Exploring the molecular clock in sympathetic preganglionic neurons

Christian Nathan

Submitted in accordance with the requirements for the degree of Doctor of Philosophy

The University of Leeds

School of Biomedical Sciences

September 2019

The candidate confirms that the work submitted is his own and that appropriate credit has been given where reference has been made to the work of others.

Acknowledgments

First off, I would like to thank my primary supervisor Jim Deuchars; your guidance through my PhD was amazing not only did you provide me with a number of opportunities to improve my research repertoire but you invited me into your home and made me feel welcome in Leeds. Thank you for all the knowledge you've given me as we've perused over my IHC slides or qPCR/RNA-seq results. A big thank you to my co-supervisor Julie Aspden, your passion for science is inspiring. You helped me get through the numerous genetic experiments of my project and provided invaluable advice. Another big thank to Sue Deuchars, your patient and measured approach at meetings helped guide my research and planning. A huge thank you to the people at the RNA-seq facility Ian Carr, Ummey Hany, Morag Raynor. Special thanks to Dapeng Wang for his invaluable and crucial work processing the RNA-seq. Next I'd like to thank my Mom and Dad, your support through my PhD was so important for me to reach this stage. I would like to especially thank my Mom for your patience and kind words when times were tough and I felt I was going in circles your calm demeanour and positive attitude helped me so much! I would also like to mention my supervisor's labs who were a tremendous help. To Aspden lab members Aikaterina Douka, Eleanor Walton, Ioannis Tsagakis, Michaela Agapiou and Tayah Hopes thank you for all the fun times! Aaron Murray, Andreea Pantiru, Badre Ahmed, Beatrice Bretherton, Brenda Frater, Cat Colquhoun, Claudia MacLean, Emily Johnson, Hanan El-Kuwaila, Jessica Haigh, Kaisan Mahadi, Lauryn New, Lucy Peers, Nazlahshaniza Shafin, Norah Altuwaijri, Nurhafizah Ghani, Pierce Mullen, Yazi Al'Joboori and more: thanks for the advice and the fun times over the course of my PhD! A massive thank you to all my friends here in Leeds, there are too many to name here but know that you all were so crucial in helping me get to this stage as all the hangouts were so important to me! I hope I can make you all proud with my future endeavours!

Abstract

Sympathetic preganglionic neurons (SPNs) are the final point of influence the central nervous system has on sympathetic nerve activity. These cells are predominantly located in the intermediolateral cell column (IML) of the thoracic spinal cord. Sympathetic nerve activity exhibits a diurnal rhythm which is evident in blood pressure variations. This project examines if there is evidence of a molecular clock in SPNs and aims to characterize SPN gene expression profile in mice.

The first aim was to identify a marker to isolate SPNs for flow cytometry so gene expression could be studied. Data mining from on-line resources identified potential candidates, immunofluorescence (IF) was applied to test selectivity of identified SPN markers. IF identified Galectin-3, previously undescribed in mouse spinal cord tissue, as a selective label for IML SPNs. Galectin-3 and other candidate markers did not label all SPNs.

The presence of a molecular clock with the potential to directly influence sympathetic activity was examined. Quantitative polymerase chain reaction (qPCR) revealed molecular clock genes Bmal1 and Per2 were diurnally expressed in IML samples. Immunofluorescence revealed SPNs expressed Per2 and Bmal1 proteins which displayed diurnal rhythmicity, suggesting SPNs possess a molecular clock.

Gene expression in IML samples and SPNs was examined with RNAseq was performed. A new method to obtain single SPNs and IML samples from frozen tissue was devised. RNA-seq from IML and single cells revealed gene expression profiles detailing receptor/channel subtypes and subunits present. RNA-seq identified a potential selective marker for SPNs which was confirmed with immunofluorescence as the $GABA_A$ θ subunit. qPCR of genes that influence SPN activity selected from RNAseq results revealed diurnal rhythm of expression levels in the IML.

These studies indicate that SPNs contain molecular clock machinery which may control expression of genes/proteins that influence SPN and sympathetic nerve activity.

Table of contents

Chapter 1 14
1.1 Biological circadian and diurnal rhythms 16
1.2 Many physiological processes display diurnal rhythms 17
1.3 Generation of circadian and diurnal rhythms 17
1.4 The SCN keeps time through a ‘molecular clock’ 19
1.5 Clock mechanism are also present outside of the SCN 21
1.6 Molecular clock in cardiovascular tissues 23
1.7 Diurnal physiological rhythms in the cardiovascular system 26
1.8 Sympathetic nerve activity exhibits diurnal activity 27
1.9 The autonomic nervous system – the sympathetic nervous system 29
1.10 Sympathetic preganglionic neurons 31
1.11 Neurochemistry of SPNs 39
1.12 Central nervous system influences on SPN activity 42
1.13 Rostral ventrolateral medulla 43
1.14 A5 influence on SPNs 44
1.15 The paraventricular nucleus of the hypothalamus 45
1.16 Is the PVN the link between the SCN and SPNs? 47
1.17 Role of the SNS in peripheral circadian rhythms 48
1.18 Could SPNs contain a clock mechanism to control sympathetic function 49
1.19 Hypothesis and aims 50
Chapter 2 51
2.1 Common buffers, solutions and media 52
2.1.1 General Buffers 52
2.2 Immunohistochemical techniques 52
2.2.1 IHC overview 533
2.2.2 Online screen of potential SPN/MN markers 53
2.2.3 Animals 53
2.2.4 Fluorogold injections in mice 54
2.2.5 Transcardial perfusion for tissue fixation 55
2.2.6 Tissue preparation 56
2.2.7 Reagents 56
2.2.8 Fluorescent immunohistochemistry 56
2.2.9 Controls 588
2.2.10 Microscopy and image capture 58
2.2.11 Statistics 58
2.3 Quantitative real-time polymerase chain reaction (qRT-PCR) 58
2.3.1 Reagents and equipment 58
2.3.2 qRT-PCR overview 59

2.3.3 Primer design 59
2.3.4 Animals 59
2.3.5 Tissue preparation 60
2.3.6 RNA extraction and purification 60
2.3.7 DNAse treatment 62
2.3.8 Nanodrop reading of RNA concentration 62
2.3.9 Reverse transcription 62
2.3.10 qRT-PCR 62
2.3.11 Statistics 63
2.4 Single cell RNA sequencing (scRNA-seq) 63
2.4.1 Animals 63
2.4.2 Tissue preparation 64
2.4.3 RNA extraction and cDNA synthesis 65
2.4.4 cDNA amplification 66
2.4.5 Purification of amplified cDNA 67
2.4.6 Quality control 67
2.4.7 Library preparation and RNA sequencing 69
2.4.8 RNA sequencing data processing 70
2.4.9 Statistics 81
Chapter 3 82
3.1 Introduction 83
3.2 Objectives 86
3.3 Materials and Methods 86
3.4 Results 91
3.4.1 Use of FG as a label for SPNs, MNs and pericytes 91
3.4.2 Candidate markers for SPNs and MNs 93
3.4.3 Galectin-3 labels a subset of SPNs as well as ependymal cells 109
3.4.4 Anti-nitric oxide synthase labels SPNs 110
3.4.5 Comparison between antibodies that labelled SPNs 110
3.5 Discussion 116
3.5.1 Galectin-3 is a novel non-specific marker for SPNs and ependymal cells in mice 116
3.5.2 NOS1 labels SPNs and tends to label more SPNs than Galectin 118
3.5.3 Comparisons between FG and antibodies 119
3.6 Conclusion 120
Chapter 4 121
4.1 Introduction 122
4.2 Summary and objectives 125
4.3 Materials and methods 126

4.4 Results 128
4.4.1 Diurnal rhythm of expression of select mRNA in IML region of thoracic spinal cord 128
4.4.2 Fluorescent intensity of clock proteins in SPNs 128
4.5 Discussion 136
4.5.1 Diurnal rhythm of mRNA expression 136
4.5.2 Bmal1 and Per2 are present in SPNs 137
4.5.3 Diurnal rhythm of clock proteins in SPNs 138
4.6 Conclusion 141
Chapter 5 143
5.1 Introduction 144
5.2 Materials and Methods 147
5.3 Results 156
5.4 Discussion 2012
Chapter 6 2201
6.1 Summary 2212
6.2 Identification of a selective marker for SPNs/VHMNs 2223
6.3 Diurnal rhythms of Bmal1 and Per2 mRNA/protein expression within the IML 2223
6.4 Producing the first transcriptome of signle IML SPNs 224
6.5 Future Experiments 226
6.6 Conclusion 2278
References 2209

List of Figures

Figure 1.1 Architecture of the molecular clock 21
Figure 1.2 Diurnal rhythm of cardiovascular parameters……26
Figure 1.3 Overview of autonomic nervous system anatomy……..…….31
Figure 1.4 Location of SPNs within spinal cord……33
Figure 1.5 Overview of inputs and outputs of SPNs……..36
Figure 1.6 Spinal cord regions and innervation of target organs……..……..39
Figure 1.7 SCN-SPN pathway……44
Figure 2.1 Summary of immunohistochemistry protocol……55
Figure 2.2 Online database search for SPN and MN markers…….....56
Figure 2.3 Overview of quantitative polymerase chain reaction (qPCR) workflow…….62
Figure 2.4 Overview of single-cell processing for RNA-seq……..……67
Figure 2.5 Overview of SMART cDNA synthesis……69
Figure 2.6 Overview of quantitative polymerase chain reaction (qPCR) workflow…….72
Figure 2.7 FastQC quality report graphs: Per base sequence quality…….……74
Figure 2.8 FastQC quality report graphs: Per sequence quality score……..……...…….75
Figure 2.9 FastQC quality report graphs: Per base sequence content……..……...…….76
Figure 2.10 FastQC quality report graphs: Per sequence GC content…..……..……..……77
Figure 2.11 FastQC quality report graphs: Per base N content……..……...……..78
Figure 2.12 FastQC quality report graphs: Sequence length distribution…..……..……...……79
Figure 2.13 FastQC quality report graphs: Sequence duplication level……..……..…….80
Figure 3.1 Online database search for SPN and MN markers…….....91
Figure 3.2 Fluorogold labelling of SPNs and MNs in thoracic spinal cord slice…....93
Figure 3.3 Allen Brain Atlas candidates CD44 and CART..…….....97
Figure 3.4 CD24 labelling in thoracic spinal cord slice …….....98
Figure 3.5 ChAT labelling of SPNs and MNs in thoracic spinal cord slice…….....99
Figure 3.6 ChAT labelling of SPNs and MNs in FG-labelled thoracic spinal cord slice……..…..…….....100

Figure 3.7 Galectin-3 labelling of SPNs and MNs in thoracic spinal cord slice…….....102

Figure 3.8 Galectin-3 labelling of SPNs and MNs in FG-labelled thoracic spinal cord slice……...103

Figure 3.9 GPR68 labelling in thoracic spinal cord slice..……...104

Figure 3.10 Allen brain atlas candidate GPX3……...……..……...105

Figure 3.11 JAM-C labelling in thoracic spinal cord slice..……..……...106

Figure 3.12 NOS1 labelling of SPNs in thoracic spinal cord slice..……...107

Figure 3.13 NOS1 labelling of SPNs in FG-labelled thoracic spinal cord slice.……...108

Figure 3.14 Allen brain atlas candidate PSA-NCAM……..…….……...109

Figure 3.15 PSA-NCAM antibody labelling of SPNs in thoracic spinal cord……..…….……...112

Figure 3.16 S100A11 labelling in thoracic spinal cord slice…….……...113

Figure 3.17 Allen brain atlas candidate S100β…… ….…….……...114

Figure 3.18 Percentage of FG-positive SPNs that were labelled by a primary antibody (ChAT, NOS1, Gal-3) in thoracic spinal cord…….…….……...115

Figure 4.1 The effect of light-dark cycle on clock gene Bmal1 in IML micropunches .130

Figure 4.2 The effect of light-dark cycle on clock gene Per2 in IML micropunches….131

Figure 4.3 Representative confocal images of Bmal1 and Per2 immunofluorescence (red) in the lateral horn of the spinal cord ……..…132

Figure 4.4 Representative confocal images of Bmal1 and Per2 immunofluorescence (red) in the central autonomic area of the spinal cord ……133

Figure 4.5 Comparison of immunofluorescence of all SPNs labelled by Bmal1 or Per2 antibodies ……..……134

Figure 4.6 Comparison of immunofluorescence of IML SPNs labelled by Bmal1 or Per2 antibodies……135

Figure 4.7 Comparison of immunofluorescence of IPPe SPNs labelled by Bmal1 or Per2 antibodies……..……136

Figure 5.1 Aspiration of single cells from fresh frozen section for scRNA-seq…….158

Figure 5.2 Images of IML micropunch and multi-cell and DNA ScreenTape library quality checks ..……..……159

Figure 5.3 Images of single cell aspiration and DNA ScreenTape library quality checks ……..……160

Figure 5.4: Relative expression (FPKM values) of mRNA coding for adrenergic α1/2 receptor subtypes in IML RNA-seq data ……166

Figure 5.5: Relative expression (FPKM values) of mRNA coding for adrenergic α1/2 receptor subtypes in scRNA-seq data ……..……166

Figure 5.6: Relative expression (FPKM values) of calcium channel subunit mRNAs in IML RNA-seq data……..……167

Figure 5.7: Relative expression (FPKM values) of highly expressed (over 15 FPKM) calcium channel α2/Δ subunit mRNAs in IML RNA-seq data……..……167

Figure 5.8: Relative expression (FPKM values) of calcium channel subunit mRNAs in scRNA-seq data ……168

Figure 5.9: Relative expression (FPKM values) of mRNA coding for calcium channel α2/Δ subunits in scRNA-seq data ……169

Figure 5.10: Relative expression (FPKM values) of mRNA coding for muscarinic receptor types in IML RNA-seq data……..….172

Figure 5.11: Relative expression (FPKM values) of mRNA coding for muscarinic receptor types in scRNA-seq data ……172

Figure 5.12: Relative expression (FPKM values) of mRNA coding for nicotinic receptor subtypes in IML RNA-seq data ……..……173

Figure 5.13: Relative expression (FPKM values) of mRNA coding for nicotinic receptor subtypes in scRNA-seq data ……..……173

Figure 5.14: Relative expression (FPKM values) of mRNA coding for GABA receptor subunits in IML RNA-seq data.……..177

Figure 5.15: Relative expression (FPKM values) of mRNA coding for GABA receptor associated proteins in IML RNA-seq data ……178

Figure 5.16: Relative expression (FPKM values) of GABA receptor subunit mRNAs in IML RNA-seq data ……..……...178

Figure 5.17: Relative expression (FPKM values) of mRNA coding for all GABA receptor subunits in scRNA-seq data ……..179

Figure 5.18: Relative expression (FPKM values) of mRNA coding for GABA receptor associated proteins in scRNA-seq data ……179

Figure 5.19: Relative expression (FPKM values) of mRNA coding for GABA receptor subunits (within 20-80 FPKM range) in scRNA-seq data ……180

Figure 5.20: Relative expression (FPKM values) of mRNA coding for GABA receptor subunits (within 5-20 FPKM range) in scRNA-seq data ……..180

Figure 5.21: ChAT and GARBQ labelling in thoracic spinal chord determined using IF/IHC ……..……181

Figure 5.22: Relative expression (FPKM values) of mRNA coding for AMPA glutamate receptor types in IML RNA-seq data ……..185

Figure 5.23: Relative expression (FPKM values) of mRNA coding for AMPA glutamate receptor types in scRNA-seq data ……185

Figure 5.24: Relative expression (FPKM values) of mRNA coding for ionotropic glutamate receptor types in IML RNA-seq data ……186

Figure 5.25: Relative expression (FPKM values) of mRNA coding for ionotropic glutamate receptor types in scRNA-seq data ……186

Figure 5.26: Relative expression (FPKM values) of mRNA coding for glutamate [NMDA] receptor subunits in IML RNA-seq data……...187

Figure 5.27: Relative expression (FPKM values) of mRNA coding for glutamate [NMDA] receptor subunits in scRNA-seq data ……..……...188

Figure 5.28: Relative expression (FPKM values) of mRNA coding for metabotropic glutamate receptor types in IML RNA-seq data…….189

Figure 5.29: Relative expression (FPKM values) of mRNA coding for metabotropic glutamate receptor types in scRNA-seq data ……..…….189

Figure 5.30: Relative expression (FPKM values) of mRNA coding for 5-HT receptor subtypes in IML RNA-seq data ……..…….194

Figure 5.31: Relative expression (FPKM values) of mRNA coding for 5-HT receptor subtypes in scRNA-seq data ……..…….195

Figure 5.32: Relative expression (FPKM values) of mRNA coding for sodium channel α/β subunits in IML RNA-seq data.....195

Figure 5.33: Relative expression (FPKM values) of mRNA coding for sodium channel α/β subunits in scRNA-seq data ……..……..196

Figure 5.34: The effect of light-dark cycle on candidate genes in IML micropunches.197

List of Tables

Table 1.1 Disturbances in clock genes and cardiovascular effects in mice models……24
Table 1.2 Neurochemistry profile of SPNs……41
Table 3.1 List of all primary antibodies used……88
Table 3.2 Percentage of FG-positive SPNs labelled by a primary antibody (ChAT, NOS1, Gal-3) in thoracic spinal cord sections..……..115
Table 5.1 PCR program prescribed for sample type according to SMART-seq v4 kit……..151
Table 5.2 qPCR program used for investigating potential diurnal rhythms in IML micro punch samples……..……..……..154
Table 5.3 Comparison of RNA-seq data to ABA ISH images of thoracic spinal cord..160
Table 5.4 Summary of relative gene expression of adrenergic (alpha 1 and alpha 2) receptor subtypes in IML and scRNAseq data set……..……...161
Table 5.5 Summary of relative gene expression of voltage-gated calcium channel subunits in IML and scRNAseq data set……...……...164
Table 5.6: Summary of relative gene expression of muscarinic acetylcholine receptor subtypes in IML and scRNA-seq data set..……169
Table 5.7: Summary of relative gene expression of nicotinic acetylcholine receptor subtypes in IML and scRNA-seq data set..……170
Table 5.8: Summary of relative gene expression of GABAA/B receptor subunits in IML and scRNA-seq data set..……..……..175
Table 5.9: Summary of relative gene expression of glutamate receptor subunits and subtypes in IML and scRNA-seq data set…..……..183
Table 5.10: Summary of relative gene expression of 5HT receptors in IML and scRNA-seq data set……..……..……..190
Table 5.11: Summary of relative gene expression of sodium channel α/β subnits in IML and scRNA-seq data set……...……..……..191
Table 5.12: Comparison of differential mean FPKM expression between ChAT- and GAD-positive single cell samples..……..……..197

Abbreviations

ABA	Allen brain atlas
aCSF	Artificial cerebrospinal fluid
ANS	Autonomic nervous system
BP	Blood pressure
cDNA	complementary DNA
CNS	Central nervous system
FG	Fluorogold
HR	Heart rate
IC	Intercalated nucleus
IF	Immunofluorescence
IHC	Immunohistochemistry
ISH	*In situ* hybridization
IML	Intermediolateral cell column
IP	Intraperitoneal
MN	Motoneurone
mRNA	messenger RNA
PBS	Phosphate buffered saline
PCR	Polymerase chain reaction
PFA	Paraformaldehyde
PNS	Peripheral nervous system
qPCR	Quantitative polymerase chain reaction

RNA-seq	RNA-sequencing
SC	Spinal cord
SCN	Suprachiasmatic nucleus of the hypothalamus
scRNA-seq	Single cell RNA-sequencing
SNA	Sympathetic nervous activity
SNS	Sympathetic nervous system
SPN	Sympathetic preganglionic neurone
VHMN	Ventral horn motoneurone

Chapter 1
General Introduction

1.1 Biological Circadian and Diurnal Rhythms

Life on Earth is governed by a 24 hour day-night cycle. The predictable change in light and temperature has resulted in the evolution of mechanisms for biology to function to obtain maximum benefit from different times of day. Such mechanisms are driven by biological clocks through which the 24 hour day-night cycle influences gene regulation and biological function (Panda *et al.*, 2002a; Bhadra *et al.*, 2017). The development of biological clocks therefore confers a survival advantage for organisms, allowing them to adapt their physiology and behaviour in accordance to changes in light and temperature. Physiological activities such as sleep-wake patterns, mental alertness, organ movement and eating habits display rhythms, peaking at specific times of the day. Behavioural activities, such as venturing out for hunting, are also rhythmic and important for an organism's survival. In addition, storing food for unfavourable seasons and hibernation displays a rhythm, thus clocks not only serve as daily timers but seasonal timers as well (Panda *et al*., 2002; Bhadra *et al.*, 2017).

The rhythms of physiology and behaviour in organisms conferred by biological clocks can be broadly defined as the oscillation between active and inactive phases. There are a number of such rhythms defined in organisms - circadian, diurnal and ultradian. Circadian rhythms are endogenously produced rhythms with an oscillation over ~24 hours that persists under constant environmental conditions. Diurnal rhythms are synchronized to the day-night cycle and so are not produced endogenously. Although it is possible to have circadian rhythms that are not influenced by day/night cycle, most studies tend to use the terms interchangeably particularly in experimental animals on a 12/12 hour light/dark cycle. In contrast, ultradian rhythms are synchronized to biological processes

such as feeding and occur more frequently over a 24 hour period (Bell-Pedersen *et al.*, 2005).

1.2 Many physiological processes display circadian rhythms

Many physiological processes are synchronised to the day-night cycle and so display diurnal rhythms. For example, the sleep-wake pattern and mental alertness are characterized by active phases occurring during light periods, while inactive or rest phases occur during the dark periods (although this pattern is reversed in nocturnal animals such as mice). Diurnal rhythms are also exhibited by a number of organs and systems. Examples of systems that display diurnal rhythmicity in some of their parameters include the cardiovascular, gastrointestinal and renal systems. In the cardiovascular system, heart rate (HR) and blood pressure (BP) display diurnal rhythmicity, dipping during the night in humans (Crnko *et al.*, 2019). The gastrointestinal system displays ultradian rhythmicity in activation of peristaltic muscle movement and the release of hunger associated hormones such as ghrelin at feeding times (Challet, 2019). Within the renal systems, several processes related to urine output undergo diurnal rhythms including renal plasma flow and glomerular filtration rate (Firsov and Bonny, 2018).

1.3 Generation of circadian/diurnal rhythms

In the 1950's, Jürgen Aschoff defined the term 'zeitgeber' as an external signal that synchronises rhythms. The process by which a rhythm synchronizes to a zeitgeber is known as entrainment. Whilst there are a number of different zeitgebers, light is the zeitgeber which produces diurnal rhythms in biological clocks (Aschoff, 1951).

In mammals, light levels are sensed via intrinsically photoreceptive retinal ganglion cells and transmitted via the retinohypothalamic tract within the optic chiasm to the suprachiasmatic nucleus of the hypothalamus (SCN) (Sharma and Chandrashekaran, 2005; Herzog, 2007; Do and Yau, 2010). The SCN is composed of roughly 10,000 cells clustered at the base of the third ventricle directly above the optic chiasm. The SCN has two parts, referred to as the core and shell distinguished by retinal and efferent connections and neuropeptide expression. The core receives the retinal input and expresses vasoactive intestinal peptide (VIP) and gastrin-releasing peptide (GRP) while the shell receives input from the core and contains arginine vasopressin (AVP)-expressing cells. In summary, light sensed by retinal ganglion cells directly innervates neurones in the core of the SCN, which in turn entrains rhythmic oscillations within the shell of the SCN. (Evans *et al.*, 2015; Hastings *et al*., 2018).

The output of SCN neurons can synchronise rhythmicity within other brain regions, and therefore light levels can indirectly influence a wide range of physiological functions. For example, SCN efferents project directly to the medial preoptic, paraventricular and dorsomedial nuclei and the subparaventricular zone of the hypothalamus (Hastings *et al.*, 2018). In addition, SCN efferents project to the basal forebrain and midline thalamus. As a result SCN activity can modulate a number of processes such as wakefulness (reticular activating system, a set of nuclei within the brainstem), thermoregulation feeding and cardiovascular parameters (hypothalamus), memory and learning (hippocampus), mental performance (neocortex) and endocrine secretion (pituitary gland) (Hastings *et al.*, 2018).

1.4 The SCN keeps time through a ‘molecular clock’

Light input to the SCN regulates its rhythmicity and thereby the influence of the SCN on biological clocks. These clocks are endogenous genetic circuits which keep track of time (see Figure 1.1). A number of researchers have contributed to the discovery of various gene and protein components that comprise the molecular clock. In 2017, the Nobel Prize in Physiology or Medicine was awarded to Jeffrey C. Hall, Michael Rosbash and Michael W. Young, each of whom isolated and characterized the protein Period (PER) in the fruit fly. The PER protein was shown to exhibit a circadian rhythm, aggregating during the evening and being broken down in the morning (Hastings *et al.*, 2018). In following years other clock genes and proteins have been discovered in a range of different species, such as: aryl hydrocarbon receptor nuclear translocator-like protein 1 (BMAL1), circadian locomotor output cycles kaput (CLOCK) and cryptochrome (CRY). Collectively these studies have enabled identification of the molecular determinants and mechanisms by which the molecular clock is established and maintained (King *et al.*, 1997; Gekakis *et al.*, 1998; Kume *et al.*, 1999; Shearman *et al.*, 2000). The mechanism by which the molecular clock functions is described as a transcription-translational feedback loop (TTFL). There are positive and negative transcriptional modulators that comprise a negative feedback loop, resulting in the cyclic activation of clock gene transcription components. The positive arm consists of transcription activators, Bmal1 and Clock while the negative arm is comprised of PER and CRY. The transcription and translation of the Bmal1 gene is driven by the protein retinoic acid-related orphan receptor (ROR) and repressed by another protein REV-ERB. CLOCK and BMAL1 proteins form heterodimers which bind to promoters of PER and CRY genes, leading to activation of their transcription. PER proteins

are phosphorylated and can form complexes with CRY proteins and the enzyme casein kinase 1ε/δ. Some of these complexes are degraded by proteasomes while others translocate from the cytoplasm to the nucleus. The PER/CRY protein complex can suppress CLOCK/BMAL1 mediated transcription of the PER and CRY genes. The same complex can also decrease the influence of CLOCK/BMAL1 on other core clock genes which in turn modulates clock outputs and rhythmic biological processes (von Schantz and Archer, 2003; Ko and Takahashi, 2006; Albrecht and Ripperger, 2009; Takeda and Maemura, 2011; Takahashi, 2016). This TTFL mechanism persists in all biological clocks across the body. In summary, the CLOCK/BMAL1 protein complex of the molecular clock binds to transcription factors, which in turn bind to target genes to influence their transcription and ultimately cellular functions (Ueda *et al.*, 2005; Takahashi, 2016).

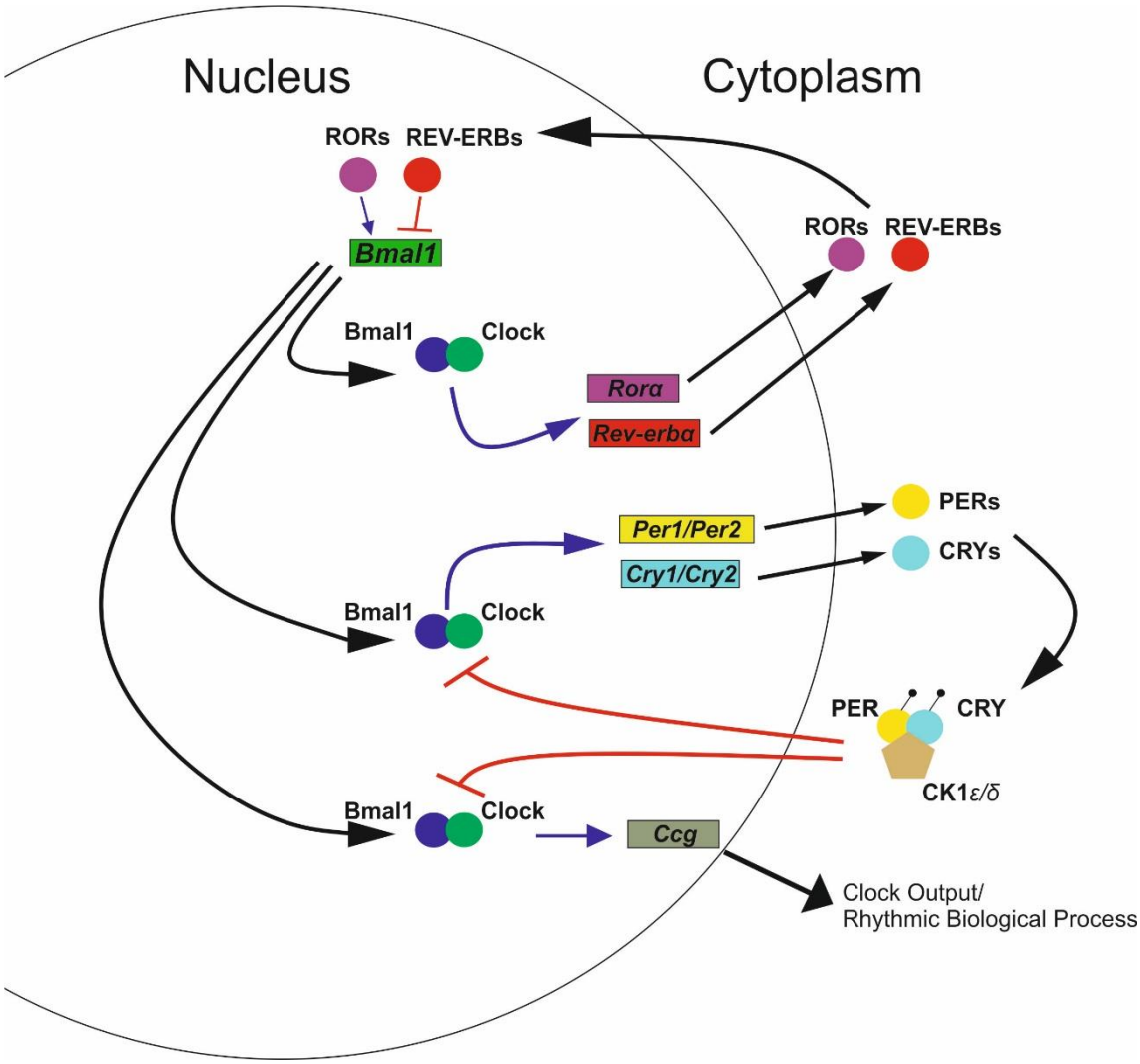

Figure 1.1 Architecture of the molecular clock
The molecular clock is comprised of a set of genes and the proteins they encode locked in a transcriptional-translational feedback loop. The positive arm consists of the Bmal1 and Clock proteins while the negative arm consists of Per and Cry proteins. Adapted from (Ko and Takahashi, 2006).

1.5 Clock mechanisms are also present outside of the SCN

In mammals, the biological clock system is composed of multiple clocks organized in a hierarchy. The SCN serves as the master clock setting the rhythms of clock gene/protein expression in peripheral tissues, referred to as peripheral clocks. Peripheral clocks have been described in a number of organs including the heart, liver, lungs, kidneys, thyroid gland, pineal gland and spleen (Mohawk *et al*., 2012). Indeed, clocks in the cultured explants of the cornea,

liver, kidney and pituitary gland among others have maintained rhythmic oscillations of clock protein PER2, as measured by the PER2: luciferase fluorescence assay. These findings illustrate how peripheral clocks can be self-sustained, persisting in the absence of SCN input. Interestingly, rhythms were also evident in cultured explants obtained from SCN-lesioned animals, indicating that the SCN was not required for establishing peripheral CLOCK gene rhythms. SCN lesions did however result in phase desynchrony among the tissues of these animals, implicating an important role of the SCN in setting the timing of peripheral rhythms.(Yoo *et al.*, 2004). The SCN's hierarchical dominance over peripheral clocks was demonstrated in cellular clocks of cultured fibroblasts from PER1 gene deficient mice. These mice exhibited a shorter rhythmic oscillation of PER2 gene, as measured by RNA levels. When PER1 deficient fibroblasts were transplanted into a wild-type host, the PER2 gene rhythm was restored. This study demonstrates the control that the SCN master clock has over peripheral clocks, likely achieved through neuronal or hormonal pathways (Pando *et al.*, 2002). The SCN is therefore an important structure that serves to entrain and synchronize peripheral clocks across the body, capable of restoring normal rhythmic oscillations in defective peripheral clocks (Pando *et al.*, 2002; Stratmann and Schibler, 2006).

The presence of biological clocks in peripheral tissues and cells raises the question of how much of global transcription is under circadian control. This question is now easier to answer with the advent of genome-wide analysis techniques and tools. Regarding the liver, heart and skeletal muscle, roughly 2-10% of the total genome is transcribed with a circadian rhythm, as measured by whole genome microarray and quantitative polymerase chain reaction (qPCR) of selected target genes. Specifically, 337 genes showed rhythmic transcription

in the liver while 450 genes displayed rhythmic transcription in the heart (Panda *et al.*, 2002b; Storch *et al.*, 2002; Miller *et al.*, 2007). Rhythmic transcription of genes has been attributed to diurnal rhythms of organ function. The peripheral clock within the liver affects a number of different physiological processes. A qPCR study conducted on mouse liver samples taken at different times of day revealed that target genes involved with nutrient metabolism were highly expressed during the evening. Genes encoding enzymes involved in intermediate metabolism were also found to vary with time of day. Specifically, transcripts coding for cholesterol biosynthesis enzymes peaked during the evening while cholesterol degradation enzyme transcripts peaked several times throughout the day (Panda *et al.*, 2002b). Furthermore, peripheral clocks within organ systems such as the cardiovascular system also have the potential to drive rhythmic gene expression in a number of associated tissues and cell types, thereby influencing a host of physiological processes.

1.6 Molecular clocks in cardiovascular tissues

Rhythmic gene expression has been observed in major organs involved with the cardiovascular system, particularly the heart within the cardiomyocytes comprising the atrial and ventral myocardium (Storch *et al.*, 2002; Evans *et al.*, 2015). Rhythmic expression of clock genes has been observed in the atrium, ventricle and aorta of the human heart. The mRNA levels of *Per1*, *Per2*, *BMAL1* and *Cry1* were assessed using real time polymerase chain reaction (PCR) and differential mRNA expression. Peak *Per1* and *Per2* mRNA expression occurred in the morning with *Per1* occurring earlier in the morning that *Per2*. *BMAL1* mRNAs occurred later in the evening (Leibetseder *et al.*, 2009). In blood vessels, the clock genes, Bmal1 and Clock were identified in mouse aortas using northern blot analysis. These clock genes exhibited diurnal

rhythms with both shown to peak during the early morning (McNamara *et al.*, 2001). The presence of Per2 genes, exhibiting a diurnal rhythm, within mouse aortas was identified by a separate study. Northern blot analysis demonstrated that Per2 expression peaked during the evening (Nonaka *et al.*, 2001). Rhythmic oscillations of PER1 protein have also been observed in vein and artery cultures, using the fluorescence intensity of immuno-localised proteins as a measure of rhythm (Davidson *et al.*, 2005). Numerous other studies have also characterized molecular clocks within individual cell types found within blood vessel walls. *Bmal1* and *Per2* mRNA diurnal rhythms were observed in vascular endothelial cells, present in the inner layer of blood vessels. qPCR revealed *Bmal1* mRNA peaked during the morning whilst *Per2* mRNA peaked during the evening (Takeda *et al.*, 2007). Vascular smooth muscle cells, found within the middle layer of blood vessels, also show diurnal oscillations of a number of key clock components. *Per1/2* and *Rev-erb* mRNAs have been shown to be highly expressed during the middle of the day and evening whereas *Bmal1* mRNA expression was higher during the morning, as determined by qPCR (Chalmers *et al.*, 2008). Similar observations have been made for fibroblasts, present within the outer walls of blood vessels. A study conducted using cultured fibroblasts, revealed that expression of BMAL1 and PER2 proteins displayed rhythmic oscillations, as measured by fluorescence intensity (Welsh *et al.*, 2004). In addition to cells comprising vasculature, other cell types within the cardiovascular system have also been shown to exhibit rhythmic oscillations of gene expression. Cultured adult rat cardiomyocytes displayed diurnal rhythms of *Bmal1* and *Per2* mRNA expression. Once again qPCR illustrated how *BMAL1* mRNA peaked in the morning and *Per2* mRNA peaked during the evening (Durgan *et al.*, 2005). Cultured cardiac progenitor-

like cells from human fetal and adult hearts also exhibit diurnal rhythms, with *Bmal1* mRNA expression peaking in the morning (Du Pré *et al.*, 2017).

Given the prevalence of diurnal expression patterns of clock genes within cardiovascular organs, tissues and cell types, it is not surprising that cardiovascular functions also exhibit diurnal rhythms. As summarised in Figure 1.2, diurnal rhythms have been reported for BP, HR, circulating catecholamines, platelet aggregability and blood clot formation (Takeda and Maemura, 2016). Concurrently, a variety of animal studies have demonstrated how genetic manipulation of clock genes directly perturbs diurnal rhythmicity and ultimately cardiovascular physiology, as detailed in Table 1.1.

Table 1.1 Disturbances in clock genes and cardiovascular effects in mice models.

Clock disturbance	Effects	Reference
Bmal1-knockout mice	Loss of physiological rhythms in heart rate and blood pressure. Dilated cardiomyopathy	(Curtis *et al.*, 2007; Lefta *et al.*, 2012)
Per2-knockout mice	Endothelial dysfunction	(Viswambharan *et al.*, 2007)
Cardiomyocyte-specific Clock-mutant mice	Disruption of physiological variation of the transcriptome; bradycardia and mitochondrial dysfunction	(Bray *et al.*, 2008; Durgan *et al.*, 2010; Podobed *et al.*, 2014)
Bmal1-knockout mice and Clock-mutant mice	Vascular injury, endothelial dysfunction and pathological vascular remodelling	(Anea Ciprian *et al.*, 2009)
Cardiomyocyte-specific Clock-mutant plus cardiomyocyte-specific Bmal1-knockout mice	Drug-induced hypertrophic cardiomyopathy	(Durgan *et al.*, 2011)
Mice with inducible, cardiomyocyte-specific disruption of Bmal1	Bradycardia, prolonged QRS duration and ventricular arrhythmias	(Schroder *et al.*, 2013)
Cardiomyocyte-specific Bmal1-knockout mice	Disruption of physiological variation in 10% of the transcriptome; cardiac metabolism changes, dilated cardiomyopathy and premature death	(Young *et al.*, 2014)
Vascular-smooth-muscle-cell-specific Bmal1-knockout mice	Diminished 24-h rhythm in blood pressure and change in timing of blood pressure peak	(Xie *et al.*, 2015)

Table obtained from (Crnko *et al.*, 2019).

1.7 Diurnal physiological rhythms in the cardiovascular system Human studies implementing spectroscopic measurement of blood samples have also examined diurnal cardiovascular rhythms. Within vasculature, thrombomodulin, an important co-factor in blood coagulation, levels peak during the early evening (Takeda *et al.*, 2007). Furthermore platelet aggregability exhibits two diurnal acrophases, with peaks observed during the late phases of both light and dark periods (Scheer *et al.*, 2010, 2011). Plasminogen activator inhibitor-1 (PAI-1) is a protein that inhibits the enzymatic breakdown of fibrin (aka fibrinolysis), a key component of blood clots. PAI-1 has also been shown to be especially high during the early phase of the light period (Scheer and Shea, 2014). Collectively the diurnal rhythms of these parameters likely contribute to the high incidence of adverse cardiovascular events in the early morning and evening in human subjects (Scheer *et al*., 2010).

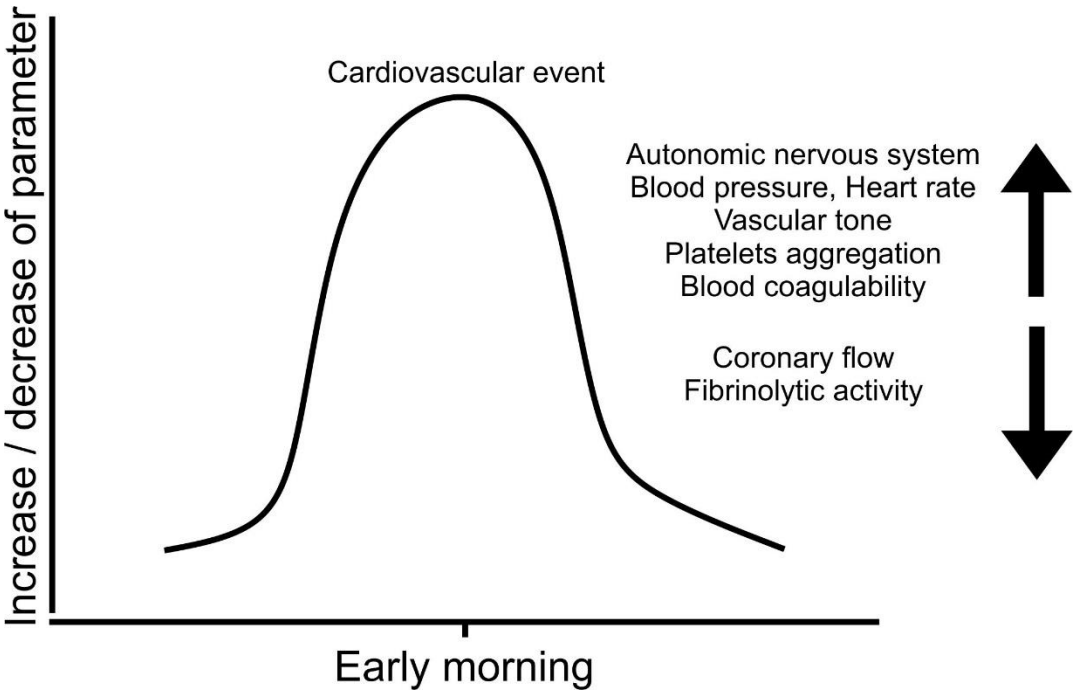

Figure 1.2: Diurnal rhythms of cardiovascular parameters
The cardiovascular system has a number of parameters that express diurnal rhythmicity. Loss of normal diurnal rhythm of these parameters results in an increased risk of a cardiovascular event in the early morning. Adapted from (Takeda and Maemura, 2015).

Cardiovascular functions follow diurnal rhythms, exemplified by the decreases in BP and HR at night in humans, with reciprocal increases in the morning (Millar-Craig *et al*., 1978; Seifalian and Hart, 2019). Disrupted diurnal rhythms are predictive of acute cardiovascular events suggesting that these rhythms are important mediators of homeostasis. Morning BP surges (MBPS) are established phenomena which can lead to hemodynamic stress (Bilo *et al*., 2018). MBPS plays a critical role in an elevated risk of cardiovascular events such as stroke in the early morning, independent of 24-hour BP values (Kario, 2010; Douma and Gumz, 2018). Other specific disruptions in circadian BP rhythm are also associated with various cardiovascular pathologies. For example, inversion of the typical circadian BP rhythm, known as reverse dipping, is associated with metabolic syndrome and predictive of end stage renal failure in diabetic patients (Nakano *et al.*, 1999; Yan *et al.*, 2015). Reduced dipping of BP at night-time, observed in some hypertensive patients, is associated with increased left ventricular hypertrophy and predicts mortality and cardiovascular events (Nakano *et al.*, 2001; Fagard *et al.*, 2009; Douma and Gumz, 2018). To provide a more generalised example, people with abnormal circadian rhythms such as night shift workers or healthy elderly subjects with sleep fragmentation, have an increased risk of developing cardiovascular disease (Knutsson *et al.*, 1986; Karlsson *et al.*, 2005).

1.8 Sympathetic nerve activity exhibits diurnal activity

As noted in section 1.7, cardiovascular variables such as HR and BP exhibit diurnal rhythms, loss of which is associated with cardiovascular dysfunction. This diurnal rhythm is related to levels of sympathetic nerve activity (SNA). For

example, in humans, circulating epinephrine and norepinephrine peak throughout the light period and trough during the dark period (Curtis *et al.*, 2007; Scheer *et al.*, 2010, 2019). Indeed, MBPS in humans is accompanied by increases in plasma noradrenergic transmitter levels, suggesting increases in sympathetic outflow (Tuck *et al*., 1985). SNA activity has been shown to influence HR and BP in many studies (Malpas, 1998, Guyenet, 2006, Mancia and Grassi, 2014). Direct demonstration of sympathetic neural involvement has been obtained with microneurography. Specifically, increased muscle SNA (MSNA) during the day compared to night correlates with BP values and increases in SNA accompany MBPS (Grassi *et al.*, 2008; Lambert *et al.*, 2014). Furthermore, when measuring BP variability in human patients over 24 hours, researchers found that higher MSNA is associated with greater day-night differences in BP (Narkiewicz *et al.*, 2002). These findings suggest that sympathetic neural mechanisms could contribute to the regulation of BP over the 24-hour cycle.

Animal studies also indicate that the sympathetic nervous system is involved in diurnal cardiovascular rhythms. In freely moving mice with and without exercise wheels, BP and HR show clear and sustained rhythmic oscillations over 24 hour periods (V K Lall *et al.*, 2017). In the rat working heart brainstem preparation, which is an anaesthetic-free preparation decerebrated at the pre-collicular level (thus removing the SCN), there are significant differences in HR and importantly in SNA. These differences were found to be dependent on the timing of the preparation. Thus those that were recorded in the morning (equivalent to the sleep phase) had significantly lower SNA and HR compared to the evening (the normal active phase for rats) (Mahadi *et al.*, 2019).

Diurnal rhythmic activity in the sympathetic nervous system is clearly important in physiological and pathophysiological function of the cardiovascular system. The final common pathway through which the central nervous system (CNS) influences sympathetic nervous activity is at the level of the sympathetic preganglionic neurones (SPNs) in the intermediolateral cell column (IML) of the spinal cord (Deuchars and Lall, 2015). However, to date, there are no reports as to whether the neuronal circuits controlling cardiovascular activity are also intrinsic circadian clocks. This thesis asks whether SPNS could act as intrinsic clocks and contribute to the neural circadian system involved in cardiovascular control.

1.9 The autonomic nervous system – the sympathetic nervous system

The autonomic nervous system (ANS) comprises the sympathetic and parasympathetic branches, as well as the enteric nervous system. It is responsible for maintaining homeostasis and so influences a number of body functions such as HR, digestion and respiration rate without conscious control. Whilst the enteric is considered part of the ANS, it is located in the gastrointestinal tract and will not be discussed further here. The sympathetic and parasympathetic nervous systems project to many of the same structures across the body and generally function in opposition to one another, typically considered as preparing the body for either fight-or-flight or rest-and-digest' responses to stimuli (See Figure 1.3). For example within the cardiovascular system, the parasympathetic nervous system slows HR whereas the sympathetic accelerates HR (Wehrwein *et al*., 2016; Karemaker, 2017).

The parasympathetic nervous system is responsible for 'rest-and-digest' and other activities the body performs when at rest. The parasympathetic efferent

projections arise from 3 main nerves: cranial nerves III (oculomotor), VII (facial), IX (glossopharyngeal), X (vagus) and the pelvic splanchnic nerves and innervate many of the same end organs as the sympathetic nervous system such as the heart, lungs and gastrointestinal tract. The parasympathetic nervous system functions to return these organs' activity to normal functions following a reaction to a stimulus. Some examples of this include decreasing HR, constricting bronchioles and increasing peristalsis (Wehrwein *et al*., 2016; Karemaker, 2017).

The CNS component of the sympathetic nervous system is located in the spinal cord, particularly in the thoracic and lumbar regions. These regions of the spinal cord are the final points at which the CNS can influence SNA, since SPNs located here project directly out of the spinal cord to sympathetic ganglia. As this thesis examines the potential for a molecular clock in SPNs, a brief review of SPNs follows.

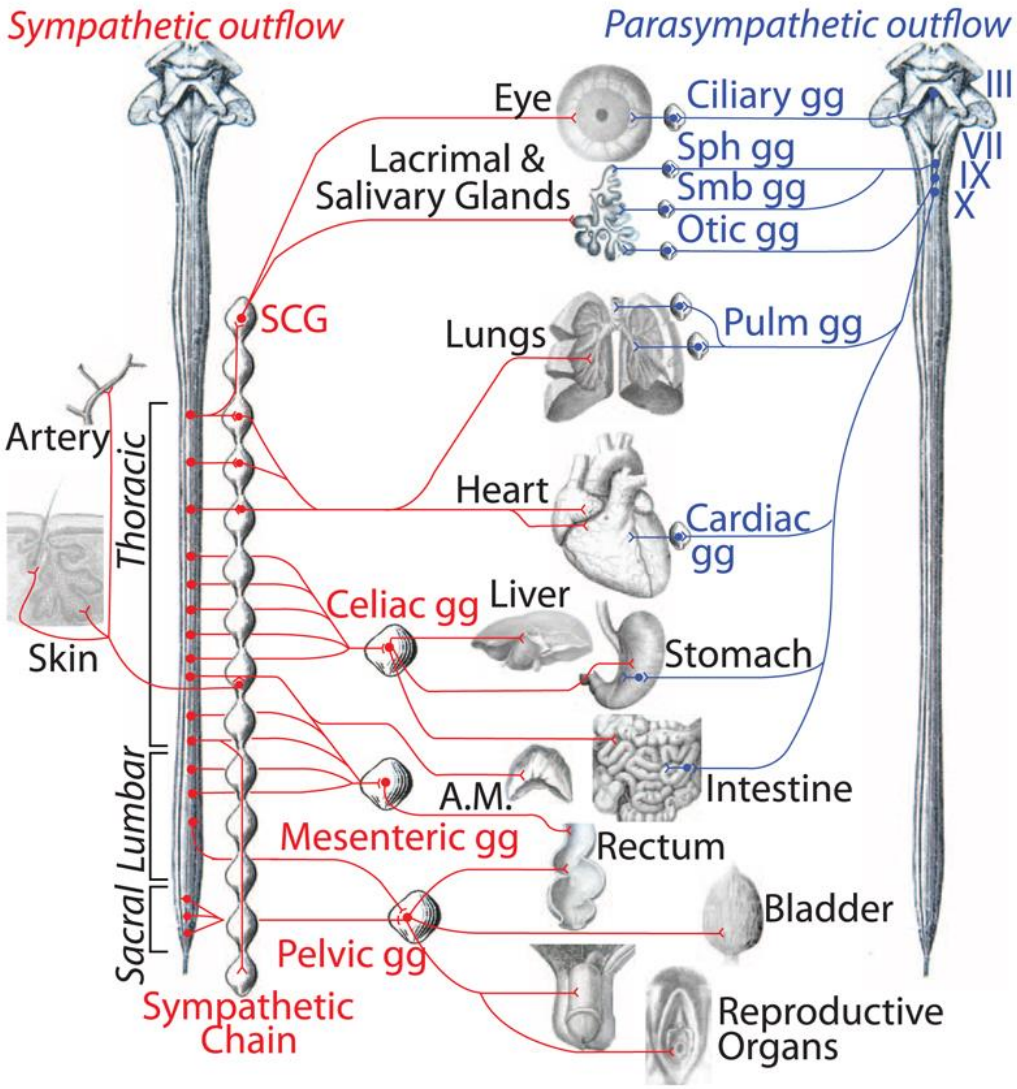

Figure 1.3 Overview of Autonomic Nervous system anatomy
Sympathetic and parasympathetic branches and their projections to organs are depicted in this diagram. Many organs receive dual input from the branches of the autonomic nervous system. Sympathetic efferent projections originating from the intermediolateral cell column project to a number of organs (red). The parasympathetic efferent projections originate from the cranial nerves and innervate many of the same structures (blue). III, oculomotor nerve; VII, facial nerve; IX, glosso-pharyngeal nerve; X, vagus nerve; A.M., adrenal medulla; gg, ganglion; Pulm, pulmonary; SCG, superior cervical ganglion; Sph, sphenopalatine; Smb, submandibular. Image obtained from (Espinosa-Medina *et al.*, 2016).

1.10 Sympathetic preganglionic neurons

SPNs are found predominately in the thoracolumbar (T1-L2) and lumbosacral levels (L6-S1) of the spinal cord. A number of techniques have been employed to study these cell types ranging from degeneration, histological staining and

retrograde and transneuronal tracing. The anatomical distribution of SPNs within the spinal cord has been demonstrated across species from rats, dogs, cats and even monkeys (Clarke, 1850; Petras and Cummings, 1972; Schramm *et al.*, 1975; Chung *et al.*, 1979; Rubin and Purves, 1980; Chung *et al*., 1980; Rando *et al*., 1981; Oldfield and McLachlan, 1981; Baron *et al*., 1985; Bennett *et al.*, 1986; Jänig and McLachlan, 1986; Bacon and Smith, 1988; Pyner and Coote, 1994; Tang *et al*., 1995a). SPNs form clusters in 4 distinct areas in the thoracic and lumbar spinal cord: intermediolateral cell column (IML), nucleus intermediolateralis thoracolumbalis pars funicularis (Ilf), intercalated nucleus (IC) and central autonomic area (nucleus intercalatus pars paraependymalis, IPPe) (Petras and Cummings, 1972; Chung *et al.*, 1979; Oldfield and McLachlan, 1981) (Figure 1.4). Most SPNs are found in the IML, forming nests in bilateral columns, which are located on the lateral edge of the grey matter on either side of the spinal cord. The nests of SPNs vary in number from 20 to 150 neurons (Petras and Cummings, 1972; Chung *et al.*, 1979; Oldfield and McLachlan, 1981; Deuchars and Lall, 2015). SPN cell bodies and dendrites display a ladder-like arrangement along the length of the spinal cord (Romagnano and Hamill, 1984; Bacon and Smith, 1988b). SPN cell bodies make up the majority of the soma within the IML, however interneurons are found in this area as well (Deuchars, 2015). SPN cell bodies within the IML are either triangular, spindle-shaped, elongated or round which was determined following their labelling with retrograde labelling studies using horseradish peroxidase (HRP) or cholera toxin-B horseradish peroxidase (Oldfield and McLachlan, 1981; Pyner and Coote, 1994, 1995). IML SPNs' dendrites project towards the white matter while some arborizations project to the central canal (Pyner and Coote, 1994, 1995; Tang *et al*., 1995b).

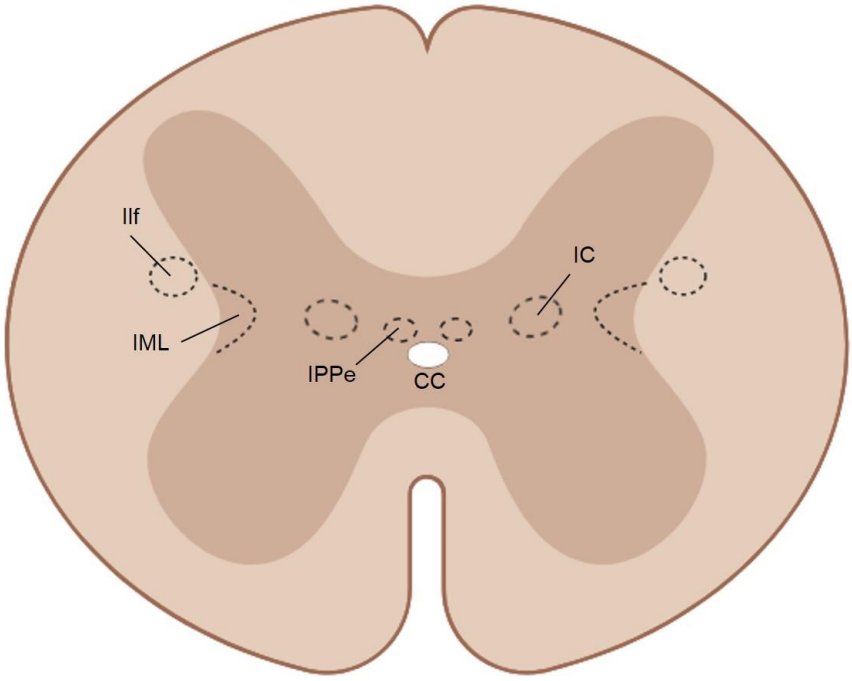

Figure 1.4 Location of SPNs within the spinal cord
There are 4 main groups of SPNs: intermediolateral cell column, IML; nucleus intermediolateralis pars funicularis, IIf; intercalated nucleus, IC; central autonomic area, IPPe; CC, central canal. Image adapted from (Deuchars and Lall, 2015).

Within the white matter is another group of SPNs located in the IIf region, the cell bodies of these SPNs are generally triangular or spindle-shaped. The dendrites of IIf SPNs extend laterally and mingle with the projections of the IML SPNs (Petras and Cummings, 1972; Chung *et al.*, 1979; Barber *et al.*, 1984; Strack *et al.*, 1988). Between the IML and the central canal is the IC region where another grouping of SPNs is found, their somata are spindle-shaped and their dendrites run laterally and associate with IML SPNs (Pyner and Coote, 1995). The fourth group of SPNs is located in the IPPe region which is above the central canal (also known as lamina X), the somata of these SPNs are triangular or spindle-shaped and the dendrites of these cells can cross the

central canal to the other side of the spinal cord allowing communication between both sides (Deuchars and Lall, 2015).

Tracing studies have attempted to map the distribution of SPNs retrogradely labelled from the adrenal gland, sympathetic nerves or ganglia using retrograde tracers HRP and/or hydroxystilbamidine (commonly known as Fluorogold). HRP was introduced via direct injection into ganglia, into axons or into nerves that were cut or transected (Schramm *et al*., 1975, Oldfield and McLachlan, 1977, Chung *et al*., 1979, Chung *et al*., 1980, Baron *et al*., 1985a, Baron *et al*., 1985b, Jänig and McLachlan, 1986). Improved retrograde tracers such as cholera toxin B conjugated to HRP allowed dendritic branches to be observed (Bacon and Smith, 1988, Pyner and Coote, 1994a, Pyner and Coote, 1995, Tang *et al*., 1995). HRP Injections in the lumbar sympathetic trunk and inferior mesenteric ganglion labelled SPNs in the IPPe and the IML (McLachlan *et al*., 1985). Retrograde tracing via application of HRP to the hypogastric nerve and lumbar sympathetic trunk paired with electrophysiological recordings of cat lumbar SPNs have revealed that the location of SPNs correlates with their function. Measurement of axon conduction velocities following hypoxic stimulation found that SPNs with vasoconstrictor functions are found in the IML or Ilf (Jänig, 1980, McLachlan, 1985).

Fluorogold is an attractive alternative to other retrograde tracers as it is delivered via intraperitoneal injection thus making it easier to deliver and less invasive than other tracers. Animals are sacrificed 2 days after the injection, resulting in widespread labelling of neurons with axons that exit the CNS, including SPNs. This tracer labels motoneurons (MNs) in the ventral horn, SPNs in the cervical segment 8 to lumbar segment 2 of spinal cord and also pericytes throughout the CNS (Ambalavanar and Morris, 1989, Anderson and

Edwards, 1994, Edwards *et al*., 2013). In an alternative study, the superior cervical, coeliac and pelvic ganglia and the adrenal gland were injected with Fast Blue or cholera B toxin. The same rats also received an i.p. injection of Fluorogold, resulting in co-labelling of different SPN populations spanning the cervical, thoracic and lumbar regions of the spinal cord. This study confirmed that Fluorogold reliably labels the entire SPN population (Anderson and Edwards, 1994).

Strack *et al*. used Fluorogold to label discrete groups of SPNs within the spinal cord, achieved by injecting the ganglia (or adrenal gland) that they projected to. This experiment found a large number of SPNs (1000-2000 per ganglion) innervate the sympathetic ganglia controlling the head or thoracic organs whereas a small number of SPNs (100-400 per ganglion) innervate the sympathetic ganglia controlling the gut, kidney and pelvic organs (Strack *et al.*, 1988). Strack *et al*. suggests the difference in number of SPN innervation of end organs may be related to the level of control of these organs, i.e. the sympathetic postganglionic neurons innervating the head or thoracic organs are capable of a fine level of adjustment as opposed to sympathetic innervation to other organs. Ilf SPNs innervate the superior, middle and inferior cervical sympathetic ganglia. IML SPNs are the predominant source of innervation to many ganglia including the superior cervical ganglion, middle cervical ganglion, inferior cervical ganglion, celiac ganglion, aorticorenal ganglion, superior mesenteric ganglion and the adrenal gland (Strack *et al*., 1988) (Figure 1.5). Simultaneous retrograde labelling using tracers Fast Blue, Diamino Yellow and Fluorogold from the superior cervical ganglion, stellate ganglion and adrenal medulla found that different groups of SPNs in the SPN-rich areas in the spinal cord innervated these ganglia. IML SPNs predominantly innervated the three

ganglia followed by Ilf SPNs. At rostral levels there was less representation of adrenal medulla projecting SPNs whereas at caudal levels there were less superior cervical ganglion and stellate ganglion projecting neurons. The results of this study indicated SPNs were arranged in target-specified columns in the thoracic spinal cord (Pyner and Coote, 1994b).

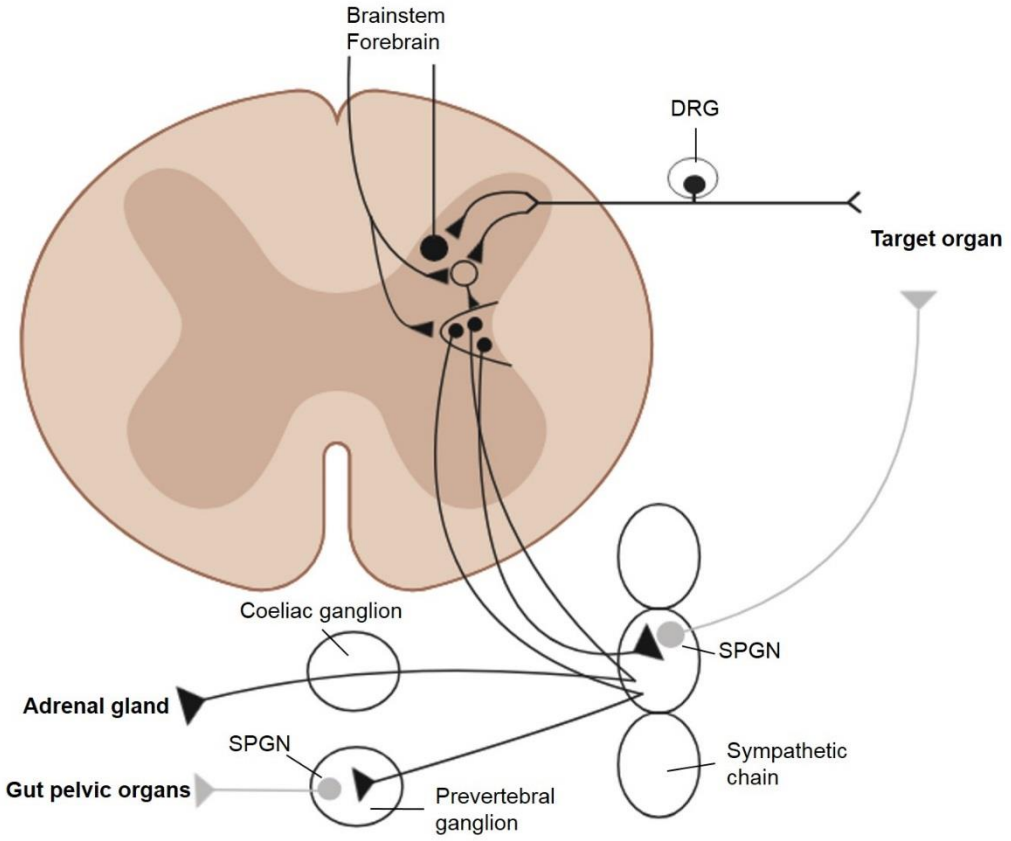

Figure 1.5 Overview of inputs and outputs of SPNs
SPNs synapse on sympathetic postganglionic neurons, SPGN. SPGNs synapse on the target organ. Sensory information is conveyed to the thoracolumbar spinal cord by afferents with their cell bodies in the dorsal root ganglion, DRG. Imaged adapted from (Deuchars and Lall, 2015).

Studies using electrical stimulation of IML SPNs or microinjections of L-glutamate have found IML SPNs may have different functions based on which side of the spinal cord they are located. Electrical stimulation of the IML SPNs in the spinal segments T1 to mid T8 on the right side elicited an increased HR and arterial hypertension. Stimulation on the left resulted in the same changes but

they were significantly lower (Henry and Calaresu, 1972, Sundaram *et al*., 1989). Electrical stimulation of the sympathetic fibres in the right vagus nerve and the right inferior cardiac nerve resulted in an increase of HR by 92 beats/min. Electrical stimulation of the left inferior cardiac nerve, the left middle cardiac nerve and the sympathetic fibres in the left vagus nerve resulted in an increase of the HR of 43 beats/min (Kamosińska *et al*., 1989, Murugaian *et al*., 1990).

Previous studies have shown SPN projections synapse on a number of ganglia and have illustrated the influence these cell types have across the body. Janig *et al*. noted in their review that a single SPN could innervate up to 200 postganglionic neurons in humans, based on previous research on SPN target organs (Jänig and McLachlan, 1992). SPNs send ipsilateral projections to thoracic ganglia and the adrenal medulla (Cummings, 1969, Petras and Cummings, 1972, Schramm *et al*., 1975, Jin Mo *et al*., 1975, Petras and Faden, 1978, Kuo *et al*., 1980). SPNs located in the lumbar region of spinal cord may send contralateral projections to the lumbar sympathetic trunk, lumbar splanchnic nerve and hypogastric nerve as suggested by the results of retrograde tracing with HRP (Faden and Petras, 1978, Baron *et al*., 1985a, Baron *et al*., 1985b). HRP labelling revealed SPN axons leave at the segmental level of their cell soma (Chung *et al*., 1979). There is a distinct topographic organization of SPNs within the spinal cord although SPNs within a spinal cord segment may innervate different ganglia as proven by retrograde tracing studies. Double labelling of SPNs, pairing either Fluorogold, Fast Blue, or Diamidino Yellow, was observed when a retrograde tracer was introduced to the adrenal medulla or more than one ganglion (Pyner and Coote, 1994b).

Transneuronal tracing has allowed for the precise labelling of SPNs innervating different end organs. This method also helped determine the SPNs involved in end organ control at each spinal cord segment (Strack *et al*., 1988, Strack and Loewy, 1990). Viruses provided a useful tool for transneuronal labelling; injected into an end organ the viruses are transported via axons to sympathetic postganglionic neurons where they replicate. Pseudorabies virus (PRV)-injections of the cranial and caudal poles of the kidney resulted in different IML SPNs being labelled in different segments of the thoracic spinal cord, thus illustrating their topographic organization. SPNs within thoracic segment 11 innervated both poles however more SPNs within thoracic segment 11 innervated the cranial pole while a small population within thoracic segment 12 innervated the caudal pole (Huang *et al*., 2002). PRV-injection into brown adipose tissue (BAT) resulted in IML SPNs labelled in thoracic level 4 and 5 (Cano *et al*., 2003). PRV injections in the ventricular myocardium resulted in bilaterally labelled IML SPNs in thoracic segment 1-7 and 8-11. Right atrial injections resulted in contralateral labelling, these SPNs are most likely to contribute to the chronotropic effects of sympathetic activation (Ter Horst *et al*., 1996). PRV injection of the kidneys resulted in labelling of SPNs in thoracic segment 6 to lumbar segment 1, with the highest number of labelled SPNs being located in thoracic segment 10 (Schramm *et al*., 1993). Most cells labelled were located in the IML, dual PRV infections of the left and right kidney confirmed lateralization of the spinal cord outputs with ipsilateral SPNs being labelled (Cano *et al*., 2004). Super cervical ganglion (SCG) injections resulted in SPNs labelled in the cervical segment 8 to thoracic segment 5, the majority were labelled in thoracic segment 1 to segment 3 (Tang *et al*., 1995b) (Figure 1.6).

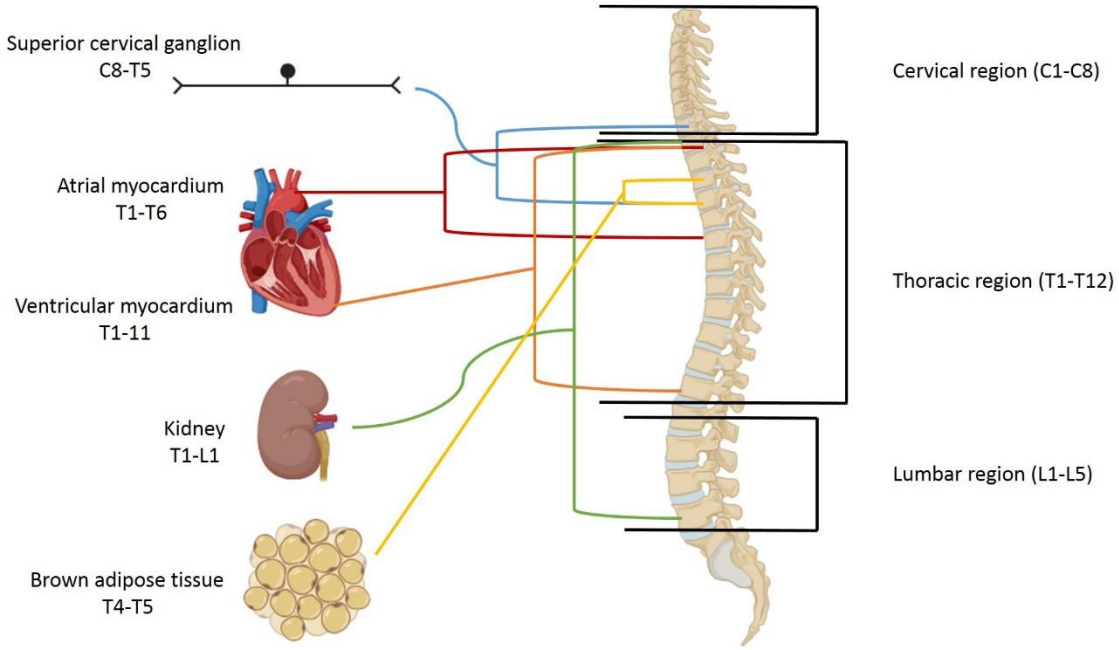

Figure 1.6 Spinal cord regions and innervation of target organs
Summary diagram of transneuronal tracing using pseudorabies virus (PRV) to label SPNs at different spinal cord segments by injecting target organs. PRV injections at each target organ labels SPNs within the spinal cord regions identified in the left column.

1.11 Neurochemistry of SPNs

The neurochemical profiles of SPNs has been studied through retrograde tracing and immunohistochemistry (IHC) using specific markers (Table 1.3). All SPNs are cholinergic and the coexpression of specific markers has been used to elucidate what structures they project to and their function. The majority of SPNs are nicotinamide adenine dinucleotide phosphate (NADPH) diaphorase positive indicating that they synthesize nitric oxide; most of the NADPH diaphorase positive SPNs were located in the more lateral regions of the IML (Anderson, 1992, Deuchars and Lall, 2015). Nitric oxide synthase expression correlates with SPN targets, NOS immunoreactivity paired with retrograde tracing revealed 54% of celiac ganglion-projecting SPN and 98% of adrenal medulla-projecting SPN were NOS immunopositive (Hinrichs and Llewellyn-Smith, 2009). Nitric oxide synthase I (NOSI) and II (NOSII) both produce nitric

oxide however their distribution within IML SPNs differs. NOSI was found primarily in the perikaryon, proximal dendrites or axons. NOSII was found on the circumference of SPNs (Poon *et al*., 2016). RL-29 is a carbohydrate-binding protein involved in immune response in neurons. RL-29 immunoreactivity was observed in IML SPNs in the thoracic and lumbosacral regions of spinal cord of the rat (Park and Chung, 1999).

Calcium-binding proteins involved in maintaining calcium levels in neurons are commonly used to identify specific neuronal subtypes. Retrograde tracing using Fast Blue, cholera toxin B and Fluorogold injected into the submandibular, thyroid and lacrimal gland, paired with antibody labelling for calretinin found that calretinin is expressed in SPNs that synapse on the secretomotor postganglionic neurons which innervate the submandibular salivary gland. Calretinin is not expressed by SPNs innervating postganglionic neurons that influence the lacrimal gland, thyroid gland, anterior chamber of the eye and skin of the forehead (Grkovic and Anderson, 1995). Pairing antibody labelling for calbindin with retrograde tracing using Fast Blue and Fluorogold injected into the superior cervical and stellate ganglion found that calbindin immunoreactivity was observed in a subset of SPNs that project to the stellate ganglion and SPNs in the rostral and caudal regions of spinal cord (Grkovic and Anderson, 1997). Grkovic *et al*. found SPNs synapsing on the postganglionic neurons innervating the iris of the eye are calcitonin-gene related peptide (CGRP) immunopositive. This was achieved via injection of Fast Blue into the anterior chamber of the eye paired with antibody labelling in the spinal cord for CGRP (Grkovic *et al*., 1999).

Signal transduction proteins are differentially expressed in neurons and can be used to identify neuronal subsets. Extracellular signal-related kinases or cyclic

AMP response element binding protein (CREB) becomes phosphorylated upon activation thus subsets of activated neurons can be identified. Springell *et al*. used antibodies against phosphorylated ERK 1/2 (p-ERK) to label SPNs within the thoracic spinal cord. P-ERK-immunopositive SPNs were observed throughout the IML, with a high proportion at rostral and caudal levels. 64% of adrenal SPNs were p-ERK positive. The high immunoreactivity of p-ERK suggests a large proportion of SPNs are tonically active (Springell *et al.*, 2005).

Neuropeptides are peptides that neurons use to communicate with one another and have diverse functions, influencing signalling in the brain and body. The presence of cocaine and amphetamine-regulated transcript (CART) was observed in SPNs. IHC and retrograde tracing experiments using cholera toxin B injected into the adrenal medulla, coeliac ganglion, right superior cervical ganglion and left pelvic ganglion conducted in rat tissue found that CART was present in SPNs targeting vasoconstrictor and cardiac-projecting postganglionic neurons. CART-immunopositive SPNs were activated in rats under hypoxic conditions, furthermore, SPNs innervating noradrenergic chromaffin cells were also CART positive (Fenwick *et al*., 2006b, Gonsalvez *et al*., 2010b). CART immunoreactivity could therefore provide a method to identify SPNs involved in cardiovascular functions, although this has not been confirmed in other species.

The neurochemical profiles of SPNs at different levels of the spinal cord have been demonstrated by previous summarized in Table 1.3. These studies have found SPNs with particular neurochemical profiles project to different ganglia potentially being involved in different functions. NOS1 and lectin RL-29 labelled SPNs located in the thoracic spinal cord segment (Park and Chung, 1999; Hinrichs and Llewellyn-Smith, 2009; Poon *et al.*, 2016). Furthermore, lectin RL-29 labelling of thoracic spinal cord SPNs has not been characterized since the

initial study therefore further work is required to describe the labelling efficiency of SPNs with antibodies against this protein. Experiments discussed later used antibodies against these proteins to label thoracic segment SPNs.

Table 1.2 Neurochemistry profile of SPNs

Protein	Type of SPN	Spinal cord segments	Projects to	Reference
Nicotinamide adenine dinucleotide phosphate diasphorase (NADPH)	IML and IPPe SPNs	Cervical segment 8 to Lumbar segment 2	Unknown	Anderson, 1992
Nitric oxide synthase (NOS1)	IML and IPPe SPNs	Thoracic segment 1 to Lumbar segment 2	Adrenal medulla, superior cervical, coeliac, major pelvic ganglia	Hinrichs and Llewellyn-Smith, 2009
Lectin RL-29	IML SPNs	Thoracic segment	Dorsal gray commissure	Park and Chung, 1999
Calretinin	IML SPNs	Thoracic segment 1 to 3	Superior cervical, dorsal root, stellate ganglia, secremotor	Grkovic and Anderson, 1995
Calbindin	IML SPNs	Thoracic segment 1 to Lumbar segment 2	Superior cervical and stellate ganglia	Grkovic and Anderson, 1997
Calcitonin	-	Upper thoracic segment	Postganglionic neurons innervating the iris	Grkovic *et al*. 1999
Extra signal-related kinases	IML SPNs	Cervical segment 8 to Lumbar segment 3	Adrenal gland, adrenergic chromaffin cells	Springell *et al*. 2005
Cocaine and amphetamine-regulated transcript (CART)	IML, IPPe and IC SPNs	Thoracic segment 1 to Lumbar segment 2	Coeliac, major pelvic, superior cervical ganglia and adrenal medulla	Fenwick *et al*. 2006, Gonsalvez *et al*. 2010

1.12 Central Nervous System Influences on SPN activity

SPNs are the final point where the CNS can influence sympathetic nervous activity. This influence is seen in the sympathetic baroreflex, which is a feedback loop involving mechanoreceptors in the arterial wall, the nucleus tractus solitarus (NTS), caudal ventrolateral medulla (CVLM) and rostral ventrolateral medulla (RVLM). The function of this feedback loop is to reduce short term fluctuations in BP but also to enable BP to rise to certain levels

during activities such as exercise without the loss of reflex sensitivity (Pilowsky and Goodchild, 2002; Schreihofer and Guyenet, 2002). The loop commences with an increase in BP detected by baroreceptors within the arterial wall. The baroreceptors located within the carotid sinus and aortic arch are stimulated by the distension in the artery wall due to high BP. The carotid sinus baroreceptor axons travel within the glossopharyngeal nerve while the aortic arch baroreceptor travel via the vagus nerve contacting NTS neurons. NTS neurons send glutamatergic projections to the CVLM which in turn excite GABAergic neurons which project to the RVLM. This resultantly inhibits glutamatergic input from presympathetic RVLM neurons to SPNs thus halting SPN input to postganglionic neurons which project to the heart and blood vessels (Schreihofer and Guyenet, 2002; Andresen *et al.*, 2006).

1.13 Rostral ventrolateral medulla

RVLM neurons involved in BP control innervate SPNs monosynaptically (Blessing and Nalivaiko, 2000, Guyenet and Stornetta, 2004, Guyenet, 2006) (Figure 1.7) and provide tonic excitatory input to barosensitive SPNs. Many lines of evidence converge to show that the RVLM influences SPNs and ultimately vasomotor tone (Guyenet, 2006). For example, key experiments include destruction of RVLM C1 cells to cause BP reduction due to removal of tonic excitatory input to SPNs (Dean *et al*., 1992, Dampney *et al*., 2005). Recent direct evidence has come from optogenetic studies utilising expression of a light-activated ion channel, channelrhodopsin-2 (ChR2), within RVLM cells via lentiviral transduction. Activation of ChR2-expressing cells is achieved by exposure to light (488nm). Photostimulation of ChR2-transduced RVLM neurons caused an increase in SNA and BP (Abbott *et al*., 2009).

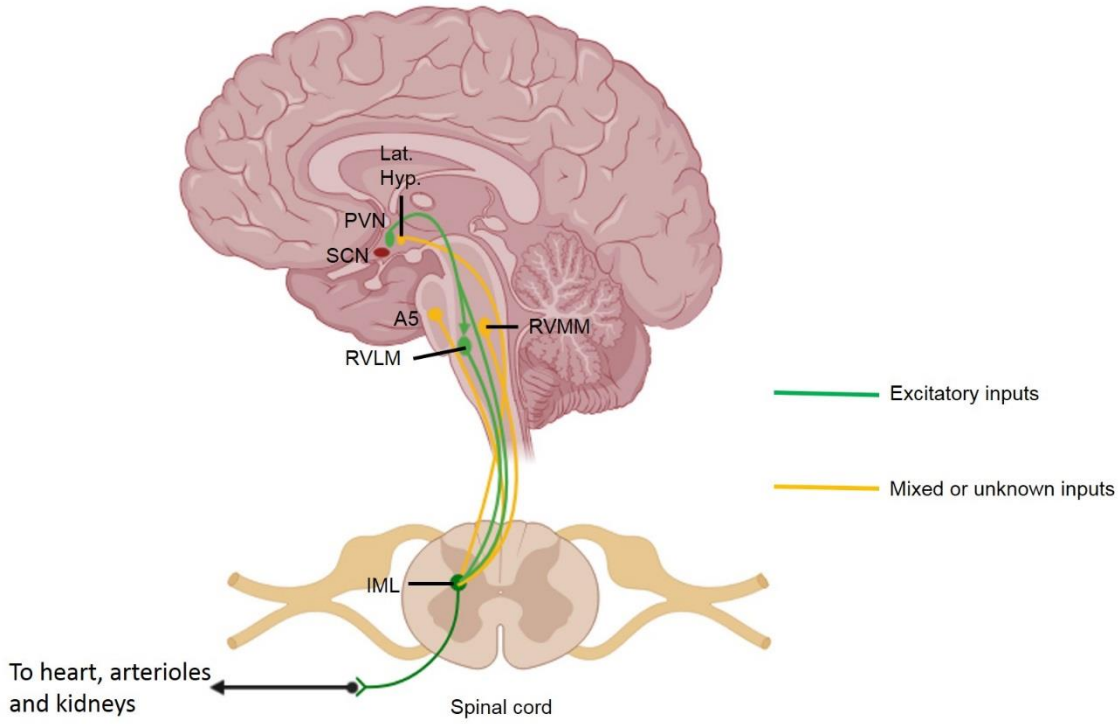

Figure 1.7 SCN-SPN pathway
SPNs receive monosynaptic inputs from overlapping subsets of neurons located in the regions indicated. Excitatory inputs to the SPNs originate from the paraventricular nucleus of the hypothalamus and rostral ventrolateral medulla. Mixed or unknown inputs to SPNs originate from the lateral hypothalamus, A5 region and rostral ventromedial medulla, RVMM. Adapted from (Guyenet, 2006; Pyner, 2009)

1.14 A5 influence on SPNs

The influence of the A5 region of the pons on SPNs is not very well studied. An anterograde tracing study, using tritiated amino acids, found dense projections from the A5 noradrenergic neurons to the spinal cord in rat tissue. Double labelling experiments using HRP injections into the spinal cord (cervical to sacral regions) and monoamine oxidase assays found that A5 neurons project to the IML. Further double labelling experiments combined HRP injections into the spinal cord at thoracic segment 1 and 2 and catecholamine fluorescence to label A5 neurons and their terminals in the IML (Loewy *et al*., 1979). A5 neurons displayed barosensitivity as most were inhibited by increases in BP suggesting that they play an excitatory role specifically on splanchnic and renal nerve

sympathetic activity (Guyenet, 1984, Guyenet and Byrum, 1985, Huangfu *et al*., 1991, Kanbar *et al*., 2011). The discharge rate of A5 neurons was reduced when mean arterial BP was increased (Guyenet, 1984). In a similar experiment, norepinephrine-induced elevation of arterial pressure silenced a majority of A5 neurons (Guyenet and Byrum, 1985). In addition to being inhibited by raising arterial pressure, a small population of A5 neurons are also inhibited by stimulation of the aortic depressor nerve. The researchers concluded that a population of A5 neurons have a vasomotor sympathoexcitatory function (Huangfu *et al*., 1991). In contrast, induced hypotension using an infusion of sodium nitroprusside resulted in an activation, as indicated by c-fos expression, of A5 neurons. Some A5 neurons were found to project to the IML in the lumbar region of the spinal cord (Li and Dampney, 1994, Polson *et al*., 2002, Dampney *et al*., 2003). Selective activation of A5 noradrenergic neurons using optogenetics revealed a greater increase in renal nerve activation as opposed to lumbar sympathetic chain which suggests a function-specific activation of sympathetic outflow; this study also found bulbospinal A5 neurons respond to peripheral chemoreceptor stimulation suggesting A5 neurons influence sympathetic responses to hypoxia (Kanbar *et al*., 2011).

1.15 The paraventricular nucleus of the hypothalamus

The PVN is one of the key regions in the hypothalamus for circulatory control. The sympathetic outflow influencing cardiovascular parameters is controlled by PVN neurons located in the parvocellular region of the nucleus, which innervate the NTS, RVLM and spinal cord, including direct innervation of SPNs (Coote *et al.*, 1998; Motawei *et al.*, 1999; Dampney *et al.*, 2005). In terms of neurochemistry, PVN autonomic neurons use a combination of glutamate and peptides such as vasopressin, oxytocin and corticotropin-releasing hormone

(CRH) as neurotransmitters to influence IML SPN activity (Coote, 2005, Benarroch, 2005, Stocker *et al*., 2006). Retrograde tracing revealed populations of PVN neurons which are immunoreactive to arginine vasopressin, oxytocin and met-enkephalin and project directly to the spinal cord and are thought to influence autonomic function (Sawchenko and Swanson, 1982; Cechetto and Saper, 1988; Motawei *et al.*, 1999; Pyner, 2009). PVN neurons project to the upper thoracic spinal cord to SPNs, predominantly to SPNs located in the IML and Ilf (Hosoya *et al*., 1991, Motawei *et al*., 1999). A combination of anterograde and retrograde tracing found that PVN axons terminated in close apposition to retrograde-labelled IML SPNs that projected to either the stellate ganglion or superior cervical ganglion. This study further supports the notion that PVN activity may directly influence cardiac-related SNA (Ranson *et al*., 1998).

An indirect influence of PVN on SPNs is also possible – PVN axons within the RVLM closely appose spinally projecting neurons (Pyner and Coote, 1999) and stimulation of the PVN results in excitation of RVLM vasomotor neurons (Motawei *et al*., 1999). There are three known possible descending PVN-sympathetic pathways: PVN neurons that project directly to the spinal cord, PVN neurons that project to RVLM neurons that then project to the spinal cord or PVN neurons that project to both RVLM neurons and spinal cord (Pyner and Coote, 1999, 2000). These pathways provide the means by which the PVN can influence cardiovascular functions or sympathovasomotor function.

The PVN also has connections with another brain area associated with influencing cardiac sympathetic outflow, the NTS (Guyenet, 2006; Pyner, 2009). Terminals labelled via anterograde tracing from the NTS were shown to appose PVN-GABA interneurons, nNOS-containing neurons and presympathetic

neurons (Affleck *et al*, 2012). It was proposed that this circuitry could contribute to plasma volume signalling from mechanoreceptors located at the venous atrial junction of the heart. Mechanoreceptor stimulation causes a reflex inhibition of cardiac sympathetic activity. The NTS axons projecting directly to presympathetic neurons could serve as the excitatory arm of the reflex while the NTS axons projecting to GABA neurons or nNOS-containing neurons may be the inhibitory arm (Affleck *et al.*, 2012).

1.16 Is the PVN the link between the SCN and SPNs?

Since the SCN does not connect directly to SPNs, the PVN may mediate SCN signals to SPNs. Indeed, the SCN has direct inputs to the sympathetic pre-autonomic neurons in the PVN, as determined by immunofluorescence using antibodies against vasopressin intestinal peptide (VIP) and retrograde tracing studies using HRP or cholera toxin B injections into the spinal cord at thoracic segment 1 or 2 in rat models (Saper *et al*., 1976, Teclemariam-Mesbah *et al*., 1997, Vrang *et al*., 1997, Cui *et al*., 2001). Physiologically, this has been shown to influence liver physiology, in particular hepatic gluconeogenesis. Hepatic gluconeogenesis displays rhythmicity with plasma glucose peaking shortly before awakening. Kalsbeek *et al*. demonstrated this daily rise in plasma glucose concentrations is caused by an SCN-mediated relief of inhibitory GABAergic inputs to sympathetic preautonomic neurons in the PVN. In addition, transneuronal labelling from the liver in rats subject to hepatic vagal denervation, resulted in labelling of neurons in the SCN (Kalsbeek *et al*., 2004). Therefore, the PVN receives direct input from the SCN and is ideally located to mediate SCN influence on the sympathetic nervous system.

1.17 Role of the sympathetic nervous system in peripheral circadian rhythms

The sympathetic nervous system is an important mediator of centrally generated circadian rhythms and may be how the SCN can set the pace of peripheral clocks. Pharmacological sympathectomy targeting noradrenergic neruons in rats resulted in a complete abolishment of circadian HR rhythms (Warren *et al*., 1994). The superior cervical ganglion (SCG) is a key ganglion of the sympathetic nervous system. Removal of this ganglion via ganglionectomy resulted in decreased sympathetic nervous system activity and loss of normal hormonal circadian rhythms. This in turn affected a number of physiological processes, particularly BP rhythmicity (Siaud, 1994, Warren, 1994, Briaud, 2004). Similarly, in the liver, the sympathetic nervous system is required to adjust plasma glucose concentrations. In a phase-shifted light/dark cycle the usual diurnal rhythm in plasma glucose concentrations was not observed in animals with denervated liver whereby nerve bundles connecting to the hepatic artery were severed. Plasma glucose concentrations of experimental animals varied from control animals, peaking at different times during the morning and evening. The researchers argued that the SCN requires input from the sympathetic nervous system to the liver, to elicit diurnal variation in plasma glucose concentrations (Cailotto *et al*., 2005, Cailotto *et al*., 2009). The SCN requires sympathetic innervation to produce diurnal rhythms in systems across the body. SPNs are an important cell type that influence SNA and could potentially act as intermediaries for the SCN master clock connecting to peripheral clocks.

1.18 Could SPNs contain a CLOCK mechanism to control sympathetic function?

Murine studies have shown that Bmal1 is indispensable for diurnal variation in BP and HR. For example, Bmal1 knockout mice loose BP and HR diurnal rhythmicity. This is likely to be influenced by a sympathetic component as evidenced by concurrently altered levels of norepinephrine and epinephrine (See also Table 1.1). However, as this study implemented a global KO model, it was not clear what cell type/CNS region imparted the disrupted cardiovascular diurnal rhythm (Curtis *et al.*, 2007).

Similarly, global KO of the gap junction protein connexin 36 (Cx36) revealed disruption of circadian BP and HR control in mice (Lall *et al*., 2017). This could have been due to the influence on SPN activity, as Cx36 mediates functionally important gap junction connections between SPNs. This is evidenced by the observation that IML SPNs displayed reduced spikelet activity in Cx36 KO mice, indicative of reduced gap junctions between neurons. Cx36 deletion resulted in disrupted sympathetic outflow which in turn affected HR and BP. However, since the SCN also expresses Cx36 any disruption in circadian rhythm in this study could also have a contribution from this nucleus (Deuchars and Lall, 2015, Lall *et al*., 2017).

Evidence of a spinal cord clock was demonstrated by rhythmic expression of clock genes Bmal1, Clock, Per1/2, Cry1 and Rev-erbα in lumbar segments 4 and 5 of rat spinal cords using qPCR. Interestingly the diurnal rhythm of clock genes and circadian hormone plasma corticosterone were disrupted by contusion injury at level 8 of the thoracic spinal cord, confirming the presence of a functioning molecular clock (Gaudet *et al*., 2018). However, which spinal cells

expressed this clock was not tested as gene expression was analysed from whole cord segments.

The existence of molecular clock genes in peripheral tissues suggests these tissue may have the ability to regulate their own clock thereby eliminating the need for SPNs to act as an intermediary. Studies using sympathectomies discussed earlier have demonstrated diurnal rhythms of physiological activities require sympathetic input to maintain rhythmicity. Chemical or surgical removal of sympathetic efferent projections to the heart and liver resulted in loss of diurnal rhythms in blood pressure and glucose production (Briaud, Zhang and Sannajust, 2004; Cailotto *et al.*, 2009). The SCN was intact in these preparations however the removal of sympathetic input to these organs resulted in the loss of regular diurnal rhythms suggesting the SNS is required. The presence of clock gene mRNA was demonstrated in whole thoracic and lumbar spinal cord segments however the specific cell type which expressed clock genes was not identified. SPNs are a prospective candidate for possessing a peripheral clock as these cells connect to a number of end organs and thus could drive diurnal rhythms in these locations. The SNS could act as an intermediary integrating diurnal rhythm information from the SCN causing clock gene/protein rhythm changes in local spinal cord peripheral clocks, SPNs, which in turn could drive peripheral clocks in end organs such as the heart and liver affecting physiological rhythms.

1.19 Hypothesis and Aims

The sympathetic nervous system maintains and influences circadian rhythms of physiology, observed in many systems including the cardiovascular system. However, the exact mechanisms by which the sympathetic nervous system

does this are unknown. Sympathectomy studies have demonstrated that the circadian rhythms of physiological processes such as BP require input from the sympathetic nervous system to maintain rhythmicity. SPNs play a critical role in determining sympathetic nervous system activity. It is therefore important to understand what influences and controls SPN activity to ultimately elicit diurnal rhythms in target tissues and organs. This project aims to determine if a molecular clock is present in SPNs and to develop a gene expression profile of this cell type.

The first aim is to label SPNs specifically in an effort to separate the cells from other cells that compose spinal cord tissue. The first aim will use immunohistochemistry (IHC) to label SPNs using candidate markers. The second aim is to characterize diurnal rhythms of gene expression in SPNs, using quantitative polymerase chain reaction (qPCR) to examine clock gene mRNA. Immunofluorescence paired with imaging to observe potential diurnal rhythms of clock proteins in SPNs will also be performed. The third aim is to develop gene expression profiles of SPNs using single cell RNA-sequencing (scRNA-seq) and to examine if circadian expression profiles are evident for any genes.

Chapter 2
General Methods

2.1 Common buffers, solutions and media

Analytical grade reagents were obtained from Alfa Aesar, Sigma Aldrich, ThermoFisher Scientific and VWR International.

2.1.1 General Buffers

Artificial cerebrospinal fluid (aCSF) – 124 mM NaCl, 26 mM $NaHCO_3$, 3 mM KCl, 2 mM $MgSO_4 \cdot 7H_2O$, 2.5 mM NaH_2PO_4, 10 mM glucose, 2 mM $CaCl_2$

Cryoprotectant – Ethylene glycol, glycerol, 0.4M phosphate buffer (PB), distilled water

Internal electrode solution – Nuclease-free water, RNAse inhibitor

Lysis buffer – Nuclease-free water, 0.1% (v/v) Triton X-100, RNAse inhibitor

Phosphate-buffered saline (PBS) – 10 mM Na_2HPO_4, 1.8 mM KH_2PO_4, 137 mM NaCl, 4 mM KCl (pH 7.4)

PBST (0.1% (v/v))- 10 mM Na_2HPO_4, 1.8 mM KH_2PO_4, 137 mM NaCl, 4 mM KCl, 0.1% (v/v) Triton X-100

2.2 Immunohistochemical techniques

2.2.1 Immunohistochemistry overview

Immunohistochemistry is based on the principle of antibodies specifically binding to antigens in tissue and uses the binding of antibodies to antigens as a way to visualise the presence of proteins in a tissue. Initial steps involve using donkey serum to prevent nonspecific binding in tissue of interest. Primary antibodies are raised against the protein of interest. Primary antibodies may be polyclonal or monoclonal meaning they either bind to multiple epitopes of a protein or to one epitope. A secondary antibody paired with a fluorescent visualisation tag is used to visualise the proteins labelled by the primary antibody (Ramos-Vara, 2017). The secondary antibody is raised against the animal that the primary antibody came from (Figure 2.1).

2.2.2 Online screen of potential SPN/MN markers

A strategy was devised to use an anti-ChAT antibody as a primary label to identify SPNs and MNs then use other antibodies to select for SPNs or MNs in order to facilitate easier selection of SPNs using flow cytometry. An online screen of neurotransmitter, enzyme or receptor subunit gene expression in IML SPNs and ventral horn MNs in adult mouse thoracic spinal cord tissue was conducted using online resources, Allen Brain Atlas (http://www.brain-map.org/) and Gensat (http://www.gensat.org/index.html). Proteins expressed exclusively in IML SPNs and MNs located in the ventral horn were selected to test for in IHC experiments using antibodies against the proteins chosen. The Allen Brain Atlas is an online database of *in situ* hybridization (ISH) images whereas Gensat is an atlas of ISH images and fluorescent microscopy images of spinal cord slice images from bacterial artificial chromosome (BAC) transgenic mice. Details on sample preparation and ISH protocol can be found on the Allen Brain Atlas website (http://mousespinal.brain-map.org/docs.html). In the Allen Brain Atlas the ISH images for the intermediolateral cell column (IML) were selected, this brought up a list of all the genes that are expressed in the IML where a large population of SPNs are located, see Figure 2.2. In Gensat, the search annotations function was used and “sympathetic preganglionic neurons” or “motor neurons” were searched for, which brought up a list of genes expressed in those particular cell types, refer to Figure 2.2.

2.2.3 Animals

All experiments were performed under Home Office Licence, in accordance with the regulations of the UK Animals (Scientific Procedures) Act 1986.

Experiments were carried out on C57Bl/6 adult male mice, bred in house.

2.2.4 Fluorogold injections in mice

Adult male C57/BL6 mice (4-6 weeks old, n=20) were injected intraperitoneally (IP) with hydroxystilbamidine using a 0.5 cc syringe (0.05 ml injection, 1% (w/v) in water, 5 mg/kg, Abcam, Cambridge, UK (ab138870, GR119160-9). For diurnal immunohistochemistry experiments, adult male C57/BL6 mice (4-6 weeks old, n=20) were housed in cages in groups of 5. The mice were sacrificed at specific time points: 7:30 AM and 7:30 PM. The 7:30 PM group was housed in a light cabinet with the lights on at 1 AM and lights off at 1 PM.

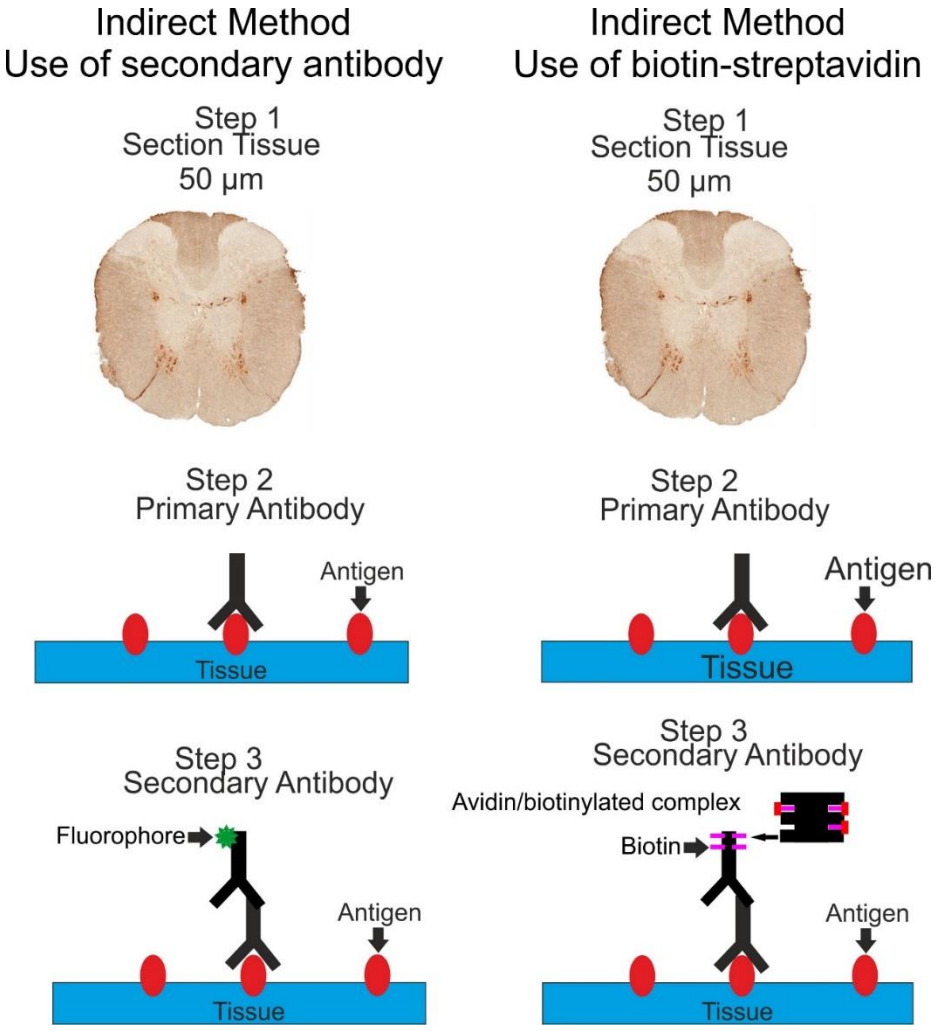

Figure 2.1 Summary of immunohistochemistry protocol
Spinal cord tissue was sectioned at 50 µm. Following initial washes the sections were incubated in primary antibody overnight. The primary antibody was washed off and the sections were incubated in secondary antibody or with biotin then streptavidin conjugated to a fluorophore.

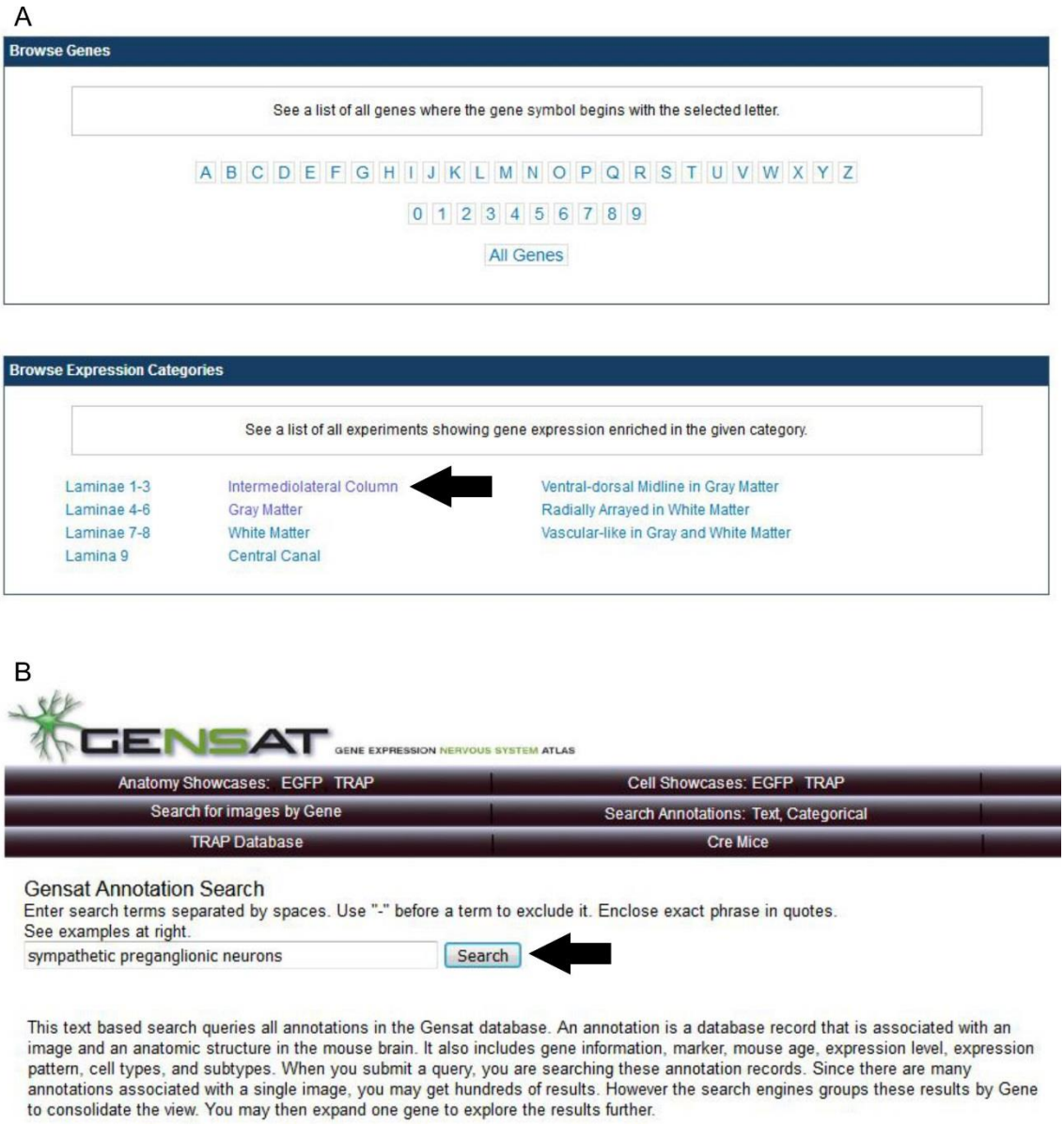

Figure 2.2 Online database search for SPN and MN markers
(A) Allen Brain Atlas gene search page, the arrow indicates the area of spinal cord selected to view gene expression. Following this, the images for individual marker candidates were selected and viewed for selective labelling of either SPNs or MNs (B) Gensat search annotations page, the arrow indicates the search box where criteria were added. Search term: sympathetic preganglionic neuron(s) or motor neuron(s) were used. A similar method as described with Allen Brain Atlas images was applied to Gensat images to identify selective markers for SPNs or MNs.

2.2.5 Transcardial perfusion for tissue fixation

Animals were deeply anaesthetised using IP injection of sodium pentobarbitone (60 mg/kg, Pentoject). Limb withdrawal and blink reflexes were tested to verify full sedation of the animal. An incision was made across the abdomen and then

the thorax was dissected to expose the heart. A blunt needle was inserted into the left ventricle and clipped into place following which the right atrium was cut and the animal was flushed with 0.1 M PB followed by perfusion using 200 mL of 4% (w/v) paraformaldehyde (PFA) (Sigma-Aldrich, S65772-488). The brain and spinal cord were placed in 4% (w/v) PFA overnight at 4ºC following the removal of the meninges.

2.2.6 Tissue preparation

Following post-fixing, both brain and spinal cord were sectioned transversely at 50 µm thickness on a vibrating microtome (Leica, VT1000S) and the free floating slices were collected and placed in PBS or stored in cryoprotectant. Cassettes that contained slices in cryoprotectant were wrapped in parafilm and placed in a -20ºC freezer.

2.2.7 Reagents

PBS tablets (Oxoid), Triton X-100 (BDH Chemicals), Tween20 (FisherScientific), Alexa Fluor ®488 and ®555 (Invitrogen), biotinylated secondary antibodies (Vector Labs), Streptavidin Red (Invitrogen), Vectashield mounting medium, Vectashield mounting medium with 4′,6-diamidino-2-phenylindole (DAPI) (Vector Labs).

2.2.8 Fluorescent immunohistochemistry

Thoracic spinal cord sections underwent three 10 minute washes in PBS and were incubated with 10% (v/v) donkey serum diluted in PBST for 30 minutes. Following this step, they were incubated in the appropriate primary antibodies diluted in PBST for 12-24 hours at 4 °C. Following three 10 minute washes in PBS, the sections were incubated in secondary antibodies conjugated to Alexa Fluor ®488 or ®555 at 1:1000, or a biotinylated secondary antibody at 1:250

followed by Streptavidin 555; all for approximately two to three hours. Sections were then washed in PBS, air-dried onto glass microscope slides and mounted under a coverslip with Vectashield mounting medium with or without DAPI.

2.2.9 Controls

No primary antibody controls were performed with each antibody used IHC experiments. This control ensures the labelling observed in the tissue is due to the primary antibody and not due to the secondary antibody or auto-fluorescence of the tissue.

No primary antibody controls were used on thoracic spinal cord tissue. Briefly thoracic spinal cord slices were incubated in PBS alone. Following this step, tissue was incubated in secondary antibodies conjugated to Alexa Fluor ®488 or ®555 at 1:1000 for two hours. Sections were then washed in PBS, air-dried on a glass microscope slides and mounted under a coverslip with Vectashield mounting medium with or without DAPI.

Further investigations into the specificity of antibodies were performed by first referring to the manufacturer's website to confirm tests for antibody specificity were performed using western blot which indicated the antibody forms a band at the molecular weight of the protein of interest. Additionally primary research literature using the antibody of interest was used to confirm antibody specificity by examining for use of antibody in a western blot experiment or lack of antibody labelling in IHC experiment conducted on tissue from a knock out animal which has the gene coding for the protein knocked out.

2.2.10 Microscopy and image capture

Tissue sections were visualised and captured using a confocal microscope (Zeiss LSM 700 Confocal Microscope) and Zeiss LSM Image browser software. High resolution images were captured with the Zeiss LSM 880 Confocal Microscope with Airyscan.

For diurnal immunohistochemistry, a 13 image Z-stack was taken of the IML region of thoracic spinal cord slice using the Zeiss LSM 700 Confocal Microscope. The 13 image Z-stack was summed into a composite image in FIJI Image processing software and then used to analyse relative fluorescent intensity. In FIJI image processing software, a free-form outline was traced around the nuclei of ChAT-positive and clock-protein positive SPNs then a measurement was taken using the measure feature of the software. A background measurement of fluorescent intensity was obtained by tracing a free-form outline in an area of general labelling.

2.2.11 Statistics

The relative intensity of clock protein were obtained by subtracting the background fluorescence intensity from the clock protein intensity. The mean relative intensity of clock protein was calculated and compared between the two time points using GraphPad Prism 7 software. Statistical analyses were performed using GraphPad Prism 7, a Student’s unpaired T-test was used.

2.3 Quantitative real-time polymerase chain reaction (qRT-PCR)

2.3.1 Reagents and equipment

TRI reagent (Zymo research), Direct-zol RNA kit (Zymo research), Turbo DNAse (Thermo fisher scientific), RNA clean and concentrator kit (Zymo research), qScript cDNA supermix (Quanta Biosciences), primer sequence

(Integrated DNA technologies), PowerUp SYBR Green Master Mix (Thermo fisher scientific).

Thermocycler (Bio-rad), Nanodrop 2000 spectrophotometer (Thermo Scientific).

2.3.2 qRT-PCR overview

qRT-PCR provides a number advantages over traditional PCR. qRT-PCR has the reverse transcription step, conversion of RNA into complementary DNA (cDNA), integrated at the start of this process. The quantification of specific, accumulating PCR products during the PCR process is made possible through the use of fluorescent dyes or probes. This aspect of qRT-PCR makes it an attractive alternative to PCR as the PCR product of interest can be tracked throughout the experiment. Sybr Green dye is the most commonly used method, the dye binds to the minor groove of double stranded (ds) DNA, so that the fluorescence reflects increasing product (Figure 2.3) (Bartlett and Stirling, 2003).

2.3.3 Primer design

Sequences of genes of interest were obtained from online genome browser, Ensembl (Frankish et al., 2017). Primers were designed using Primer3 software (Untergasser et al., 2012). Primers were designed with the following parameters: melting temperature of 60^{o}C, size range of 60-150 base pairs and a GC content of 50%. Primer sequence specificity was confirmed using BLAST analysis (Ye et al., 2012). Their properties were confirmed using the Integrated DNA technologies OligoAnalyzer tool (Owczarzy et al., 2008).

2.3.4 Animals

Adult male C57/BL6 mice (4-6 weeks old, n=10) were housed in cages in groups of 5. The mice were sacrificed at specific time points: 7:30 AM and 7:30

PM. The 7:30 PM group was housed in a light cabinet with the lights on at 1:30 AM and lights off at 1:30 PM. The mice were deeply anaesthetised with an IP injection of sodium pentobarbital as described previously. Limb withdrawal and blink reflexes were tested to verify full sedation of the animal. The mice were perfused transcardially with sucrose aCSF.

2.3.5 Tissue preparation

The brain was dissected out of the skull and was divided into 3 regions: olfactory bulb, anterior part of the brain and brainstem; these regions were stored in Tri reagent until processed further using RNA extraction and purification kits. The spinal cord was dissected out from the body cavity, the cervical, thoracic and lumbar regions were isolated, the meninges were removed and embedded in 3% (w/v) agar (Sigma-Aldrich) and 300 µm sections cut using a microtome (Campden Instruments, Integraslice 7550 PSDS). Sections were kept in aCSF bubbled with oxygen. The IML was separated from the surrounding tissue using a 0.35 mm micropunch (Electron Microscopy Sciences, 69039-03) and transferred via pipette into an RNAse free tube filled with TRI reagent.

2.3.6 RNA extraction and purification

The RNA extraction and purification steps were performed using Zymo research kits each kit contains buffers and specialized Zymo-Spin IC columns designed to remove contaminants and concentrate and purify sample RNA. The sample stored in TRI reagent was transferred to the Zymo Spin IC column where the RNA binds to column and the TRI reagent is removed by centrifuging the column. The column was filled with RNA Prewash and wash buffers which were removed by centrifuging the column. The RNA was eluted from the column using 15 µL of nuclease-free water.

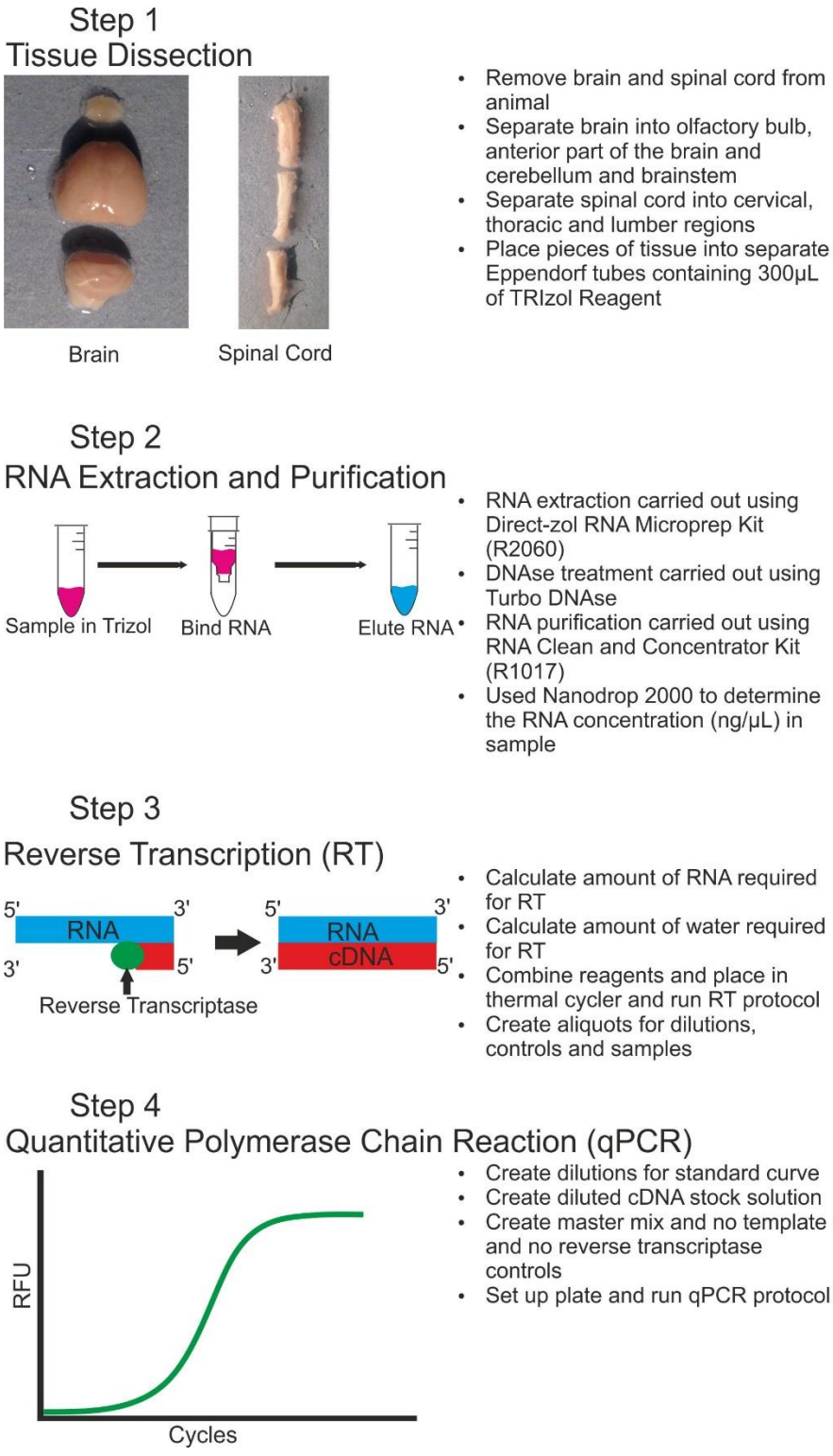

Figure 2.3 Overview of quantitative polymerase chain reaction (qPCR) workflow

Brain and spinal cord tissue were dissected from the animal and separated into different areas of interest. These tissue samples were homogenized in Trizol reagent and subsequent RNA extraction and purification was performed. The RNA was reverse transcribed into cDNA and further purified before being used in qPCR experiments.

2.3.7 DNAse treatment

The Turbo DNase reaction mix (25 µL total) consisted of RNA, nuclease-free water, 10X Turbo DNAse buffer, Turbo DNase. The thermocycler program ran for 30 minutes at 37^{o}C for enzyme activation and the temperature was held at 4^{o}C until the RNA was removed from the thermal cycler.

2.3.8 Nanodrop reading of RNA concentration

A Nanodrop 2000 spectrophotometer was used to determine the RNA concentration of the samples. The machine was first blanked using nuclease-free water and then 1 µL of RNA was used to measure the RNA concentration and quality. The Nanodrop also provides readings for the 260/230 ratio which indicates the quality of nucleic acid and 260/280 ratio which indicates whether there is protein contamination in the sample.

2.3.9 Reverse transcription

1 µg of RNA was used in a reverse transcription reaction to produce cDNA for qPCR. The RT reaction mix (20 µL total) consisted of RNA (1 µg), nuclease-free water, qScript reaction mix (5x) and qScript reverse transcriptase. The thermocycler program ran for 1 cycle of primer annealing at 22^{o}C for 5 minutes, 1 cycle of reverse transcription at 42^{o}C for 30 minutes and 1 cycle of enzyme deactivation at 85^{o}C for 5 minutes then the temperature was held at 4^{o}C until the cDNA was removed from the thermal cycler.

2.3.10 qRT-PCR

PCR reactions were carried out in triplicate using 12.5 ng of cDNA per reaction and Power SYBR Green master mix (Applied Biosystems) in 20 µl reactions. PCR product was measured using SYBR Green fluorescence on a CFX connect real time PCR detection system thermal cycler (Bio-Rad). The program

ran for 10 minutes at 95ºC for the initial melt, then 30 seconds at 95ºC for melting and separating the strands, annealing at 60ºC for 30 seconds, extension at 72ºC for 40 seconds followed by a final extension at 72ºC for 5 minutes. The melting, annealing and extension steps were repeated 39 times. The temperature was held 10ºC until samples were removed from the machine. Standard curve and melting point analyses were performed to confirm amplification efficiency and single amplified products, respectively. The delta-delta Ct analysis was used to normalize gene expression to beta actin reference gene expression.

2.3.11 Statistics

GraphPad Prism 7 was used to generate bar plots for genes of interest. Statistical tests were performed in GraphPad, a Mann-Whitney Test was used to test for significance.

2.4 Single cell RNA sequencing (scRNA-seq)

2.4.1 Animals

For the first scRNA-seq experiment, a mix of GAD-positive and wild type C57/BL6 mice (9-13 days old, n=10) were used. The mice were deeply anaesthetised with an IP injection of sodium pentobarbital as described previously. Limb withdrawal and blink reflexes were tested to verify full sedation of the animal. The mice were perfused transcardially with sucrose aCSF.

For the second scRNA-seq experiment, adult male C57/BL6 mice (4-6 weeks old, n=10) were housed in cages in groups of 5. The mice were deeply anaesthetised with an IP injection of sodium pentobarbital as described previously. Limb withdrawal and blink reflexes were tested to verify full sedation of the animal.

2.4.2 Tissue preparation

For the first experiment, the thoracic spinal cord was prepared as described previously (Section 2.3.5). Briefly, the cord was embedded in 3% (w/v) agar and was cut at 300 µm thickness on a microtome. Sections were kept in aCSF bubbled with oxygen. The section was viewed under an Olympus BX50WI microscope using Qcapture imaging software. The IML region was identified based on morphology of the spinal cord and a glass electrode was lowered into the tissue, negative pressure was applied through a syringe to aspirate a single cell. The single cell was expelled into an Eppendorf tube using positive pressure applied through a syringe. The single cell was stored in 0.5-1 µL of nuclease free water. The tube was stored in -80^{o}C freezer until processed.

For the second experiment, the mouse was decapitated, the skin, limbs and surrounding viscera were removed. A body segment of the back of the animal remained the rostral and caudal ends of the segment were cut exposing the spinal cord still within the vertebrae. The spinal cord was then expelled from the body cavity using hydraulic pressure of warm aCSF applied through a syringe at the rostral end of cord. This method provides an efficient and less invasive way to extract the spinal cord from the body cavity. The meninges were removed via the hydraulic process. The spinal cord was then segmented into the cervical, thoracic and lumbar regions and embedded in boats containing optimal cutting temperature (OCT) compound and frozen using dry ice. Frozen OCT boats were stored in -80^{o}C freezer until processed. The OCT block containing the thoracic section of spinal cord was cut at 60 µm using a cryostat (Leica, CM 1850). Sections were mounted on polysine coated slides (Thermo scientific) and stored in -80^{o}C freezer until processed. When attempting single cell or IML aspirations, sections were thawed and washed three times with aCSF. The

section was viewed under a Nikon Eclipse E600FN microscope using Qcapture imaging software. The IML region was identified based on spinal cord morphology and single cell/IML aspirations were carried out as previously described. The single cell was stored in 3.5 µL of lysis buffer. The tube was stored in -80^{o}C freezer until processed.

2.4.3 RNA extraction and cDNA synthesis

The SMART-seq v4 Ultra Low Input RNA kit (Takara Biotech) is a specialized kit designed to extract RNA and produce high quality full length cDNA from minute input RNA amounts. The kit relies on a template switching oligonucleotide which provides a new template for the reverse transcriptase to switch to and continue synthesis thus producing full length cDNA.

RNA from single cell and IML samples was extracted using the SMART-seq v4 Ultra Low Input RNA kit. Reaction buffer and Smart-seq CDS primer II A was added to the sample and the sample was placed in a thermal cycler for 3 minutes at 72^{o}C to allow the primer to anneal to the RNA. Reverse transcription master mix was added to the sample consisting of 5x Ultra Low First Strand buffer, SMART-seq oligonucleotide and SMARTScribe Reverse Transcriptase and the sample was placed in a thermal cycler. The program was as follows: 42^{o}C for 90 minutes, 70^{o}C for 10 minutes followed by a 4^{o}C holding temperature until the sample is removed from the thermal cycler. The sample now contains cDNA (Figure 2.4).

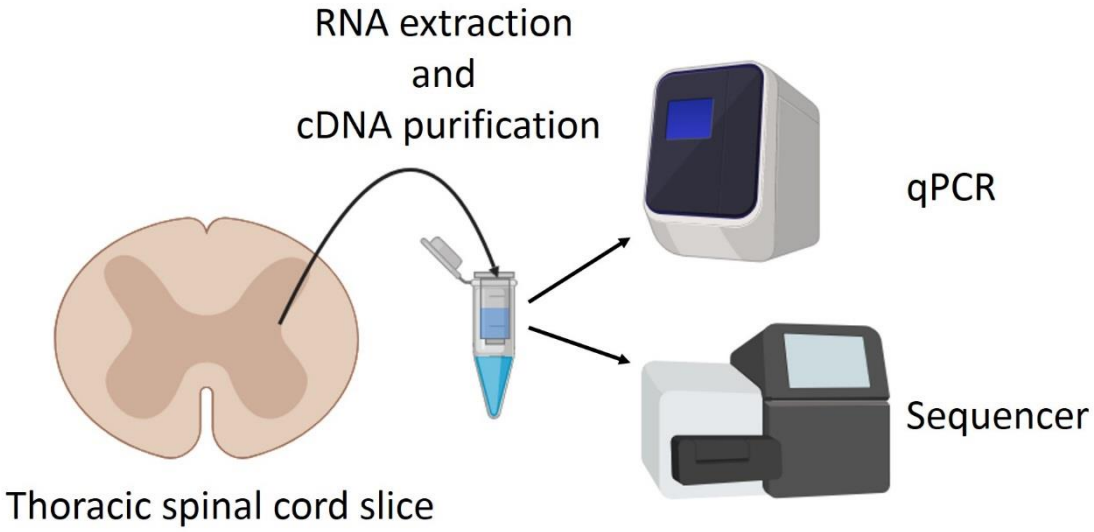

Figure 2.4 Overview of single-cell processing for RNA-seq
Single cell or IML sample were aspirated from IML region and stored in nuclease-free water or lysis buffer. The sample was then processed using a SMART-seq v4 Ultra Low Input RNA kit for sequencing producing cDNA that was used for either qPCR or sequencing.

2.4.4 cDNA amplification

The SMART-seq v4 Ultra Low Input RNA kit has a specialized protocol for long-distance PCR (LD-PCR) in order to amplify the full length cDNA produced in the cDNA synthesis step. The number of repeats for the denaturing, annealing and extension phase in the PCR protocol is determined by the input amount of RNA.

PCR master mix is added to the samples consisting of 2x SeqAmp PCR buffer, PCR primer II A and SeqAMP DNA polymerase. The samples are placed in the thermal cycler to amplify the cDNA within the sample. The number of cycles varies based on the input amount of RNA based on a reference table provided with the SMART-seq v4 RNA kit manual. The program for cDNA amplification is as follows 98^{o}C for 10 seconds, 65^{o}C for 30 seconds, 68^{o}C for 3 minutes. These three steps are repeated either for 8 cycles (IML cDNA samples) or 18 cycles (single cell cDNA samples). The final step is a 10 minute incubation at 72^{o}C. The amplified cDNA samples are held at 4^{o}C until removed from the thermal cycler (Figure 2.5).

2.4.5 Purification of amplified cDNA

Lysis buffer and AMPure XP beads are added to the amplified cDNA samples. The beads are mixed into the solution and bind to the cDNA. The samples are placed on a magnetic rack which causes the beads to pellet. The liquid was discarded and the pellet was washed twice with 80% (v/v) ethanol to remove contaminants. The purified cDNA was eluted from the beads using elution buffer.

2.4.6 Quality control

1 µL of purified cDNA from each sample was used for quality control. The population of base pair fragments making up cDNA were examined using an Agilent 2100 Bioanalyzer. The bioanalyzer uses a chip which has microchannels, each of which has a sieving polymer and fluorescence dye in it. The cDNA are electrophoretically driven by a voltage gradient similar to gel electrophoresis. The molecules are separated by size due to the sieving polymer, data is translated into gel-like images. The fluorescence dye intercalates with the cDNA and a plot of fluorescent intensity versus migration time is produced known as an electropherogram. An upper and lower marker are internal standards in the chip that align the ladder with readings from the sample wells. The upper and lower markers are visualised in the

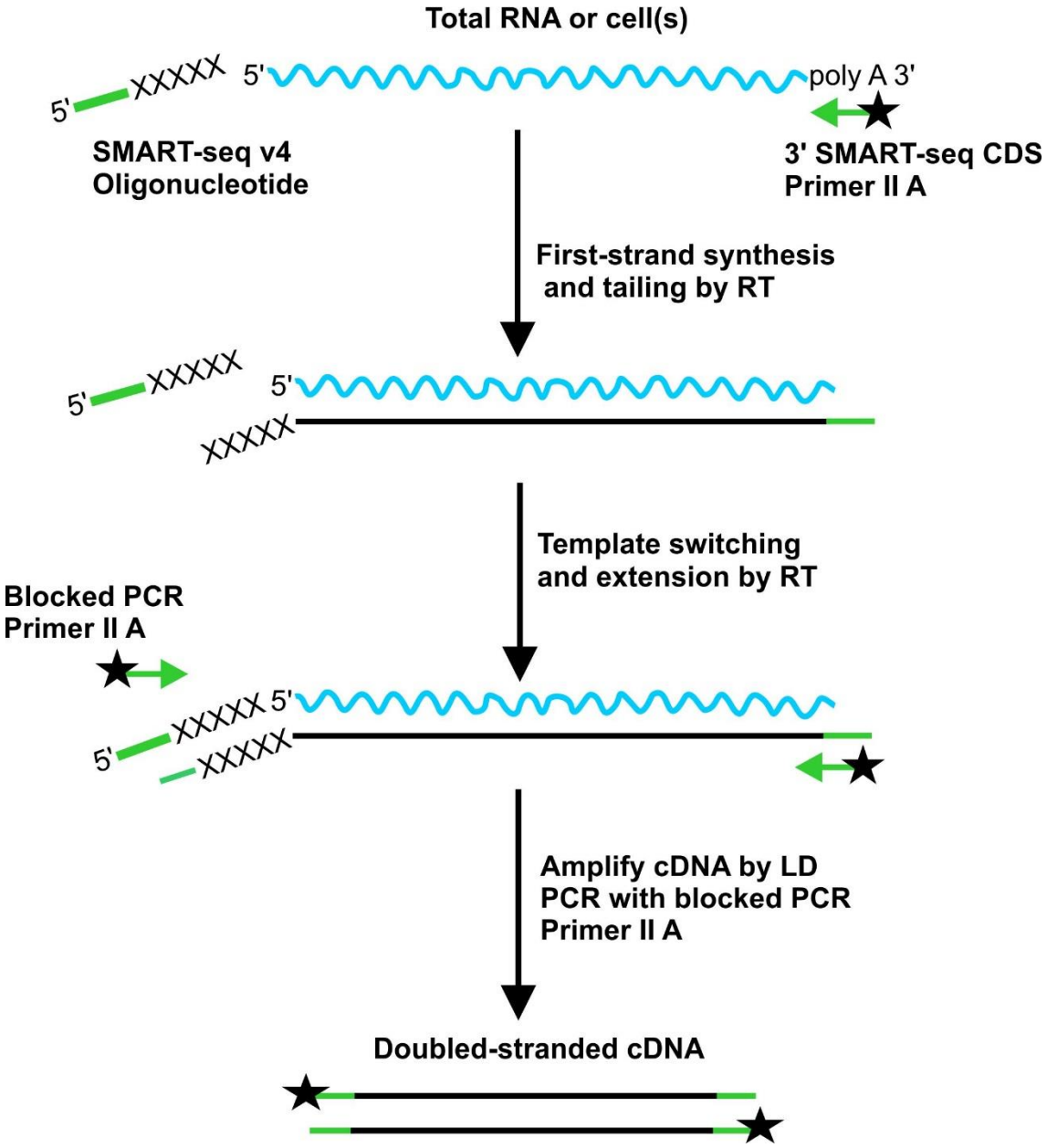

Figure 2.5 Overview of SMART cDNA synthesis
RNA from tissue or single cell is reverse transcribed using the SMART reverse transcriptase, oligonucleotide and primer. The cDNA produced from the first-strand synthesis undergoes PCR amplification and produces full-length double stranded cDNA.

electropherogram and are used to determine cDNA quality. If the sample peaks in the electropherogram were between the lower and upper markers this indicates the sample is of good cDNA quality (Qiu et al., 2012).

A Qubit fluorometer was used to determine the concentration of the cDNA samples, an additional 1 µL of cDNA was combined with Qubit assay dye and a concentration reading was taken using the fluorometer.

2.4.7 Library preparation and RNA sequencing

The Nextera XT DNA Library Preparation kit is designed to produce libraries for sequencing on Illumina platforms. The kit uses an engineered transposon, a DNA sequence, to tag cDNA (tagmentation). Tagmentation is a process that fragments the cDNA and then tags the cDNA with adapter sequences in one step. The sequences are required for PCR amplification and sequencing, the adaptor sequences are used by the sequencing machine to recognize the fragments. Limited cycle PCR uses the adapters to amplify the cDNA fragments. The PCR step also adds index adapter sequences on both ends of the cDNA fragments, which enables indexed sequencing of pooled libraries on Illumina sequencing platforms.

An Illumina Hiseq 3000 instrument was used to sequence the IML and single cell libraries produced from live tissue samples. An Illumina Nextseq 500 instrument was used to sequence the IML and single cell libraries produced from frozen tissue samples. Within the sequencing machine is a flow cell, a glass slide with lanes on the surface of these lanes is a lawn of oligonucleotides that are complementary to the adaptor sequences added to the cDNA fragments in the tagmentation process. The machine has fluorescent probes which are colour coded to the type of nucleotide they bind to. The nucleotides

attach to their complementary base pair on the fragment, the nucleotide-fluorescent probes are excited by a light source and the machine takes a picture and the colour is washed off the probes. This process continues until the whole fragment is sequenced according to the base pair length specified, in this case the live tissue and frozen tissue libraries were sequenced at 150 base pairs, paired-end on each machine respectively. Pair end sequencing refers to sequencing the fragment from both ends, this allows for more accurate read alignment to the reference genome. The sequencing machine provides a quality score for each read based on how confident the machine is that it correctly called a base and stores this information in the output file.

Samples put forward for library preparation were selected based on concentration and the data displayed in the electropherogram. The library was prepared using the Nextera XT DNA library preparation kit. Library quality was analysed using Agilent High Sensitivity D1000 ScreenTape instrument. 2 µL of cDNA was combined with High Sensitivity D1000 sample buffer and run on the ScreenTape instrument alongside standards. The instrument produces a graphical readout with fluorescent intensity on the y axis and size of fragments on the x axis. A good sample put forward for sequencing was indicated by its sample peak being between the upper and lower markers in the readout. The cDNA libraries were then pooled on a single lane in an Illumina Hiseq 3000 and sequenced at 150 base pairs, paired end (Figure 2.6).

2.4.8 RNA sequencing data processing

The output files from sequencing are fastq files, the files are uploaded and analysed using an online platform, Galaxy (Guerler et al., 2018). Galaxy analysis produces FastQC reports which indicate the quality of the reads

produced from sequencing. The quality parameters for the FastQC report were set for a cut-off quality score of 30, this meant that reads that do not have

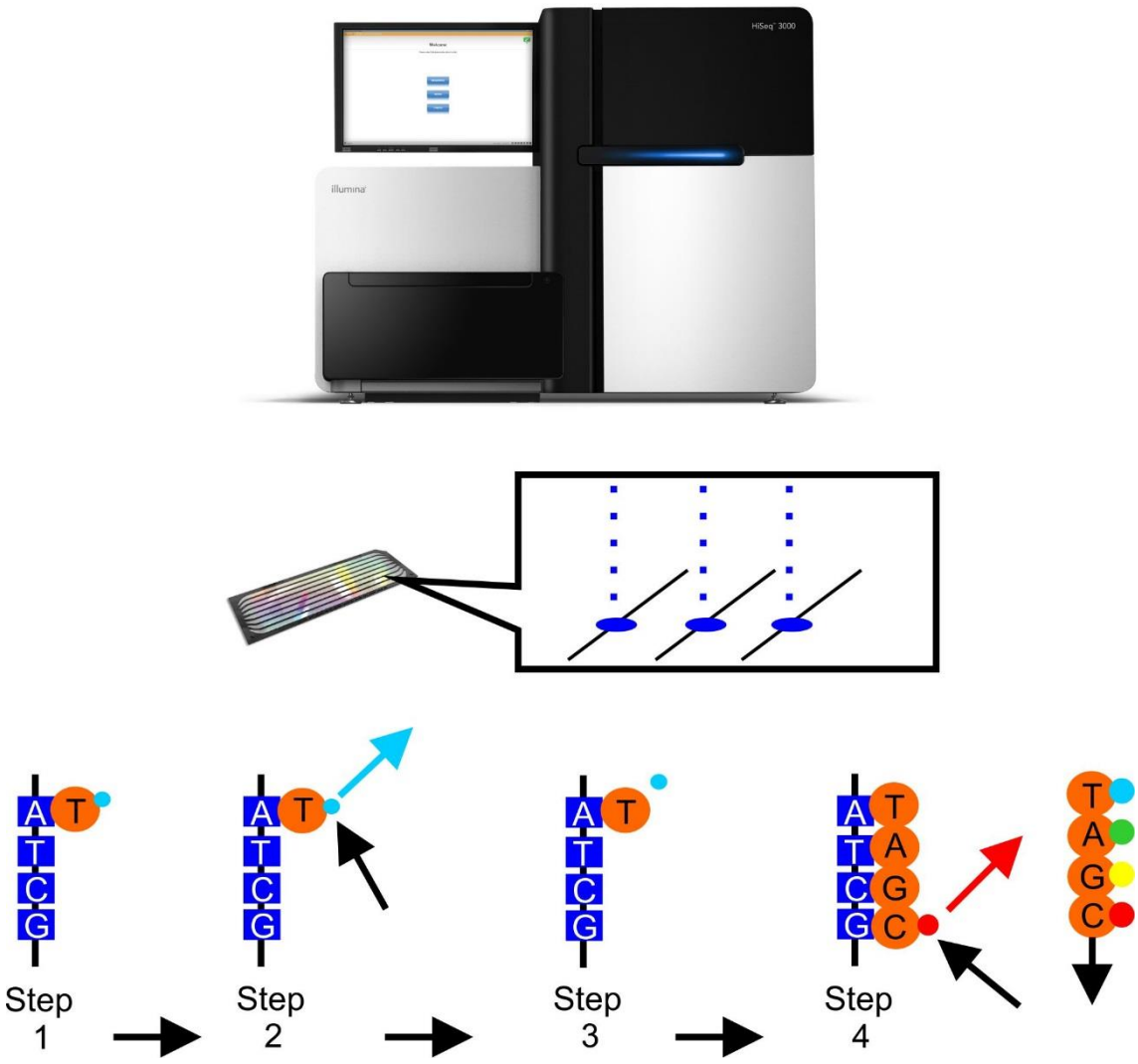

Figure 2.6 Overview of RNA-sequencing
Pictured above is an image of a Hiseq 3000 which was used in these experiments. Second, a flow cell where the cDNA library is pooled, the single strands of cDNA attach themselves to the base of the flow cell and create lawns. Finally, the bases the cDNA are comprised of are identified by the binding of complementary nucleotides that are tagged with a fluorophore.

quality equal to or higher than 30 will be discarded. A quality score of 30 is a standard cut-off and reflects a base-call accuracy of 99.9% with a probability of an incorrect base call being 1 in 1000. FastQC reports provide a quick overview of the sample quality and mark the different sections of the report with either a

green tick indicating the data passes the check or a yellow exclamation mark or red x to signify there is an anomaly or if the data does not pass the quality parameters. The graphs included in the FastQC report are per base sequence quality, per sequence quality scores, per base sequence content, per base GC content, per sequence GC content, per base N content, sequence length distribution, sequence duplication levels and overrepresented sequences. The per base sequence graph depicts the sequencing read length and the quality score for the reads at each read position, the whisker-box representing the reads should be above a quality score of 30 (Figure 2.7). The per sequence quality scores depicts the mean quality score for all the reads for that library, the mean quality score for the reads should peak at a quality score of 30 (Figure 2.8). The per base sequence content depicts the proportion of bases in each read position with percentage on the y axis, ideally these lines should be linear as a good library should have an equal number of each base (Figure 2.9). Per sequence GC content tracks the proportion of GC bases along the length of the reads and should be a straight line. The per sequence GC content depicts the mean GC content across all the reads, ideally the GC content peak for all the reads should fit over the theoretical distribution for the reads indicating normal GC content distribution (Figure 2.10). Per base N content indicates whether there were any uncalled bases in the sample (Figure 2.11). Sequence length distribution indicates whether all the reads are the same length (Figure 2.12). Sequence duplication levels indicates how many reads are not unique in the library (Figure 2.13). Overrepresented sequences is a table that provides a list of reads that are overrepresented in a dataset, provides a count and a percentage for that read and runs the sequence against a list of

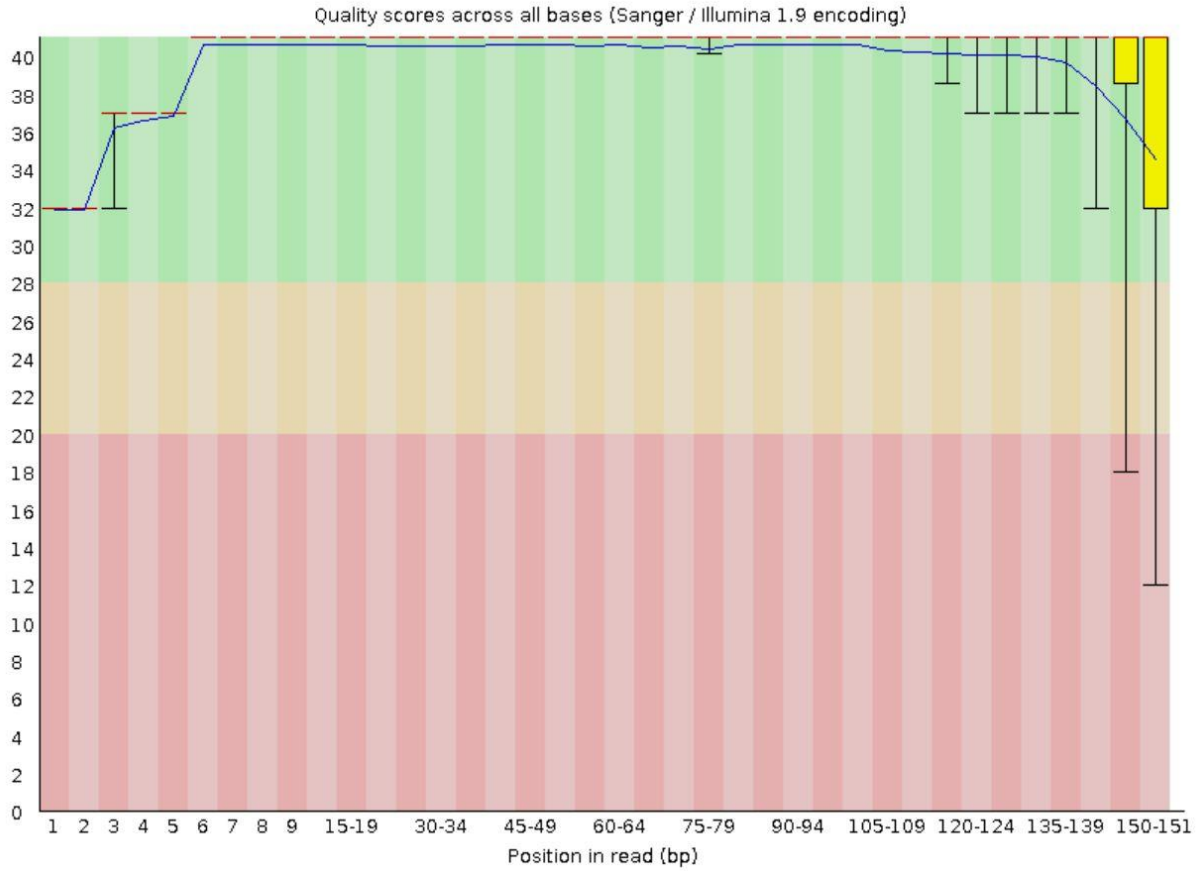

Figure 2.7 FastQC quality report: Per base sequence quality
Per base sequence quality depicts how precise the sequencing instrument calls the correct base at each read position (X-axis). This information is assigned a quality score of from 0-40 (Y-axis) which is used to separate the reads into bins of good, medium and poor quality.

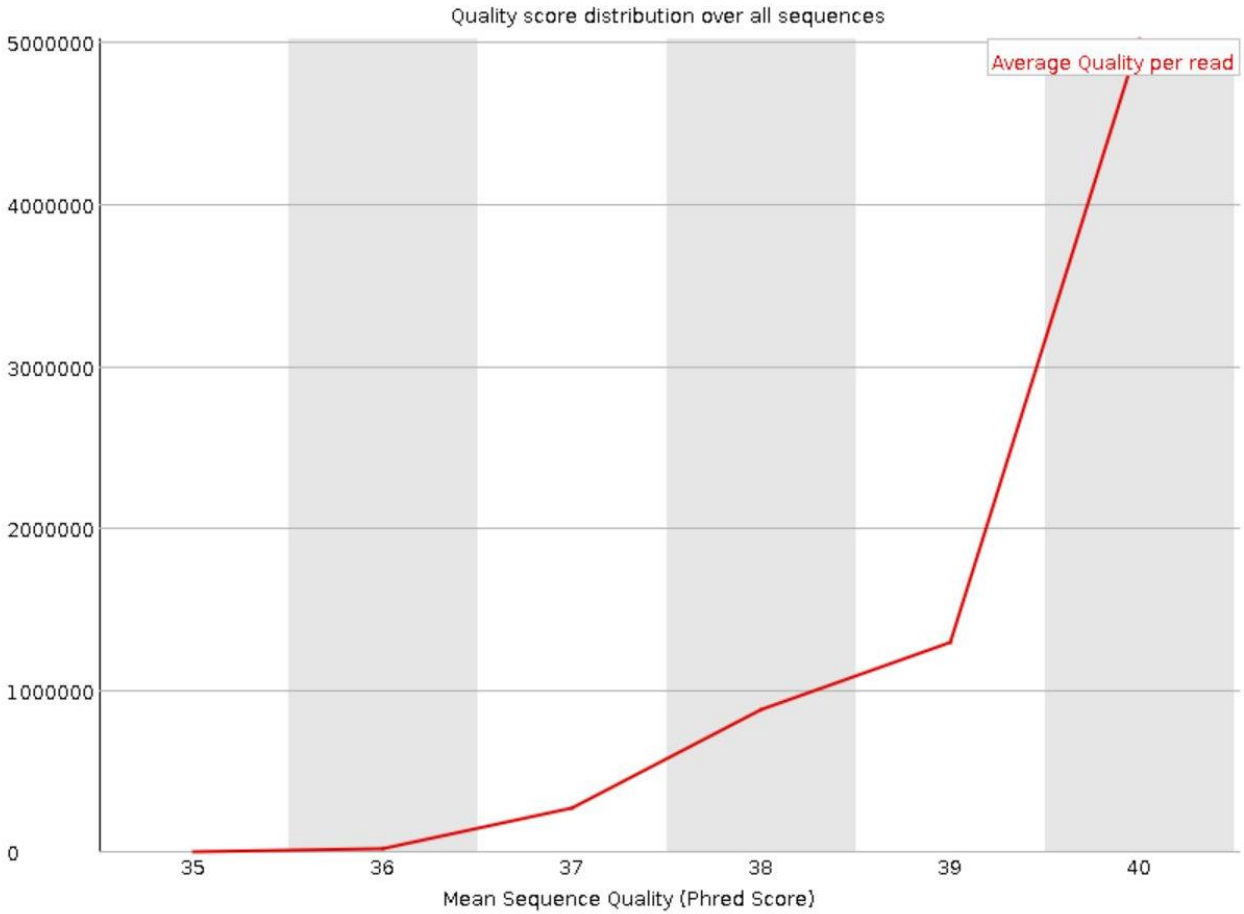

Figure 2.8 FastQC quality report: Per sequence quality scores
Per sequence quality scores depicts the mean read quality score (X-axis) for all reads within a sample library (Y-axis). Ideally mean read quality scores should be within the 30-40 score range as this denotes good quality reads.

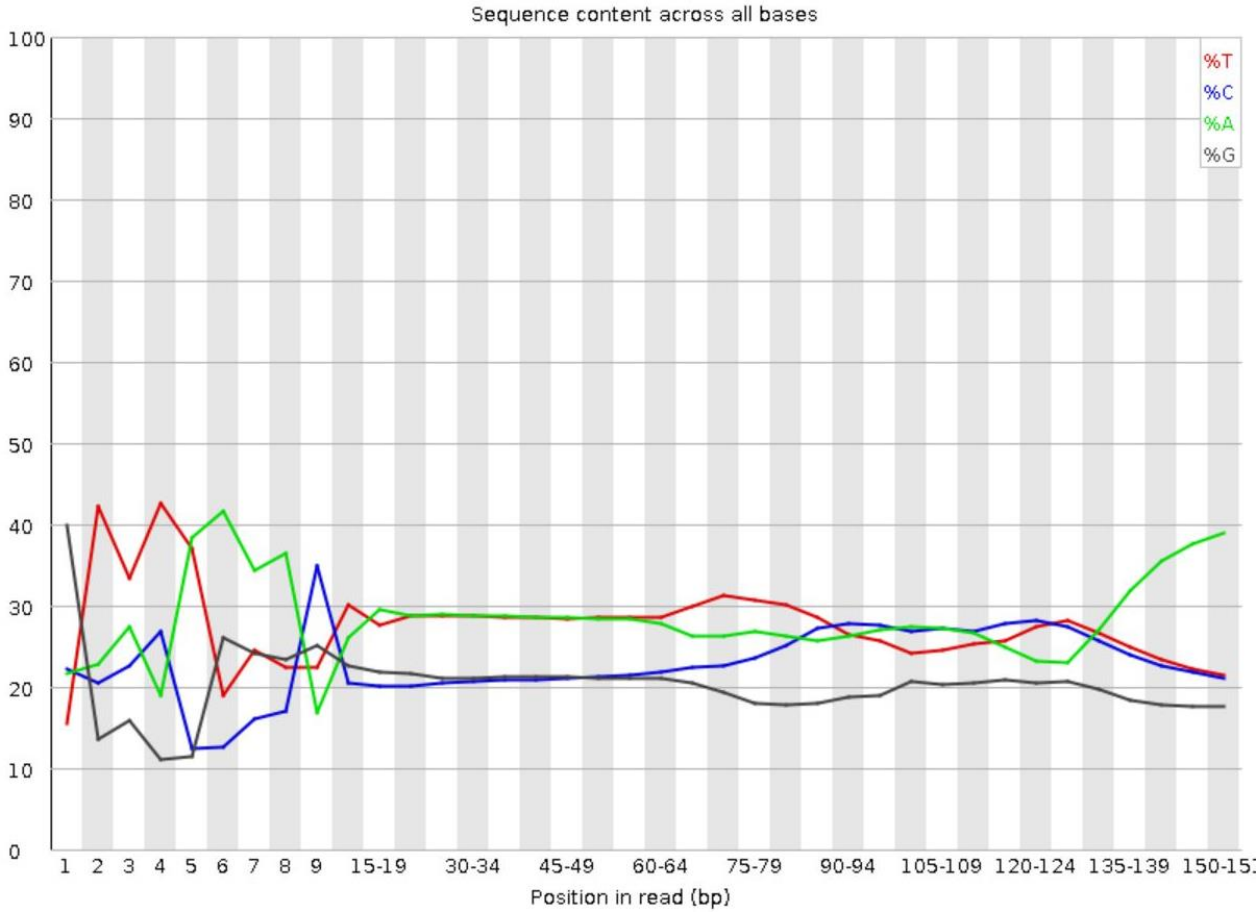

Figure 2.9 FastQC quality report: Per base sequence content
Per base sequence content depicts the percentage of bases (Y-axis) at each read position (X-axis).

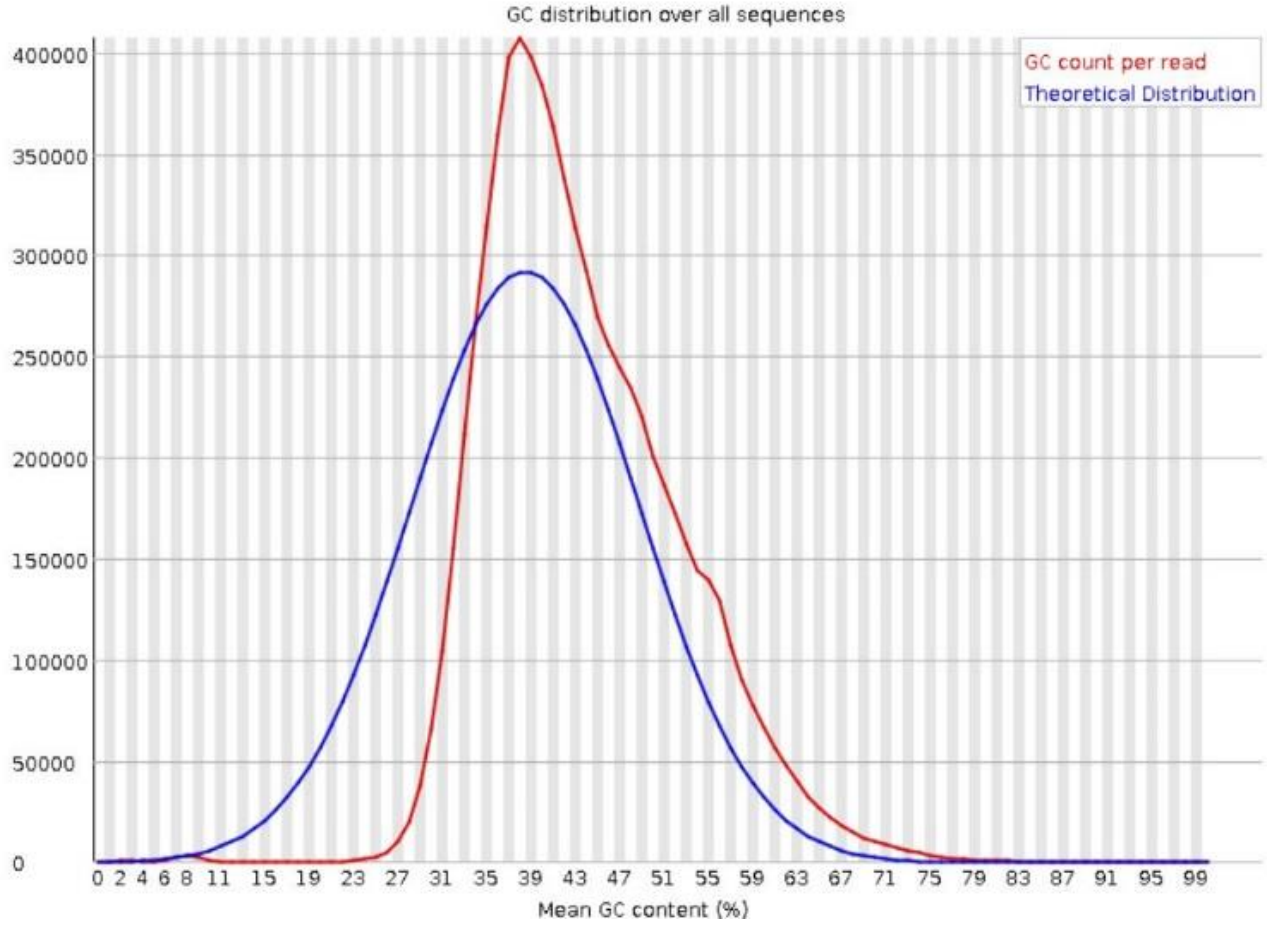

Figure 2.10 FastQC quality report: Per sequence GC content
Per sequence GC content depicts the mean GC content (Y-axis) across the read length (X-axis).

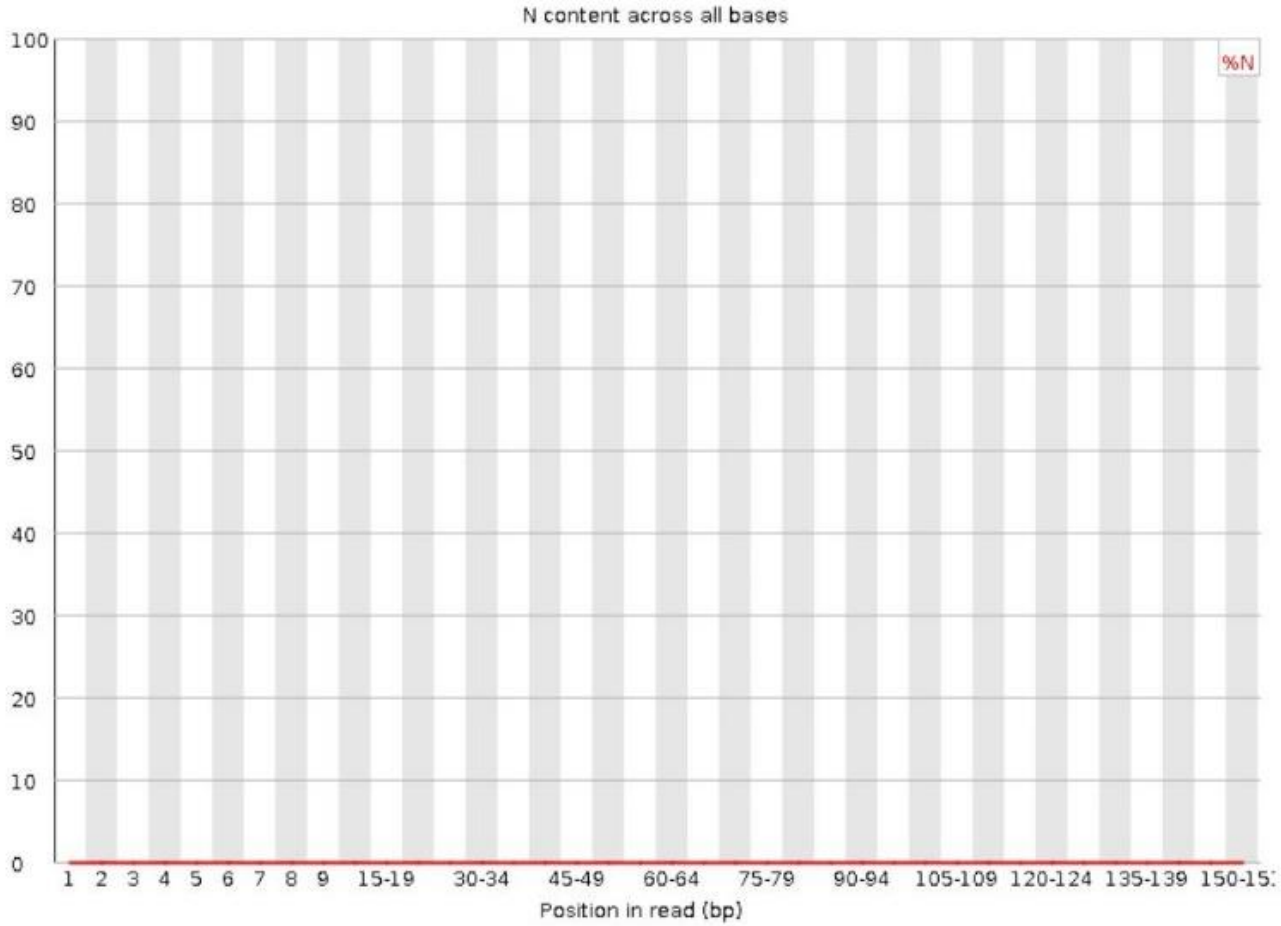

Figure 2.11 FastQC quality report: Per base N content
Per base N content indicates whether there were any bases (Y-axis) that were not identified by the sequencer within the sample along the read length (X-axis).

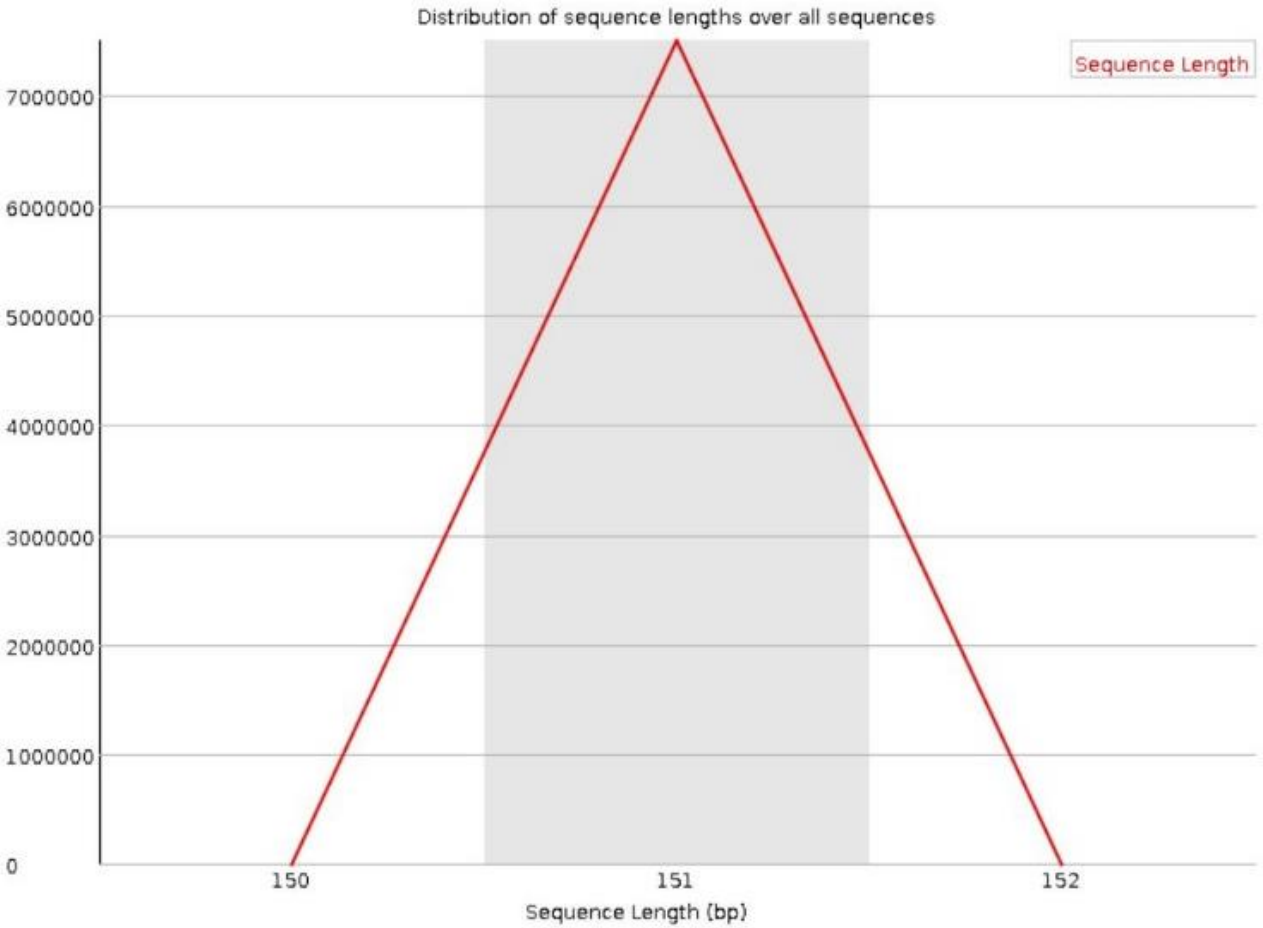

Figure 2.12 FastQC quality report: Sequence length distribution
Sequence length distribution indicates whether the reads (X-axis) within a sample library are all the same length (Y-axis) as determined by the type of sequencing set by the experimenter. In this study the 150 base pairs, paired-end sequencing was used to analyse the sample libraries.

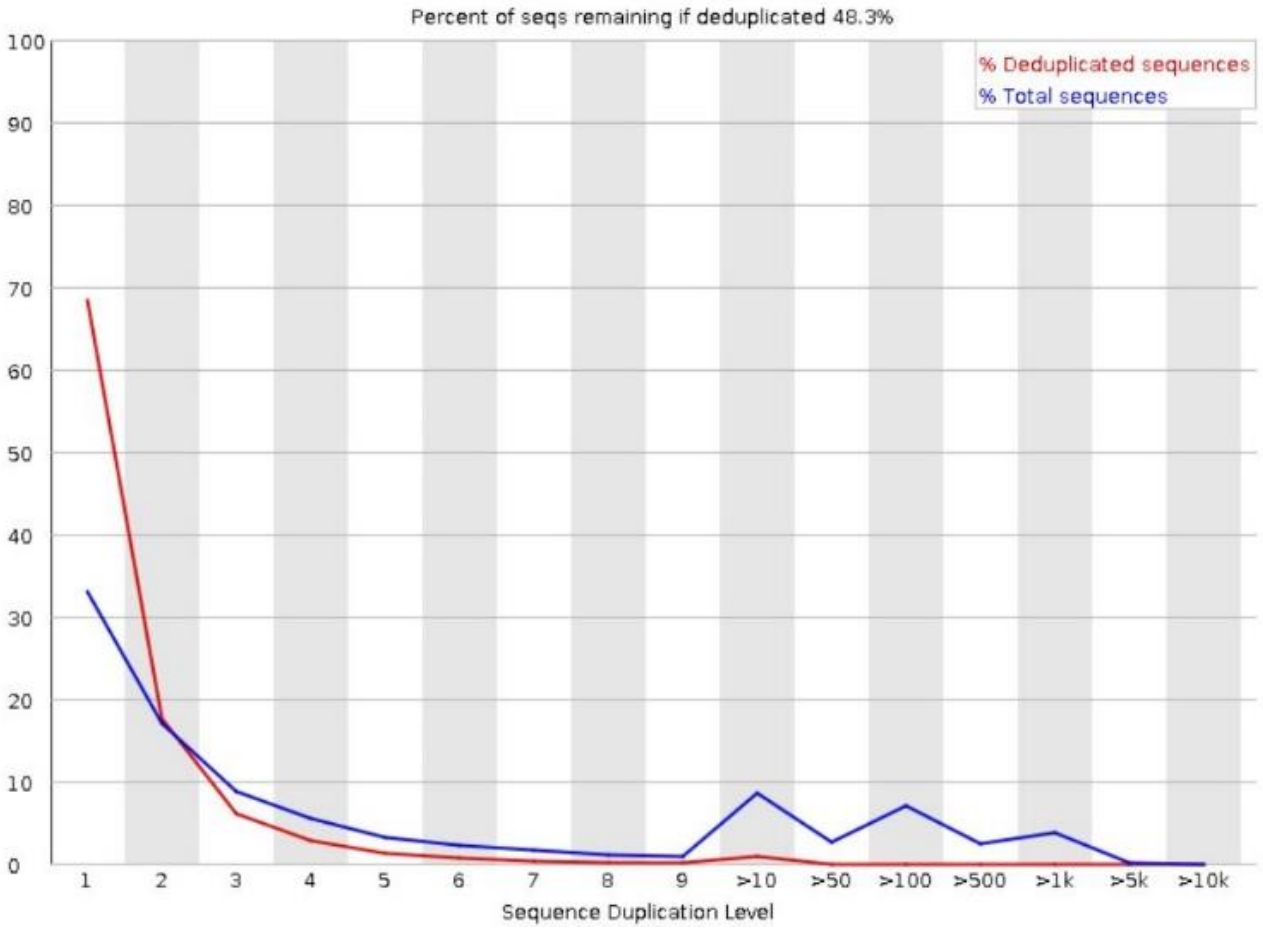

Figure 2.13 FastQC quality report: Sequence duplication level
Sequence duplication level depicts how many reads (Y-axis) are duplicated (X-axis) within the sample library and not unique.

contaminants such as the primers and adaptors that may not have been removed by the clean-up steps.

Once the data has gone through quality control using the FASTQC reports, the data must be aligned to a genome. For this purpose, the RNA-seq alignment algorithm, Spliced Transcripts Alignment to a Reference (STAR), was used to produce a genome index and align the reads to the genome index. STAR pre-processes the reference sequences to make a genome index, the index allows reads to be quickly aligned (Dobin et al., 2012). The genome index was produced using the Mouse Dec. 2011 (GRCm38/mm10) Assembly genome downloaded from the University of California, Santa Cruz (UCSC) genome browser. STAR is used to align the reads in the fastq files to the genome which produces a BAM file. The BAM file contains reads ordered by their position in the genome. The BAM file can be opened in a genome browser application to view the aligned reads and their position in the genome index. Golden Helix GenomeBrowse ® was used to visualize the aligned reads, to observe insertions or deletions, how well aligned the reads are to the genome and which genes have reads aligned to them. The next step is obtaining read counts for the data by counting how many reads map to each gene/transcript. Two analysis pipelines were used with different cut-off values for the read counts as this was the first time RNA-sequencing data was analysed in the lab. The two pipelines used were: Tophat_Cufflinks_Cuffdiff and Subread_featureCounts_DESeq2. Cut-off for the read counts were ≥0.5, ≥1, ≥5 and ≥10. Tophat is a read mapping algorithm that aligns the reads to a reference genome. Cufflinks is an algorithm that assembles transcriptomes from

RNA-seq data and quantifies their expression. Cuffdiff is an algorithm that counts the reads mapping to each transcript in each sample. Subread is a read-aligner algorithm that performs the same function as the Tophat algorithm. featureCounts is an algorithm that counts reads in RNA-seq data. DESeq2 is an algorithm that provides differential analyses on count data (Trapnell et al., 2009, Trapnell et al., 2012, Trapnell et al., 2013, Liao et al., 2013, Smyth et al., 2013, Love et al., 2014). The analysis pipelines generate output files with the read count data, read count values are expressed as the number of reads mapped per kilobase of transcript per million reads (Fragments Per Kilobase Million, FPKM). This value normalises the data for different transcript lengths and library sizes. Graphs were produced using R software or GraphPad Prism 7.

2.4.9 Statistics

R software was used to produce heat maps and conduct principal component analysis (PCA) for single cell and IML RNA-seq data. Heat maps provided global overview of the differences in gene expression in the single cell and IML samples. PCA plots were generated for single cell and IML samples, the samples are spaced according to the genes that have a FPKM value of ≥1. PCA plots were also generated for ChAT-positive and ChAT-negative samples, these samples are spaced according to the gene that have a FPKM value of ≥1. PCA plots are useful for viewing how close or distant the samples are to each other. PCA plots can be used to identify outliers and confounding variables.

GraphPad Prism 7 was used to generate bar plots for genes of interest to compare between the single cell and IML samples.

Chapter 3

Can SPNs be differentiated from other spinal neurones for cell isolation?

3.1 Introduction

In order to study gene expression within IML SPNs a method needed to be devised to separate these cell types from the general population of cells that comprise the thoracic spinal cord. Fluorescence-activated cell sorting (FACS) provides a useful method by which cell types could be separated into distinct populations based on labelling these cells using fluorescently tagged antibodies. FACS is a flow cytometry method by which a piece of tissue is reduced to the heterogeneous population of cells that it is comprised of, labelled with fluorescently tagged antibodies and individual cells sorted based on the fluorescent properties of the tag (St. John et al., 1986, Arlotta et al., 2005, Guez-Barber et al., 2012).

Previous research has demonstrated that all SPNs can be labelled by FG however, ventral horn motoneurons (VHMNs) and pericytes are also labelled by the retrograde tracer (Ambalavanar and Morris, 1989; Anderson and Edwards, 1994; Edwards *et al.*, 2013). FACS of cells on the basis of the presence of FG would therefore isolate these three cell types. Pericytes can be separated from other FG-labelled cells by labelling them using an antibody against platelet derived growth factor beta (PDGFRβ) (Edwards *et al.*, 2013). The resulting cell mixture would therefore contain SPNs and MNs. To separate SPNs from MNs using FACS, a selective marker for either cell type therefore needs to be identified.

Since it is unknown if FG effects gene transcription, another strategy may be to isolate SPNs using a combination of antibodies. For example, antibodies against the acetylcholine synthesising enzyme choline acetyltransferase (ChAT), nitric oxide synthase I (NOS1) and lectin RL-29 also known as

Galectin-3 (Gal-3) label SPNs, but since none label only SPNs a combination of these, perhaps with other, markers may be required.

In terms of immunohistochemistry, antibodies against ChAT reliably labelled a large number of SPNs in spinal cord tissue in the IML, intercalated nucleus (IC) and central autonomic area (IPPe) (Barber *et al*., 1984). ChAT is a transferase enzyme which catalyzes the transfer of an acetyl group from the co-enzyme Acetyl-CoA to choline to yield acetylcholine, a neurotransmitter. Additionally, ChAT labels MNs in the ventral horn (Barber *et al.*, 1984) and interneurones around the central canal (Gotts *et al*., 2016), making it a non-specific marker for SPNs. ChAT is therefore a useful marker to use for IHC but more selective markers for either SPNs or MNs are required for separating cells using FACS.

NOS1 is another candidate for a selective marker for SPNs. NOS1 is an enzyme that catalyzes the production of nitric oxide from L-arginine; nitric oxide produced by NOS1 has been shown recently to play a role in heterogeneous modulation of sympathetic firing behaviours (Anderson, 1992, Hinrichs and Llewellyn-Smith, 2009). Intense labelling was observed in lamina I-IV and X corresponding to the IML in the thoracic and sacral segments as well as the central canal (Hinrichs and Llewellyn-Smith, 2009). Dual labelling with NOS1 and ChAT confirmed the identity of the neurons located in the IML as SPNs. Another study examining double labelling of SPNs in the IML in mid-thoracic segments 7 to 10 with ChAT and NOS1 found at least half of ChAT-positive SPNs were labelled identifying a subpopulation of cholinergic SPNs labelled by NOS1. Of the NOS1-labelled SPNs, 22% of these cells were identified as sympathoadrenal projection neurons through use of the retrograde tracer, cholera toxin B (Hinrichs and Llewellyn-Smith, 2009). NOS1 is a potential candidate to label IML SPNs selectively however further work is required to

determine the effectiveness of using NOS1 antibodies to label IML SPNs in comparison to FG.

A potential marker specifically for SPNs is Gal-3, a protein which binds to beta-galactoside. Gal-3 has been implicated in cellular metabolism and injury response. RL-29 is a lectin that is expressed in a subset of adult rat dorsal root ganglion neurons and a large percentage of RL-29 immunoreactive neurons in the spinal cord are SPNs (Park and Chung, 1999). Interestingly, RL-29 labelled fewer IML SPNs in the thoracic segment as compared to the lumbosacral segment. Conversely, RL-29 labelling of ependymal cells was more prominent in the thoracic segment (Park and Chung, 1999). A comparison of Gal-3- and FG-labelled IML SPNs would be useful to determine whether this protein could be used to select for IML SPNs.

In addition to the above candidates, there may be other potential markers for SPNs and MNs, although literature searches did not reveal any selective for either cell type. Recent open science innovations have provided free access to databases of research information. Such databases include the Allen Spinal Cord Atlas, which reveals *in situ hybridisation* for a wide selection of genes in mouse spinal cord sections (http://mousespinal.brain-map.org/). Another such resource is GENSAT, which reveals images of expression of reporter proteins in the CNS of mouse lines generated using bacterial artificial chromosomes (http://www.gensat.org/search.jsp). Such resources are searchable to varying degrees to reveal expression in specific areas or cell types, for example SPNs and/or MNs.

3.2 Objectives

The aim of this chapter was to develop an approach to enable isolation of SPNs by flow cytometry for subsequent gene expression analysis.

Research questions:

1. Are there primary antibodies that label SPNs or MNs selectively?
2. Do primary antibodies that label SPNs label all SPNs or subsets?

Primary antibody candidates were chosen using the online databases Allen Brain Atlas and Gensat and assessed using immunohistochemistry (IHC) in WT tissue and FG-labelled tissue. FG-labelled tissue was used to assess the number of SPNs labelled with primary antibody candidates.

3.3 Materials and Methods

All IHC experiments were conducted on tissue from C57Bl/6 mice (N=30). Some mice (N=15) were injected intraperitoneally with 1% (w/v) hydroxystilbamidine (25 mg/kg, Fluorogold, FG). All tissue was prepared as described in the General Methods section. All antibodies used in IHC experiments are listed in Table 3.1. Fluorescent images were obtained as described in section the General Methods section.

A strategy was devised to use an anti-ChAT antibody as a primary label to identify IML SPNs and MNs then use other antibodies to specifically label IML SPNs or MNs to facilitate easier selection of IML SPNs using FACS. An online screen of neurotransmitter, enzyme or receptor subunit gene expression in IML SPNs and VHMNs in adult mouse thoracic spinal cord tissue was conducted using online resources, Allen Brain Atlas (ABA) (http://www.brain-map.org/) and Gensat (http://www.gensat.org/index.html). Proteins expressed exclusively in IML SPNs and MNs located in the ventral horn were selected to test for in IHC experiments using antibodies against the proteins chosen. The Allen Brain Atlas

is an online database of *in situ* hybridization (ISH) images whereas Gensat is an atlas of ISH images and fluorescent microscopy images of spinal cord slice images from bacterial artificial chromosome (BAC) transgenic mice (Figure 3.1). Details on sample preparation and ISH protocol can be found on the Allen Brain Atlas website (http://mousespinal.brain-map.org/docs.html). In the Allen Brain Atlas, the ISH images for the intermediolateral cell column (IML) were selected, this brought up a list of all the genes that are expressed in the IML where a large population of SPNs are located. In Gensat, the search annotations function was used and “sympathetic preganglionic neurons” or “motor neurons” were searched for, which brought up a list of genes expressed in those particular cell types.

Table 3.1 List of all primary antibodies used

Primary antibody to	Abbreviation	Raised in	Dilution	Source	Catalogue number	IML Allen/Gensat	Result
Cocaine and amphetamine regulated transcript	CART	Goat	1:50 1:200 1:1000	R&D Systems	AF163	Allen	SPN processes labelled possibly dendrites or axons
CD24 antigen	CD24	Mouse	1:50 1:100 1:200	BD Biosciences	561777	Allen - MNs	Dorsal horn labelling, no SPNs, no MNs
CD24 antigen	CD24	Mouse	1:50 1:100 1:200	Miltenyi Biotech	130-102-731	Allen - MNs	Dorsal horn labelling, no SPNs, no MNs
CD44 antigen	CD44	Rabbit	1:100 1:1000 1:2000 1:5000 1:10000	Abcam	AB51037	Allen	Dorsal horn labelling, no SPNs
CD44 antigen	CD44 Biotin	Mouse	1:50 1:100	Miltenyi Biotech	130-110-082	Allen	Dorsal horn labelling, no SPNs
Choline acetyltransferase	ChAT	Goat	1:500	Merck Millipore	AB144P	Allen	IML and IC SPNs and MNs
Galectin-3	Gal-3	Rat	1:50 1:100 1:200	Miltenyi Biotech	130-101-314	Allen	1-3 IML SPNs
Galectin-3	Gal-3	Goat	1:50 1:100 1:250	R&D Systems	AF1197	Allen	3-4 IML SPNs, 1-3 IC SPNs (injured tissue)

G protein coupled receptor 68	Gpr68	Mouse	1:100 1:200 1:500 1:1000	NeoScientific	A7348	Allen	Non-specific labelling
Glutathione peroxidase 3	Gpx3	Mouse	1:100 1:250 1:500 1:1000	Abcam	AB7325	Allen	Dorsal horn labelling, no SPNs
Junctional adhesion molecule 3	Jam-C	Goat	1:200	R&D Systems	AF1213	Gensat	Central canal labelling
Nitric oxide synthase 1	Nos1	Mouse	1:50 1:200	Santa Cruz Biotechnology	SC5302	Allen	2-6 IML SPNs
Polysialylated neural adhesion molecule	PSA-NCAM	Mouse	1:50 1:200 1:1000	Invitrogen	14-9118-80	Allen	SPN processes labelled possibly dendrites or axons
Calgizzarin, calcium-binding protein A11	S100A11	Mouse	1:50 1:100 1:200 1:500 1:1000	Santa Cruz Biotechnology	SC390250	Allen	Non-specific labelling
Calcium-binding protein β	S100β	Rabbit	1:100 1:500 1:1000 1:2000	Abcam	AB52642	Allen	Astrocytes labelled

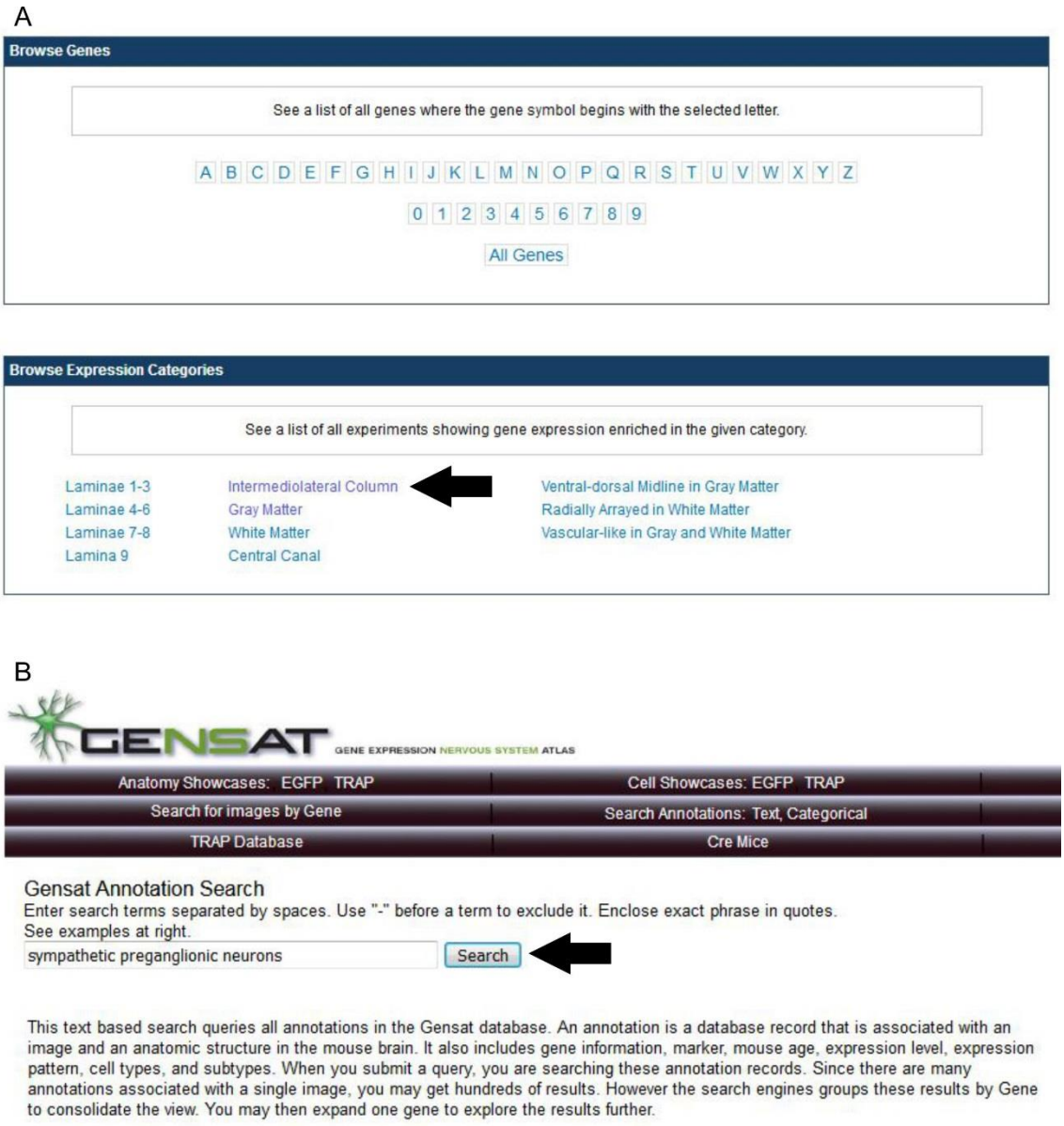

Figure 3.1 Online database search for SPN and MN markers
(A) Allen Brain Atlas gene search page, the arrow indicates the area of spinal cord selected to view gene expression. Following this, the images for individual marker candidates were selected and viewed for selective labelling of either SPNs or MNs (B) Gensat search annotations page, the arrow indicates the search box where criteria were added. Search term: sympathetic preganglionic neuron(s) or motor neuron(s) were used. A similar method as described with Allen Brain Atlas images was applied to Gensat images to identify selective markers for SPNs or MNs.

3.3.1 Controls

The omission of primary antibody in first incubation was performed with each antibody used in IHC experiments as described in the General Methods section. This control ensures the labelling observed in the tissue is due to the primary antibody and not due to the secondary antibody or auto-fluorescence of the tissue. The manufacturer's website was consulted to determine antibody specificity to the protein of interest confirmed by western blot experiments. Additionally, primary research literature was consulted to determine whether the antibody labelled the protein of interest in western blot experiments or there was a lack of labelling in tissues from a knock out mouse model for the gene encoding for protein of interest.

3.4 Results

3.4.1 Use of FG as a label for SPNs, MNs and pericytes

Initial experiments confirmed that intraperitoneal injections of FG resulted in fluorescent labelling in SPNs, motoneurons (MNs) and pericytes as described previously (Edwards et al., 2013). Punctate FG labelling was observed in the cell bodies of SPNs, MNs and pericytes (Figure 3.2Ai-Aii). SPNs in the IML and IC regions were labelled. The processes of these cell types were also labelled (Figure 3.2Aii). MNs and MN processes were labelled in the ventral horn and pericytes labelled with FG were present in multiple areas in the tissue (Figure 3.2Aiii). Identification of SPNs and MNs in this way allowed examination of other potential markers present in either of these cell types.

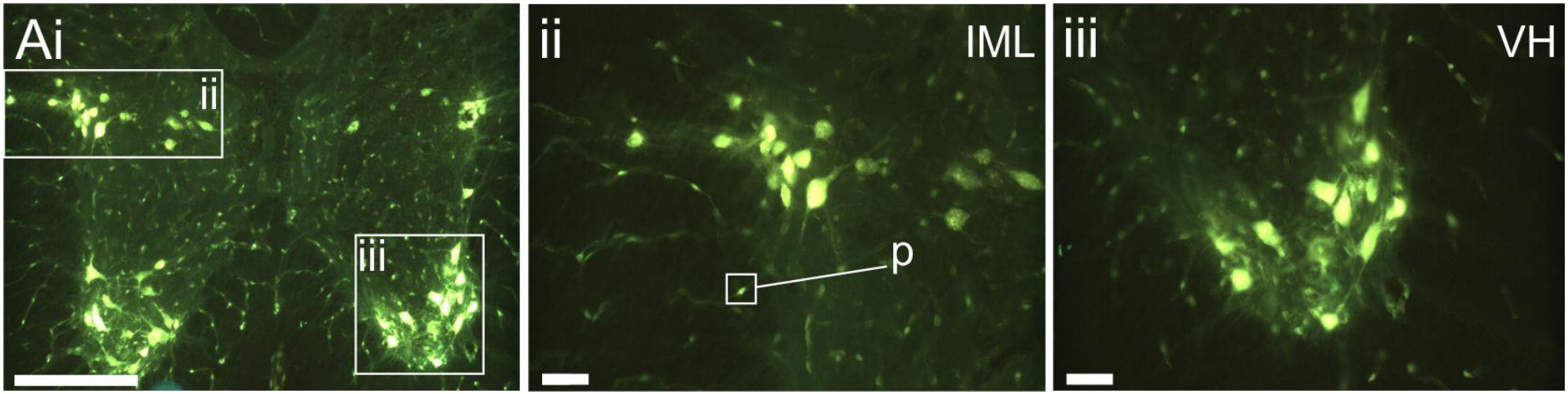

Figure 3.2 Fluorogold labelling of SPNs and MNs in thoracic spinal cord section.
Mice were injected IP with 25 mg/kg of Fluorogold and were fixed three days post injection. Thoracic spinal cord sections were obtained from removed spinal cords. A) Whole thoracic spinal cord section labelled with FG (gold, Ai), SPNs labelled with FG located in the IML, p indicates an example of a labelled pericyte (Aii). MNs labelled with FG located in the ventral horn (Aiii). Scale bars: Ai = 200 µm. Aii-iii = 10 µm.

Online screen of potential SPN and MN markers

The Allen Brain Atlas yielded 132 marker candidates for the IML region whereas Gensat yielded 33 marker candidates for SPNs and 193 for MNs. All candidates that were chosen to test using IHC displayed expression specifically in IML SPNs or VHMNs according to the Allen Brain or Gensat images; Allen Brain atlas *in situ* hybridization (ISH) images were viewed first followed by the expression mask to confirm expression in SPNs located in the IML. The Allen brain atlas was used to select the following markers: Cocaine and amphetamine regulated transcript (CART), CD44, Galectin-3 (Gal-3), Glutathione peroxidase 3 (Gpx3), G protein-coupled receptor 68 (Gpr68), Polysialylated neural cell adhesion molecule (PSA-NCAM), S100 calcium binding protein A11 (S100a11) were chosen as potential markers for SPNs whereas CD24 and S100 protein, beta polypeptide (S100β) were chosen to label MNs.

3.4.2 Candidate markers for SPNs and MNs

Most IHC experiments that attempted to label SPNs or MNs had negative results as they did not label either of these populations (summarised in Table 3.1). These included: CART, CD24, CD44, GPR68, GPX3, Jam-C, PS-NCAM, S100A11, S100β and XCR1. Since it was necessary to obtain an antibody that labelled cells selectively, whether the staining was non-selective (e.g. antibody was not specific) or whether the expression atlases were incorrect was not further examined. However, antibodies that did result in labelling of SPNs or MNs that were selected for further study included the following antibodies:

CART

Allen Brain Atlas ISH and expression mask images for CART labelling showed CART expression in IML SPNs, cells in the central canal as well as MNs in the ventral horn. Anti-CART labelled processes close in proximity to the IML which

could be SPNs processes or dendrites but did not label the soma (Figure 3.3Bi-iii).

CD24

According to the Allen Brain Atlas CD24 is highly expressed in MNs. Two directly conjugated CD24 antibodies (BD Biosciences and Miltenyi Biotech) were used in an attempt to label the MNs however both failed to label the cells of interest, anti-CD24 labelling was only observed in the dorsal horn (Figure 3.4). No MNs were labelled however ependymal cells located in the central canal were labelled.

CD44

According to the Allen Brain Atlas CD44 has low levels of expression in IML SPNs, SPNs displayed labelling in ISH and expression mask images. Following both antigen retrieval and standard IHC protocols, no labelling was observed with the initial CD44 antibody tested (Abcam). A second directly conjugated antibody from Miltenyi Biotech was used but no labelling of the SPNs was observed however only the dorsal horn exhibited fluorescence indicating that the antibody has bound to antigen in the tissue (Figure 3.3Ai-iii). These could potentially be axons of cells located in the dorsal root ganglia as DRG neurones are seen to express CD44 in Allen Brain Atlas. Anti-CD44 only labelled the dorsal horn.

ChAT

ChAT labelling of SPNs has been confirmed and documented in previous studies and is observed in the images from the Allen Brain Atlas, ChAT

antibody labels SPNs located in the IML, IC and IPPE region in thoracic spinal cord. Anti-ChAT also labels MNs located in the ventral horn (Figure 3.5-3.6).

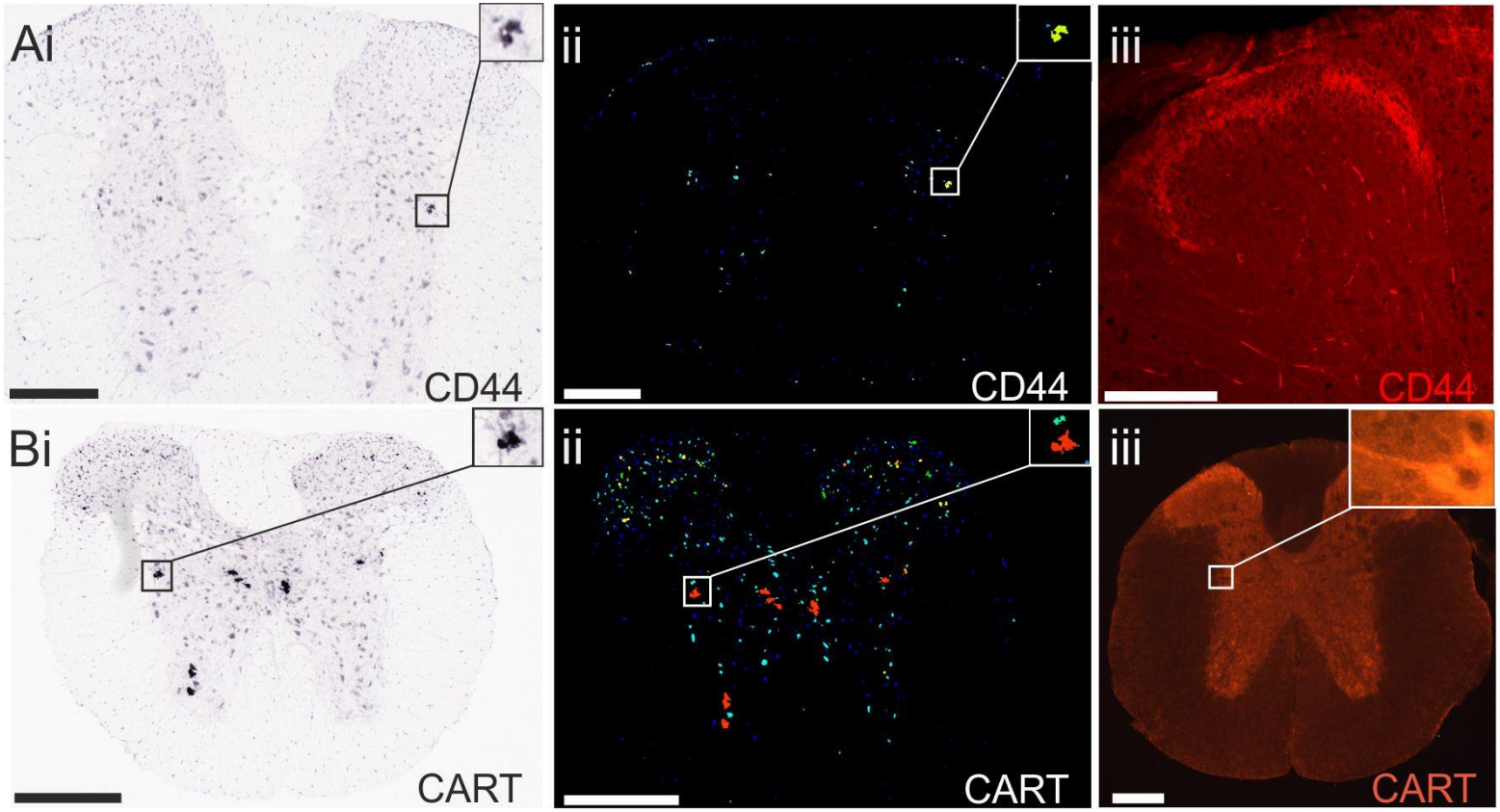

Figure 3.3 Allen Brain Atlas candidates, CD44 and CART. Image of IF attempt of IML SPN labelling using CD44 and CART antibodies in thoracic spinal cord section.
Ai-Bi) ISH image from ABA of thoracic spinal cord section labelled with candidate marker, inset displays SPNs labelled in IML. Aii-Bii) Expression mask image of ISH image, colour indicates intensity of expression of candidate marker, inset indicates expression in IML SPNs. Aiii-Biii) IF image of thoracic spinal cord section labelled with candidate marker, dorsal horn labelled with anti-CD44 and nonspecific labelling of thoracic spinal cord section by CART antibody. Biii) Inset depicts labelling of anti-CART process near IML. Scale bars: Ai-Biii = 200 μm.

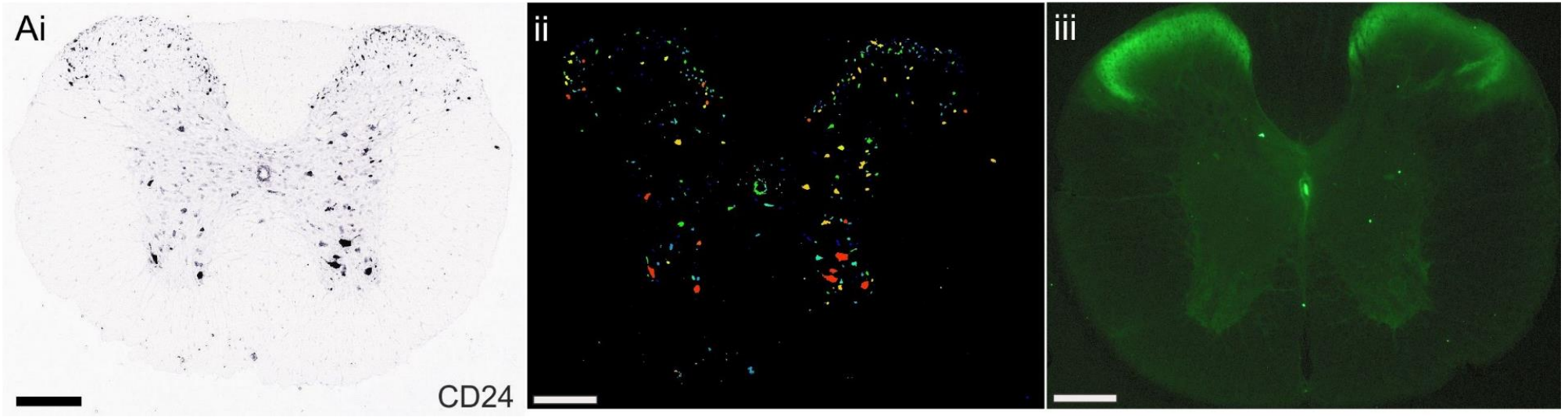

Figure 3.4 CD24 antibody labelling in thoracic spinal cord section. Anti-CD24 does not label VHMNs.
Ai) Allen brain atlas image of whole thoracic spinal cord section revealing expression of CD24 using ISH. Aii) Expression mask image of ISH image, colour indicates intensity of expression of candidate marker, CD24. Aiii) CD24-labelled thoracic spinal cord section using IF, labelling in the dorsal horn is observed however there is a distinct lack of labelling of VHMNs. Scale bars: Ai-iii = 200 μm.

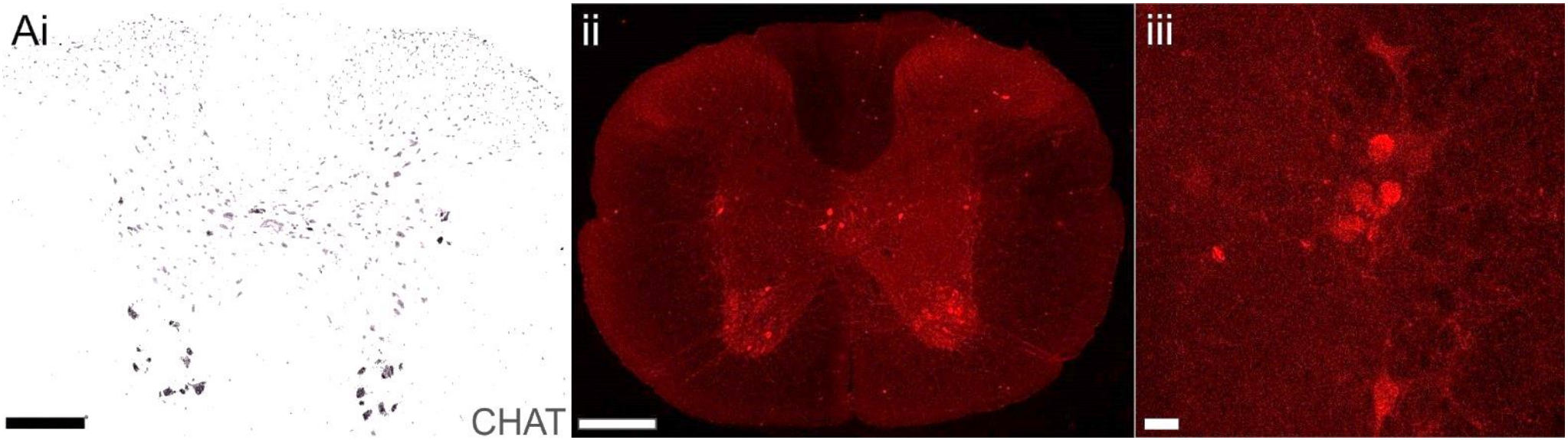

Figure 3.5 ChAT antibody labelling of SPNs and MNs in thoracic spinal cord section. Anti-ChAT reliably labels SPNs in the IML, IC and IPPe regions of thoracic spinal cord and VHMNs.
Ai) Allen brain atlas image of whole thoracic spinal cord section labelled with anti-ChAT using ISH. Aii) Whole thoracic spinal cord section labelled with ChAT antibody using IHC. Anti-ChAT labels SPNs in 3 areas: IML, IC and IPPe area as well as VHMNs. Aiii) Chat-labelled SPNs located in the IML. Scale bars: Ai-ii = 200 μm. Aiii = 10 μm.

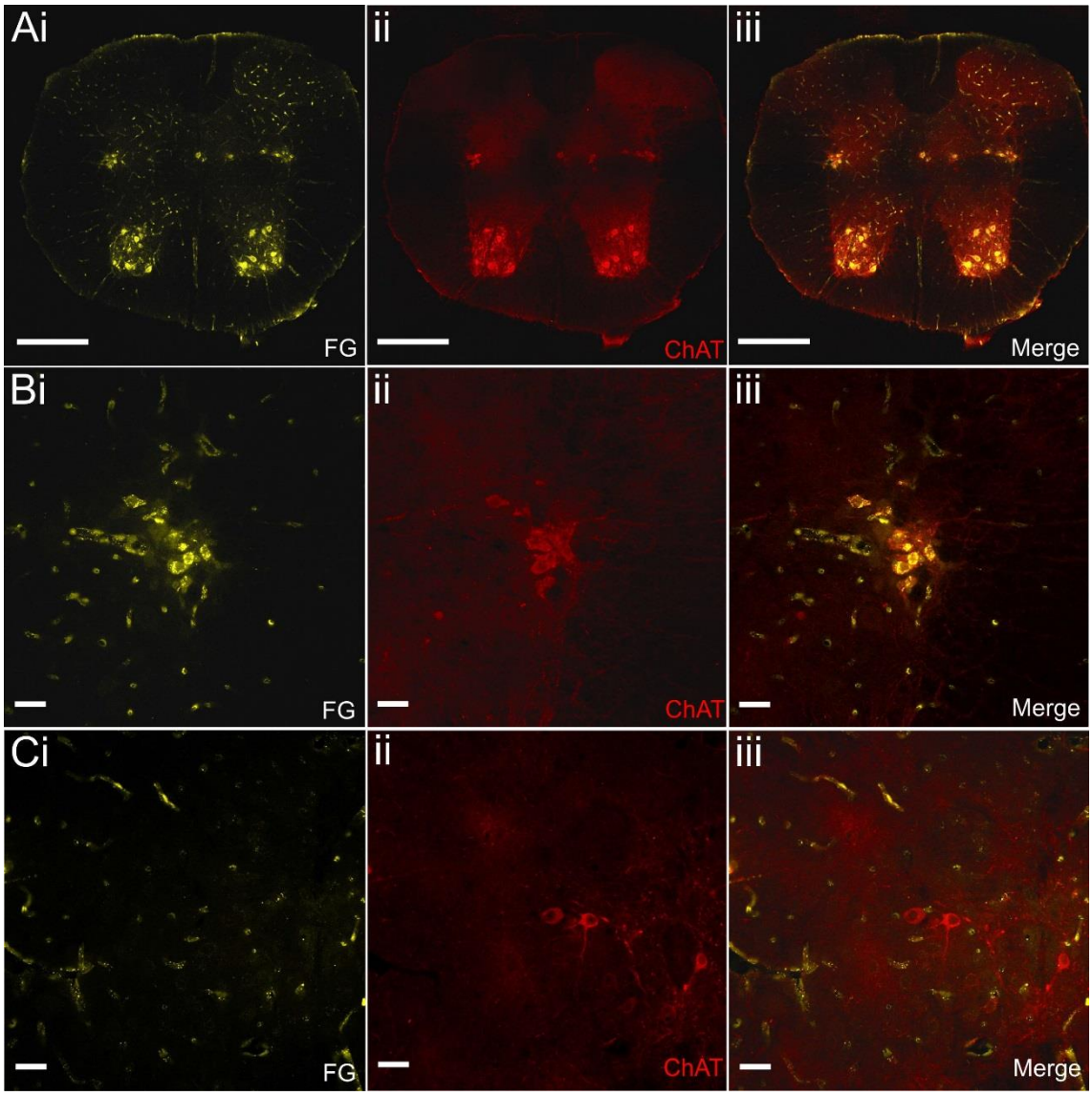

Figure 3.6 ChAT labelling of SPNs and MNs in FG-labelled thoracic spinal cord section. FG labels pericytes, VHMNs and SPNs in the IML, IC and IPPe. ChAT antibody labels SPNs in the IML, IC and IPPe and VHMNs. Mice were injected IP with 25 mg/kg of fluorogold and were fixed three days post injection. Thoracic spinal cord sections were subjected to immunohistochemistry. Ai-iii) Whole FG-labelled thoracic spinal cord section labelled with ChAT antibody. Many of the same cell types are labelled such as SPNs and VHMNs. Bi-iii) FG and ChAT-labelled SPNs located in the IML display colocalization of FG and anti-ChAT. Ci-iii) FG and Chat-labelled SPNs located in the IPPe. Scale bars: Ai-iii = 200 μm. Bi-Ciii = 10 μm.

Galectin-3

The Allen Brain Atlas images for Gal-3 have low levels of expression in SPNs in the IML (Figure 3.7Ai-ii). Gal-3 antibody labelled SPNs in the IML and the IC as well as cells in the ependymal cell layer around the central canal and some cells with morphology of microglia (Figure 3.7-3.8 Aiii-vi).

GPR68

GPR68 expression was observed in IML SPNs in the Allen Brain Atlas ISH images however, following IHC experiments antibody did not label SPNs (Figure 3.9).

GPX3

According to the Allen Brain Atlas GPX3 is expressed in SPNs within the IML however anti-GPX3 was found only to label the dorsal horn (Figure 3.10Ai-iii).

Jam-C

According to Gensat ISH images Jam-C is highly expressed in multiple SPNs within the IML. When tested using IHC, anti-Jam-C did not label IML SPNs but did label the central canal (Figure 3.11).

NOS1

Allen Brain Atlas ISH images of thoracic spinal cord slices labelled for NOS1 display punctate labelling of IML SPNs. Anti-NOS1 successfully labelled SPNs in the IML and IC specifically (Figure 3.12-3.13).

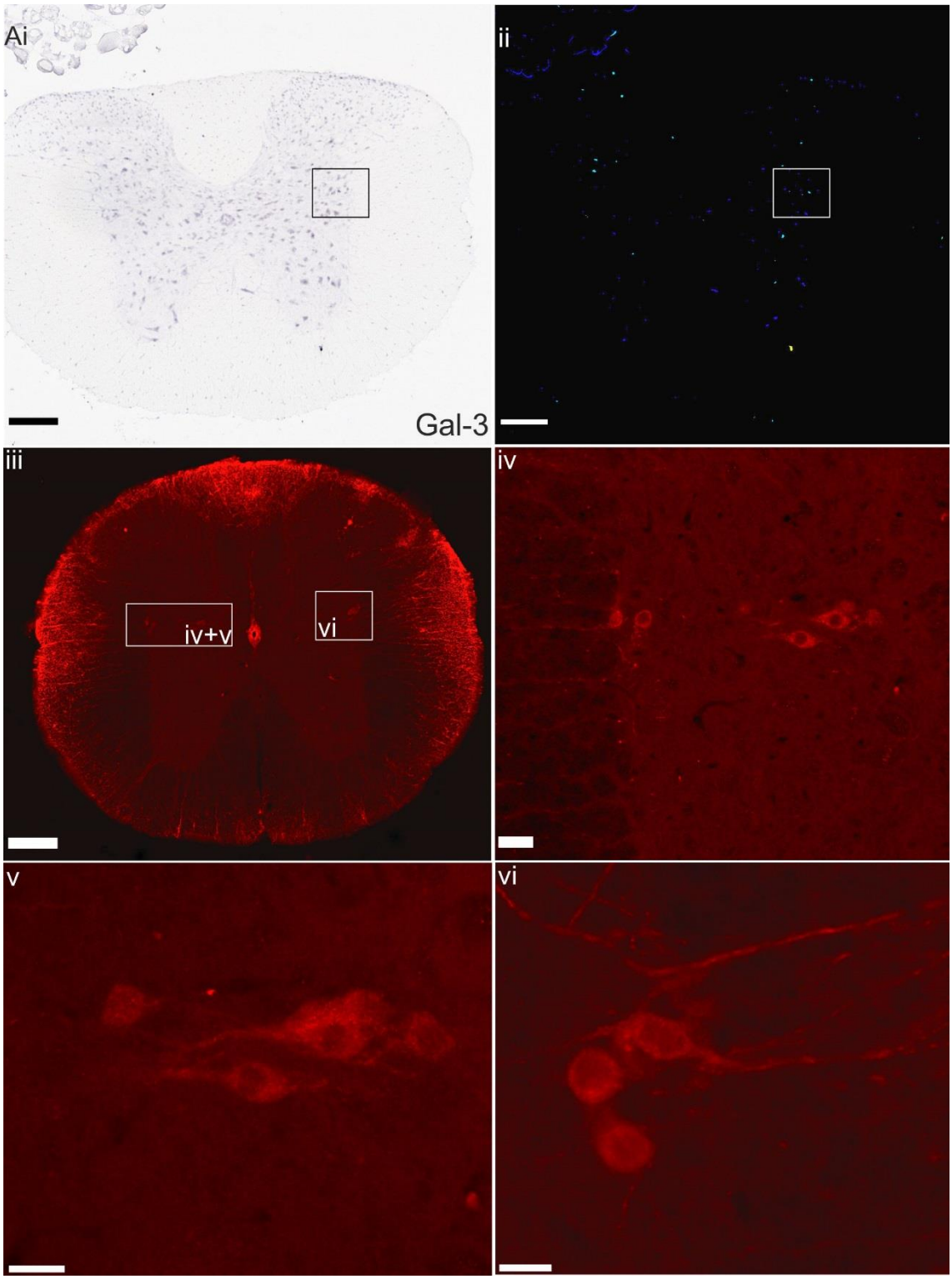

Figure 3.7 Anti-Galectin-3 labelling of IML and IC SPNs in thoracic spinal cord section.
Ai) Allen brain atlas image of whole thoracic spinal cord section labelled with Gal-3 using ISH. Aii) Expression mask image of ISH image, colour indicates intensity of expression of candidate marker, Gal-3. Aiii) Whole thoracic spinal cord section labelled with Gal-3 using IHC. SPNs labelled with Gal-3 located in the IML (Aiv,Avi) and IC (Av). Anti-Gal3 labels soma (Aiv-vi) and some processes of SPNs (Avi). Scale bars: Ai-ii = 200 μm. Aiii = 40 μm. Aiv-vi = 10 μm.

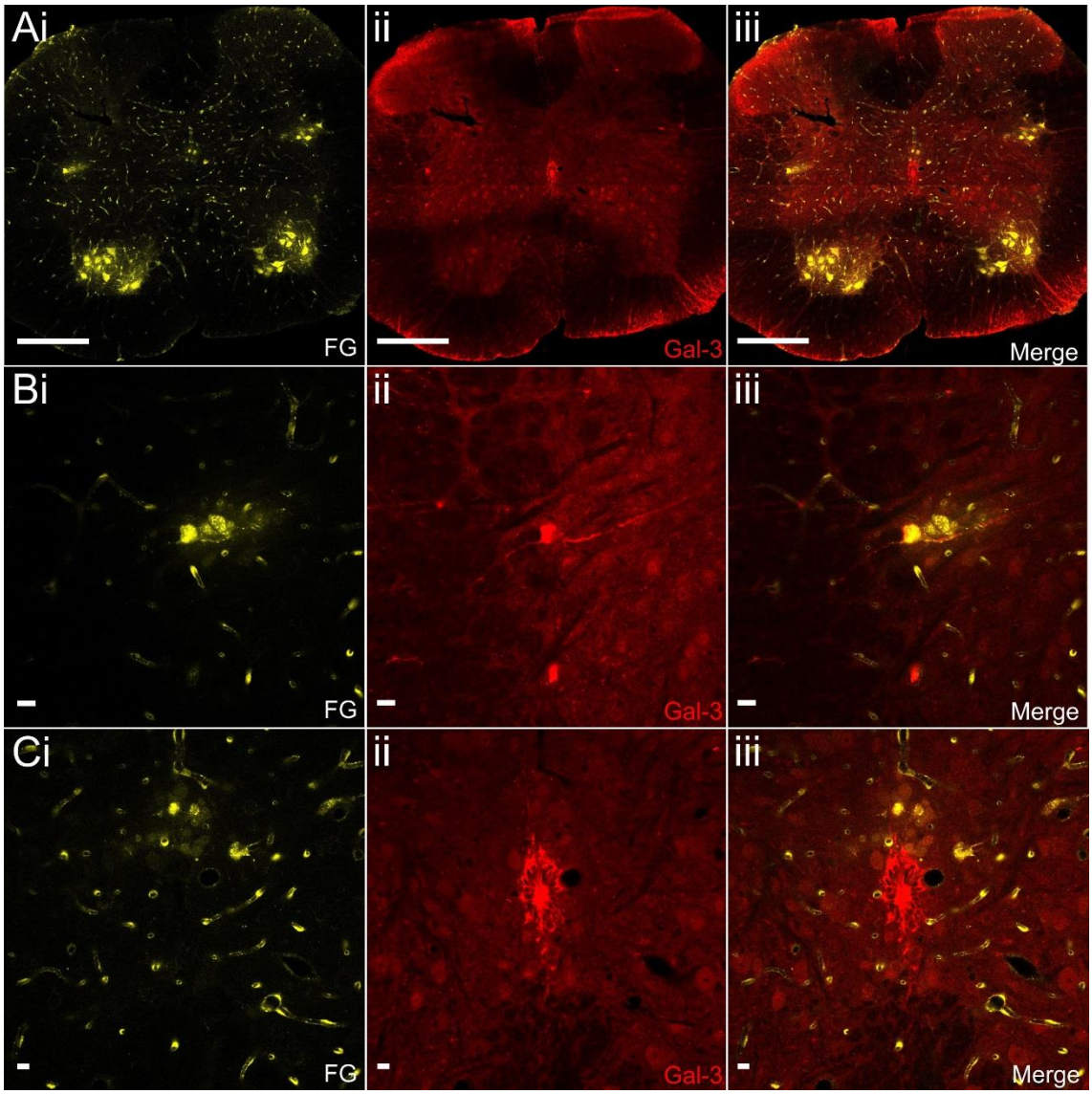

Figure 3.8 Galectin-3 labelling of SPNs and MNs in FG-labelled thoracic spinal cord section. Anti-Galectin-3 labels IML SPNs and ependymal cells in the central canal.

Mice were injected IP with 25 mg/kg of fluorogold and were fixed three days post injection. Thoracic spinal cord sections were subjected to immunohistochemistry. Ai-iii) Whole FG-labelled thoracic spinal cord section labelled with anti-Gal-3. Galectin-3 antibody labelled IML SPNs and ependymal cells. FG labelling was observed in IML, IC and IPPe SPNs, VHMNs and pericytes. Bi-iii) FG and Gal-3-labelled SPNs located in the IML. Anti-Gal-3 labels a few IML SPNs in comparison to FG. Ci-iii) FG-labelled SPNs located near the central canal. Gal-3 antibody labels ependymal cells in the central canal. Scale bars: Ai-iii = 200 µm. Bi-iii = 20 µm. Ci-Ciii = 10 µm.

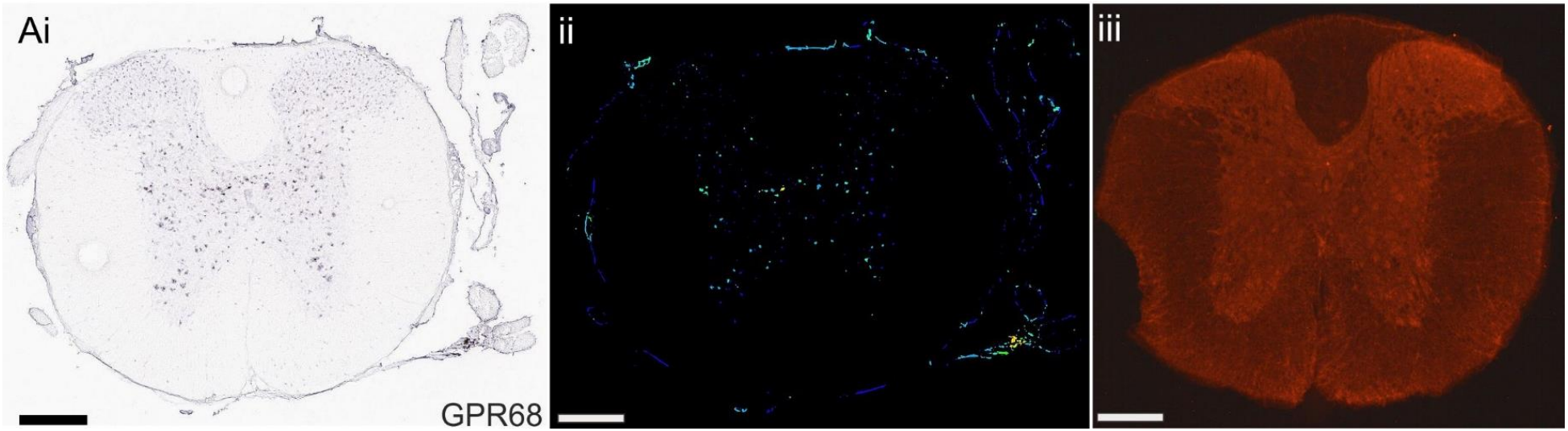

Figure 3.9 IF image of GPR68 antibody labelling in thoracic spinal cord section.
Ai) Allen brain atlas image of whole thoracic spinal cord section labelled with GPR68 using ISH. Aii) Expression mask image of ISH image, colour indicates intensity of expression of candidate marker, GPR68. Aiii) Anti-GPR68 IF resulted in nonspecific labelling of the thoracic spinal cord section. Scale bars: Ai-iii = 200 μm.

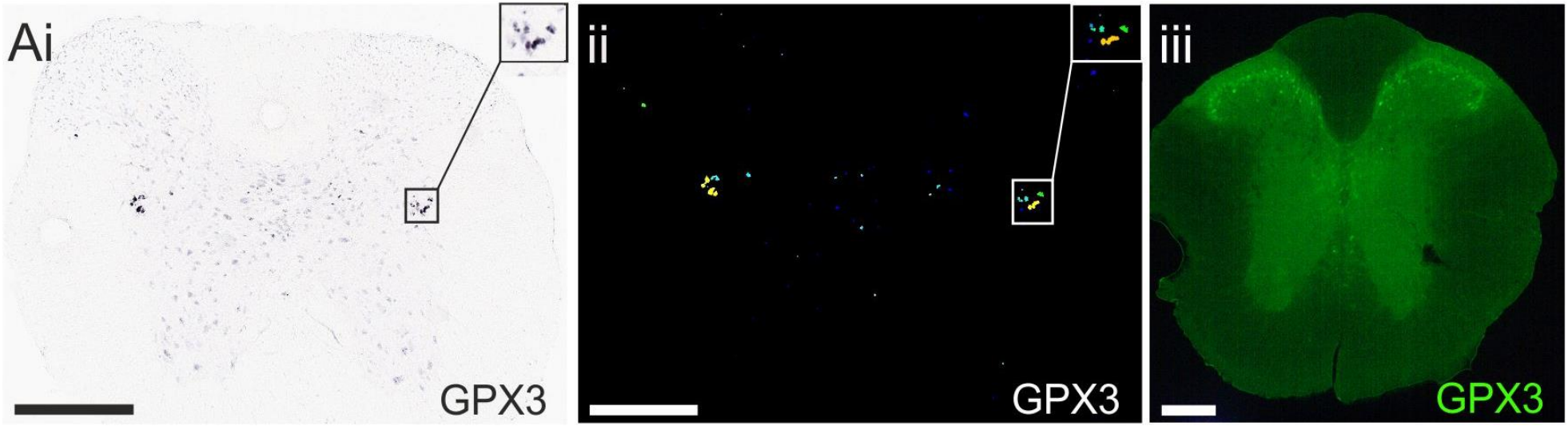

Figure 3.10 Allen Brain Atlas candidate, GPX3. Image of IF attempt of IML SPN labelling using GPX3 antibody in thoracic spinal cord section.
Ai) ISH image of thoracic spinal cord section labelled with candidate marker, inset displays SPNs labelled in IML. Aii) Expression mask image of ISH image, colour indicates intensity of expression of candidate marker. Inset: moderate levels of candidate expression observed in IML. Aiii) IF image of thoracic spinal cord section labelled with candidate markers, anti-GPX3 labelling observed in thoracic spinal cord sections. Scale bars: Ai-Aiii = 200 μm.

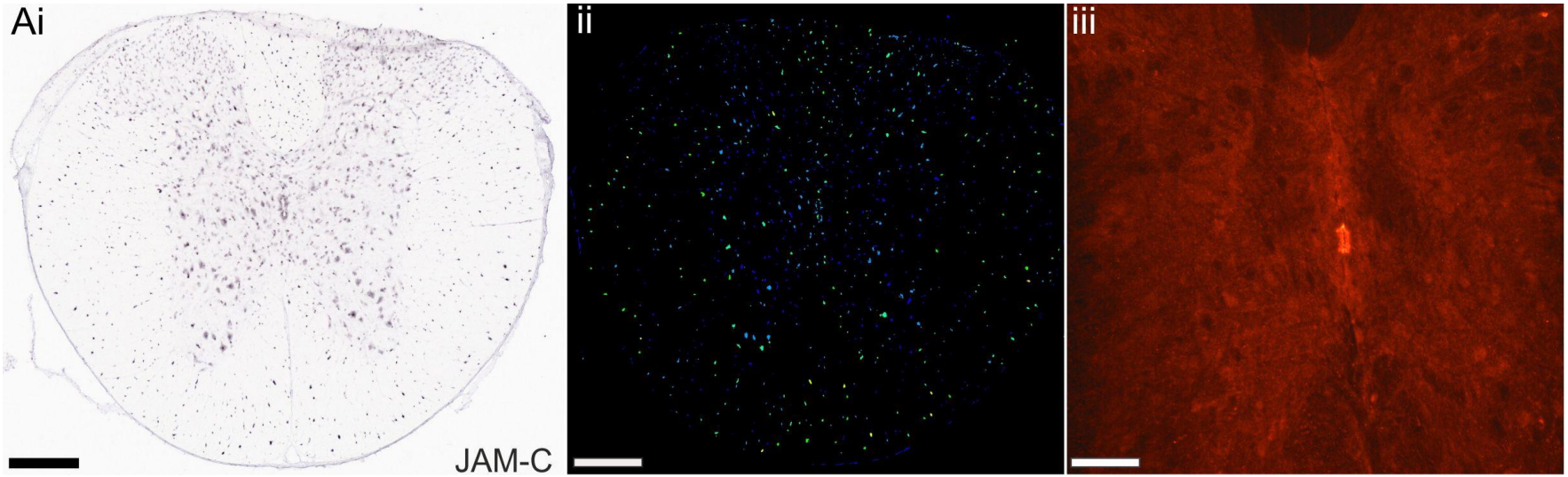

Figure 3.11 IF image of JAM-C antibody labelling in thoracic spinal cord section.
Ai) Allen brain atlas image of whole thoracic spinal cord section labelled with JAM-C using ISH. Aii) Expression mask image of ISH image, colour indicates intensity of expression of candidate marker, JAM-C. Aiii) JAM-C antibody labelled ependymal cells in the central canal however no labelling of IML SPNs was observed. Scale bars: Ai-iii = 200 μm.

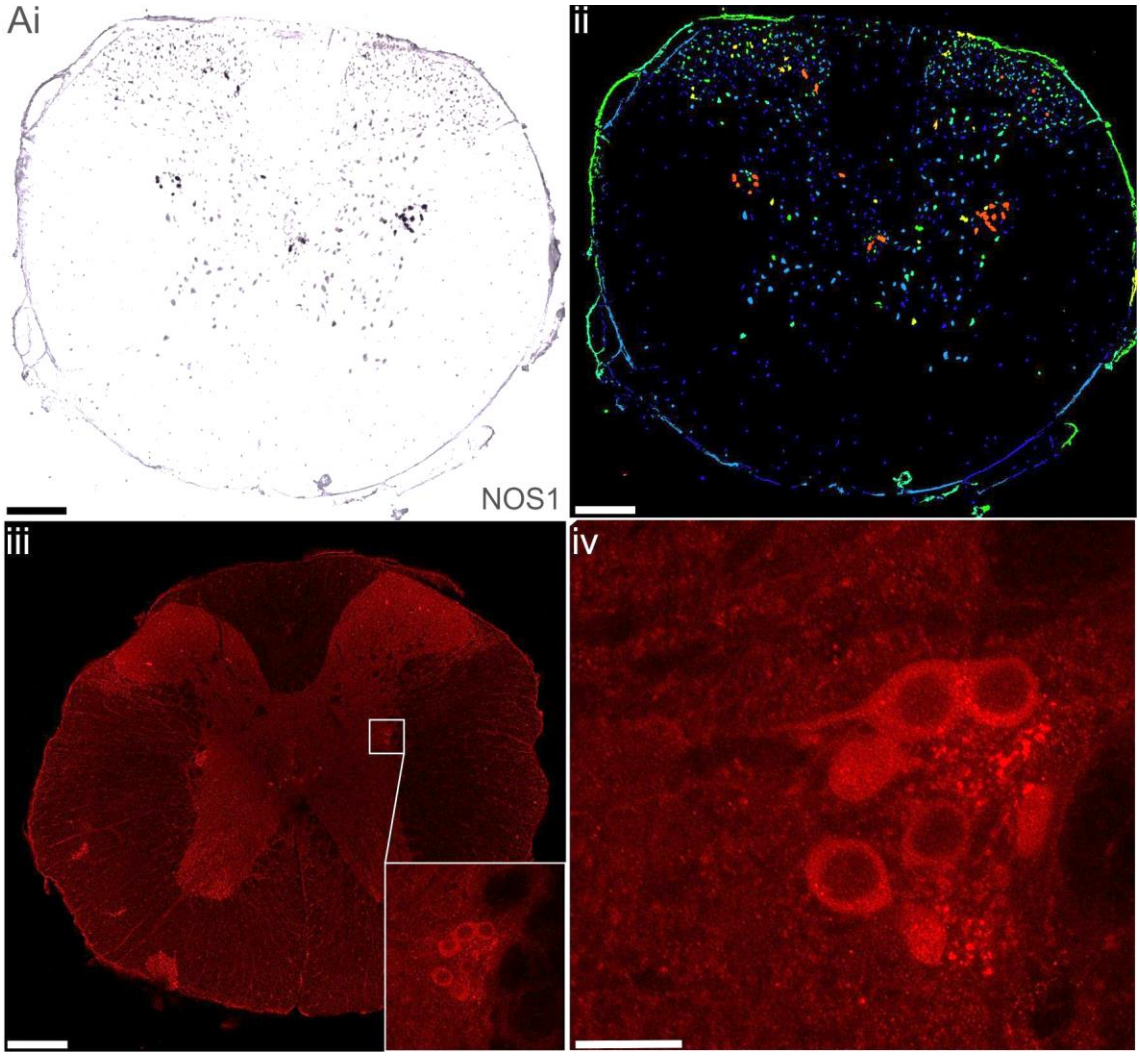

Figure 3.12 NOS1 antibody labelling of SPNs in thoracic spinal cord section.
Thoracic spinal cord section was labelled with anti-NOS1. Ai) Allen brain atlas image of whole thoracic spinal cord section labelled with NOS1 using ISH. Aii) Expression mask image of ISH image, colour indicates intensity of expression of candidate marker in IML SPNs, NOS1. (Aiii) Whole thoracic spinal cord section labelled with anti-NOS1, SPNs in the IML are labelled (see inset, Aiii), NOS1 antibody labels SPNS located in the IML (Aiv). Scale bars: Ai-iii = 200 m. Aiv = 20 µm.

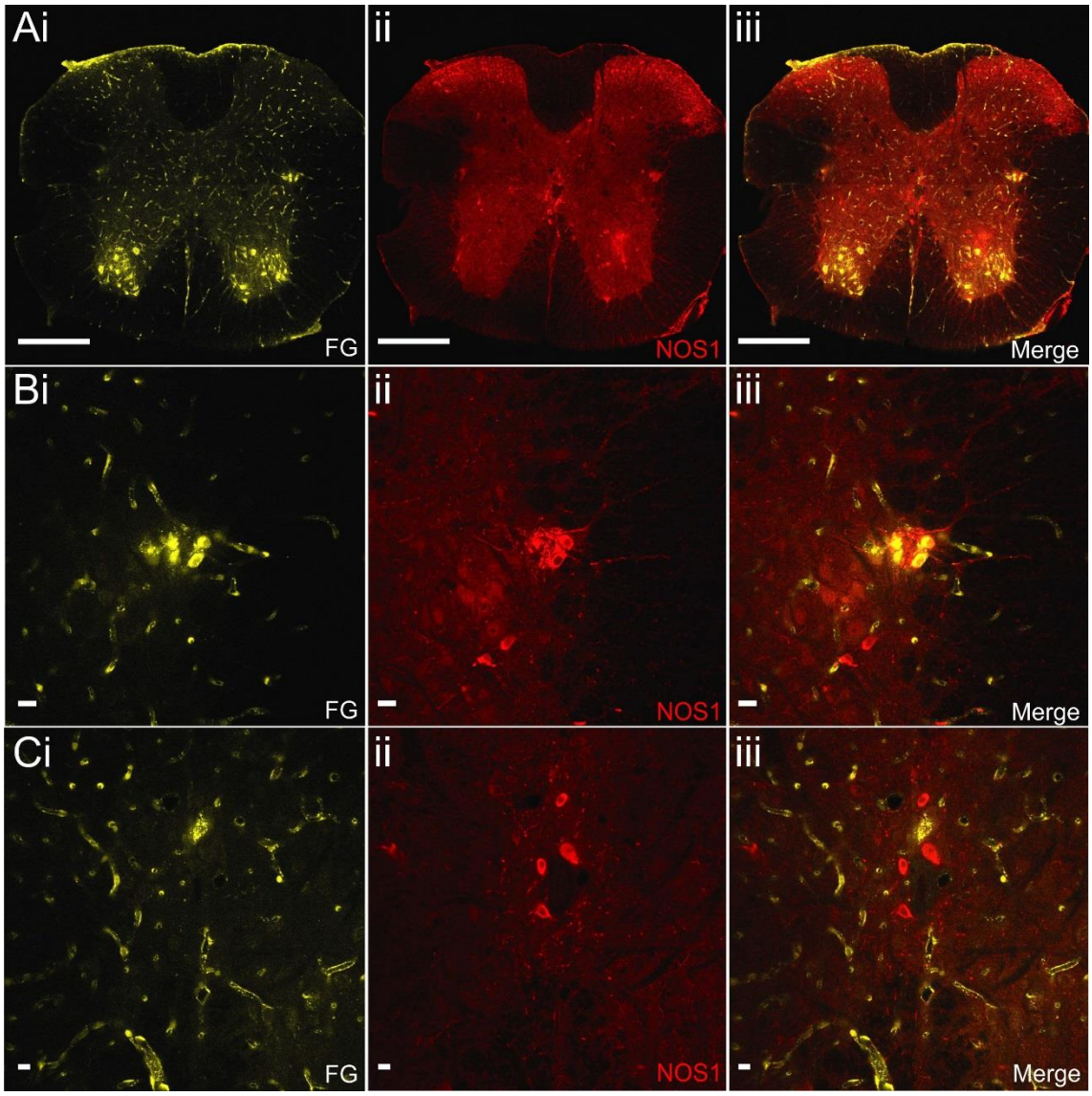

Figure 3.13 NOS1 labelling of SPNs in FG-labelled thoracic spinal cord section. FG-labelled IML, IC and IPPe SPNs, VHMNs and pericytes. Anti-NOS1 labelled IML and IPPe SPNs.

Mice were injected IP with 25 mg/kg of fluorogold and were fixed three days post injection. Thoracic spinal cord sections were obtained from removed spinal cords and subjected to immunohistochemistry. Ai-iii) Whole FG-labelled thoracic spinal cord section labelled with NOS1 antibody. Bi-iii) FG and NOS1-labelled SPNs located in the IML. Colocalization of the FG and anti-NOS1 observed in some of the cells. Ci-iii) FG and NOS1-labelled IPPe SPNs located near the central canal. Scale bars: Ai-iii = 200 µm. Bi-iii = 20 µm. Ci-Ciii = 10 µm.

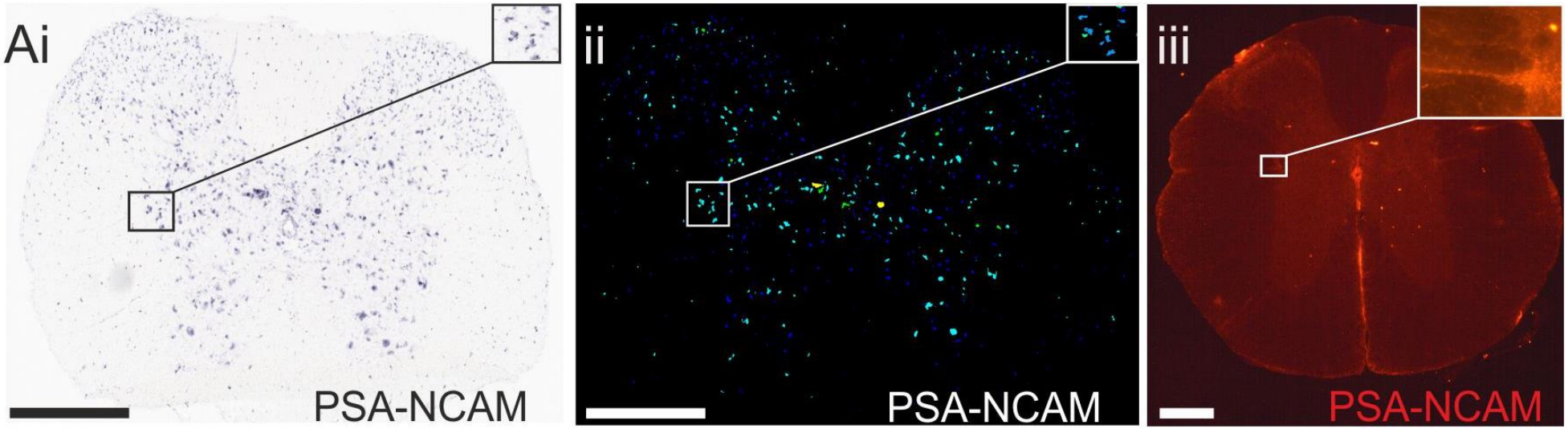

Figure 3.14 Allen Brain Atlas candidate, PSA-NCAM. Image of IF attempt of IML SPN labelling using PSA-NCAM antibody in thoracic spinal cord section.

Ai) ISH image of thoracic spinal cord section labelled with candidate marker, inset displays SPNs labelled in IML. Aii) Expression mask image of ISH image, colour indicates intensity of expression of candidate marker. Inset: moderate levels of candidate expression observed in IML. Aiii) IF image of thoracic spinal cord section labelled with candidate marker, anti-PSA-NCAM labelling observed in thoracic spinal cord sections. Aiii) Inset depicts process from IML labelled by anti-PSA-NCAM. Scale bars: Ai-Aiii = 200 μm.

PSA-NCAM

The Allen Brain Atlas images for PS-NCAM showed expression in 1-2 IML SPNs however when tested using IHC no SPN somas were labelled however it may be possible SPN processes such as axons or dendrites were labelled (Figure 3.14Ai-iii). When conducting IHC using anti-PS-NCAM on FG-labelled tissue it seemed PS-NCAM labelled in the extracellular vicinity of 3-4 SPNs in the IML, this is evident from the PS-NCAM antibody labelling the periphery of the FG-labelled somas of the SPNs (Figure 3.15).

S100a11

According the Allen Brain Atlas S100a11 is expressed within SPNs in the IML, which is seen with the punctate labelling of IML SPNs. Anti-S100a11 labelled the spinal cord section non-specifically (Figure 3.16).

S100β

According to Allen Brain Atlas ISH images S100β is highly expressed in MNs however when tested using IHC anti-S100β labelled the spinal cord section non-specifically (Figure 3.17Ai-iii).

3.4.3 Galectin-3 labels a subset of SPNs as well as ependymal cells

SPNs within the IML were labelled with the Gal-3 antibody, the identity of these cells were confirmed through FG labelling (N= 5 animals, n= 30 sections, Figure 3.8). Not all SPNs in the IML were labelled as confirmed by FG labelling, only 20% of FG-labelled SPNs were labelled with anti-Gal-3 (N= 5 animals, n= 30 sections). Anti-Gal-3 labelled ependymal cells in the central canal and some microglia as well as SPNs within the IML (N=10 animals, n= 90 sections). Gal-3 did not label MNs.

3.4.4 Anti-nitric oxide synthase labels SPNs

SPNs were labelled with anti-nitric oxide synthase (NOS1). Anti-NOS1 labelled 2-6 SPNs in the IML (N= 2 animals, n= 85 sections, Figure 3.12). NOS1 IHC performed on FG labelled thoracic spinal cord tissue found that while NOS1 antibody labels more SPNs than Gal-3, the antibody does not label all SPNs within the IML as NOS1 antibody labelled 43% of FG-labelled SPNs (Figure 3.13).

3.4.5 Comparison between antibodies that labelled SPNs

IHC was performed on FG labelled tissue to compare the percentage of IML SPNs labelled by the antibodies that labelled SPNs. When comparing whether FG-labelled SPNs were also labelled with ChAT, Gal-3 and NOS1 antibody, ChAT antibody labels the most SPNs in the IML with 73.2 ± 2.43% of FG-labelled SPNs also being labelled by ChAT antibody while anti-NOS1 labelled 43.9 ± 3.51% of FG-labelled SPNs and anti-Gal-3 labelled 20.6 ± 1.88% of FG-labelled SPNs (N= 5 animals, n= 30 sections, Figure 3.18). When comparing the percentage of SPNs labelled per area, FG labelled a larger number of SPNs in the IML and IC compared to the antibodies with the exception of the IPPe area. FG labelled 100% of IML and IC SPNs and 50.5% of IPPe SPNs compared to the ChAT antibody which labelled 71.6% of IML SPNs, 93.5% of IC SPNs and 100% of IPPe SPNs (Table 3.2). When compared to NOS1 antibody labelling, FG labelled 100% of IML and IC SPNs and 23.4% of IPPe SPNs while anti-NOS1 labelled 45.4% of IML SPNs, 34.9% of IC SPNs and 100% of IPPe SPNs (Table 3.2). FG labelled 100% of IML, IC and IPPe SPNs compared to Gal-3 antibody which labelled 29.7% of IML SPNs, 2.94% of IC SPNs and 2.22% of IPPe SPNs. Interestingly, ChAT and NOS1 labelled more cells in the IPPe than FG.

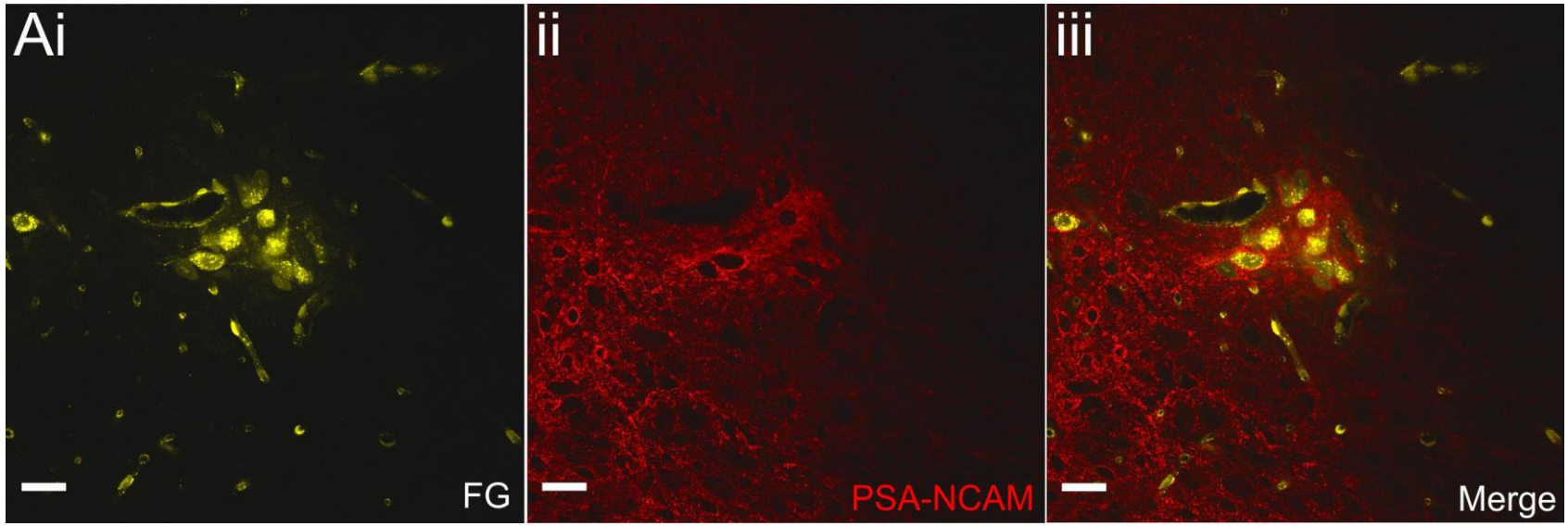

Figure 3.15 PSA-NCAM antibody labelling of SPNs in thoracic spinal cord section.
Ai) FG labelling of SPNs located in the IML. Aii) IHC image of SPNs located in the IML labelled with PSA-NCAM. Labelling appears to be extracellular surrounding the soma of the IML SPNs. Aiii) Merged image indicates SPNs located in the IML are double labelled with FG and PSA-NCAM. PSA-NCAM could potentially label IML SPNs extracellularly as depicted in this image. Scale bars: Ai-iii = 10 μm.

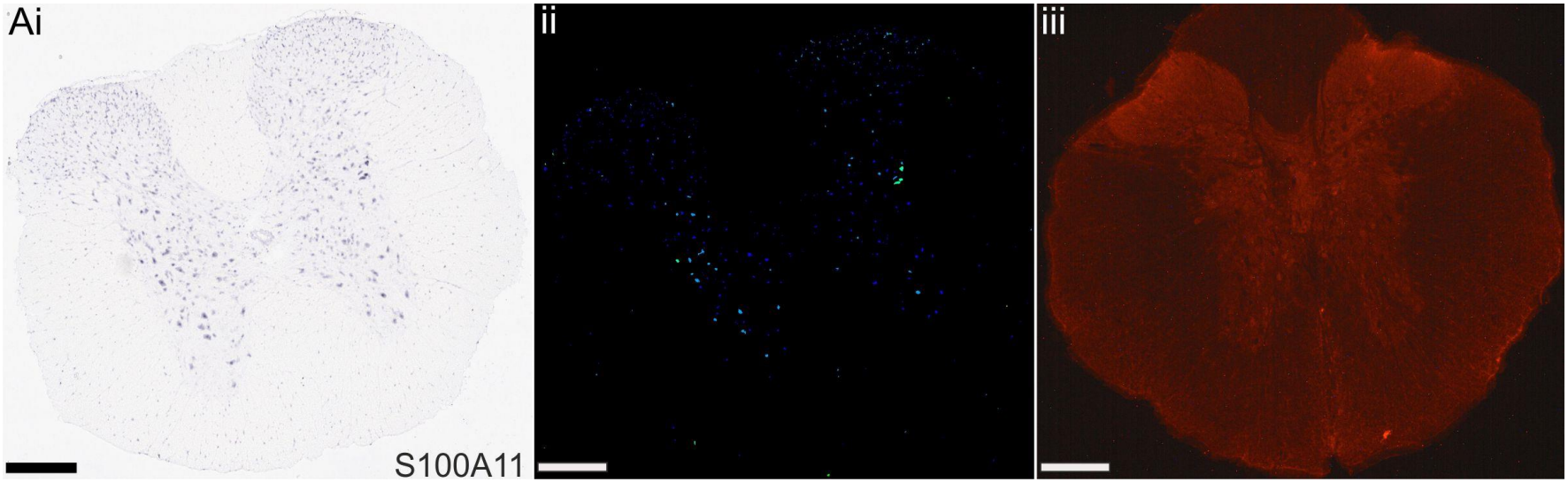

Figure 3.16 Anti-S100A11 labelling in thoracic spinal cord section.
Ai) Allen brain atlas image of whole thoracic spinal cord section labelled with S100A11 using ISH. Aii) Expression mask image of ISH image, colour indicates intensity of expression of candidate marker, S100A11. Aiii) Anti-S100A11 labelling was nonspecific in thoracic spinal cord section with no labelling observed in IML SPNs. Scale bars: Ai-iii = 200 μm.

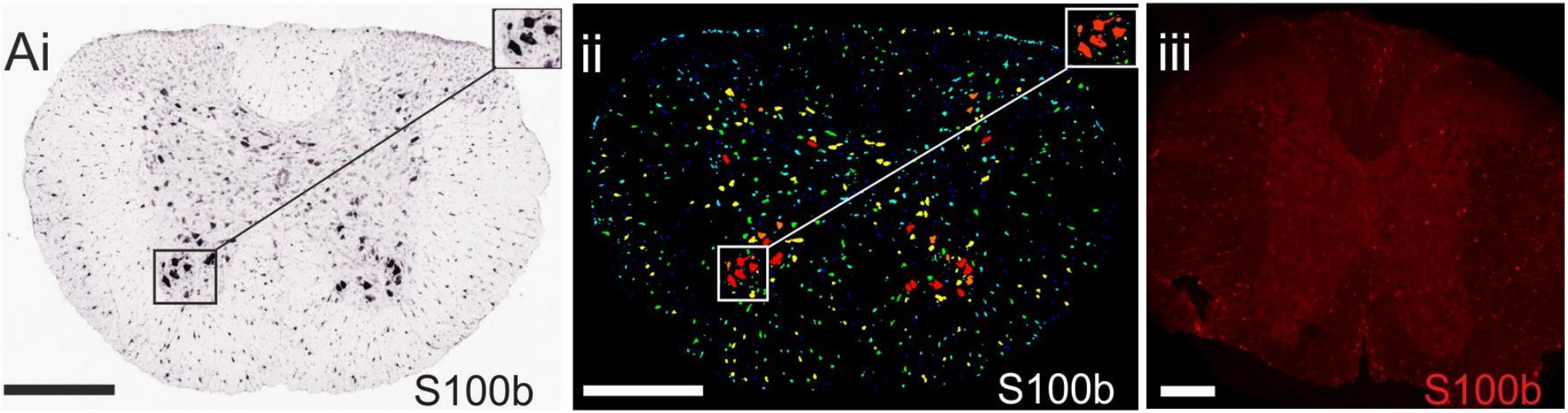

Figure 3.17 Allen Brain Atlas candidate S100β. Image of IF attempts of labelling of VHMNs with S100β antibody in thoracic spinal cord section.
Ai) ISH image of thoracic spinal cord section labelled with candidate marker S100β, inset displays expression of marker in VHMNs. Aii) Expression mask image of ISH image, colour indicates intensity of expression of candidate marker in VHMNs. Aiii) IF image of thoracic spinal cord section labelled with S100β antibody. Nonspecific labelling was observed with no anti-S100β labelling of VHMNs. Scale bars: Ai-Aiii = 200 μm.

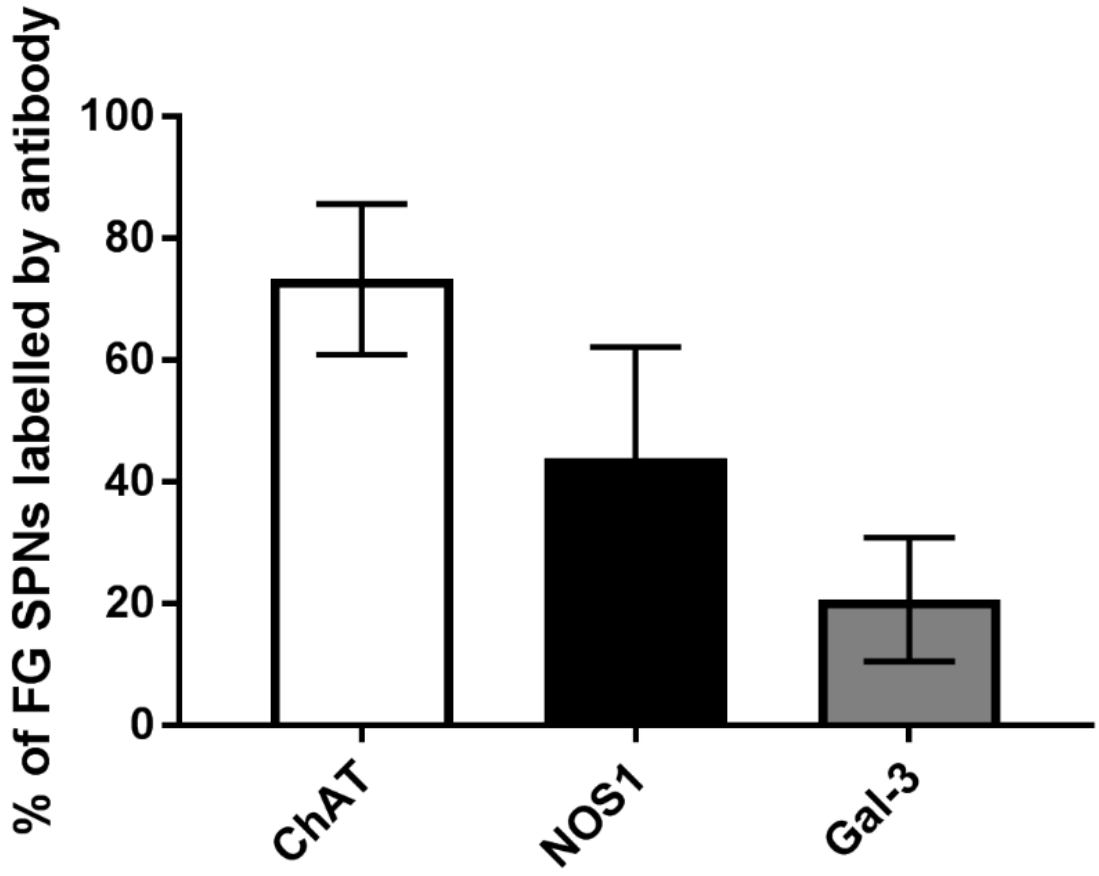

Figure 3.18 Percentage of FG-positive SPNs that were labelled by a primary antibody (ChAT, NOS1, Gal-3) using IF in thoracic spinal cord sections. ChAT antibody labelled the highest percentage of FG-positive SPNs.

The average percentage of antibody labelled (ChAT, NOS1, Gal-3) SPNs from the population of FG-positive SPNs ±SEM as measured by immunohistochemistry after IP injection of 1% (5 mg/kg) of FG. Mice were injected IP with 25 mg/kg of Fluorogold and were fixed three days post injection. Thoracic spinal cord sections were obtained from removed spinal cords and were subjected to immunohistochemistry. Results are average of 30 sections from each animal (n=5).

Table 3.2 Percentage of FG-positive SPNs labelled by a primary antibody (ChAT, NOS1, Gal-3) in thoracic spinal cord sections. When comparing the percentage of FG-positive SPNs in the IML, IC and IPPe labelled by the 3 candidate antibodies, ChAT antibody labelled the highest number of FG-positive SPNs in all areas.

	IML SPNs	IC SPNs	IPPe SPNs
% of ChAT-positive cells	71.6	93.5	100 (% FG-positive cells 50.5)
% of NOS1-positive cells	45.4	34.9	100 (% FG-positive cells 23.4)
% of Gal-3-positive cells	29.7	2.94	2.22

The percentage of primary antibody labelled SPNs from the population of FG-positive SPNs as measured by immunofluorescence after IP injection of 1% (5 mg/kg) of FG. Results are percentage of sum of SPNs counted labelled by primary antibody divided by sum of SPNs counted labelled by FG from 30 sections from each animal (n=5). Percentage of IPPe SPNs labelled by antibodies against ChAT and NOS1 were greater than the percentage of FG-labelled IPPe SPNs therefore percentage of FG-labelled IPPe SPNs was calculated as sum of IPPe SPN counted labelled by FG was divided by sum of SPNs counted labelled by primary antibody against ChAT or NOS1.

3.5 Discussion

The immunohistochemistry experiments in this chapter have identified two markers for SPNs, Galectin-3 and NOS1 which could be used to select IML SPNs using FACS. Additionally a comparison between antibodies against candidate markers, ChAT, NOS1 and Gal-3 and retrograde tracer FG were made in FG-labelled thoracic spinal cord sections to determine which marker labelled to most IML SPNs. Key findings include:

- Galectin-3 is a novel non-specific marker for some IML SPNs and ependymal cells in the central canal.
- NOS1 labels IML and IC SPNs and tends to label more FG-labelled SPNs in thoracic spinal cord sections than Galectin-3 but less than ChAT.
- FG labels the most SPNs in the IML and IC in thoracic spinal cord sections while ChAT antibody is a better marker for SPNs than Gal-3 and NOS1.

3.5.1 Galectin-3 is a novel non-specific marker for SPNs and ependymal cells in mice

Galectin-3 is a protein which binds to beta-galactoside and has been implicated in a number of biological processes most notably in inflammatory response to injury and is abundant in neutrophils and macrophages (Barondes et al., 1994, Dumic et al., 2006). Gal-3 expression has been documented in neuroglia and neurons in a number of brain regions including the cerebral cortex, hypothalamus and brainstem and other areas associated with these regions, however the function of Gal-3 in these areas was unclear (Yoo et al., 2017). Previous research on Gal-3 labelling within nervous system tissue has found that Schwann cells express Gal-3 (Narciso et al., 2009). Gal-3 labelling of SPNs in the mouse thoracic spinal cord has not been observed in previous research.

Gal-3 labelling of SPNs was intracellular however given the number of roles Gal-3 plays within a cell it is difficult to determine the role it plays within SPNs. Ependymal cells in the central canal of thoracic spinal cord sections were labelled with intracellular Gal-3. Gal-3 expression in ependymal cells and astrocytes has been described in the brain specifically in the forebrain. Within the forebrain, Gal-3 expression was concentrated in the subventricular zone (SVZ), an area of neurogenesis. Gal-1 promotes SVZ neurogenesis and recovery after stroke (Sakaguchi et al., 2006, Ishibashi et al., 2007). Gal-3 maintains and promotes neuroblast migration in the SVZ, this process might be mediated through an epidermal growth factor receptor-based mechanism (Comte et al., 2011). These previous findings suggest a similar mechanism could exist within the spinal cord with Gal-3 involved in mediating neurogenic activity of the ependymal cells.

When compared to FG labelling there were very few SPNs labelled with Gal-3. Gal-3 only labelled 1-4 SPNs in the IML region and 1-3 SPNs in the IC region. Why only a subset of SPNs are labelled with Gal-3 is open to question. Interestingly, Gal-3 is used as a biomarker of heart failure with Gal-3 expression upregulated in activated macrophages in myocardial tissue (De Boer *et al*., 2010), but a link between the Gal-3 labelled IML SPNs and cardiovascular function has not been described.

A possible explanation is that Gal-3 is only upregulated in SPNs following injury or disease. Previous research on Gal-3 upregulation following spinal cord injury at thoracic segment 9 found there was an increase in Gal-3 protein expression in microglia as measured by western blot experiments (Rotshenker *et al.*, 2008; Pajoohesh-Ganji *et al.*, 2012). Gal-3 gene expression was higher in microglia in a mouse model of amyotrophic lateral sclerosis when compared wild type

(Nikodemova *et al.*, 2014). Given Gal-3's role as a neuroinflammatory marker, it suggests SPNs could serve a function in injury response. Future experiments could investigate whether there is an increase in Gal-3 labelled SPNs in conditions associated with inflammation, such as heart failure, hypertension and spinal cord injury.

3.5.2 NOS1 labels SPNs and tends to label more SPNs than Galectin

NOS1 labelling of SPNs in the IML has been documented in previous work on mice and rats (Dun et al., 1992, Blottner and Baumgarten, 1992, Anderson et al., 1995). As described previously, NOS1 antibody only labelled a subset of SPNs when compared to FG-labelled SPNs in the same spinal cord slice (Table. 3.2). With 45.4% of IML FG-positive SPNs being labelled by NOS1 antibody. Previous research in rats by Blottner and Baumgarten compared anti-ChAT labelling of IML SPNs to a NOS1 antibody and found that NOS1 only labels a subset of SPNs within the IML (48.9% of ChAT-labelled SPNs) (Blottner and Baumgarten, 1992). A similar percentage of IML SPNs were labelled in the present study compared to Blottner and Baumgarten study suggesting NOS1 labelled IML SPNs may influence specific peripheral targets (Blottner and Baumgarten, 1992). NOS1 expression has been demonstrated to vary in SPNs according to the ganglia they innervate in a study conducted on rats; adrenal medulla (98.6%) and major pelvic ganglia (89%) projecting SPNs had the highest levels of NOS1 immunoreactivity compared to SPNs that projected to the superior cervical (75.3%) and coeliac ganglia (54.8%) (Hinrichs and Llewellyn-Smith, 2009). It is likely the FG-labelled SPNs could project to the major pelvic or coeliac ganglia given that the FG was administered intraperitoneally, as a result this also suggests that some of the NOS1 immunoreactive SPNs project to these ganglia as well. The function of these

NOS1 immunoreactive SPNs is currently unknown however previous research has shown nitric oxide produced by NOS1 has a tonic excitatory effect on sympathetic vasomotor tone. Blocking NOS1 activity using 7-nitroindazole, a specific NOS1 antagonist, in the thoracic cord resulted in a decrease MAP, HR and sympathetic activity (Poon et al., 2016).

Compared to Gal-3, NOS1 labelled more SPNs in the IML and IC region. Retrograde tracing studies have found SPNs within the IC region send axons to the inferior mesenteric and major pelvic ganglia however it is unclear whether these are the only ganglia these cells project to (Hinrichs and Llewellyn-Smith, 2009). It is possible that the NOS1 immunoreactive SPNs within the IC project to these ganglia however the exact function of these cells and how they interact with the ganglia is unknown.

While NOS1 labelled more SPNs than Gal-3, NOS1 IHC in FG-labelled tissue confirmed that NOS1 only labels a specific subset of SPNs within the general population located in the IML. NOS1 is a promising marker for SPNs due to its specificity however, it needs to be confirmed whether all NOS1 positive SPNs are involved in cardiovascular control, which would make it a useful marker to isolate subsets of SPNs with this function.

3.5.3 Comparisons between FG and antibodies

FG efficiency for labelling SPNs has been documented by previous studies (Ambalavanar and Morris, 1989, Anderson and Edwards, 1994, Pyner and Coote, 1994b). When compared to the candidate antibodies, ChAT, NOS1 and Gal-3, FG labelled more SPNs in the IML and IC region. NOS1 antibodies did label more IPPE-located cells than FG however these cells are not SPNs as FG has been demonstrated to label all SPNs; the identity of these cells is unknown at present.

3.6 Conclusion

This series of experiments has identified Gal-3, as a novel marker of a subset of SPNs in the mouse spinal cord. Gal-3 labels a small number of SPNs within the IML and IC region and ependymal cells in the central canal. Gal-3 could be used in conjunction with another SPN marker to label a larger number of SPNs. NOS1 labels a greater number of SPNs than Gal-3, however it also only labels a subset of SPNs. NOS1 could potentially be combined with Gal-3 to increase the number of SPNs labelled in the IML. ChAT therefore appears to be the best marker for SPNs as it labels the most SPNs across the thoracic spinal cord section. Despite identifying these markers of SPNS, none were suitable to allow selection of SPNs using FACS. Other methods of selecting SPNs will therefore need to be developed.

Chapter 4

The molecular clock in sympathetic preganglionic neurons in thoracic spinal cord

4.1 Introduction

As noted in the introduction, the master clock is located in the hypothalamus within a structure called the suprachiasmatic nucleus (SCN) which is composed of roughly 20,000 neurons that are coupled together (Mohawk *et al*., 2012). In addition to the master central clock, peripheral clocks have been described in a number of tissues; including the heart, lung, pituitary gland, cornea, liver and kidney.

Circadian dynamics have been primarily studied in the SCN and a few peripheral tissues using quantitative polymerase chain reaction (qPCR) or immunofluorescence paired with imaging or with real-time bioluminescence recordings. Most studies on peripheral clocks use qPCR to determine potential rhythmic expression in target genes (Akhtar *et al*., 2002, Storch *et al*., 2002, Panda *et al*., 2002, Miller *et al*., 2007, Hughes *et al*., 2009, Mohawk *et al*., 2012). For example, a study on mRNA expression in the liver using microarrays found roughly 9% of 2122 genes were rhythmically expressed between day and night periods. These genes were involved in a number of important processes in the liver ranging from glucose metabolism, cellular vesicle trafficking, cytoskeletal structure and detoxification, suggesting these processes all exhibit rhythmicity (Akhtar *et al*., 2002).

The rhythmicity of clock genes/proteins *PER1*, *PER2*, *BMAL1* and *CRY1* mRNA, has been observed in tissues in the cardiovascular system, including in the heart and cells cultured from cardiomyocytes and blood vessels (McNamara *et al.*, 2001; Nonaka *et al.*, 2001; Storch *et al.*, 2002; Davidson *et al.*, 2005; Durgan *et al.*, 2005; Takeda *et al.*, 2007; Chalmers *et al.*, 2008; Du Pré *et al.*, 2017). As discussed in section 1.6 of the introduction, rhythmic oscillation of

clock genes/proteins were observed using qPCR, bioluminescent recordings or microarray. Some of these rhythms were diurnal in response to light as a zeitgeber, while others were circadian, oscillating over a period of time. Deletion of clock genes in cell specific or whole animal knockout has been demonstrated in previous research to have effects on cardiovascular function, indeed a number of cardiovascular parameters such as HR and BP display diurnal rhythmicity and loss of BP rhythm has been attributed to the onset of cardiovascular events (see Table 1.1, Figure 1.2 in Introduction) (Takeda and Maemura, 2016; Crnko *et al.*, 2019). Diurnal rhythms in sympathetic outflow has been correlated to BP rhythmicity through measurements of MSNA using microneurography or plasma adrenaline and noradrenaline concentration (Tuck *et al*., 1985; Grassi *et al.*, 2008; Lambert *et al.*, 2014). IML SPNs are key regulators of sympathetic outflow regulating BP as they play a role in the baroreceptor reflex response increasing BP (Tuck, 1986; Pilowsky and Goodchild, 2002; Schreihofer and Guyenet, 2002; Guyenet and Stornetta, 2004; Gordan *et al*., 2015). Therefore it is likely these cell types are involved in maintaining BP rhythmicity and express clock genes/proteins.

Most studies have focused on peripheral clocks located in the liver or heart however there are no studies that have looked for potential peripheral clocks in the spinal cord cells that influence cardiovascular control. The SCN is thought to influence peripheral clocks through the autonomic nervous system and endocrine system (Mohawk *et al*., 2012, Takeda and Maemura, 2016). Indeed, there may be only a few synapses between the SCN and SPNs. The Hosoya and Ranson studies ionophoretically injected tracers, biotinylated dextran amine and phaseolus vulgaris leucoagglutinin, directly into the paraventricular nucleus (PVN) and direct injections of retrograde tracer cholera toxin subunit B into

either the superior cervical or stellate ganglion. The SCN has GABAergic projections to the PVN; the dorsal paraventricular nucleus has spinally projecting neurons which project to the thoracic intermediolateral cell column (IML), a SPN-rich region. The PVN efferents are in very close association to SPNs projecting to the stellate ganglion and the superior cervical ganglion, suggesting that the PVN could influence cardiac sympathetic outflow (Hosoya *et al*., 1991, Ranson *et al*., 1998). Stimulation of PVN neurons also elicits a response in RVLM neurons which provide excitatory and inhibitory drive to SPNs (Coote *et al*., 1998, Guyenet, 2006). Previous research has demonstrated the removal of sympathetic efferents to the liver and heart through surgical or chemical methods resulted in the loss of diurnal rhythms of plasma glucose concentration and BP rhythmicity (Siaud *et al.*, 1994; Warren *et al*., 1994; Briaud *et al*., 2004; Cailotto *et al.*, 2005, 2009). SPNs are an important cell type, influencing sympathetic nervous activity to end organs, therefore this circuit and the PVN's influence on sympathetic outflows suggests these cells can be influenced by the central clock and may play a crucial role in determining the rhythms of peripheral clocks.

The presence of a peripheral clock in the spinal cord has not been described previously. Considering that sympathetic nervous activity shows a circadian activity that has been correlated with diurnal rhythmicity in BP (see Chapter 1), sympathetic preganglionic neurones could be good candidates to express clock activity (Millar-Craig, Bishop and Raftery, 1978; Narkiewicz *et al.*, 2002; Grassi *et al.*, 2008; Lambert *et al.*, 2014). This would be functionally important, since, for example, the pulses of the sympathetic neurotransmitter norepinephrine can phase shift clock gene expression in blood vessel epithelium and liver (Terazono *et al*., 2003, Reilly *et al*., 2008).

Since a selective marker for SPNs or VHMNs was not identified in the experiments described in the previous chapter, it was not possible to isolate SPNs using flow cytometry. ChAT was still the best marker for IML SPNs, labelling the greatest number of SPNs in the IML, IC and IPPe, when compared to Gal-3 and NOS1. Anti-ChAT was therefore used in IHC/IF experiments to identify IML SPNs. Previously, micropunches of spinal tissue containing IML revealed expression of GABA receptors in the IML, hence this approach was adopted (Wang *et al*., 2008a). The experiments that follow therefore examine for the presence of clock genes, BMAL1 and PER2 in micropunch samples of the IML. The presence of the clock proteins, BMAL1 and PER2, in IML SPNs, as identified by ChaT antibody, was then examined using IHC/IF.

4.2 Summary and objectives

Peripheral clocks are found in a number of tissues and are usually characterized by the diurnal expression of clock genes/proteins BMAL1 and PER2 (Evans *et al*., 2015, Ono *et al*., 2015). Previous research has described the diurnal rhythm of BMAL1 and PER2 primarily in the SCN but this rhythmicity has also been described in other areas of the brain, liver and kidneys (Herichova *et al*., 2007, Evans *et al*., 2015, Sinturel *et al*., 2017). A long-standing question in molecular clock studies is how the central clock located in the SCN exerts influence on peripheral clocks in other tissues; previous research suggests that either the autonomic nervous system, specifically the sympathetic nervous system, could be involved (Mohawk *et al*., 2012, Takeda and Maemura, 2016). Previous research has not focused on characterizing the peripheral clock in spinal cord cell types. Sympathetic preganglionic neurons (SPNs) are the last point of influence the central nervous system has on sympathetic nervous system activity. The majority of SPNs are located in the

intermediolateral cell column (IML) region of spinal cord (Deuchars and Lall, 2015). Diurnal rhythm of BMAL1 and PER2 gene and protein expression in SPNs would be indicative of a peripheral clock being present in these cell types and would suggest they possess a diurnal rhythm of activity. Previous studies have paired quantitative polymerase chain reaction (qPCR) with immunofluorescence (IF) and microscopy to study changes in diurnal rhythms of clock genes *BMAL1* and *PER2* mRNA and protein expression in tissue culture as well as fixed tissue slices (Ramanathan *et al*., 2006, LeSauter *et al*., 2012, Leach *et al*., 2013, Evans *et al*., 2015, Barca-Mayo *et al*., 2017).

Research questions:

1. Are clock proteins BMAL1 and PER2 present in sympathetic preganglionic neurons?
2. Do BMAL1 and PER2 exhibit a diurnal rhythm in sympathetic preganglionic neurons?

4.3 Materials and methods

All immunofluorescence (IF) experiments were conducted on tissue from C57Bl/6 mice (N=5 for each time point). Mice for qPCR and immunofluorescence were sacrificed at 7:30 AM or 7:30 PM (N=5 for each time point). Antibodies are listed in Table 3.1. Fluorescent images were obtained as described in section 2 of General Methods. For qPCR, mice were terminally anaesthetized with an intraperitoneal injection of sodium pentobarbital (60 mg/kg) and transcardially perfused with sucrose artificial cerebrospinal fluid (aCSF). Following perfusion the spinal cord was dissected out and the meninges removed. Thoracic spinal cord segment was embedded in agar and sectioned at 300 µm. The region of interest, the IML, was identified based on visual observation of the spinal cord morphology; a 350 µm tissue corer was

used to select and remove the IML area from the surrounding tissue. The IML samples were then placed in Trizol and the RNA extracted and purified using a kit. cDNA was synthesized from the RNA and subsequent qPCR was performed. Mean relative mRNA expression values of BMAL1 and PER2 were calculated and compared using GraphPad Prism 7 software. Statistical analyses were performed using GraphPad Prism 7, a Mann-Whitney test was used.

Measurement of fluorescent intensity of clock proteins in IHC-labelled tissue was conducted using FIJI software. Z-stacks composed of 13 optical slices were summed into a composite image, the channel tool was used to switch between the 3 fluorescent labels. The composite image was scanned through each individual image to find a clear representation of SPNs labelled with the clock protein of interest. When a measurement was taken the red channel was selected corresponding to the Alexafluor555 labelled clock protein. A free-form outline was traced around the nuclei of ChAT-positive and clock-protein positive SPNs then a measurement was taken using the measure feature of the software. A background measurement of fluorescent intensity was obtained by tracing a free-form outline in an area of general labelling. The relative intensity of clock proteins was obtained by subtracting the background fluorescence intensity from the clock protein intensity. The mean relative intensity of clock protein was calculated and compared between the two time points using GraphPad Prism 7 software. Statistical analyses were performed using GraphPad Prism 7, a Student’s unpaired T-test was used.

4.4 Results

4.4.1 Diurnal rhythm of expression of select mRNA in IML region of thoracic spinal cord

qPCR of RNA extracted from IML-containing micropunches of the spinal cord revealed that BMAL1 mRNA expression showed a trend of being higher in the evening when compared to morning (Figure 4.1; $p = 0.6$). In contrast, PER2 mRNA expression was significantly higher in the morning compared to evening (Fig. 4.2; $p<0.0001$). These data suggest that expression of clock genes exhibit rhythms in the IML.

4.4.2 Fluorescent intensity of clock proteins in SPNs

Thoracic spinal cord tissue was labelled with both BMAL1 and PER2 antibodies (Figure 4.3) at both time points, 7:30 AM/PM (N=5 animals for each time point, n= 18 sections). Dual immunofluorescence with antibodies to ChAT confirmed the presence of clock proteins in SPNs in the IML and IPPe (Figures 4.3 and 4.4). The fluorescent intensity of clock protein labelling seemed to vary between the time points based on visual inspection of the slice using fluorescence microscopy. Furthermore DAPI labelling confirmed nuclear localization of clock proteins. Comparisons were made between the mean relative intensities of the clock proteins measured in tissue sacrificed at 7:30 AM/PM (Figure 4.5-4.7). Relative mean intensities of clock proteins in SPNs were compared in cells located in IPPe, IML or both areas combined between time points.

BMAL1: When combining all SPNs (Figure 4.5), BMAL1 intensity in SPNs from tissue perfused at 7:30 AM was 98.4 ± 3.7 relative units and 60 ± 3.3 relative units in 7:30 PM tissue ($p=0.0001$). Examining only SPNs in the IML (Figure 4.6) revealed that BMAL1 intensity was significantly higher in 7:30 AM tissue (103.5 ± 4.3 relative units) compared to 7:30 PM tissue (62.1 ± 3.9 relative units; $p=0.0001$). Similarly, in IPPe SPNs (Figure 4.7), BMAL1 intensity was

89.1 ± 6.8 relative units in 7:30 AM tissue and significantly lower at 55.3 ± 5.8 relative units in 7:30 PM tissue (p=0.0001).

PER2: when either all SPNs (Figure 4.5), SPNs in the IML only (Figure 4.6) or SPNs in the IPPE (Figure 4.7) were examined, PER2 did not significantly differ between the time points.

All SPNs: 7:30 AM: 60.9 ± 4.1 relative units, 7:30 PM: 58.2 ± 3.2;

IML SPNs: 7:30 AM: 64.5 ± 6.0 relative units, 7:30 PM: 50.1 ± 4.2

IPPe SPNs: 7:30 PM: 58.4 ± 5 relative units compared 7:30 AM: 51.7 ± 5 relative units)

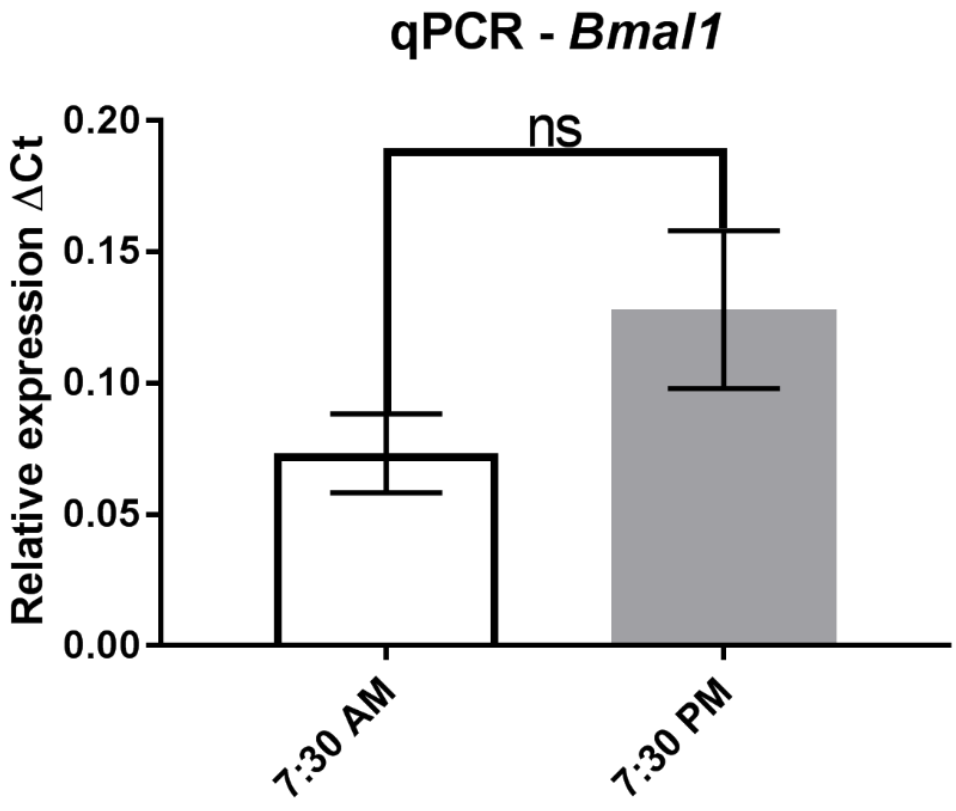

Figure 4.1 The effect of light-dark cycle on clock gene BMAL1 in IML micropunches.
qPCR analysis of BMAL1 gene expression in IML micropunches, results are average of triplicate readings for each animal ±SEM, n=5 in each group. Significance measured with Mann-Whitney test: n.s (not significant), * (p<0.05), ** (p<0.01), *** (p<0.001), **** (p<0.0001).

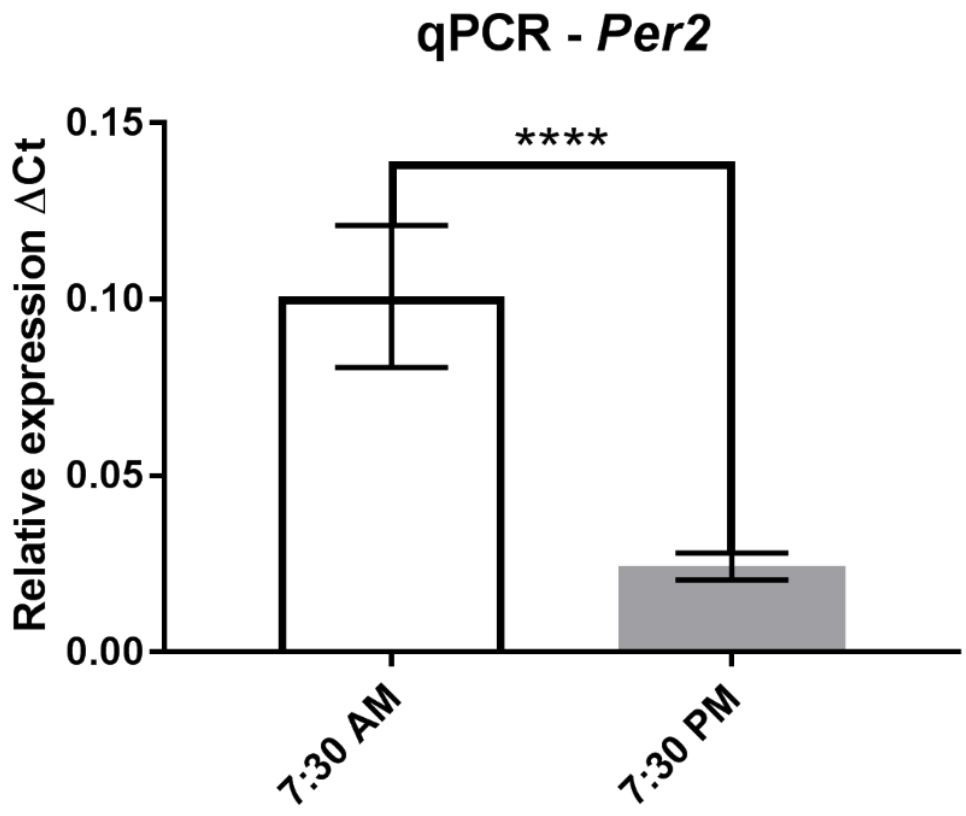

Figure 4.2 The effect of light-dark cycle on clock gene PER2 in IML micropunches.
qPCR analysis of PER2 gene expression in IML micropunches, results are average of triplicate readings for each animal ±SEM (n=5 animals in each group). Significance measured with Mann-Whitney test: n.s (not significant), * ($p<0.05$), ** ($p<0.01$), *** ($p<0.001$), **** ($p<0.0001$).

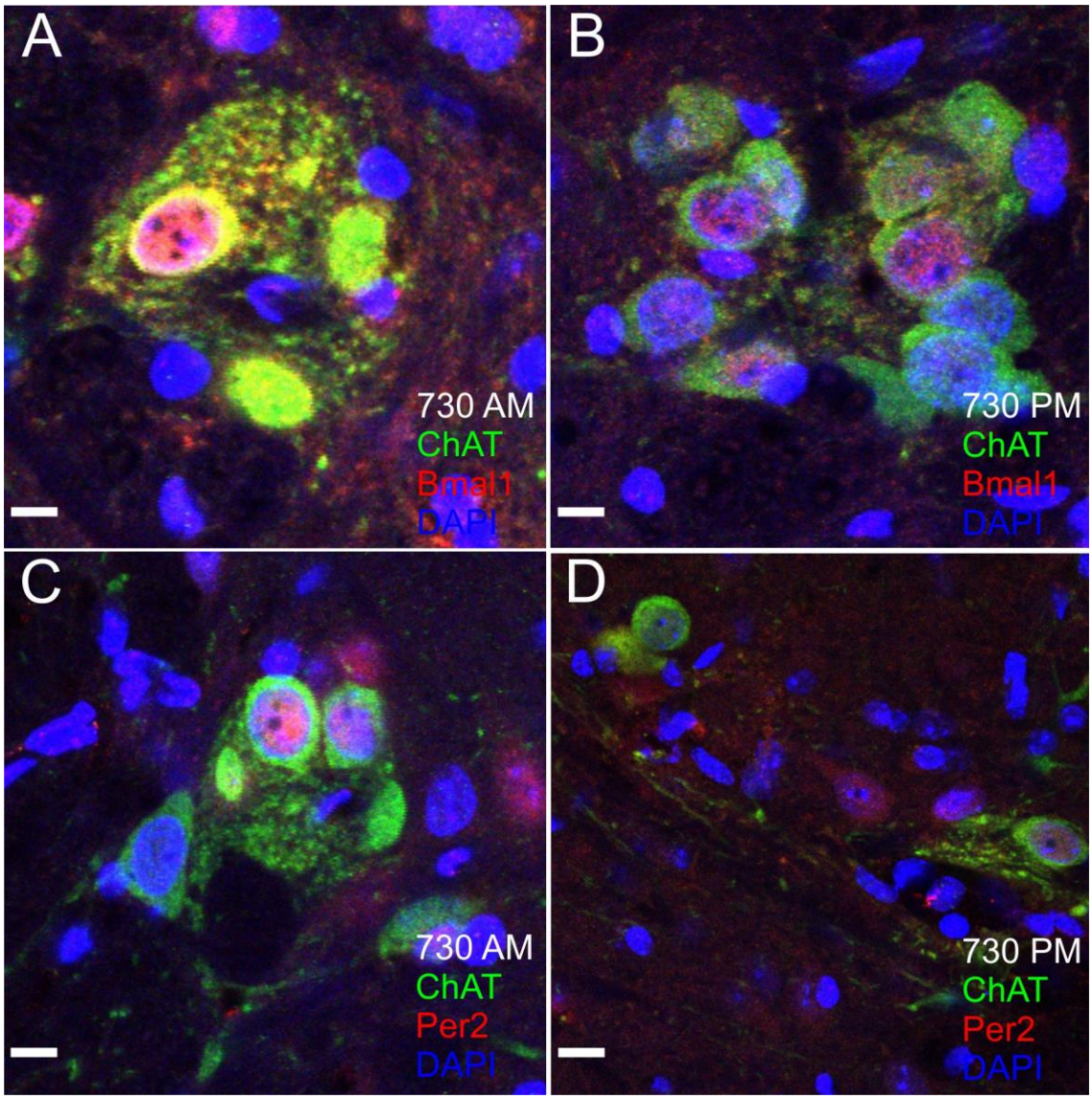

Figure 4.3 Representative confocal images of BMAL1 and PER2 immunofluorescence (red) in the lateral horn of the spinal cord.
IML SPNs are labelled with ChAT (green), clock protein BMAL1 and PER2 are labelled with antibodies against BMAL1/PER2 (red), and nuclei with DAPI (blue). Sections were obtained from mice perfuse fixed at 7.30am or 7.30pm. Scale bars: A-D = 20 μm.

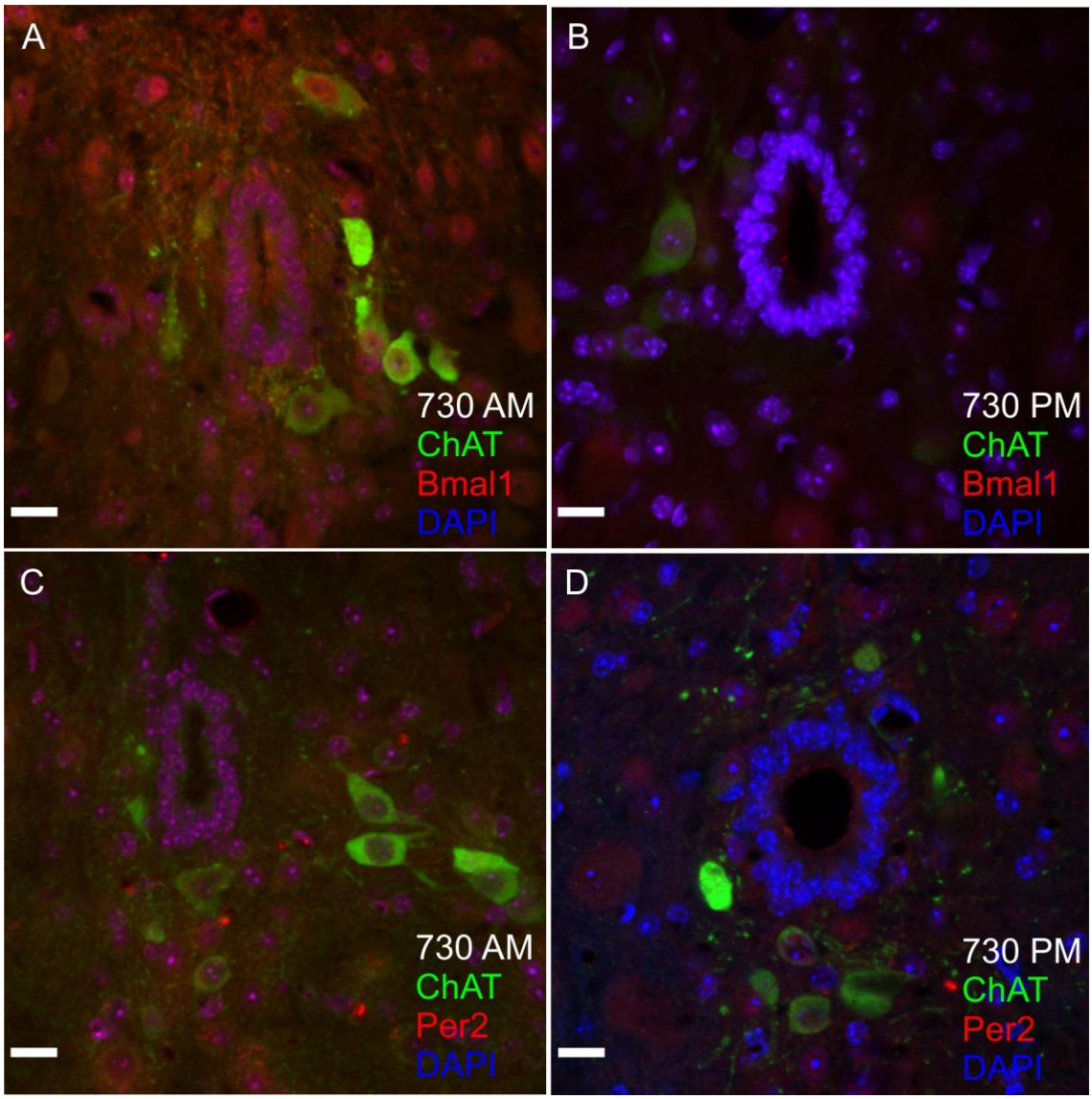

Figure 4.4 Representative confocal images of BMAL1 and PER2 immunofluorescence (red) in the central autonomic area of the spinal cord.
Cells are labelled with ChAT (green), clock protein BMAL1 and PER2 are labelled with antibodies against BMAL1/PER2 (red), and nuclei with DAPI (blue). Cells are thought to be SPNs based on location and morphology. Sections were obtained from mice perfusion fixed at 7.30am or 7.30pm. Scale bars: A-D = 20 μm.

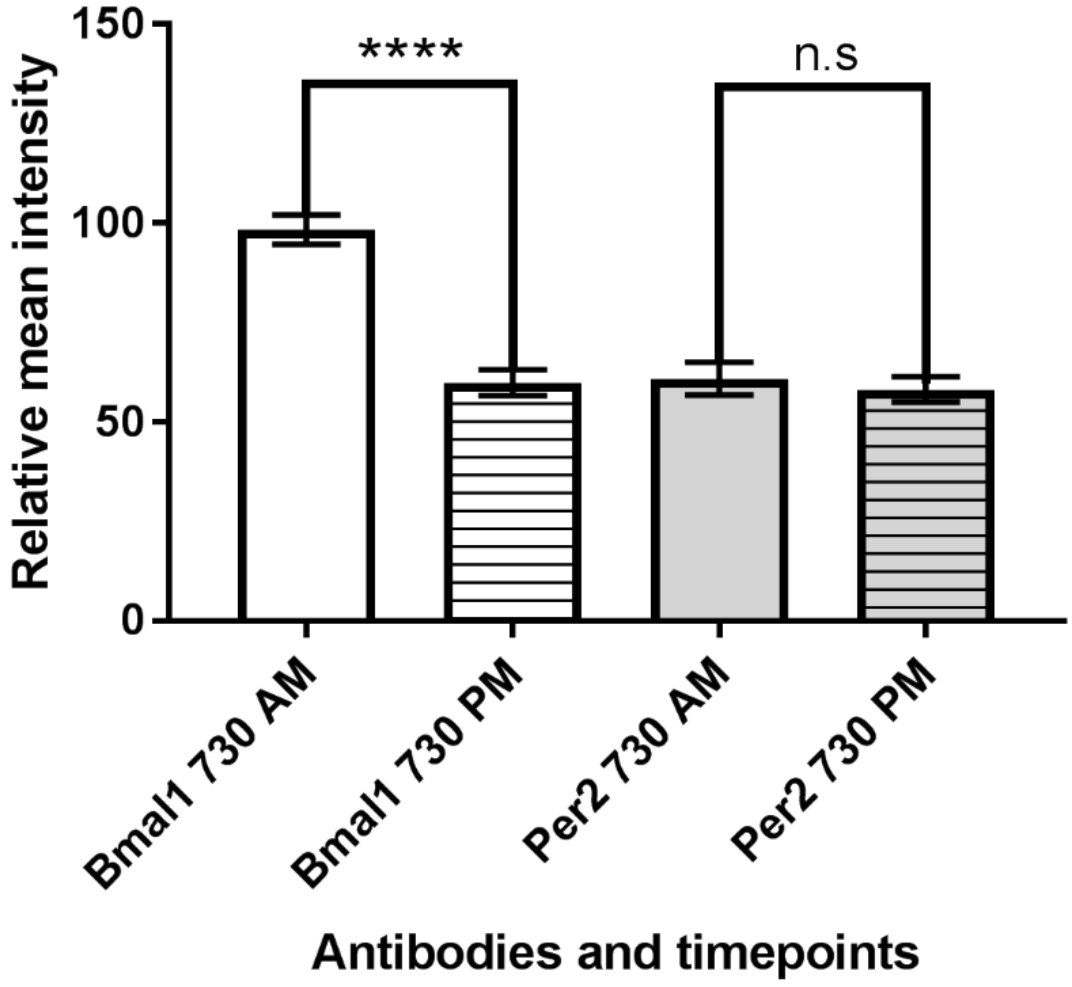

Figure 4.5 Comparison of immunofluorescence of all SPNs labelled by BMAL1 or PER2 antibodies.
Mean relative intensity ±SEM of immunofluorescence of Chat-positive SPNs that were labelled by BMAL1 or PER2. Results are an average of mean intensity measurements of the immunofluorescence of both central canal and IML SPNs from 18 sections from each animal (n=5). Significance measured with Student's unpaired t-test: n.s (not significant), * ($p<0.05$), ** ($p<0.01$), *** ($p<0.001$), **** ($p<0.0001$).

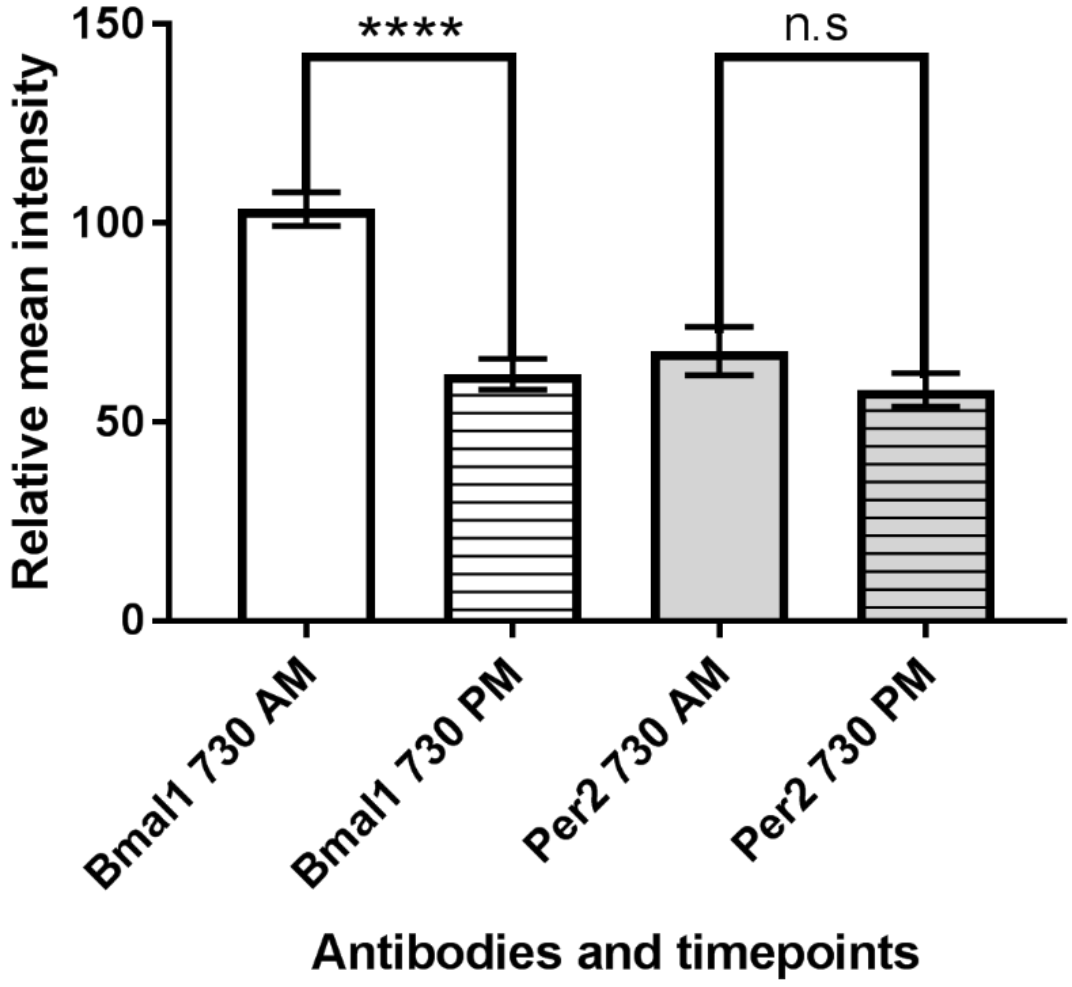

Figure 4.6 Comparison of immunofluorescence of IML SPNs labelled by BMAL1 or PER2 antibodies.
Mean relative intensity ±SEM of immunofluorescence of Chat-positive SPNs that were labelled by BMAL1 or PER2. Results are an average of mean intensity measurements of immunofluorescence of IML SPNs from 18 sections from each animal (n=5). Significance measured with Student's unpaired t-test: n.s (not significant), * ($p<0.05$), ** ($p<0.01$), *** ($p<0.001$), **** ($p<0.0001$).

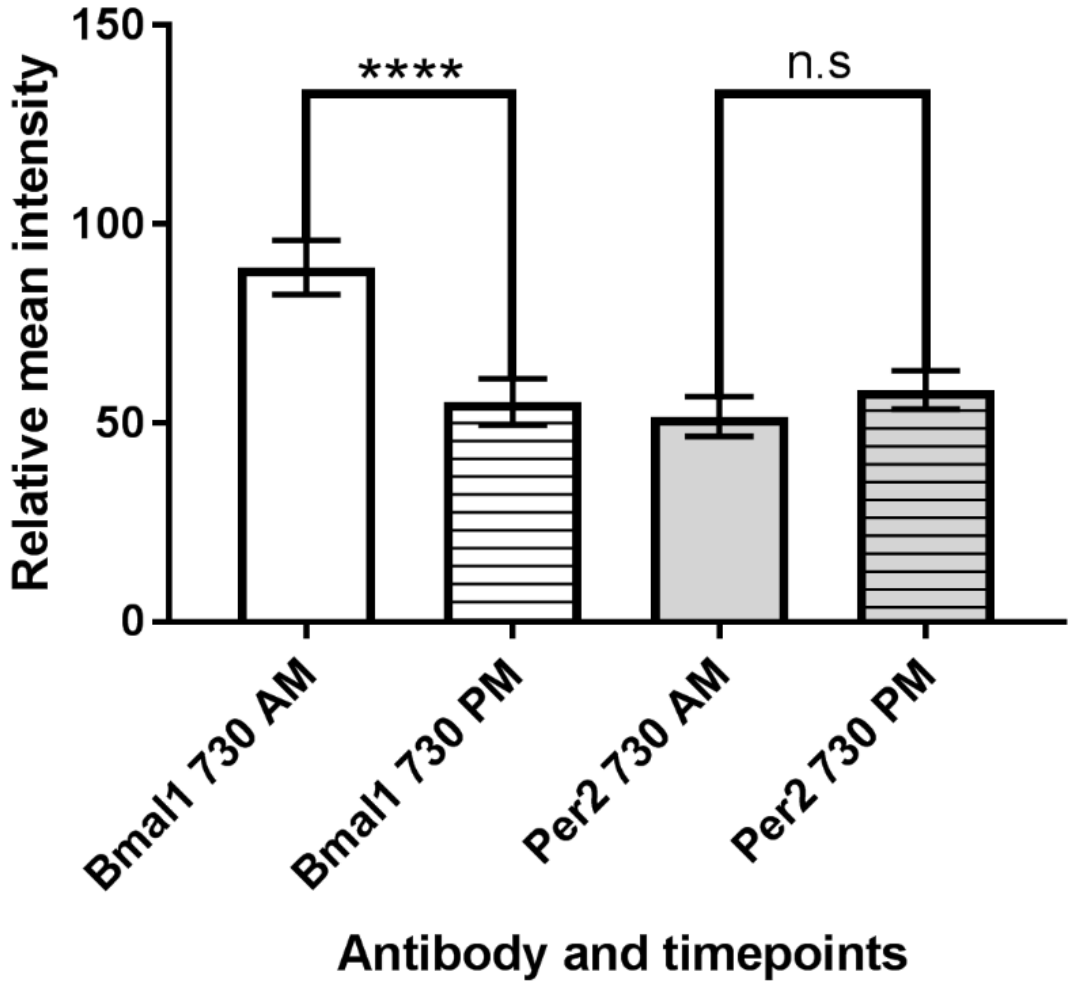

Figure 4.7 Comparison of immunofluorescence of lPPe SPNs labelled by BMAL1 or PER2 antibodies.
Mean relative intensity ±SEM of immunofluorescence Chat-positive SPNs that were labelled by BMAL1 or PER2. Results are an average of mean intensity measurements of immunofluorescence of central canal SPNs from 18 sections from each animal (n=5). Significance measured with Student's unpaired t-test: n.s (not significant), * ($p<0.05$), ** ($p<0.01$), *** ($p<0.001$), **** ($p<0.0001$).

4.5 Discussion

These experiments have demonstrated for the first time that clock genes, BMAL1 and PER2 are present in SPNs and display diurnal rhythms in both their mRNA and protein expression levels. The experiments in this chapter have determined:

- The expression of Clock genes BMAL1 and PER2 vary with the time of day
- Clock proteins, BMAL1 and PER2, are present in IML and IPPe SPNs
- Clock proteins exhibit diurnal rhythmicity with BMAL1 displaying significantly higher levels during the morning

4.5.1 Diurnal rhythm of mRNA expression

The circadian rhythm of clock genes in peripheral clocks is set by the central clock located in the suprachiasmastic nucleus of the hypothalamus therefore the rhythm of clocks across the body should be uniform with *BMAL1* mRNA peaking in the evening and *PER2* mRNA peaking in the morning in mice (Buhr and Takahashi, 2013). The results in this chapter are broadly consistent with this – *PER2* mRNA was higher in the morning (7.30am), and there was a strong trend towards *BMAL1* mRNA being significantly higher in the evening (7.30pm). Other genes involved in the molecular clock could be added to this study in future, such as Rev-Erb, which represses *BMAL1* transcription (Ko and Takahashi, 2006, Mendoza-Viveros *et al*., 2017). In addition, more select sampling of SPNs may reveal if there was a rhythm of expression of *PER2* within SPNs and not other cells in the IML, which could have diluted the signal in the micropunch approach used here. Nevertheless, the detection of some rhythmic expression in this study merited examination of protein levels.

4.5.2 BMAL1 and PER2 are present in SPNs

BMAL1 and PER2 are integral to the function of the molecular clock with BMAL1 being involved with the positive arm and PER2 with the negative arm. The cycling of these genes and the proteins they encode is how diurnal rhythmicity is controlled in mammals (Ko and Takahashi, 2006, Mohawk *et al*., 2012). BMAL1 and PER2 proteins were detected in thoracic spinal sections; with labelling observed throughout but particularly noted in the IML, central canal and ventral horn regions. ChAT labelling confirmed the presence of clock proteins in SPNs. In the IML it is likely that all ChAT cells are SPNs, but in the central canal region there is the possibility that some ChAT cells also express GAD67 (Gotts *et al*., 2016). The presence of these proteins indicates that a peripheral clock exists within SPNs and may govern SPN function which in turn suggests these cells may exhibit diurnal rhythms of activity.

The discrepancy between BMAL1 and PER2 mRNA and protein levels between the morning and evening time points may be explained by the time required for increases in mRNA to be translated and reflected in protein levels. Previous work in the mouse SCN has demonstrated peak *PER2* mRNA levels in the morning were followed by peak PER2 protein levels at midday 6 hours later (Buhr and Takahashi, 2013). This could explain the difference between *PER2* mRNA rhythmicity not being reflected in PER2 protein rhythmicity in the IF experiments. Future experiments could add more time points across the morning and evening to characterize the diurnal rhythm of clock gene and protein expression.

Diurnal rhythms of SNA has been correlated to BP rhythmicity in both human and animal models (Millar-Craig *et al*., 1978; Narkiewicz *et al.*, 2002; Grassi *et al.*, 2008; Lambert *et al.*, 2014; Mahadi *et al.*, 2019). Furthermore the removal of

sympathetic input to ganglia involved in the maintenance of BP results in disruption of BP rhythmicity (Siaud *et al.*, 1994; Warren *et al*., 1994; Briaud *et al*., 2004). IML SPNs are involved in the baroreceptor reflex response and function to increase BP (Schreihofer and Guyenet, 2002; Andresen *et al.*, 2006; Guyenet, 2006). The possession and diurnal rhythm of clock genes in this cell type suggests their functional output is likely to vary throughout the morning and evening and could potentially influence BP rhythmicity. Further work is required to characterize diurnal rhythmicity of SPN activity and link the activity of these cells to functional changes in end tissue/organs.

4.5.3 Diurnal rhythm of clock proteins in SPNs

In order to confirm the clock proteins in SPNs display a diurnal rhythm, IF was carried out in tissue from animals sacrificed at 7:30 AM and 7:30 PM. The molecular clock cycle begins with BMAL1 and another protein, Clock, forming a heterodimer within the nucleus which then activates the translation of *PER* and *CRY* genes. PER and CRY proteins heterodimerize, forming a complex with another protein casein kinase 1ε/δ and move from the cytoplasm back into the nucleus where they negatively regulate the translation of their own genes (Lowrey and Takahashi, 2011, Mohawk *et al*., 2012). Use of DAPI allowed visualization of the nucleus of the SPNs labelled with ChAT and BMAL1/PER2 thereby allowing the nuclear translocation of the clock proteins to be observed between the two time points. BMAL1 protein levels are highest in the nucleus during the morning while PER2 protein levels peak during the evening (von Schantz and Archer, 2003). This is somewhat reflected in the data with BMAL1 protein levels significantly higher in the morning in SPNs. PER2 did not display significant differences in thoracic spinal cord tissue between the two time points which suggests the molecular clock could function differently in these cell types

however further experiments are required. During the evening, PER2 forms a heterodimer with Cry proteins, translocate into the nucleus and negatively regulates the transcription of the *PER* and *CRY* genes, if PER2 protein is not upregulated during the evening in SPNs, another clock protein must be involved in the negative arm of the molecular clock. The PER1 protein could be forming a heterodimer with CRY proteins to halt *PER*/*CRY* gene expression however this was not confirmed in the current study. Previous research has determined peripheral clocks can function independent of the master clock in the SCN and furthermore, peripheral clocks can be entrained to stimuli other than the light cycle such as endocrine signalling, temperature and local signals such as the effect of feeding schedule on gastrointestinal clocks (Vujović *et al*., 2008, Mohawk *et al*., 2012, Hastings *et al*., 2018). These inputs are thought to be integrated to dictate the rhythmic output of the peripheral clock (Mohawk *et al*., 2012). Another potential explanation for lack of difference in PER2 protein levels between the two time points are regulatory mechanisms that act on the transcriptional and translational feedback loop (TTFL). Post-translational regulation of subcellular trafficking and protein degradation could affect PER2 protein levels (Mendoza-Viveros *et al*., 2017). Subcellular trafficking could lead to a lower nuclear accumulation of PER2 protein; in Drosophila the interaction between PER2 protein and Timeless protein facilitates the heterodimer's entry into the nucleus. Mutations within the subunits of the Timeless protein can result in delays to nuclear accumulation (Mendoza-Viveros *et al*., 2017). In terms of mammals the process of nuclear localization of PER2 is not well understood; unlike in Drosophila where PER2 has a narrow window in which it is transported into the nucleus, PER2 is transported gradually in mammals (Mendoza-Viveros *et al*., 2017). The enzymes, glycogen synthase kinase 3 beta (GSK3β) is

responsible for phosphorylating PER2 promoting its nuclear localization whereas casein kinase 1 epsilon (CK1ε) phosphorylates PER2 promoting degradation in the cytoplasm (Iitaka *et al*., 2005). Studies conducted in human embryonic kidney cells and rat SCN demonstrated that CK1ε phosphorylates PER2 protein and promotes its degradation. Co-immunoprecipitation and kinase/phosphatase assays determined that CK1ε and PER2 protein interact with one another and that phosphorylation by CK1ε leads to the degradation of PER2 protein over time (Keesler *et al.*, 2000; Takano *et al.*, 2000; Vielhaber *et al.*, 2000). The presence of these enzymes were not tested for, lower levels of these enzymes in the tissue could result in less PER2 being trafficked into the nucleus. G-protein-coupled receptor kinase 2 promotes phosphorylation of PER2 and supresses nuclear trafficking as demonstrated in by co-immunoprecipitation experiments conducted in mPER2 Luciferase mice; the presence of this enzyme was not tested for and could be another reason for low PER2 trafficking into the nucleus (Mehta *et al*., 2015). Future work could target more clock genes and proteins involved in the molecular clock cycle to determine how the molecular clock functions in IML SPNs.

The SCN is thought to control rhythmicity of autonomic neurons through preautonomic neurons located in the hypothalamus; these cells contact parasympathetic and sympathetic preganglionic neurons in the brainstem and spinal cord (Teclemariam-Mesbah *et al*., 1997, Kalsbeek *et al*., 2006). This could be the output pathway SCN neurons influence the circadian rhythm of SPNs. SCN terminals control the rhythmic activity of the pre-autonomic neurons using differently timed pulses of vasopressin, GABA and glutamate (Teclemariam-Mesbah *et al*., 1997, Kalsbeek *et al*., 2006). The SCN influences the PVN via GABAergic signalling which in turn influences the sympathetic

preautonomic neurons which contact SPNs (Buijs and Kalsbeek, 2001, Kalsbeek *et al*., 2004). The SPN peripheral clock and the diurnal activity of these cell types is most likely influenced by combination of SCN neurotransmitters acting on the PVN projections to preganglionic sympathetic neurons and local stimuli in the spinal cord.

4.6 Conclusion

This series of experiments has demonstrated for the first time that a peripheral clock exists within IML SPNs in the thoracic spinal cord as exemplified by the presence and diurnal rhythms of clock genes BMAL1 and PER2. The ramifications of a clock in this cell type could be significant as they project to a number of ganglia and could potentially drive diurnal rhythms of physiological activity in a number of end organs. Future work could aim to investigate diurnal rhythms in SPN activity potentially through electrophysiological experiments or conduct bioluminescent imaging of SPN activity determined by luciferase under control of ChAT at different time points. *BMAL1* and *PER2* mRNA transcripts were detected by qPCR experiments in time-point IML micropunches and displayed diurnal rhythmicity. Additionally BMAL1 protein diurnal rhythm was observed in IML SPNs by measuring relative intensity in immunofluorescence images; BMAL1 protein levels in the nucleus were higher in the morning. Image analysis confirms rhythmic levels of BMAL1 protein and nuclear translocation of BMAL1 between the time points of 7:30 AM and 7:30 PM. There were two confounding findings in this study, BMAL1 mRNA and PER2 protein did not exhibit a significant diurnal rhythm. As discussed previously this could be due to molecular modulators such transcripts and proteins that are involved in transcriptional or translational regulation that could affect the TTFL components. Future experiments could attempt to profile molecular modulators involved in

transcriptional and translational regulation more specifically in SPNs, for example using single cell or cell type specific RNAseq and possibly local stimuli in the spinal cord.

Chapter 5

Gene expression in the IML and single SPNs examined using RNA-seq

5.1 Introduction

RNA-seq has been increasingly applied to understand expression of genes in the diverse tissues, revealing previously unknown differences in regional and individual cell populations (Rosenberg *et al*., 2018). In the nervous system, RNA-seq has been used to characterize gene expression in cell types from different brain regions or to differentiate cell types based on gene expression profiles from heterogeneous RNA samples from brain regions (Lake *et al*., 2016, Chen *et al*., 2017, Romanov *et al*., 2017, Rosenberg *et al*., 2018). Applying RNA-seq to the IML could therefore reveal genes involved in autonomic control that have not yet been identified. Furthermore, single cell RNA-seq (scRNA-seq) analysis of SPNS has the potential to reveal novel genes in SPNs, or indeed different sub-populations. Transcriptomes generated from RNA-seq of the IML and scRNA-seq could therefore identify genes that affect SPN activity which in turn may influence autonomic control of end organs/systems such as the cardiovascular system.

The first essential step in RNA-seq is sample isolation. Samples can be on the scale of tissue, particular components of tissue (e.g CNS nuclei) or single cells (Nichterwitz *et al*., 2016, Fuzik *et al*., 2016, Ziegenhain *et al*., 2017). Since the IML is a small component of the thoracic spinal cord, it is preferable to isolate it from surrounding tissue in some way. In one previous approach, tissue micropunches and qPCR revealed that the $GABA_A$ α5 subunit was expressed in the rat IML and electrophysiology in spinal cord slices indicated that GABAA receptors in SPNs were likely to contain this subunit (Wang *et al*., 2008a). Therefore, the micropunch approach was first used to examine gene expression in IML of mouse.

Since the IML contains SPNs but also interneurones which may have been captured in micropunch samples, (Deuchars *et al*., 2001, Deuchars, 2015), attempts were made to target single SPNs for scRNA-seq. A number of different technologies have been combined with RNA-seq to capture single cells for processing, these techniques include laser-capture microdissection, microfluidics and aspiration of the whole cell or cytoplasmic contents using a patch electrode (Golubeva *et al*., 2013, Lovatt *et al*., 2015, Nichterwitz *et al*., 2016, Fuzik *et al*., 2016, Cadwell *et al*., 2016, Gokce *et al*., 2016, Abraham and Maliekal, 2017, Ziegenhain *et al*., 2017). A selective marker to facilitate microfluidic isolation of single SPNs was not found in chapter 3, so this approach was not possible. In any case, such isolation procedures may no longer be considered best practice since Eberwine *et al*. states that isolating single cells has the potential to change transcriptional states due to perturbations to the cell during the isolation process. The best way to overcome this problem was to isolate the cell contents while it is still within its tissue matrix or microenviroment (Eberwine *et al*., 2013). This study therefore first isolated RNA from single SPNs in living spinal cord slices by adapting the visualised patch clamp approach.

Although some success was obtained with the above approaches, neither allowed precise timing of collection of tissue, an important consideration if potential circadian rhythms in gene expression are under investigation. In addition, the smallest bore of the micropuncher was large enough to capture many cells from outside of the IML. A method to more specifically focus on the IML was developed, which allowed visualised harvesting of cells from the IML from tissue that had been frozen. This approach was then extended to single

cells, thereby developing a novel approach to isolation of single cells that allows capture from precisely timed tissue from adult animals.

Diurnal variations in SPN activity will be influenced by fluctuations in the expression pattern of specific receptors, which in turn result in variability in how these neurones respond to selective drugs. SPNs are richly innervated by descending inputs, which control their level of activity through activation of a number of receptors. Therefore, whilst RNA-seq provides a platform to analyse the whole gene expression of SPNs, prior knowledge of systems involved in cardiovascular control by the SNS allows specific analysis of influences on these systems.

Major influences are from serotonergic and noradrenergic fibres that densely target SPNs (Deuchars and Lall, 2015). SPNs are depolarised by activation of 5-HT2 receptors or α1 adrenoceptors and 5-HT induces rhythmic network activity in the intermediolateral cell column of spinal cord slice (where descending inputs are lost) or restores rhythmic sympathetic nerve activity in spinalised rats (Yoshimura, Polosa and Nishi, 1987; Marks *et al.*, 1990; Pickering, Spanswick and Logan, 1994; Marina, Taheri and Gilbey, 2006; Deuchars and Lall, 2015). SPNs are also hyperpolarised by activation of 5-HT1A receptors or α2 adrenoceptors, whilst a tonic inhibitory influence on SPNs activity is mediated through α5 containing GABAergic receptors, so the control of SPN activity at the single cell level is complex (Guyenet and Cabot, 1981; Yoshimura, Polosa and Nishi, 1987; Pickering, Spanswick and Logan, 1994; Wang *et al.*, 2008). For example, only occasional influences of 5-HT1A receptors have been reported (Pickering *et al*., 1994). Indeed, administration of 5-HT1A agonists at onset of activity significantly advanced wheel running activity under constant light conditions, suggesting that this receptor plays a

critical role on preparing for activity after rest (Tominaga *et al.*, 1992). Cx36 is gap junction protein that labels IML SPNs and has a role in sympathetic activity. Cx36-KO mice displayed a reduction in sympathetic nerve discharge and a reduction in arterial pressure (Varinder K. Lall *et al.*, 2017). It is likely Cx36 displays a diurnal rhythm within IML SPNs concurrent with the diurnal rhythms of SNA and BP. The expression patterns of genes involved in these systems was therefore analysed with RNA-Seq and, if found present at significant levels, with qPCR.

Research questions:

1. Characterize gene expression profiles of IML micropunches
2. Develop an approach to target the IML more specifically than micropunches
3. Develop a method to allow collection of RNA from SPNs in precisely timed, adult tissue
4. Characterize gene expression profiles of single SPNs

5.2 Materials and Methods

IML micropunches

Adult male C57/BL6 mice (6 weeks old, n=10) were terminally anaesthetized with 60mg/kg intraperitoneal injection of sodium pentobarbital and transcardially perfused with sucrose artificial cerebrospinal fluid (sucrose aCSF) in order to remove blood as well as limit degradation of RNA due to nucleic acid damaging enzymes, nucleases, until the sample was placed in Trizol. Following perfusion the spinal cord was dissected out and the meninges removed. Thoracic spinal cord segment was embedded in agar and sectioned at 300 µm. The region of interest, the IML, was identified based on visual observation of the spinal cord morphology; a tissue corer with a 350 µm diameter was used to select and

remove the IML area from the surrounding tissue. The IML samples were then placed in Trizol and the RNA extracted and purified using a RNA extraction kit followed by a DNAse treatment and finally the sample was purified using a RNA clean and concentrator kit (Zymo Research).

Single cell aspiration from living spinal cord slices

A mix of GAD-positive and wildtype C57/BL6 mice (9-13 days old, n=10) were terminally anaesthetized with 60 mg/kg intraperitoneal injection of sodium pentobarbital and transcardially perfused with sucrose artificial cerebrospinal fluid (sucrose aCSF). Following perfusion, the spinal cord was dissected out and the meninges removed. Thoracic spinal cord segment was embedded in agar and sectioned at 300 µm. The section was placed under an Olympus BX50WI microscope with a Rolera-XR camera and viewed using Qcapture imaging software (Qimaging, Canada). The IML region of the section was identified based on the morphology of the spinal cord slice and using the morphological landmark, the dorsal horn, to properly position the electrode to aspirate cells located in the IML. Once the IML was located, the electrode was lowered into the region and a single cell was selected to aspirate, negative pressure was applied to the electrode using a syringe to suck up the single cell. Aspiration of single cells was conducted in collaboration with a postdoctoral researcher, Claudia Maclean. The single cell was expelled into an Eppendorf tube using positive pressure applied using a syringe. The single cell was stored in 0.5-1 µL of nuclease-free water and placed in -80^{o}C freezer until processed.

Harvesting of IML and single cells from frozen sections

Adult C57/BL6 male mice (6 weeks old, n=10) were terminally anaesthetized with 60mg/kg intraperitoneal injection of sodium pentobarbital. The heads of the mice were separated from the body approximately at the brainstem-cervical spinal cord region. To remove the spinal cord, the skin, limbs and organs were removed so that only a body segment of the back of the animal remained with the spinal cord still within the vertebrae. A 60 mL syringe was filled with warm aCSF solution (temperature maintained at 37^{o}C) which was attached to piece of tubing; the tubing was placed against the opening; the plunger of the syringe was depressed slowly and the pressure was used to eject the spinal cord caudally into a glass dish containing oxygenated aCSF. If the spinal cord was not visible additional rostral body segments of the back of the animal were cut to expose the spinal cord; most ejected spinal cord samples contained thoracic and lumbar regions of spinal cord however due to trimming the rostral body segment not all samples had cervical regions intact. Following ejection the spinal cord was quickly segmented into two thoracic segments and two lumbar segments which were placed into freezing boats filled with OCT and frozen by placing them in a box of dry ice. The freezing boats were labelled to identify the location and type of spinal cord segment. The samples were stored in -80^{o}C freezer until processed. Previous work characterising SPNs in rats used 30-75 µm thick sections and determined the somal axes of IML SPNs was 14 x 30 µm to 28 x 49 µm (Navaratnam and Lewis, 1970; Barber *et al.*, 1984; Tang *et al*., 1995). The thoracic segments were cut using a cryostat, 60 µm thick sections were cut and adhered to labelled polylysine slides and frozen in -80^{o}C freezer until processed.

Slides were cleaned with 70% ethanol then RNAseZap® solution to ensure they were nuclease free. Tissue sections adhered to slides following washes with aCSF confirming that the polylysine coating was not removed by the ethanol or RNAseZap® washes.

The slides with thawed thoracic spinal cord slices were placed in a physiology recording rig, a few drops of aCSF were added to the slide to enable visualisation of the slice. The section was viewed under an Olympus BX50WI microscope using Qcapture imaging software. The IML region was identified based on morphology of the spinal cord. Following this a glass electrode was lowered into the area, negative pressure was applied through a syringe to aspirate multiple cells from the IML region. The multi-cell sample was expelled into an Eppendorf tube using positive pressure applied through a syringe. The tube was stored in -80ºC freezer until processed. The aspiration of the single cells from the IML region followed the same protocol described previously with the exception that in some aspiration experiments a Nikon Eclipse E600FN microscope paired with Qcapture imaging software was used to view the cells. The single cell samples were stored in lysis buffer and placed in -80ºC freezer until processed.

SMART-seq v4 Ultra Low Input Kit for RNA-seq

The concentration of RNA from IML micropunch samples was first determined using a Nanodrop 2000 spectrophotometer (ThermoFisher). 1 µL of the sample was used to measure to RNA concentration.

To prepare the samples for RNA-seq, the IML micropunch sample RNA was diluted to an input amount of 10 nanograms as this was the maximum amount of input RNA for the SMARTseq v4 Ultra Low Input RNA kit (Takara Biotech) to

produce cDNA. In the first step, lysis buffer, 10x reaction buffer and SMART-seq primer were added to the single cell and diluted IML micropunch samples. The solution was heated to 72°C in a preheated, hot-lid thermal cycler for 3 minutes which allowed the primer to anneal to the RNA within the samples. Following this step, the 5x ultra low first-strand buffer, Smart-seq v4 oligonucleotide and Smart-scribe reverse transcriptase were added to samples and were placed in a thermal cycler with a specialized program to reverse transcribe the RNA into cDNA. The program consisted of a 42°C incubation for 90 minutes followed by a 70°C incubation for 10 minutes and a 4°C holding temperature upon completion. The PCR step of the kit involved adding 2X SeqAmp PCR buffer, PCR primer and SeqAmp DNA polymerase to the samples and placing them in a preheated thermal cycler with a specific program based on the input amount of RNA. The programs are summarized below.

Table 5.1 PCR program prescribed for sample type according to SMART-seq v4 kit

Steps	IML micropunch/ IML multi-cell	Single cells
Initial	95ºC for 1 minute	95ºC for 1 minute
Number of cycles	8x	18x
Repeated cycles	98ºC for 10 seconds	98ºC for 10 seconds
	65ºC for 30 seconds	65ºC for 30 seconds
	68ºC for 3 minutes	68ºC for 3 minutes
Final extension	72ºC for 10 minutes	72ºC for 10 minutes
Holding temperature	4ºC	4ºC

cDNA purification using AMPure XP Bead Kit

The final step of the extraction process is cDNA purification using the Agencourt AMPure XP bead kit. Magnetic AMPure XP beads were added to each sample; the beads selectively bind to the cDNA. The samples were placed on a magnetic rack which caused the cDNA-bound beads to form a pellet against the wall of the Eppendorf tube which was held in place by the magnet. Two 70%

ethanol washes were performed. The pellet was left to air dry for two minutes then the cDNA was eluted from the beads using elution buffer. 2 µL sample of purified cDNA was obtained to perform validation using an Agilent 2100 Bioanalyzer. The purified cDNA was stored in -20°C freezer until submitted for library preparation.

Quality Control

Validation of cDNA was performed on an Agilent 2100 Bioanalyzer and Qbit fluorometer. Validation of cDNA library quality was performed on an Agilent D1000 ScreenTape system.

Sequencing

Two different sets of sequencing were conducted. 6 IML micropunches (n= 6 mice) and 26 single cells (n= 10 mice) from live tissue were submitted for library preparation using an Illumina Nextera XT DNA library preparation kit and sequenced on an Illumina HiSeq 3000 using a 150 base pairs, paired-end sequencing.

From frozen tissue, 25 samples comprised of 17 IML (n= 10 mice) and 8 single cell samples (n= 10 mice), were submitted for library preparation using an Illumina Nextera XT DNA library preparation kit. Samples were sequenced on an Illumina NextSeq 500 using a 150 base pairs, paired-end sequencing.

The samples are sequenced on a flow cell, a slide with microfluidic channels through which polymerase, deoxynucleotide triphosphates (dNTPs) and buffers. The cDNA is denatured and strands adhere to the flow cell vertically. The sequencer uses fluorescent probes that are colour coded to the type of nucleotide they bind to. Each nucleotide of each strand is bound by a

fluorescent probe, the sequencer images the bound probes then the fluorescent probe is washed off and the cycle repeats until the entire strand has been sequenced. This process produces the read of the cDNA strand consisting of all the identified nucleotides within the strand. Paired-end sequencing means that cDNA strands are sequenced from both ends of the strand thereby improving the mapping of the reads to the transcriptome improving accuracy and quality of the sequencing data (Eberwine *et al*., 2013, Poulin *et al*., 2016).

IML time point samples and qPCR on diurnal rhythms

Adult male C57/BL6 mice (4-6 weeks old, n=10) were housed in cages in groups of 5. The mice were sacrificed at specific time points: 7:30 AM and 7:30 PM. The spinal cord tissue was prepared as described earlier. The IML samples were obtained using a tissue-corer and processed for RNA extraction and cleanup as described earlier. Briefly Trizol and RNA extraction kit followed by DNAse treatment and RNA clean and concentrator kit (Zymo Research). 1 µg of RNA was used in a reverse transcription reaction to produce cDNA for qPCR using qScript cDNA synthesis kit (Quantas Biosciences). PCR reactions were carried out in triplicate using 12.5 ng of cDNA per reaction and Power SYBR Green master mix (Applied Biosystems) in 20 µl reactions. PCR product was measured using SYBR Green fluorescence on a CFX connect real time PCR detection system thermal cycler (Bio-Rad).

qPCR cycle program for diurnal rhythm samples

The qPCR program for investigating diurnal rhythm of target genes in IML micropunch samples is summarized below in Table 5.2.

Table 5.2 qPCR program used for investigating potential diurnal rhythms in IML micro punch samples

Steps	IML micropunch
Initial	95^{o}C for 10 minute
Number of cycles	39x
Repeated cycles	95^{o}C for 30 seconds
	60^{o}C for 30 seconds
	72^{o}C for 40 seconds
Final extension	72^{o}C for 5 minutes
Holding temperature	4^{o}C

Analyses and Statistics

The output files from sequencing were fastq files, which were analysed using an online platform, Galaxy (Guerler *et al*., 2018). Galaxy analysis produced FastQC reports which indicated the quality of the reads produced from sequencing. Read counts for the data were obtained by counting how many reads mapped to each gene/transcript using two analysis pipelines, Tophat_Cufflinks_Cuffdiff and Subread_featureCounts_DESeq2. The read mapping rate referred to the percentage of successfully aligned reads to a reference genome; the mapping rate was higher in the Tophat_Cufflinks_Cuffdiff pipeline, and therefore further analysis was conducted using the data from this pipeline. The output files from the algorithm pipeline contained read count data, read count values were expressed as the number of reads mapped per kilobase of transcript per million reads (Fragments Per Kilobase Million, FPKM). This value normalised the data for different transcript lengths and library sizes. Graphs and statistical analyses were produced using R software or GraphPad Prism 7.

IML and single cell analyses

For single cell samples, RNA-seq data was analysed from cells expressing mRNA encoding choline acetyltransferase (ChAT), the acetylcholine synthesising enzyme which was used to define the IML samples as likely to contain SPNs and single cells as likely to be SPNs. ChAT-positive samples were determined as having ChAT FPKM values higher than of 5. Using this cut-off limit, 6 IML samples from live tissue out of 6 IML samples were deemed ChAT-positive IML samples; 9 IML samples from the 17 frozen tissue samples were deemed ChAT-positive IML samples. These datasets were merged and were referred to as the IML RNA-seq data and processed as described below. Using this cut-off limit, 5 single cells from live tissue out of 26 single cells were deemed ChAT-positive single cells; 2 single cells from the 8 frozen tissue samples were deemed ChAT-positive single cells. These datasets were merged and were referred to as the scRNA-seq data and processed as described below. The RNA-seq datasets produced from sequencing were large given the number of genes expressed within the IML or single cells so specific attention was paid to groups of channel and receptors that were known or suspected to affect SPN activity. When examining the relative expression of channel and receptor subtype and subunit mRNA, the individual FPKM values measured in each ChAT positive sample of each subunit or subtype mRNA were compared within the respective groups of receptors/channels to determine which subtype or subunit mRNA had the highest expression for each group.

In addition to Chat-positive cells, GAD-positive single cells were selected from the single cell data set for comparison to the Chat-positive cells. GAD-positive cells were identified based on their FPKM values, samples that had GAD FPKM values that were higher than a cut-off FPKM value of 1 were identified as GAD-

positive samples. Differential gene analysis was performed using the Tophat_Cufflinks_Cuffdiff comparing ChAT-positive single cells to GAD-positive single cells in order to identify genes specifically expressed in SPNs.

5.3 Results

IML and single cell library quality control

Single cells were successfully aspirated from fresh and fresh-frozen sections using a pipette (Figure 5.1). Prior to being run on the sequencer, the IML and SC libraries underwent a final quality control step using the Agilent D1000 ScreenTape system. This instrument measures the base pair length of cDNA fragments or reads within a library based on fluorescence intensity measurements. An ideal library is composed of reads between 200 and 500 base pairs in length. Both the IML and SC libraries are composed of reads of this length (Figure 5.2-3). The IML micropunch sample (Figure 5.2A) and IML multi-cell samples (Figure 5.2B) produced libraries that were similar in quality of reads. No difference in read quality was observed when comparing SC libraries obtained from fresh (Figure 5.3A) or frozen sections (Figure 5.3B).

Comparing RNA sequencing with Allen Brain Atlas *In situ* Hybridisation

The RNA-seq results were paired with *in situ* hybridization (ISH) images for the same genes (when available) from the Allen brain atlas (ABA) to depict mRNA expression using a different method, but also to help determine whether mRNA expression was observed in IML SPNs (Table 5.3). Genes studied, described below in alphabetical order were: adrenergic alpha 1/2 receptors, voltage-gated calcium channels, muscarinic acetylcholine receptors, nicotinic acetylcholine receptors, $GABA_A$ and $GABA_B$ receptors, glutamate receptors, 5-HT receptors and sodium channels.

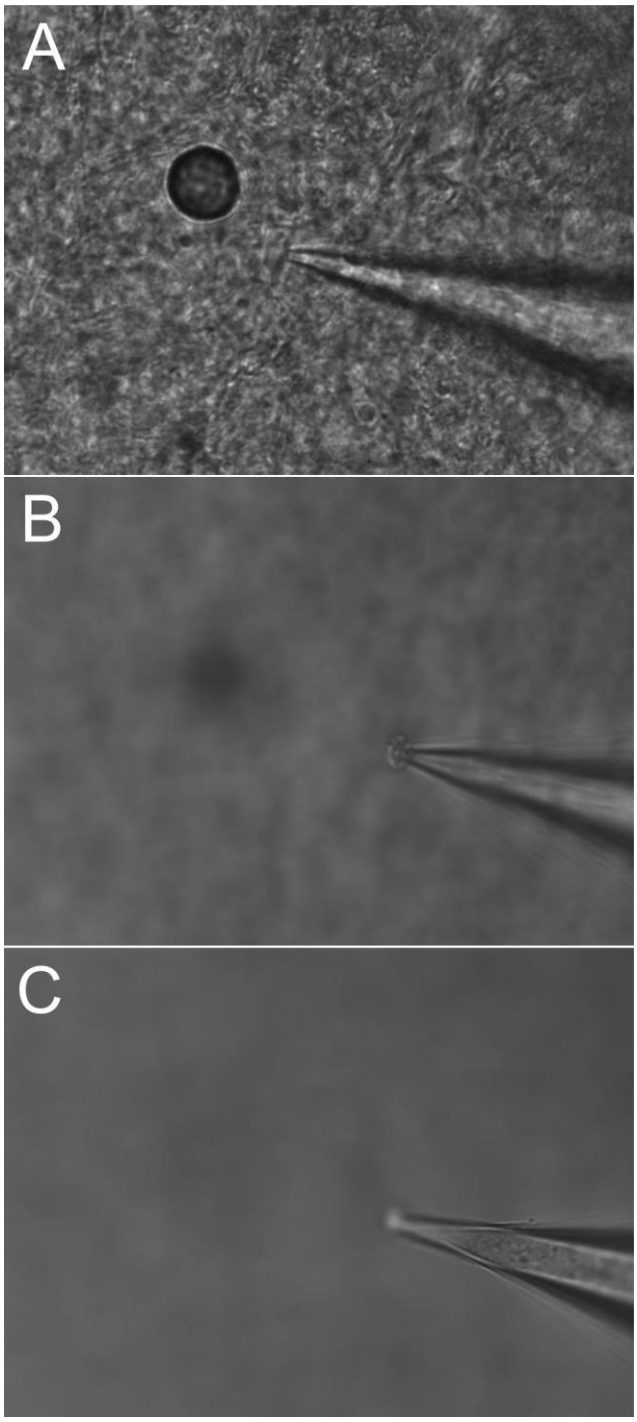

Figure 5.1: Aspiration of single cell from fresh frozen section for scRNA-seq.
A) Photograph of initial aspiration of single cell using pipette from a fresh frozen section. B) Single cell successfully aspirated, single cell can be viewed at the tip of the pipette. C) Aspirated single cell within the pipette, successful picking. The cell was deposited in nuclease-free water and stored in -80^{o}C.

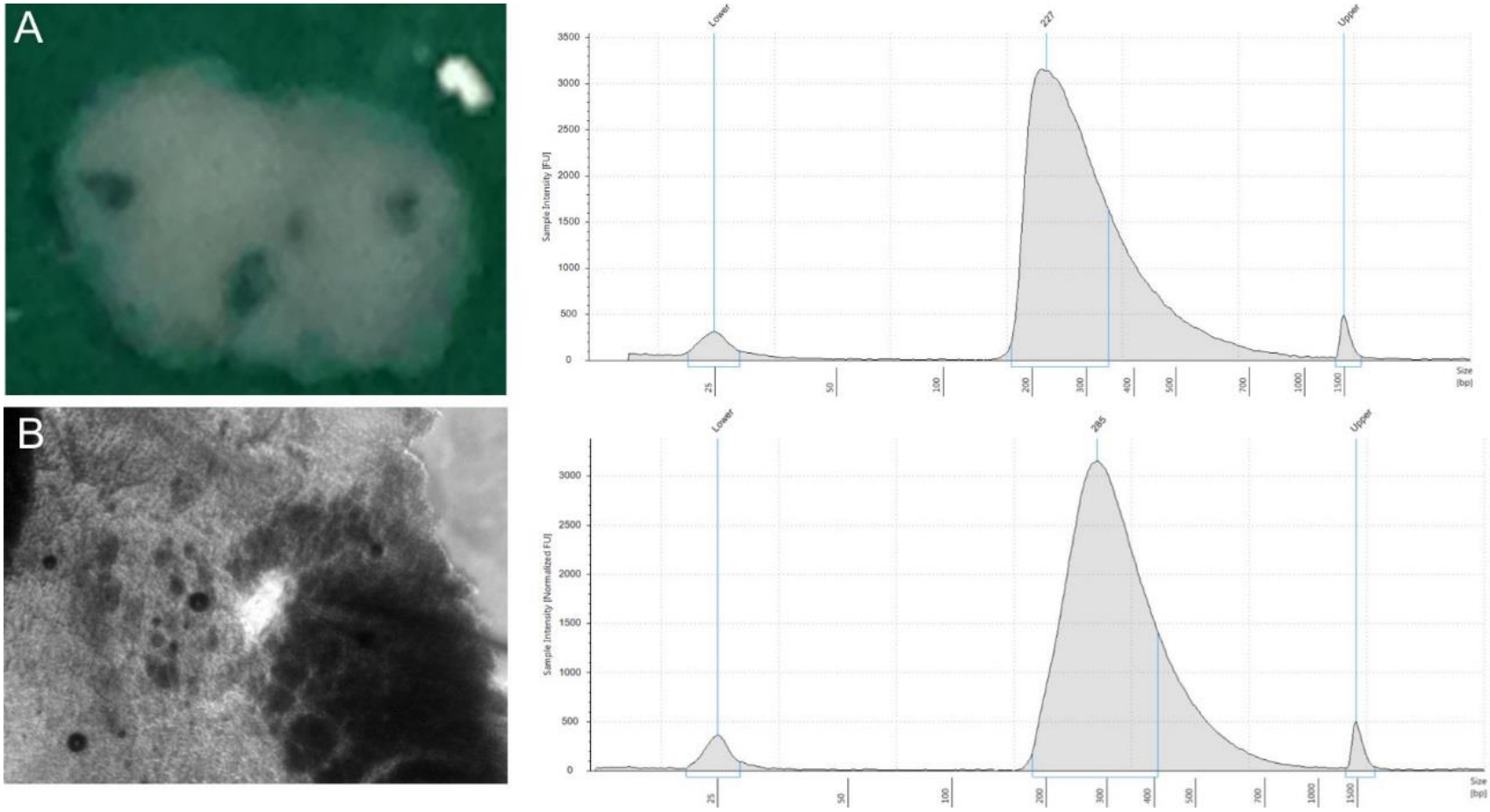

Figure 5.2: Images of IML micro punch and multi-cell and DNA ScreenTape library quality checks.
A) Photograph of IML micro punch from fresh section and sample library quality check. B) Photograph of IML multi-cell from fresh frozen section and corresponding sample library quality check. All libraries exhibit fluorescent intensity peak at 200 base pairs and peak spans 200 to 500 base pairs indicating optimal library read length for sequencing.

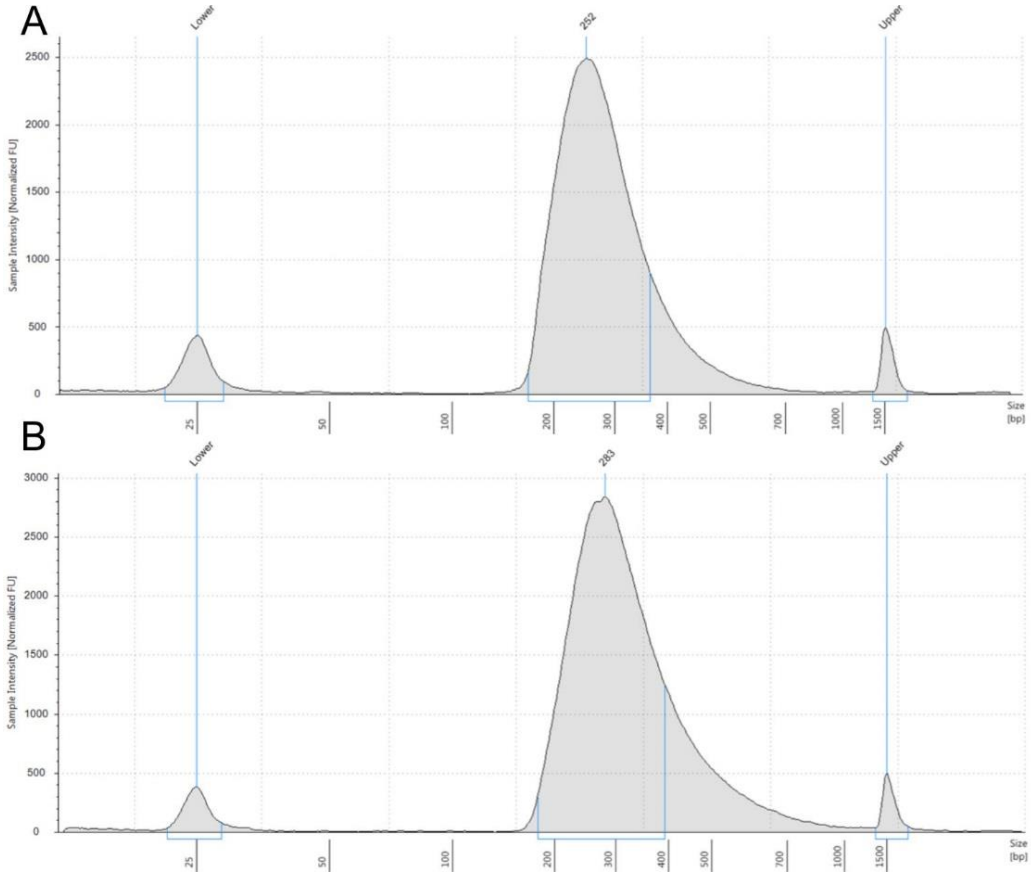

Figure 5.3: Images of single cell aspiration and DNA ScreenTape library quality checks.
A) Library quality check of single cell sample aspirated from fresh section. B) Library quality check of single cell sample aspirated from fresh frozen section. All libraries exhibit fluorescent intensity peak at 200 base pairs and peak spans 200 to 500 base pairs indicating optimal library read length for sequencing.

Table 5.3: Comparison of RNA-seq data to ABA ISH images of thoracic spinal cord.

Receptor/Channel	Gene	IML RNA-seq data	Single cell RNA-seq data	ABA images
Adrenergic α1 receptor	Adra1b	✓	✓	x
Adrenergic α2 receptor	Adra2a	✓	✓	✓
L-type calcium channel subunit	Cacna1c	x	✓	✓
	Cacna1d	x	✓	✓
	Cacna1f	✓	x	x
	Cacna1s	✓	x	✓
T-type calcium channel subunit	Cacna1g	✓	✓	✓
	Cacna1i	✓	✓	✓
Voltage-dependent calcium channel subunit	Cacna2d1	✓	✓	✓
	Cacna2d2	✓	✓	x
	Cacna2d3	✓	✓	✓
Muscarinic acetylcholine receptor	Chrm3	✓	✓	✓
	Chrm4	✓	✓	✓
Nicotinic acetylcholine receptor	Chrna1	✓	✓	✓
	Chrna4	✓	✓	✓
$GABA_A$ receptor α subunit	Gabra5	✓	✓	✓
$GABA_A$ receptor β subunit	Gabrb1	✓	✓	x
	Gabrb2	✓	✓	x
$GABA_A$ receptor γ subunit	Gabrg2	✓	✓	✓
$GABA_A$ receptor ρ subunit	Gabrr1	✓	✓	✓
	Gabrr2	✓	✓	✓
GABA receptor θ subunit	Gabrq	✓	✓	✓
$GABA_B$ receptor subunit	Gabbr1	✓	✓	✓
GABA receptor associated protein	Gabarapl2	✓	✓	x
AMPA glutamate receptor	Gria2	✓	✓	✓
	Gria3	✓	✓	✓
	Gria4	✓	✓	✓
Ionotropic glutamate receptor	Grik4	✓	✓	✓
	Grik5	✓	✓	✓
Glutamate [NMDA] receptor subunit 3	Grin3a	✓	✓	✓
Glutamate [NMDA] receptor subunit ε	Grin2b	✓	✓	✓
Metabotropic glutamate receptor	Grm1	✓	✓	✓
	Grm3	✓	✓	✓
	Grm4	✓	✓	✓
	Grm5	✓	✓	✓
$5HT_1$ receptor	Htr1A	✓	✓	✓
$5HT_2$ receptor	Htr2C	✓	✓	✓
$5HT_3$ receptor	Htr3B	✓	✓	✓
$5HT_5$ receptor	Htr5B	✓	✓	✓
Sodium channel α subunit	Scn1a	✓	✓	✓
Sodium channel β subunit	Scn1b	✓	✓	✓

Adrenergic (alpha 1 and 2) Receptors

Adrenergic receptors are G-protein coupled receptors that are targets for norepinephrine and epinephrine. The relative expression of both α1 and α2 receptor subtype mRNA were observed in the IML dataset, with the α_{2A} adrenergic receptor being the highest among the subtypes expressed within the IML (Figure 5.4). When comparing relative expression (Normalised FPKM) between α1 and α2 receptor subtypes, α_{1B} adrenergic receptor mRNA was the highest amongst the α1 adrenergic receptor subtypes while α_{2A} adrenergic receptor mRNA was highest among the α2 receptor subtypes (Table 5.4). When examining relative expression of α1 and α2 receptor subtype mRNA in the single cell dataset a similar group of subtypes were observed, α_{2A} adrenergic receptor was highest expressed subtype which is similar to that detected in the IML dataset (Figure 5.5). Comparing between the relative expression (Normalised FPKM) of α1 and α2 receptor subtype mRNA revealed that the α_{1B} adrenergic receptor and α_{2A} adrenergic receptor were highly expressed in ChAT-positive single cells (Table 5.4). α_{2A} adrenergic receptor mRNA expression was observed in IML and was selective to SPNs in ISH and expression mask images of the thoracic spinal cord from the ABA.

Table 5.4: Summary of relative gene expression of adrenergic (alpha 1 and alpha 2) receptor subtypes in IML and scRNA-seq data set.

Gene of interest	Sample type	Level of relative gene expression (Normalised FPKM)
Adrenergic α1 receptors	IML	Adra1b > Adra1a > Adra1d
	Single cell	Adra1b > Adra1a > Adra1d
Adrenergic α2 receptors	IML	Adra2a > Adra2c > Adra2b
	Single cell	Adra2a > Adra2c > Adra2b

Voltage-Gated Calcium Channels

Voltage-gated calcium channels (VGCCs) are a subgroup of ion channels, widely expressed throughout the CNS. VGCCs, located on the plasma membrane, are activated in response to depolarisation and facilitate calcium entry from the extracellular environment with a high degree of specificity. VGCCs are broadly categorised into 2 subgroups: high voltage activated (HVA) and low voltage activated (LVA) referring to the magnitude of depolarisation required to open the channel. HVA channels include L-, N-, P/Q- and R-type channels, whereas LVA channels include only T-type VGCCs which are activated by relatively smaller amounts of depolarisation. A common feature of all VGCCs is that they express a single pore-forming α1 subunit. Auxiliary subunits such as β, α2, γ and α2Δ form heteromeric complexes with HVA α1 subunits, whereas LVA channels typically only consist of the α1 subunit (Spanswick and Logan, 1990, Gonzalez Burgos *et al*., 1995, Talley *et al*., 1999, Perez-Reyes, 2003).

All of the VGCCs identified in the single cell dataset were also detected in the whole IML samples. This observation was expected as IML tissue samples should contain multiple SPNs and also glial cells and potentially interneurons. In addition to the VGCC genes also seen in the single cell data set, L-type isoforms ($\alpha1_F$ and $\alpha1_S$) and the T-type isoform ($\alpha1_H$) were present at low levels in the IML data set. This suggests that these 3 genes are not present in SPNs, instead selectively expressed by glial cells or interneurons. Further differences between the data sets were apparent in the relative expression levels. Regarding the IML dataset, the N-type subunit ($\alpha1_B$) and the T-type subunit ($\alpha1_I$) showed the highest mRNA expression, for HVA and LVA VGCCs respectively. In addition the α2Δ3 subunit was the most prominent auxiliary

subunit (Figure 5.6-5.7). When comparing relative expression (Normalised FPKM) between subunits of different VGCC types, calcium channel, voltage-dependent, L type, $\alpha 1_S$ subunit (Cacna1s) was the higher expressed L-type calcium subunit, calcium channel, voltage-dependent, T type, $\alpha 1_G$ subunit (Cacna1g) and calcium channel, voltage-dependent, T type, $\alpha 1_I$ subunit (Cacna1i) were highly expressed T-type calcium subunits and voltage-dependent calcium channel subunit α2/Δ-1 (Cacna2d1) and calcium channel, voltage-dependent, α2/Δ subunit 3 (Cacna2d3) were the highly expressed voltage-dependent calcium channel complex subunits (Table 5.5).

In the single cell data set, mRNA coding for the voltage-dependent calcium channel subunit α2/Δ1 (Cacna2d1) was the highest expressed subunit when comparing relative expression (individual FPKM) of the different VGCC subunits. Other L-type ($\alpha 1_C$), N-type ($\alpha 1_B$), R-type ($\alpha 1_E$) and P-type ($\alpha 1_A$) HVA channels were also detected in single cell samples (Figure 5.8-5.9). When comparing the relative expression (Normalised FPKM) in the single cell data within the L-type calcium channel subunit group, calcium voltage-gated channel subunit $\alpha 1_C$ (Cacna1c) and calcium voltage-gated channel subunit $\alpha 1_D$ mRNA (Cacna1d) were highest (Table 5.5). When comparing the relative expression (Normalised FPKM) in the T-type calcium channel subunit group, calcium channel, voltage-dependent, T type, $\alpha 1_G$ subunit (Cacna1g) and calcium channel, voltage-dependent, T type, $\alpha 1_I$ subunit (Cacna1i) were highly expressed which is similar to the trend observed in the IML data (Table 5.5). Voltage-dependent calcium channel subunit α2/Δ-1 mRNA (Cacna2d1) was the highest expressed voltage-dependent calcium channel complex subunit when comparing relative expression (Normalised FPKM) (Table 5.5).

When consulting the ABA, Cacna1c and Cacna1d mRNA expression was observed in IML SPNs in the thoracic spinal cord as well as other cell types throughout the dorsal and ventral horns. Cacna1g mRNA was expressed primarily in the dorsal horn with some expression observed in the IML area. Cacna1i mRNA expression was observed throughout the slice however no expression seems to be present in IML SPNs. Expression within SPNs was not as clear in the ISH and expression mask image of Cacna1s mRNA. Cacna2d1 mRNA is expressed in the dorsal horn primarily however high expression is observed in IML SPNs. Cacna2d3 mRNA is highly expressed throughout the spinal cord slice, high expression is observed in the ventral horn motoneurons and IML SPNs.

Table 5.5: Summary of relative gene expression of voltage-gated calcium channel subunits in IML and scRNA-seq data set.

Gene of interest	Sample type	Level of relative gene expression (Normalised FPKM)
L-type calcium channel subunits	IML	Cacna1c > Cacna1d > Cacna1f > Cacna1s
	Single cell	Cacna1d > Cacna1c > Cacna1s = Cacna1f
T-type calcium channel subunits	IML	Cacna1g > Cacna1i > Cacna1h
	Single cell	Cacna1i > Cacna1g > Cacna1h
Voltage-dependent calcium channel subunits	IML	Cacna2d3 > Cacna2d1 > Cacna2d2 > Cacna2d4
	Single cell	Cacna2d1 > Cacna2d3 > Cacna2d2 > Cacna2d4

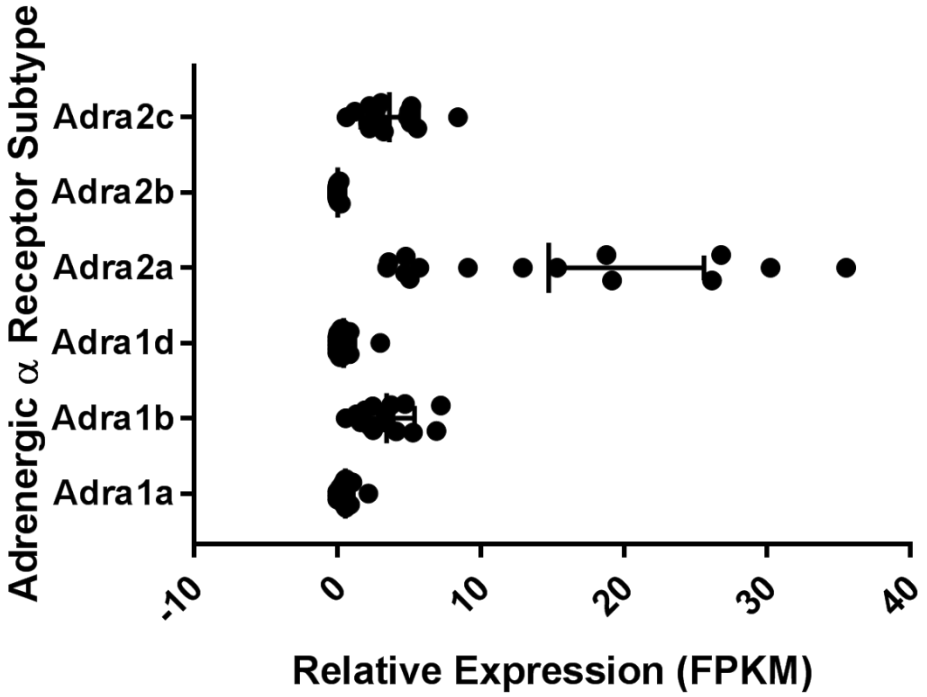

Figure 5.4: Relative expression (FPKM values) of mRNA coding for adrenergic α1/2 receptor subtypes in IML RNA-seq data. mRNA coding for adrenergic α2 receptor subtype 2a (Adra2a) is highest expressed in the IML RNA-seq data set.

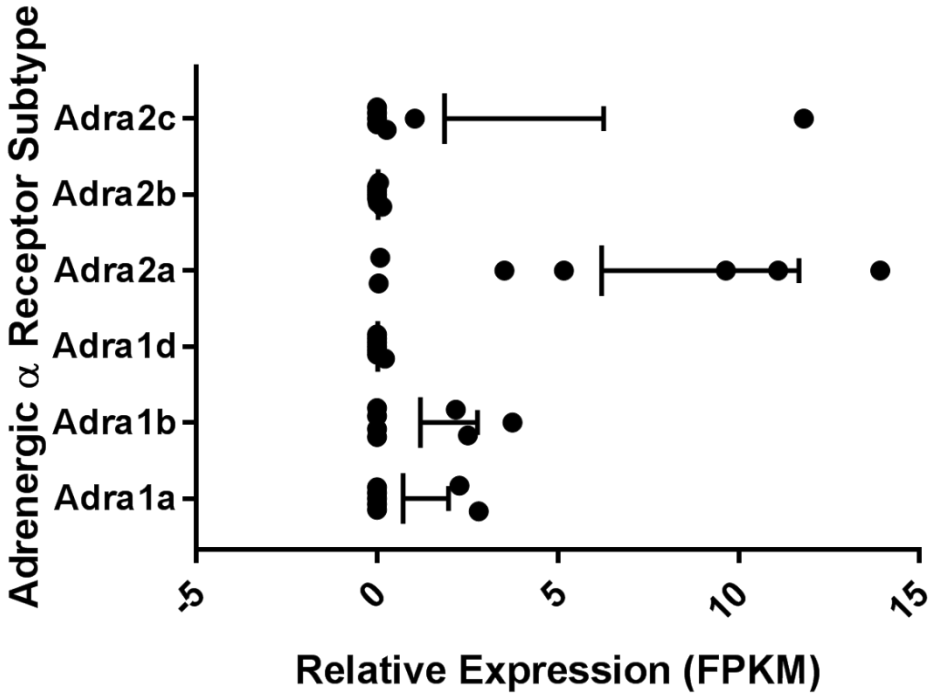

Figure 5.5: Relative expression (FPKM values) of mRNA coding for adrenergic α1/2 receptor subtypes in scRNA-seq data. mRNA coding for adrenergic α2 receptor subtype 2a (Adra2a) is highest expressed in the scRNA-seq data set.

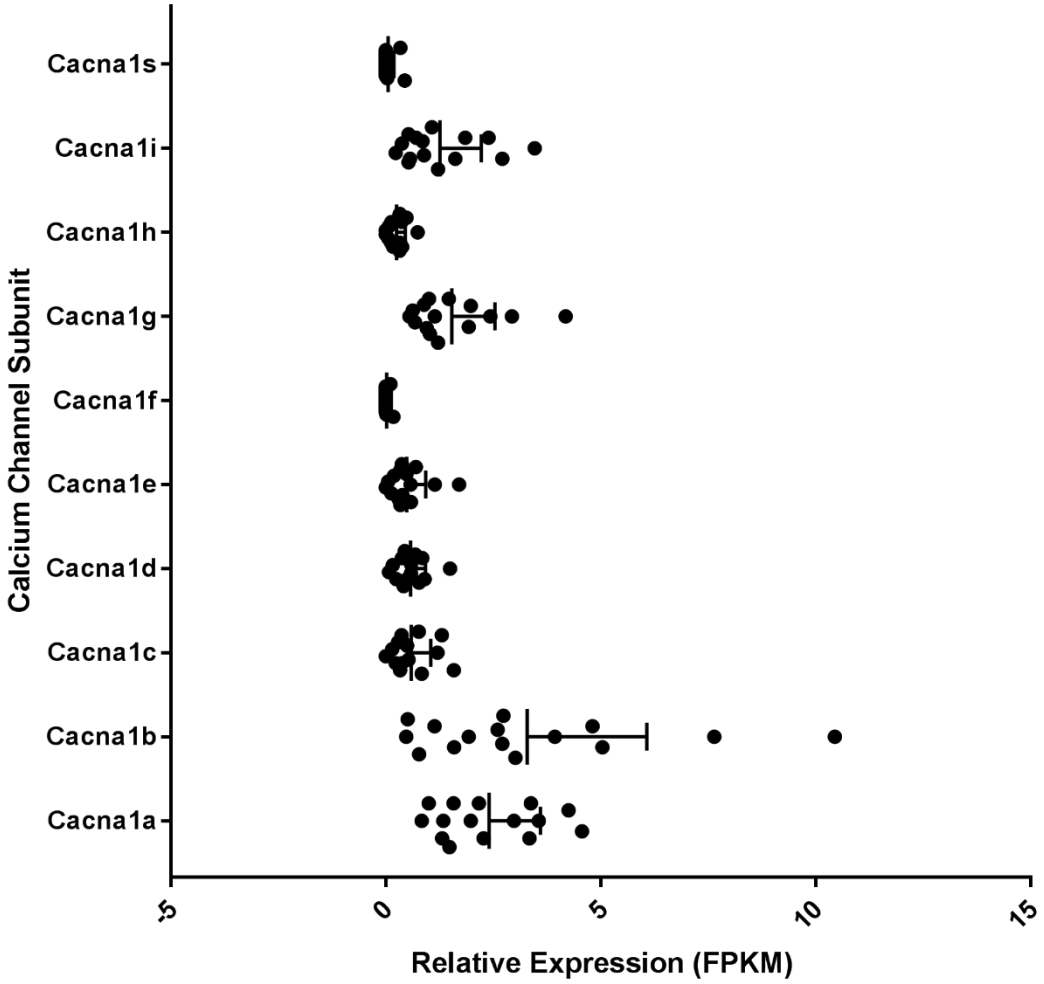

Figure 5.6: Relative expression (FPKM values) of calcium channel subunit mRNAs in IML RNA-seq data.

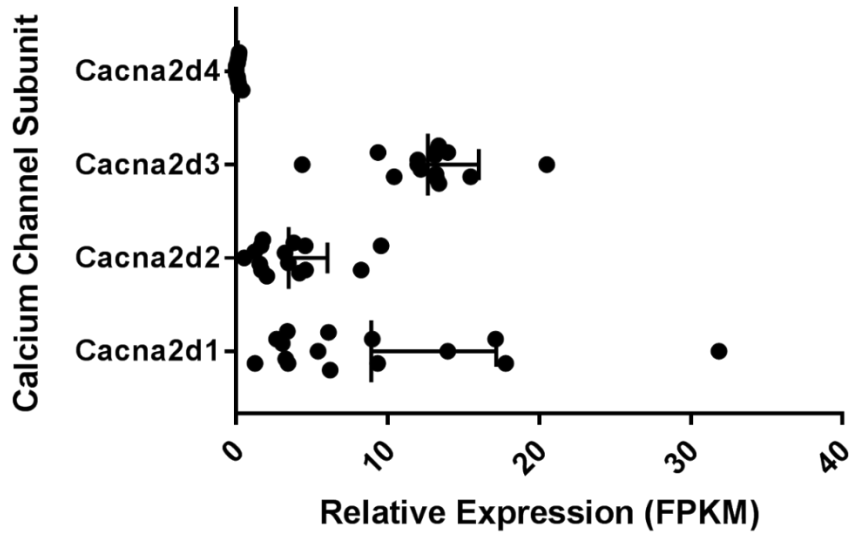

Figure 5.7: Relative expression (FPKM values) of highly expressed (over 15 FPKM) calcium channel α2/Δ subunit mRNAs in IML RNA-seq data.

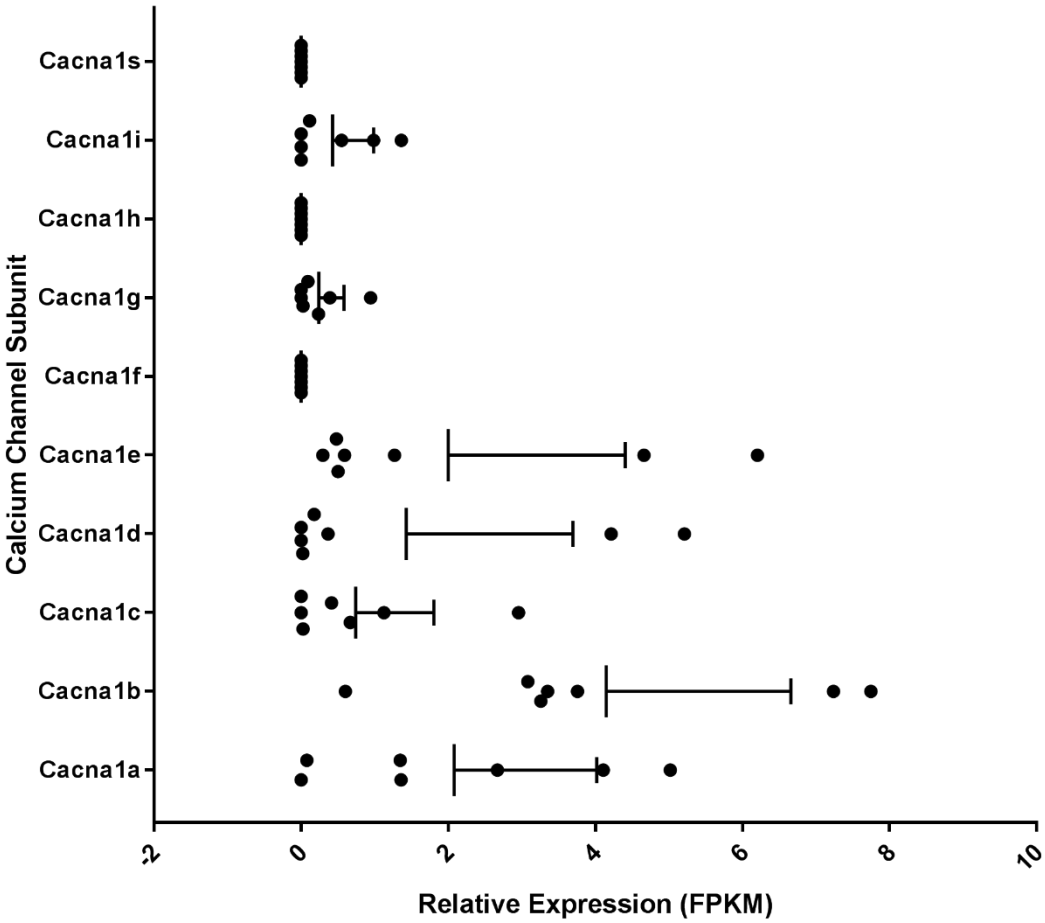

Figure 5.8: Relative expression (FPKM values) of calcium channel subunit mRNAs in scRNA-seq data.

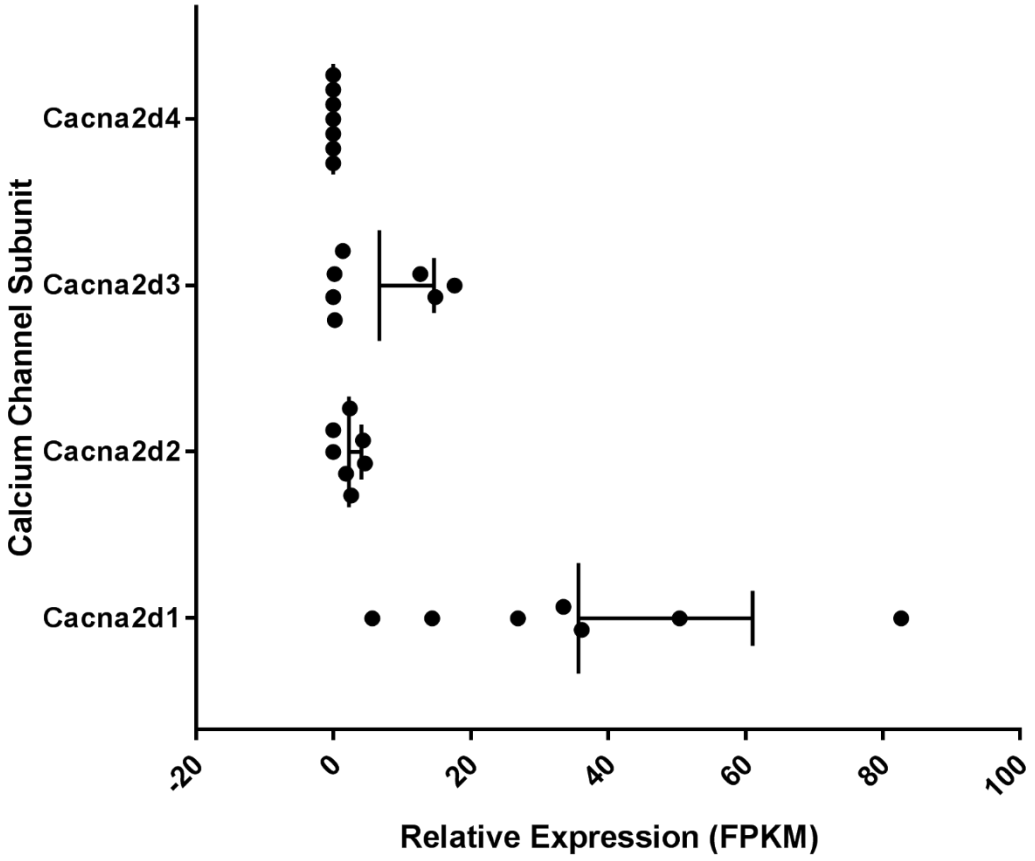

Figure 5.9: Relative expression (FPKM values) of mRNA coding for calcium channel α2/Δ subunits in scRNA-seq data. mRNA coding for voltage-dependent calcium channel subunit α2/Δ1 (Cacna2d1) was highly expressed in the single cell data.

Chrm genes - Muscarinic Receptors

Muscarinic receptors are acetylcholine receptors which form G protein-coupled receptor complexes located on the cell membranes of some neurons. In the IML data set, mRNA coding for muscarinic acetylcholine receptor M3 (Chrm3) was the highest expressed when comparing relative expression via individual FPKM values and (Normalised FPKM) to the other receptor types (Figure 5.10, Table 5.6).

A different trend was observed in the single cell data with mRNA coding for muscarinic acetylcholine receptor M2 (Chrm2) and muscarinic acetylcholine receptor M4 (Chrm4) being highly expressed compared to the individual FPKM values of other receptor types (Figure 5.11), but with muscarinic acetylcholine receptor M1 (Chrm1) and muscarinic acetylcholine receptor M3 (Chrm3) being expressed lower than Chrm2 and Chrm4 (Figure 5.11, Table 5.6). M3 and M4 muscarinic receptor type expression was observed in many regions of the thoracic spinal cord as depicted in the ABA images. The expression mask view for the M4 muscarinic receptor type suggests more cells across the spinal cord slice express the mRNA coding for this subtype than the M3 muscarinic receptor mRNA.

Table 5.6: Summary of relative gene expression of muscarinic acetylcholine receptor subtypes in IML and scRNA-seq data set.

Gene of interest	Sample type	Level of relative gene expression (Normalised FPKM)
Muscarinic acetylcholine receptors	IML	Chrm3 > Chrm5 > Chrm1 = Chrm4
	Single cell	Chrm2 =Chrm 4 > Chrm3 > Chrm1 > Chrm5

CHRNA - Nicotinic Receptors

Nicotinic receptors are ionotropic acetylcholine receptors. These receptors are composed α, β, δ and ε subunits and receptor subtypes can be composed of

one type of subunit or at least one α and one β subunit. All neuronal nicotinic receptors possess an α subunit therefore these were examined more closely in the RNA-seq data sets (Taylor, 2012). mRNA coding for acetylcholine receptor subunit α1 (CHRNA1) was highest in terms of individual FPKM values and normalised FPKM when compared to the other nicotinic receptor types in the IML data set (Figure 5.12, Table 5.7). mRNA coding for neuronal acetylcholine receptor subunit α3 (CHRNA3) and neuronal acetylcholine receptor subunit α7 (CHRNA7) had the second highest relative expression as determined by normalised FPKM whereas neuronal acetylcholine receptor subunit α2 (CHRNA2), neuronal acetylcholine receptor subunit α5 (CHRNA5) and neuronal acetylcholine receptor subunit α6 (CHRNA6) were the lowest (Table 5.7).

When comparing individual FPKM values in the single cell data set, neuronal acetylcholine receptor subunit α1 (CHRNA1) and neuronal acetylcholine receptor subunit α4 mRNA (CHRNA4) had the highest expression (Figure 5.13). Unlike in the IML data set, when comparing relative expression (Normalised FPKM), neuronal acetylcholine receptor subunit α4 mRNA (CHRNA4) had highest expression followed by neuronal acetylcholine receptor subunit α1 (CHRNA1) (Table 5.7).

Similar to the ABA images of the muscarinic receptor subtypes, the nicotinic receptor subtypes are expressed ubiquitously throughout the thoracic spinal cord slice, neuronal acetylcholine receptor subunit α4 mRNA appears to be expressed in more cells across the spinal cord slice.

Table 5.7: Summary of relative gene expression of nicotinic acetylcholine receptor subtypes in IML and scRNA-seq data set.

Gene of interest	Sample type	Level of relative gene expression (Normalised FPKM)
Nicotinic acetylcholine receptors	IML	Chrna1 > Chrna3 = Chrna7 > Chrna6 > Chrna2 = Chrna5
	Single cell	Chrna 4 > Chrna 1

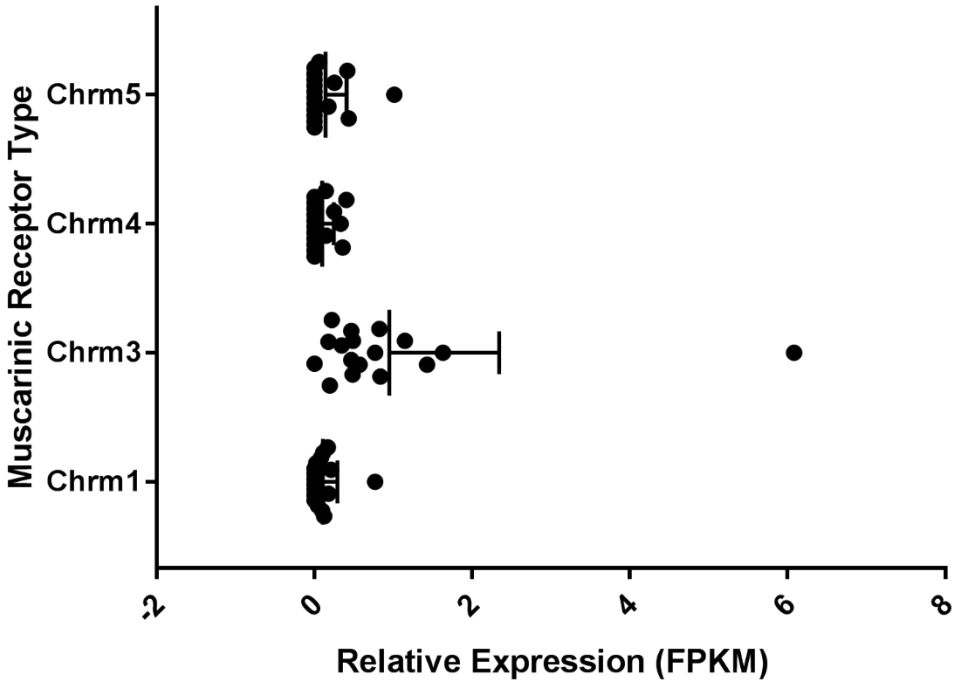

Figure 5.10: Relative expression (FPKM values) of mRNA coding for muscarinic receptor types in IML RNA-seq data.

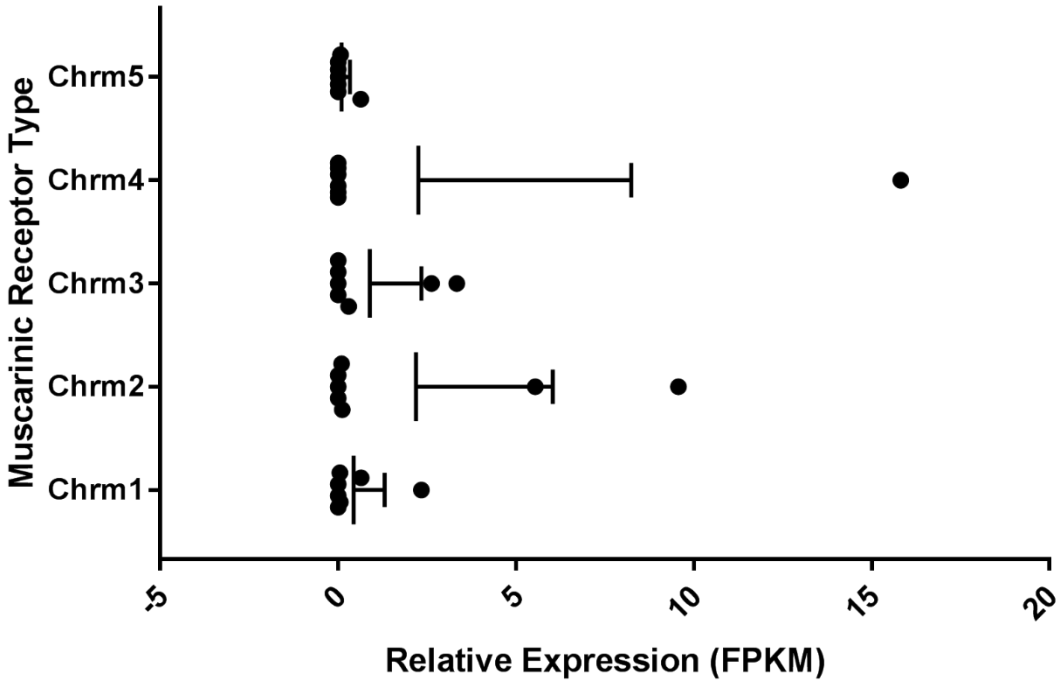

Figure 5.11: Relative expression (FPKM values) of mRNA coding for muscarinic receptor types in scRNA-seq data.

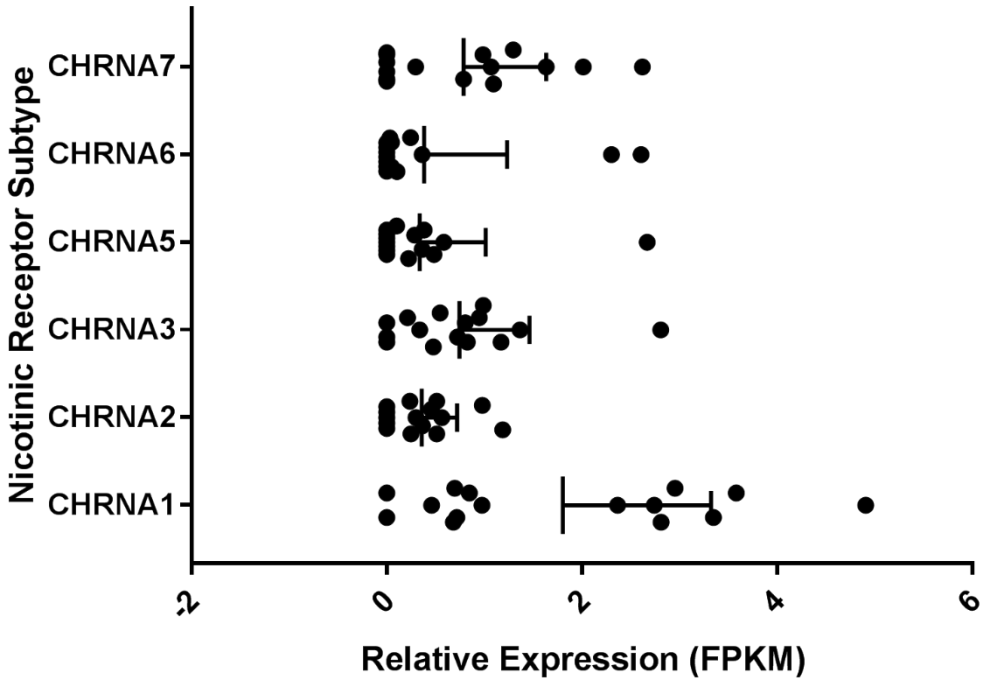

Figure 5.12: Relative expression (FPKM values) of mRNA coding for nicotinic receptor subtypes in IML RNA-seq data.

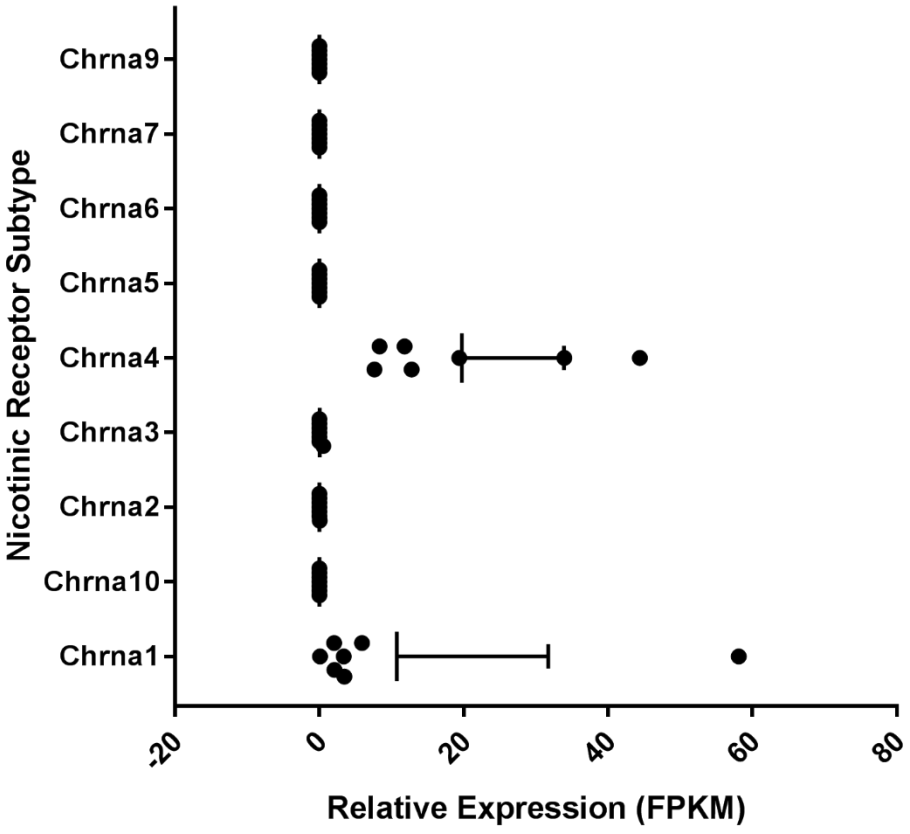

Figure 5.13: Relative expression (FPKM values) of mRNA coding for nicotinic receptor subtypes in scRNA-seq data.

$GABA_A$ and $GABA_B$ Receptors

GABA receptors respond to the inhibitory neurotransmitter GABA: there are two classes of GABA receptors, ionotropic $GABA_A$ and metabotropic $GABA_B$ receptors. The expression of all GABA receptor subunits were examined in the IML and scRNA-seq data sets.

When comparing all the $GABA_A$ receptor subunits it is interesting to note that several less commonly expressed subunits were present in both the IML and single cell data sets, GABA receptor subunit Δ (Garbd), Gamma-aminobutyric acid receptor subunit ε (Gabre), $GABA_A$ receptor subunit ρ2 (Gabrr2) and GABA receptor subunit θ (Gabrq) (Figure 5.14, 5.17).

In the IML data set, GABA receptor γ2 mRNA (Gabrg2) had the highest individual FPKM values when compared to other GABA receptor subunits (Figure 5.14, 5.16). GABA receptor associated proteins (Gabarap, Gabarapl1 and Gabarapl2) had the highest individual FPKM values (Figure 5.15). When comparing relative expression (Normalised FPKM) in $GABA_A$ receptor α subunits, $GABA_A$ receptor subunit α1 (Gabra1) was highest with $GABA_A$ receptor subunit α5 (Gabra5) and $GABA_A$ receptor subunit α3 (Gabra3) being second and third highest (Table 5.8). $GABA_A$ receptor subunit β2 (Gabrb2) had the highest relative expression (Normalised FPKM) compared to the other β subunits (Table 5.8). $GABA_A$ receptor subunit γ2 (Gabrg2) had the highest relative expression (Normalised FPKM) compared to the other γ subunits (Table 5.8). $GABA_A$ receptor subunit ρ2 (Gabrr2) had the highest relative expression (Normalised FPKM) compared to the other ρ subunits (Table 5.8). Rarer GABA receptor subunits GABA receptor subunit Δ (Garbd), GABA receptor subunit ε (Gabre) and GABA receptor subunit θ (Gabrq) were present when comparing

individual FPKM values in the IML RNA-seq data set (Figure 5.14). $GABA_{B1}$ receptor 1 (Gabbr1) had the highest relative expression (Normalised FPKM) compared to the other $GABA_B$ receptors (Table 5.8). When comparing the relative expression (Normalised FPKM) of the GABA receptor associated proteins, GABA receptor protein-like 2 mRNA (Gabarapl2) was the highest in the IML (Table 5.8).

Similar GABA receptor subunits were expressed in the single cell data set, rare GABA receptor subunits GABA receptor subunit Δ (Garbd), GABA receptor subunit ε (Gabre), and GABA receptor subunit θ (Gabrq) were present when comparing individual FPKM values as seen in the IML data set (Figure 5.16). In the scRNA-seq data set, GABA receptor associated proteins had the highest individual FPKM values and $GABA_A$ receptor subunit γ2 (Gabrg2) had the second highest individual FPKM values which is similar to the IML data set (Figure 5.18-5.19). When comparing GABA receptor subunits with lower individual FPKM values, $GABA_A$ receptor subunit α4 (Gabra4) had higher individual FPKM values (Figure 5.20). When comparing relative expression (Normalised FPKM) of the GABA α subunits in the single cell data $GABA_A$ receptor subunit α1 (Gabra1) was highest with $GABA_A$ receptor subunit α5 (Gabra5) and $GABA_A$ receptor subunit α3 (Gabra3) being second and third highest which is similar to the findings in the IML data set (Table 5.8). When comparing the GABA receptor β subunits, $GABA_A$ receptor subunit β1 (Gabrb1) had the highest relative expression followed by $GABA_A$ receptor subunit β2 (Gabrb2) (Table 5.8). Similar to the IML data set, $GABA_A$ receptor subunit γ2 (Gabrg2) had the highest relative expression (Normalised FPKM) compared to the other γ subunits (Table 5.8). $GABA_A$ receptor subunit α5 (Gabra5) and $GABA_A$ receptor subunit ρ2 (Gabrr2) are highly expressed, in terms of individual

FPKM values and normalised FPKM, in both IML and single cell data sets. When comparing relative expression (Normalised FPKM) of $GABA_B$ subunits, $GABA_{B1}$ receptor 1 (Gabbr1) had the highest relative expression as seen with the IML dataset (Table 5.8). $GABA_{B1}$ receptor 1 (Gabbr1) and GABA receptor associated protein-like 2 mRNA (Gabarapl2) had the highest relative expression when compared to other $GABA_B$ receptors and GABA receptor associated proteins (Table 5.8).

In ABA, GABRA5 expression was observed across the thoracic spinal cord sections. GABA receptor subunit θ (Gabrq) mRNA was highly expressed in IML SPNs while $GABA_A$ receptor subunit ρ1 (Gabrr1) expression was uniform throughout the spinal cord slice. Both $GABA_B$ receptor β subunits were highly expressed across the thoracic spinal cord slice with the IML being an area of particularly high expression as depicted in ABA images. Anti-Gabrq was tested using IHC in thoracic spinal cord slices and IML SPNs were labelled however ventral horn motoneurons were also labelled (Figure 5.21).

Table 5.8: Summary of relative gene expression of $GABA_{A/B}$ receptor subunits in IML and scRNA-seq data set.

Gene of interest	Sample type	Level of relative gene expression (Normalised FPKM)
$GABA_A$ receptor α subunits	IML	Gabra1 > Gabra5 > Gabra3 > Gabra2 > Gabra4 > Gabra6
	Single cell	Gabra1 > Gabra5 > Gabra3> Gabra4 > Gabra2 > Gabra6
$GABA_A$ receptor β subunits	IML	Gabrb2 > Gabrb1 > Gabrb3
	Single cell	Gabrb1 > Gabrb2 > Gabrb3
$GABA_A$ receptor γ subunits	IML	Gabrg2 > Gabrg1 > Gabrg3
	Single cell	Gabrg2> Gabrg1 > Gabrg3
$GABA_A$ receptor ρ subunits	IML	Gabrr2 > Gabrr1 > Gabrr3
	Single cell	Gabrr1 > Gabrr2
$GABA_B$ receptor subunits	IML	Gabbr1 > Gabbr2
	Single cell	Gabbr1 > Gabbr2
GABA receptor associated proteins	IML	Gabarapl2 > Gabarap > Gabarapl1
	Single cell	Gabarapl2 > Gabarap = Gabarapl1

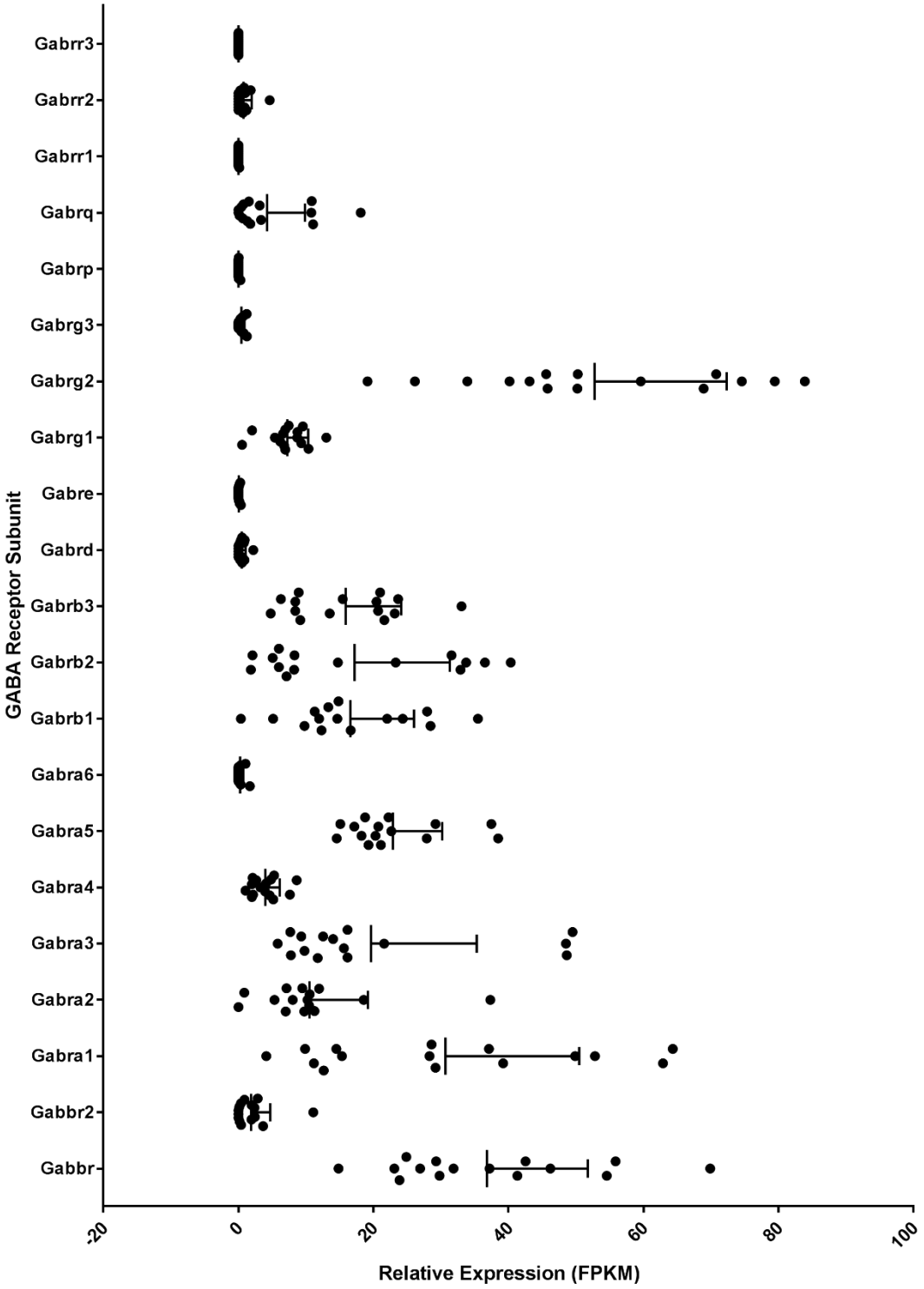

Figure 5.14: Relative expression (FPKM values) of mRNA coding for GABA receptor subunits in IML RNA-seq data.

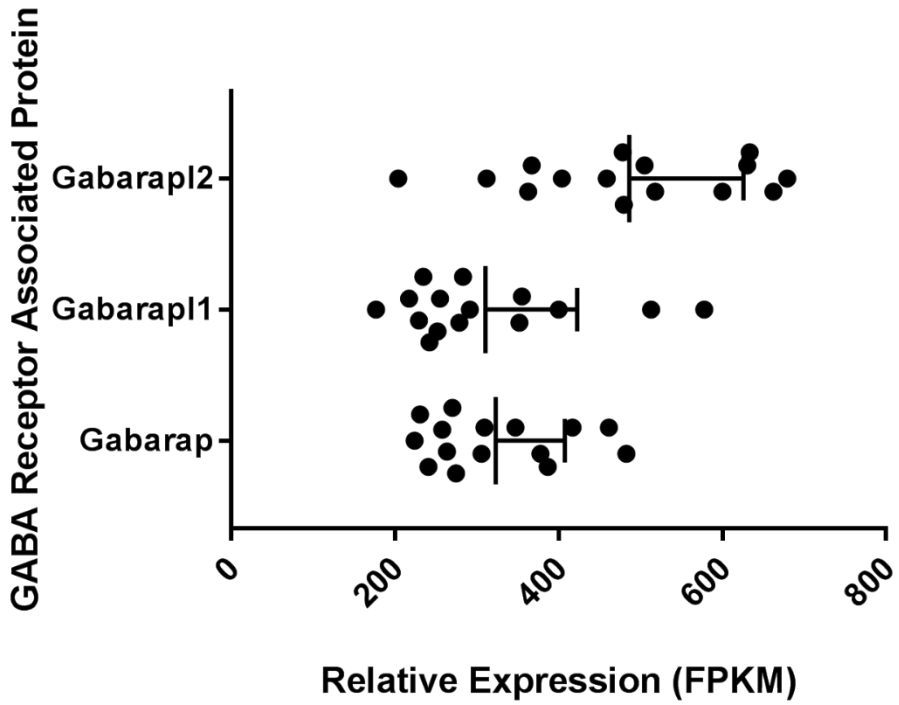

Figure 5.15: Relative expression (FPKM values) of mRNA coding for GABA receptor associated proteins in IML RNA-seq data.

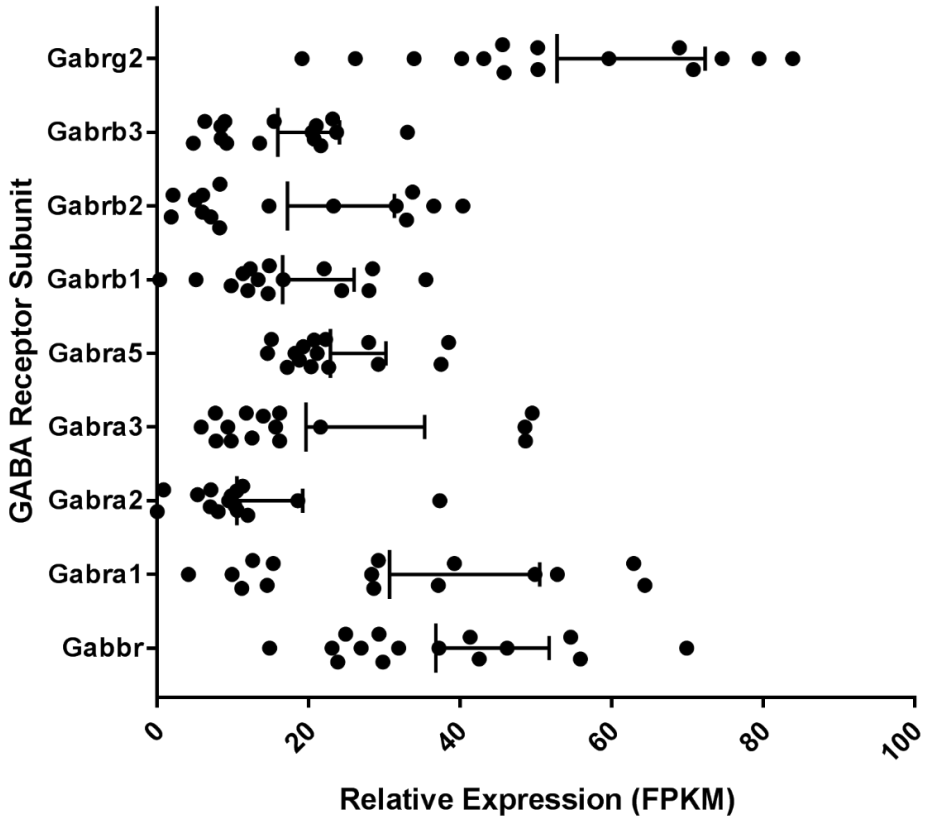

Figure 5.16: Relative expression (FPKM values) of GABA receptor subunit mRNAs in IML RNA-seq data. mRNA coding for GABA receptor γ2 subunit (Gabrg2) was highly expressed in the IML RNA-seq data.

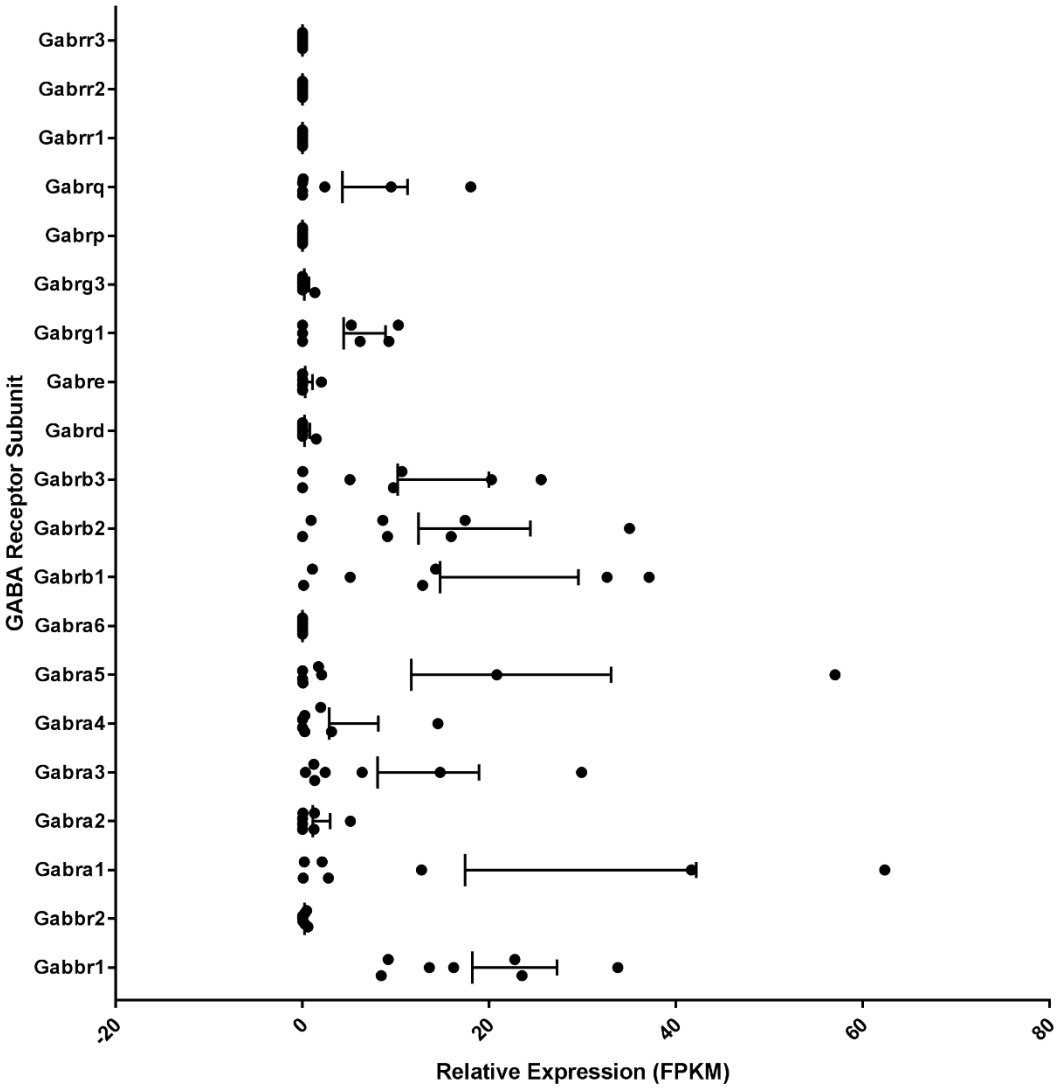

Figure 5.17: Relative expression (FPKM values) of mRNA coding for all GABA receptor subunits in scRNA-seq data.

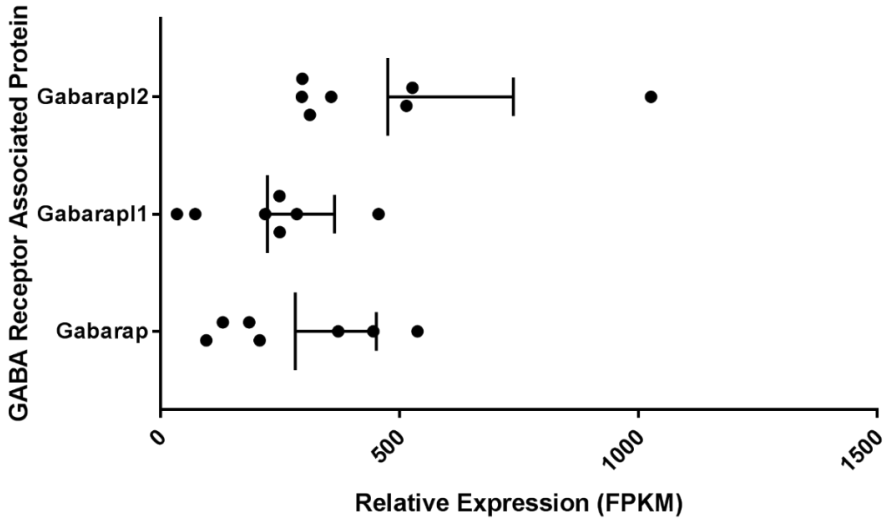

Figure 5.18: Relative expression (FPKM values) of mRNA coding for GABA receptor associated proteins in scRNA-seq data.

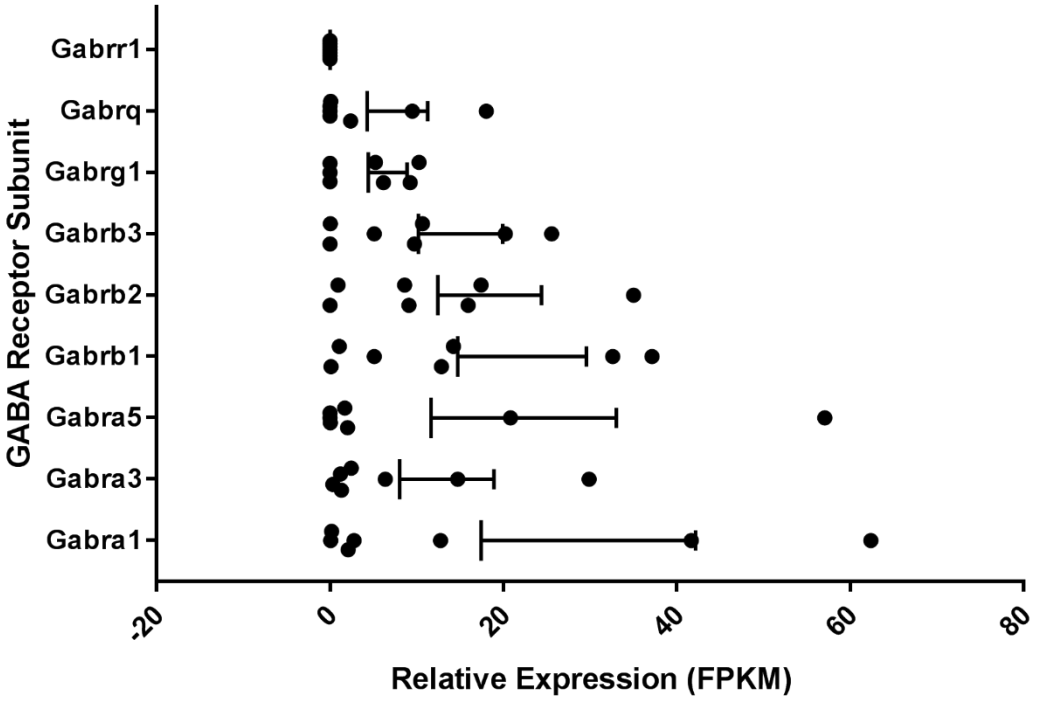

Figure 5.19: Relative expression (FPKM values) of mRNA coding for GABA receptor subunits (within 20-80 FPKM range) in scRNA-seq data.

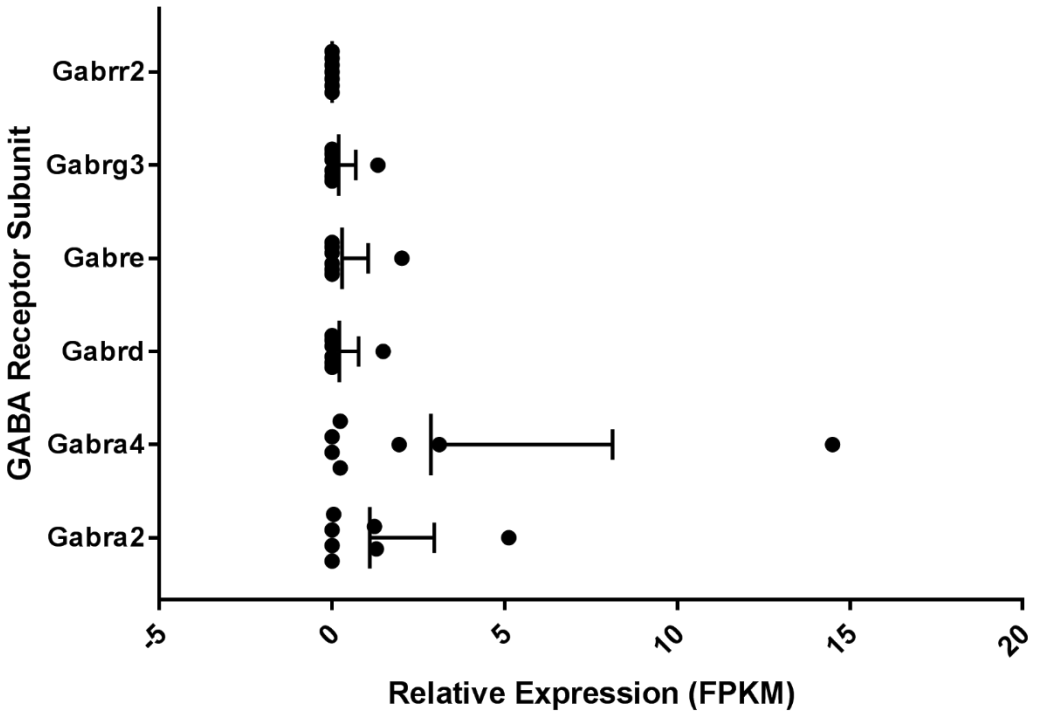

Figure 5.20: Relative expression (FPKM values) of mRNA coding for GABA receptor subunits (within 5-20 FPKM range) in scRNA-seq data.

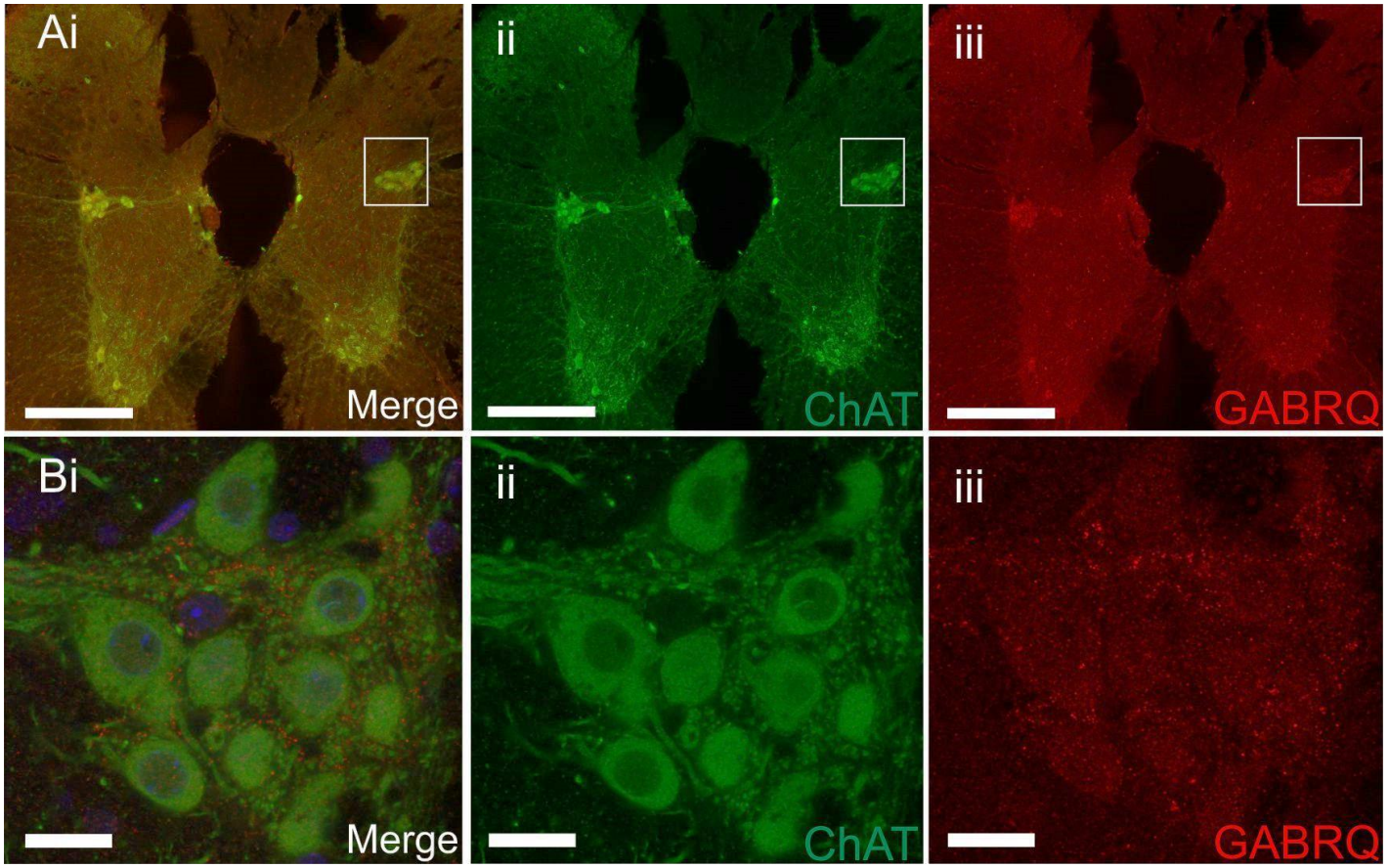

Figure 5.21: ChAT and GARBQ labelling in thoracic spinal chord determined using IF/IHC.
Ai-iii) Whole thoracic spinal cord slice labelled with anti-ChAT and anti-GABRQ, at 1:200 dilution, using IHC. Bi-iii) ChAT and GARBQ-labelled SPNs located in the IML. Scale bars: Ai-iii = 200 μm. Bi-iii = 10 μm.

Glutamate Receptors

Glutamate receptors can be divided into metabotropic and ionotropic receptors, ionotropic receptors can be further subdivided into AMPA, kainate and NMDA receptors.

AMPA receptor subunits – AMPA receptors are composed of four subunits Gria1, Gria2, Gria3 and Gria4 which combine to form a tetramer, most AMPA receptors are composed of tetramers made from different subunits (Mayer, 2005). When comparing individual FPKM values and relative expression (Normalised FPKM) between AMPA receptors in the IML data set, a similar trend was observed with glutamate ionotropic receptor AMPA type subunit 2 (Gria2), glutamate receptor 3 (Gria3) and glutamate receptor 3 (Gria4) having similar levels of expression (Figure 5.22, Table 5.9). Individual FPKM values and normalised FPKM of glutamate ionotropic receptor AMPA type subunit 2 (Gria2) was highest when compared to other AMPA receptors in the single cell data (Figure 5.23, Table 5.9).

In ABA, all three AMPA glutamate receptor mRNA showed high expression, Gria2 had higher expression in the dorsal horns whereas Gria3 and Gria4 mRNA was more highly expressed towards the central region, lateral and ventral horns.

Kainate receptor subunits – There are five kainate receptor subunits, Grik1, Grik2, Grik3, Grik4 and Grik5, which can be combined different ways to form tetramers. Grik1-3 can form functional receptors entirely composed of that particular subunit (Collingridge *et al*., 2009). When comparing individual FPKM values between kainate glutamate receptors in the IML data set found that most receptor subunits had low individual FPKM values with the exception of

glutamate receptor, ionotropic kainate 5 (Grik5) which had the highest relative expression measured by normalised FPKM (Figure 5.24, Table 5.9).

Individual FPKM values of kainate receptors did not vary greatly in the single cell data set however when comparing normalised FPKM, mRNA coding for glutamate receptor, ionotropic kainate 4 (Grik4) had the highest relative expression followed by glutamate receptor, ionotropic kainate 1 (Grik1) and glutamate receptor, ionotropic kainate 5 (Grik5) (Figure 5.25, Table 5.9).

In the ABA, Grik4 is expressed across the thoracic spinal cord, whereas the expression mask of Grik5 seems to indicate that mRNA expression of Grik5 is concentrated in the IML.

NMDA receptor subunits – The NMDA receptor is formed from Grin1 and Grin2 subunits forming a heterotetramer (Gambrill and Barria, 2011). In the IML data set, glutamate [NMDA] receptor subunit 3A (Grin3A) and glutamate [NMDA] receptor subunit ε2 (Grin2B) had the highest individual FPKM values and high expression as measured by normalised FPKM (Figure 5.26, Table 5.9).

In the single cell data, glutamate receptor, ionotropic, N-methyl D-aspartate-associated protein 1 (GRINA) had the highest individual FPKM values however, similar to the IML data set, mRNA coding for glutamate [NMDA] receptor subunit 3A (Grin3A) and glutamate [NMDA] receptor subunit ε2 (Grin2B) were highly expressed as measured by normalised FPKM (Figure 5.27, Table 5.9). In the ABA, expression of these receptor subunits was observed in the dorsal, lateral and ventral regions of the thoracic spinal cord.

mGLuR receptors – There are a number of different types of metabotropic glutamate receptors (mGLuRs), they are divided into different groups based on how the respond to NMDA (Alvarez *et al*., 2000). In the IML data set,

metabotropic glutamate receptor 5 (GRM5) had the highest individual FPKM values (Figure 5.28). Additionally comparison of normalised FPKM revealed that metabotropic glutamate receptor 5 (GRM5) had the highest relative expression followed by metabotropic glutamate receptor 7 (GRM7) while metabotropic glutamate receptor 1 (GRM1), metabotropic glutamate receptor 3 (GRM3), metabotropic glutamate receptor 4 (GRM4) having similar levels of expression (Table 5.9). Comparisons of individual FPKM values in the single cell data found metabotropic glutamate receptor 5 (GRM5) and metabotropic glutamate receptor 7 (GRM7) having the highest values (Figure 5.29). Like the IML data set, relative expression of metabotropic glutamate receptor 5 (GRM5) was highest followed by metabotropic glutamate receptor 7 (GRM7) (Table 5.9).

ABA images showed mRNA expression for metabotropic glutamate receptor 1 (GRM1), metabotropic glutamate receptor 3 (GRM3) and metabotropic glutamate receptor 4 (GRM4) was present across the slice with high expression observed in the IML region. mRNA coding for the metabotropic glutamate receptor 5 was expressed in the dorsal and lateral horn of the thoracic spinal cord slice. The ABA had no images for the metabotropic glutamate receptor 7 (GRM7).

Table 5.9: Summary of relative gene expression of glutamate receptor subunits and subtypes in IML and scRNA-seq data set.

Gene of interest	Sample type	Level of relative gene expression (Normalised FPKM)
AMPA glutamate receptors	IML	Gria2 > Gria3 > Gria4 > Gria1
	Single cell	Gria2 > Gria3 > Gria4 > Gria1
Ionotropic glutamate receptors	IML	Grik5 > Grik2 > Grik1 > Grik4 > Grik3
	Single cell	Grik4 > Grik1 > Grik5 > Grik2 > Grik3
Glutamate [NMDA] receptor subunit 3	IML	Grin3a > Grin3b
	Single cell	Grin3a > Grin3b
Glutamate [NMDA] receptor subunit ε	IML	Grin2b > Grin2c > Grin2d > Grin2a
	Single cell	Grin2b > Grin2a > Grin2d > Grin2c
Metabotropic glutamate receptors	IML	Grm5 > Grm7 > Grm1 > Grm3 > Grm4 > Grm8 > Grm2 > Grm6
	Single cell	Grm5 > Grm7 > Grm1 > Grm4 > Grm3 > Grm2 > Grm8 > Grm6

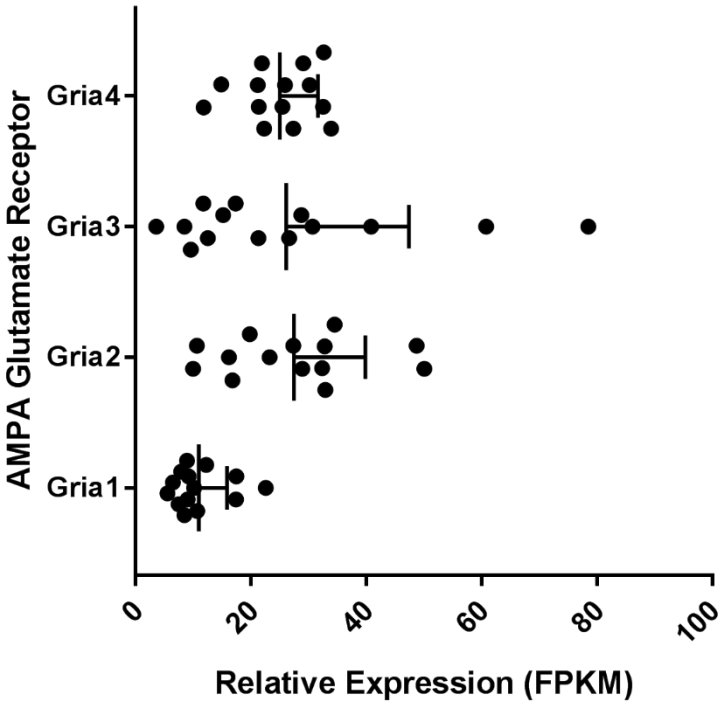

Figure 5.22: Relative expression (FPKM values) of mRNA coding for AMPA glutamate receptor types in IML RNA-seq data.

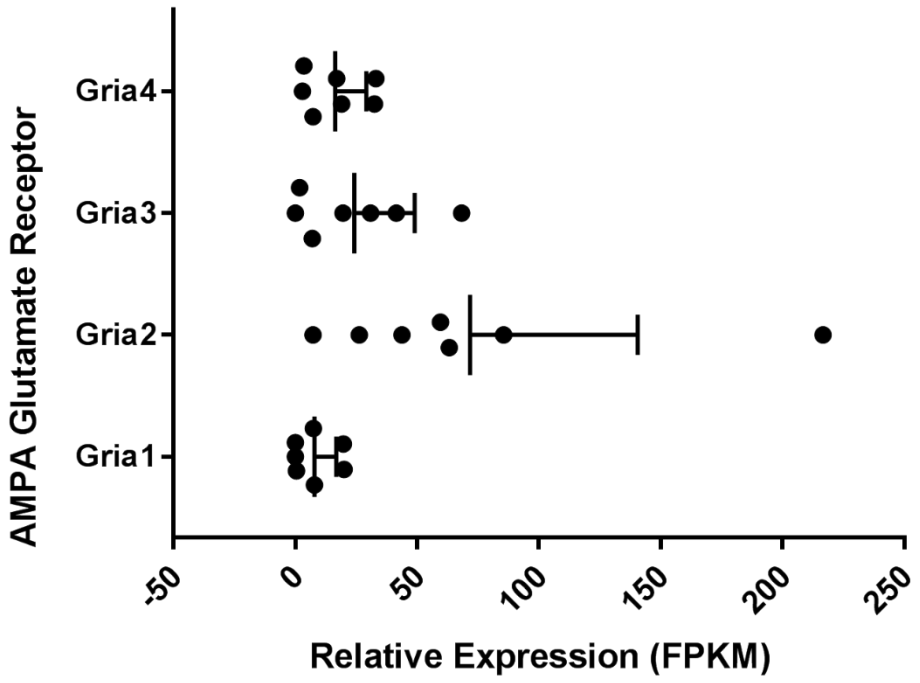

Figure 5.23: Relative expression (FPKM values) of mRNA coding for AMPA glutamate receptor types in scRNA-seq data.

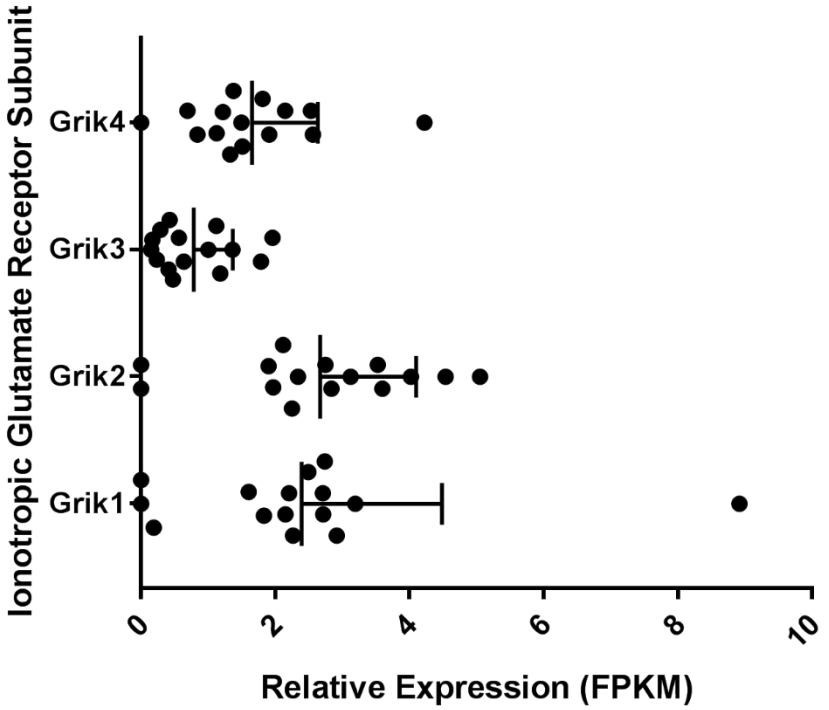

Figure 5.24: Relative expression (FPKM values) of mRNA coding for ionotropic glutamate receptor types in IML RNA-seq data.

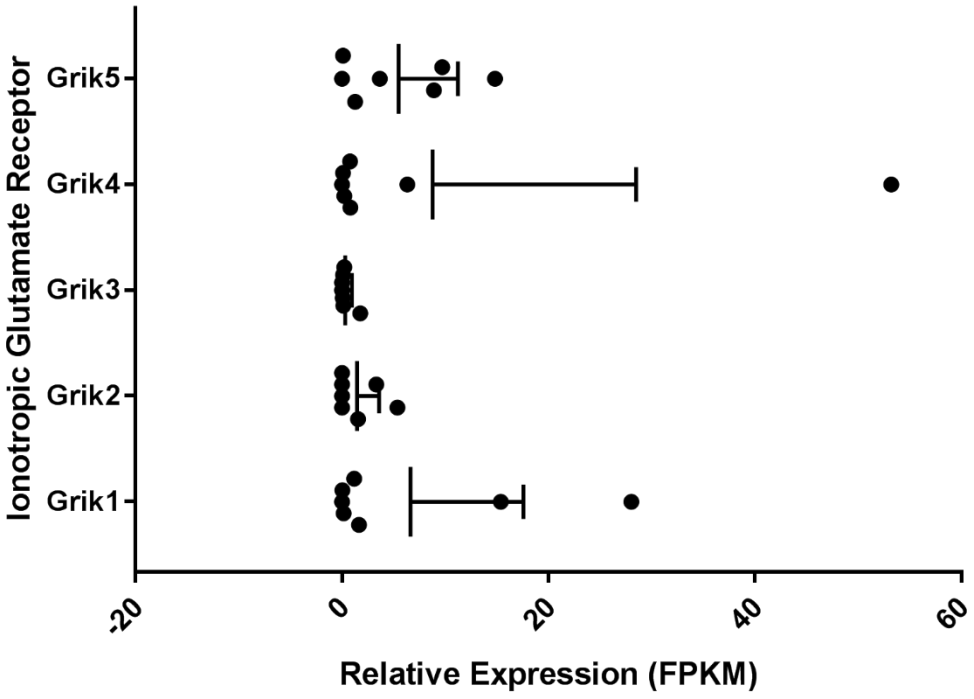

Figure 5.25: Relative expression (FPKM values) of mRNA coding for ionotropic glutamate receptor types in scRNA-seq data.

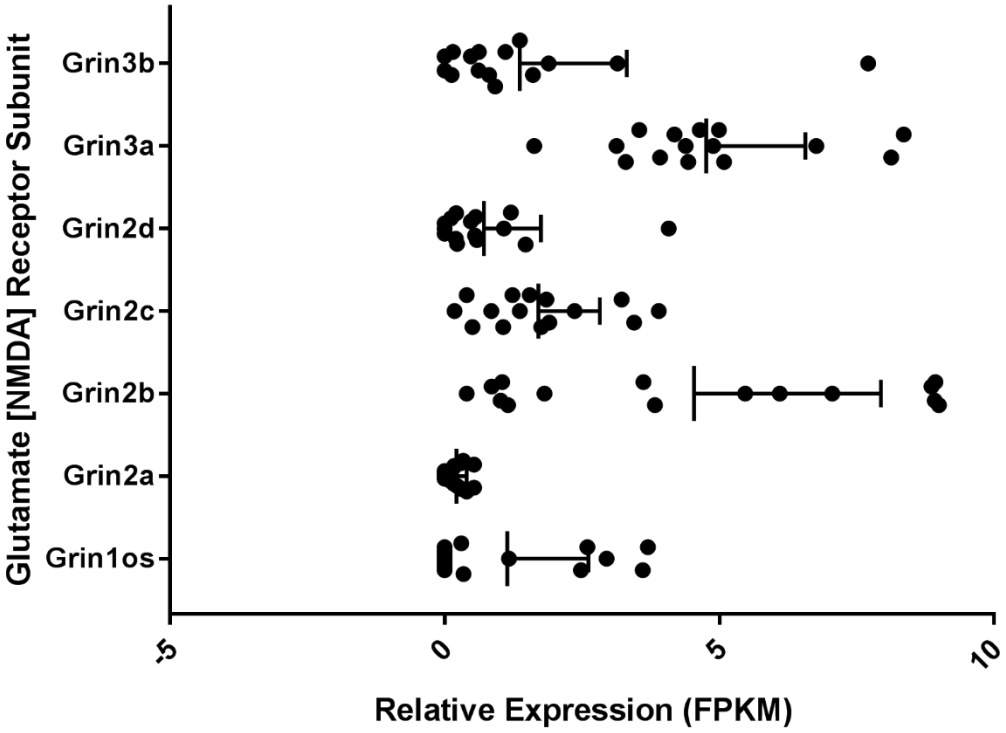

Figure 5.26: Relative expression (FPKM values) of mRNA coding for glutamate [NMDA] receptor subunits in IML RNA-seq data.

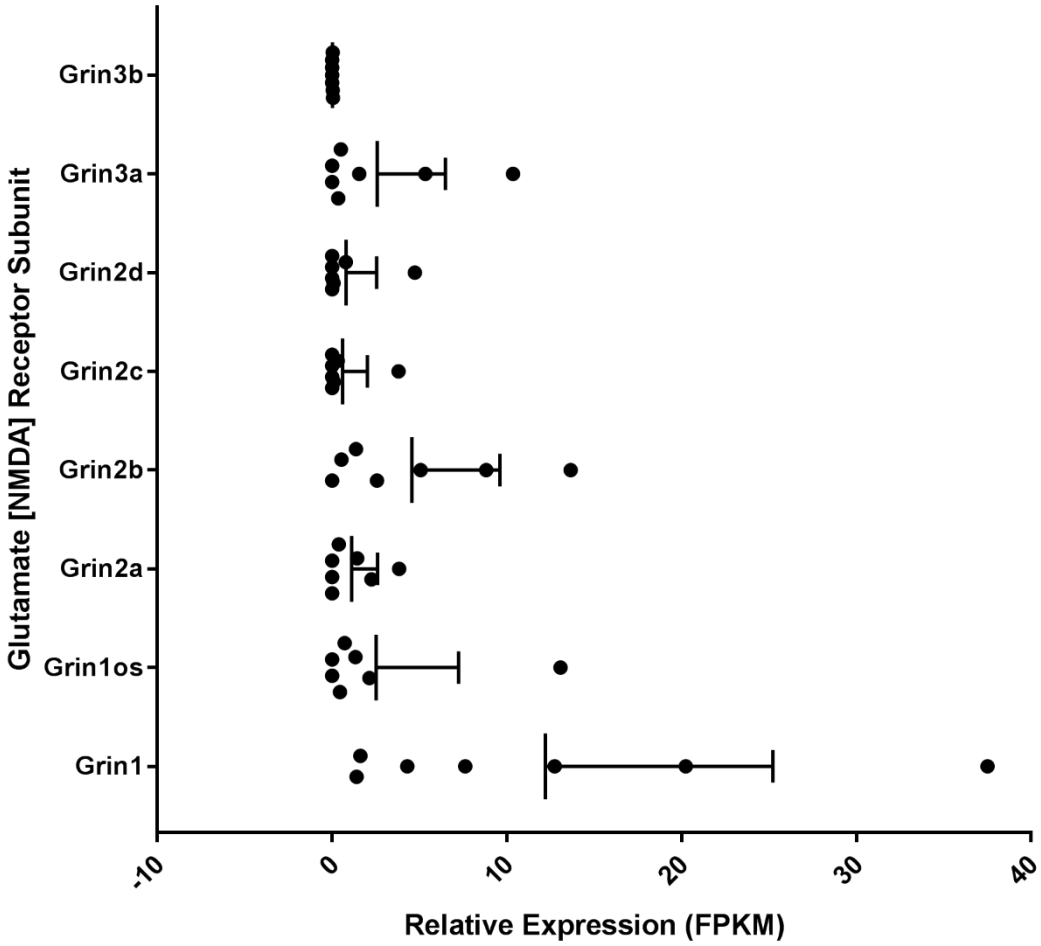

Figure 5.27: Relative expression (FPKM values) of mRNA coding for glutamate [NMDA] receptor subunits in scRNA-seq data.

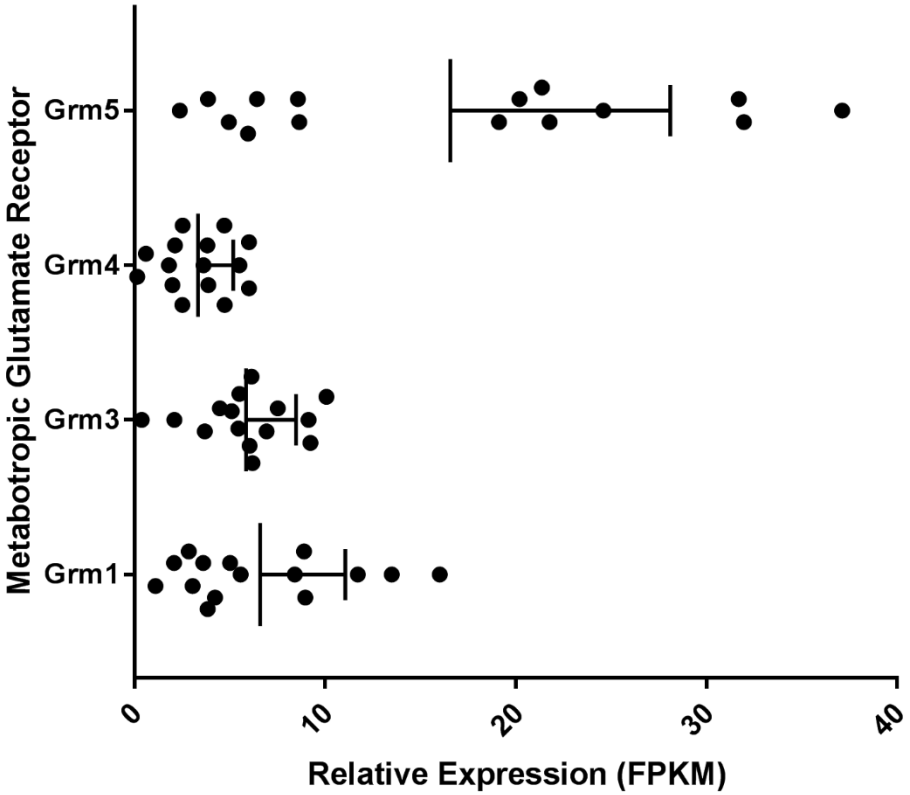

Figure 5.28: Relative expression (FPKM values) of mRNA coding for metabotropic glutamate receptor types in IML RNA-seq data.

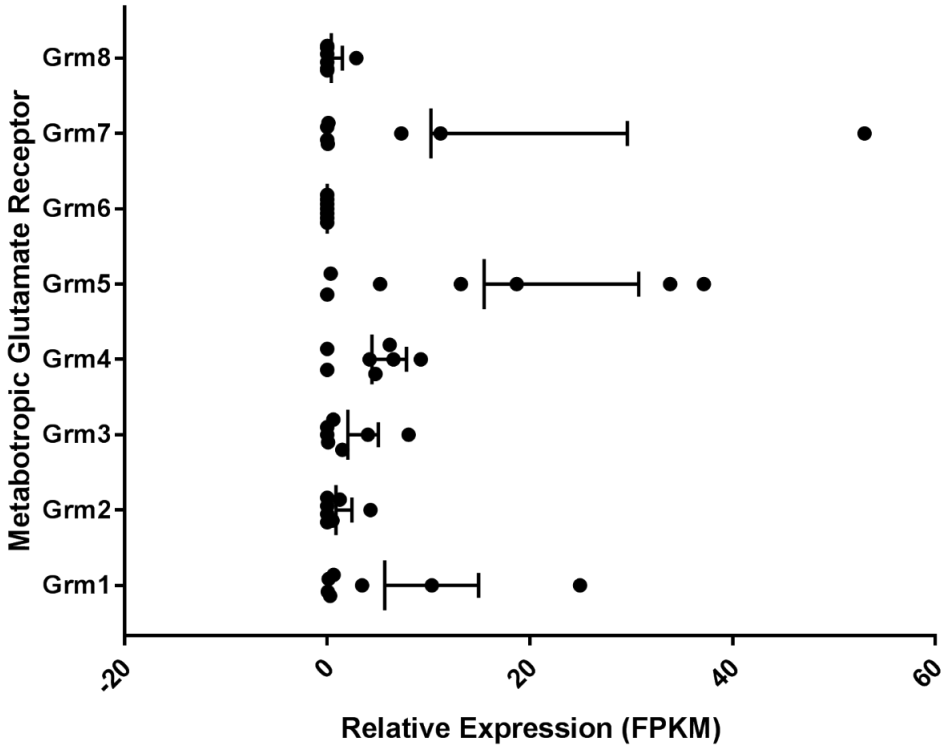

Figure 5.29: Relative expression (FPKM values) of mRNA coding for metabotropic glutamate receptor types in scRNA-seq data.

5-HT Receptors

5-HT receptors are a group of G protein-coupled receptors and ligand-gated ion channels that respond to 5-HT (Collingridge *et al*., 2009). In the IML data set, 5-HT_{2C} receptor (Htr2c) and 5-HT_{7} receptor (Htr7) had the highest FPKM values (Figure 5.30). Comparing between 5-HT receptor subtypes, 5-HT_{1A} receptor (Htr1a) and 5-HT_{1D} (Htr1d) receptor were highly expressed as measured by normalised FPKM (Table 5.10). 5-HT_{2C} receptor (Htr2c) had the highest expression when compared to other 5-HT_{2} receptor subtypes (Table 5.10). 5-HT_{3A} receptor (Htr3a) and 5-HT_{5A} receptor (Htr5a) were highly expressed compared to other 5-HT_{3} and 5-HT_{5} receptor subtypes respectively (Table 5.10). In the single cell data set, individual FPKM values were highest for 5-HT_{2C} receptor (Htr2c) and 5-HT_{5b} receptor (Htr5b) (Figure 5.31). Similar trends seen in the IML data set were observed when comparing relative expression (Normalised FPKM) in the $5HT_{1}$ and $5HT_{2}$ receptor subtype groups, 5-HT_{1A} receptor (Htr1a) and 5-HT_{2C} receptor (Htr2c) were highly expressed (Table 5.10).

A difference between the IML and single cell data set was observed when comparing relative expression (Normalised FPKM) in the $5HT_{3}$ and $5HT_{5}$ receptor subtype groups, 5-HT_{3B} receptor (Htr3b) and 5-HT_{5B} receptor (Htr5b) were highly expressed in the single cell data? (Table 5.10).

In ABA, mRNA expression of 5-HT_{1A} receptors is prevalent in the dorsal and lateral horns of the thoracic spinal cord. 5-HT_{2C} receptors were highly expression in the dorsal and lateral horns of the thoracic spinal cord. ISH images showed 5-HT_{3B} subunit mRNA expression in the lateral horn. mRNA expression of the 5-HT_{5B} receptor in IML SPNs was not observed in ABA

images however minor expression of the receptor was present in the thoracic spinal cord.

Table 5.10: Summary of relative gene expression of 5HT receptors in IML and scRNA-seq data set.

Gene of interest	Sample type	Level of relative gene expression (Normalised FPKM)
$5HT_1$ receptors	IML	Htr1a = Htr1d > Htr1f > Htr1b
	Single cell	Htr1a > Htr1f >Htr1d >Htr1b
$5HT_2$ receptors	IML	Htr2c > Htr2a > Htr2b
	Single cell	Htr2c > Htr2a = Htr2b
$5HT_3$ receptors	IML	Htr3a > Htr3b
	Single cell	Htra3b > Htr3a
$5HT_5$ receptors	IML	Htr5a > Htr5b
	Single cell	Htr5b > Htr5a

Sodium Channels

Sodium channels are membrane proteins composed of a mixture of α and β subunits that conduct sodium ions into the cell through the cell's plasma membrane (Wang *et al*., 2017). In the IML data set, FPKM values were highest for the sodium channel subunit β1 (Scn1b) (Figure 5.32). When comparing relative expression (Normalised FPKM) between sodium channel α subunits, sodium channel, voltage-gated, type I, α subunit (Scn1a) was highest followed by sodium channel, voltage gated, type VIII, α subunit (Scn8a) (Table 5.11). Sodium channel subunit β1 (Scn1b) was highest followed by sodium channel β subunit 4 (Scn4b) when comparing relative expression (Normalised FPKM) between sodium channel β subunits (Table 5.11).

Unlike the IML data set, the individual FPKM values for the sodium channel α and β subunits was highly variable in the single cell data set (Figure 5.33). Sodium channel, voltage-gated, type I, α subunit (Scn1a) and Sodium channel, voltage-gated, type III, α subunit (Scn3A) followed by sodium channel, voltage gated, type VIII, α subunit (Scn8a) and sodium channel, voltage-gated, α

subunit 9 (Scn9a) when comparing relative expression (Normalised FPKM) between sodium channel α subunits in the single cell data set (Table 5.11). When comparing relative expression (Normalised FPKM) between sodium channel β subunits in the single cell data set, sodium channel subunit β1 (Scn1b) was highest followed by sodium channel β subunit 3 (Scn3b) and sodium channel β subunit 4 (Scn4b) (Table 5.11). ABA images indicated both mRNA expression of the subunits was high across the thoracic spinal cord slice with SCN1b mRNA being especially high.

Table 5.11: Summary of relative gene expression of sodium channel α/β subnits in IML and scRNA-seq data set.

Gene of interest	Sample type	Level of relative gene expression (Normalised FPKM)
Sodium channel α subunits	IML	Scn1a > Scn8a > Scn3a
	Single cell	Scn3a > Scn1a > Scn8a > Scn9a
Sodium channel β subunits	IML	Scn1b > Scn4b > Scn2b > Scn3b
	Single cell	Scn1b > Scn3b = Scn4b > Scn2b

qPCR analysis of target genes in time point IML micropunches

A number of target mRNAs were measured in time point IML micropunches using qPCR based on the findings of the RNA-seq data. The target mRNAs coded for proteins such as a receptor, enzyme or neuropeptide which affect SPN activity these included: 5-HT_{2A} receptor (Htr2a), α2 adrenergic receptor (Adra2a), cocaine- and amphetamine-regulated transcript (CART), choline acetyltransferase (ChAT), connexin-36 (Gjd2) and $GABA_A$ receptor, α5 (Gabra5). 5-HT_{2A} receptor (Htr2a) mRNA expression showed a trend of being higher at 7:30 PM than 7:30 AM (Figure 5.34A, p=0.5). Adra2a mRNA expression was significantly higher at 7:30 AM than 7:30 PM (Figure 5.34B, $p<0.05$). CART RNA expression was also higher at 7:30 AM, however it was not found to be statistically significant (Figure 5.34C, p=0.3). ChAT and Gjd2 mRNA

expression were significantly higher at 7:30 AM (Figure 5.34D-E, $p<0.05$). Gabra5 mRNA expression was significantly higher at 7:30 AM (Figure 5.34F, $p<0.01$). Some of the target mRNAs exhibit diurnal rhythms, therefore suggesting that there is a diurnal regulation of gene expression in SPNs which may result in a diurnal rhythm of activity.

Comparison of differentially expressed genes between Chat-positive or GAD-positive single cells

When comparing ChAT-positive and GAD-positive cells several potential SPN markers were identified based on FPKM values; these genes coded for proteins that had diverse functions ranging from cell differentiation, immune response or were channel subunits (Table 5.12). The Allen Spinal Cord Atlas was used to examine whether these genes were expressed specifically in IML SPNs. The majority of candidates with high FPKM values in ChAT-positive cells labelled IML SPNs as well as other cell types such as ependymal cells and ventral horn motor neurons. Of the group of genes that were highly expressed in ChAT-positive cells, three genes appeared specifically expressed in IML SPNs. The first was immunorepressive gene 1 (Irg1) which is a protein involved in the immune response to pathogens (Michelucci, 2013). The second was TNFAIP3 interacting protein 2 (Tnip2) which is also involved in cellular immune response specifically by activating the MAP/ERK signalling pathway (Xie, 2017). The third gene was phospholipid scramblase 4 (Plscr4) which is thought to be involved in movement of phospholipids in activated or apoptotic cells (Wiedmer, 2000). The Allen Brain Spinal Cord Atlas was consulted to determine whether the marker candidates labelled IML SPNs specifically. Most markers candidates were nonspecific labelling IML SPNs, ependymal cells and ventral horn motoneurons. Irg1, Tnip2 and Plscr4 were specifically found in IML SPNs.

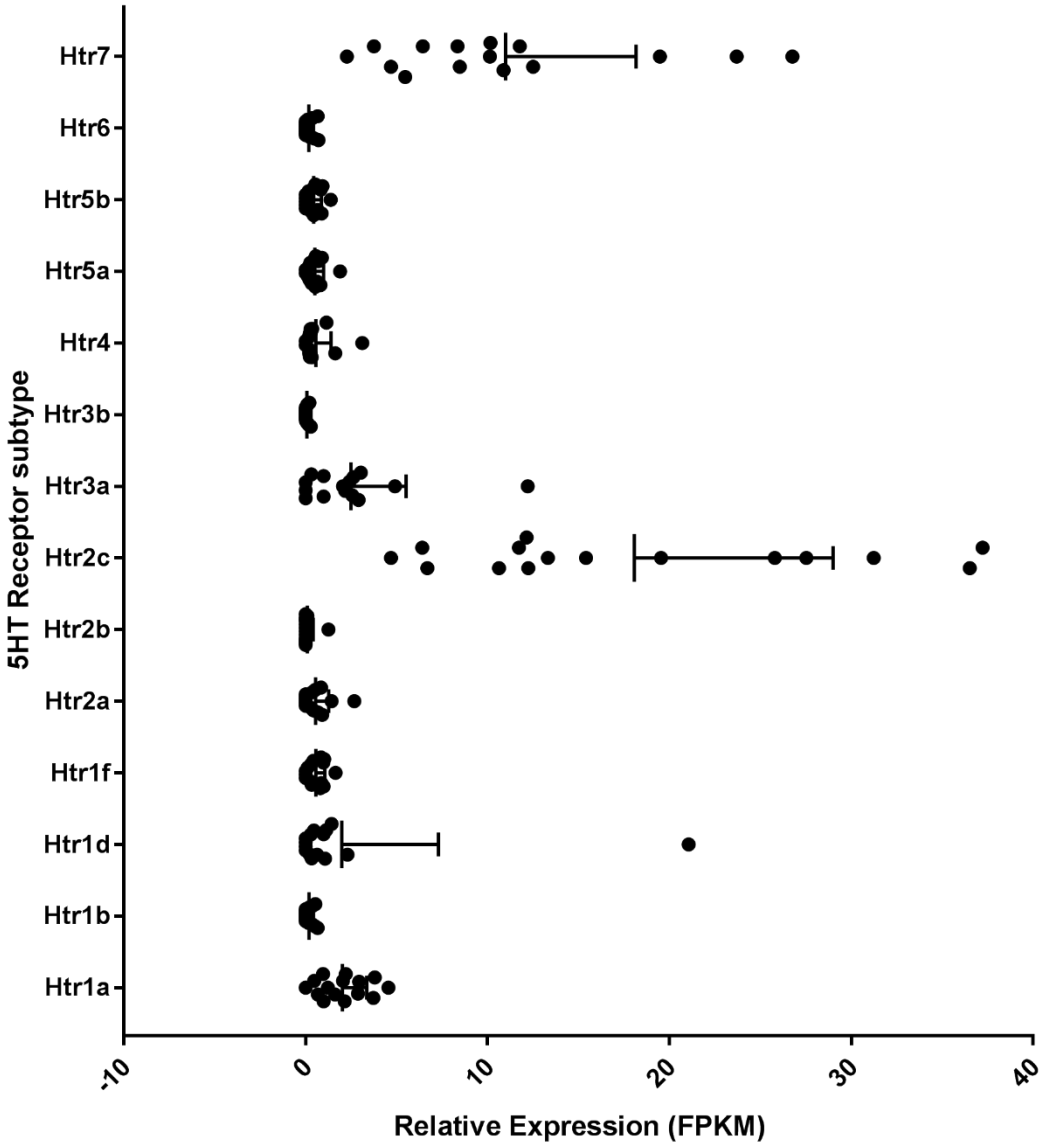

Figure 5.30: Relative expression (FPKM values) of mRNA coding for 5-HT receptor subtypes in IML RNA-seq data. mRNA coding for 5-HT_{2C} receptor (Htr2c) and 5-HT_7 receptor (Htr7) subtypes were highest expressed in the data set.

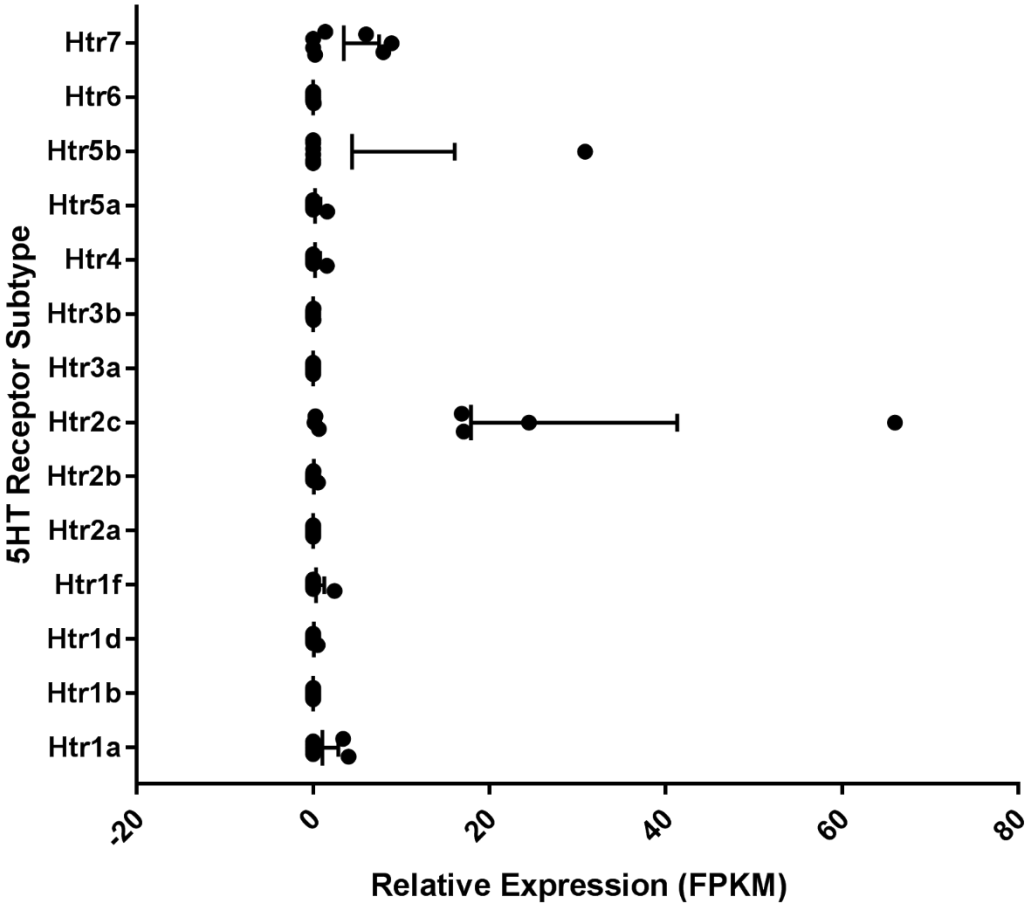

Figure 5.3: Relative expression (FPKM values) of mRNA coding for 5-HT receptor subtypes in scRNA-seq data.

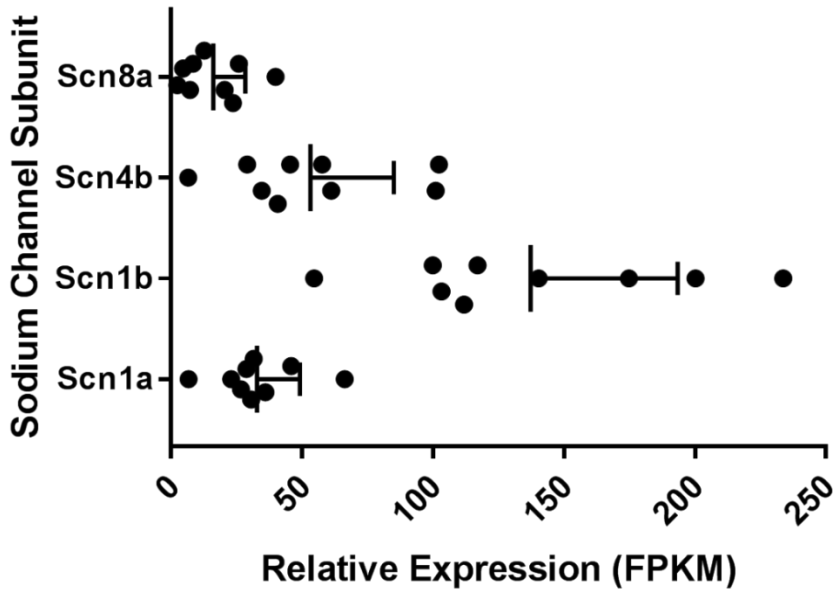

Figure 5.4: Relative expression (FPKM values) of mRNA coding for sodium channel α/β subunits in IML RNA-seq data. mRNA coding for sodium channel β1 subunit was highly expressed in the dataset.

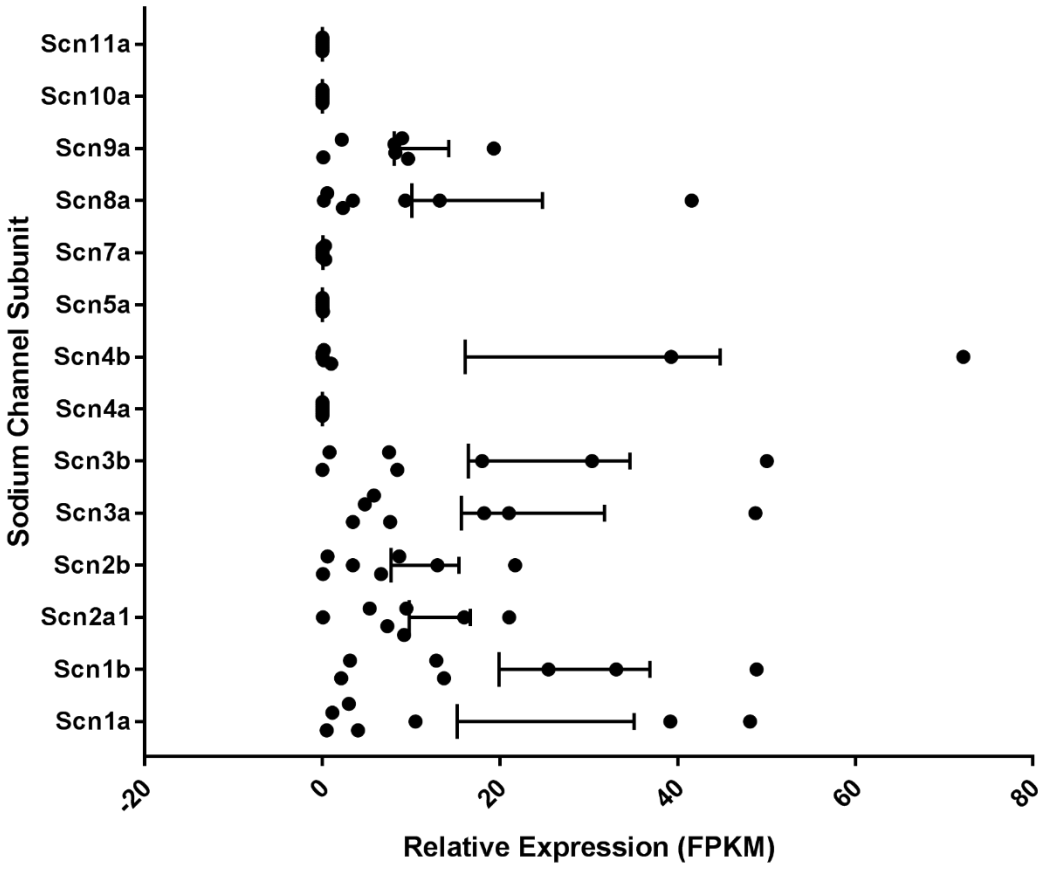

Figure 5.5: Relative expression (FPKM values) of mRNA coding for sodium channel α/β subunits in scRNA-seq data.

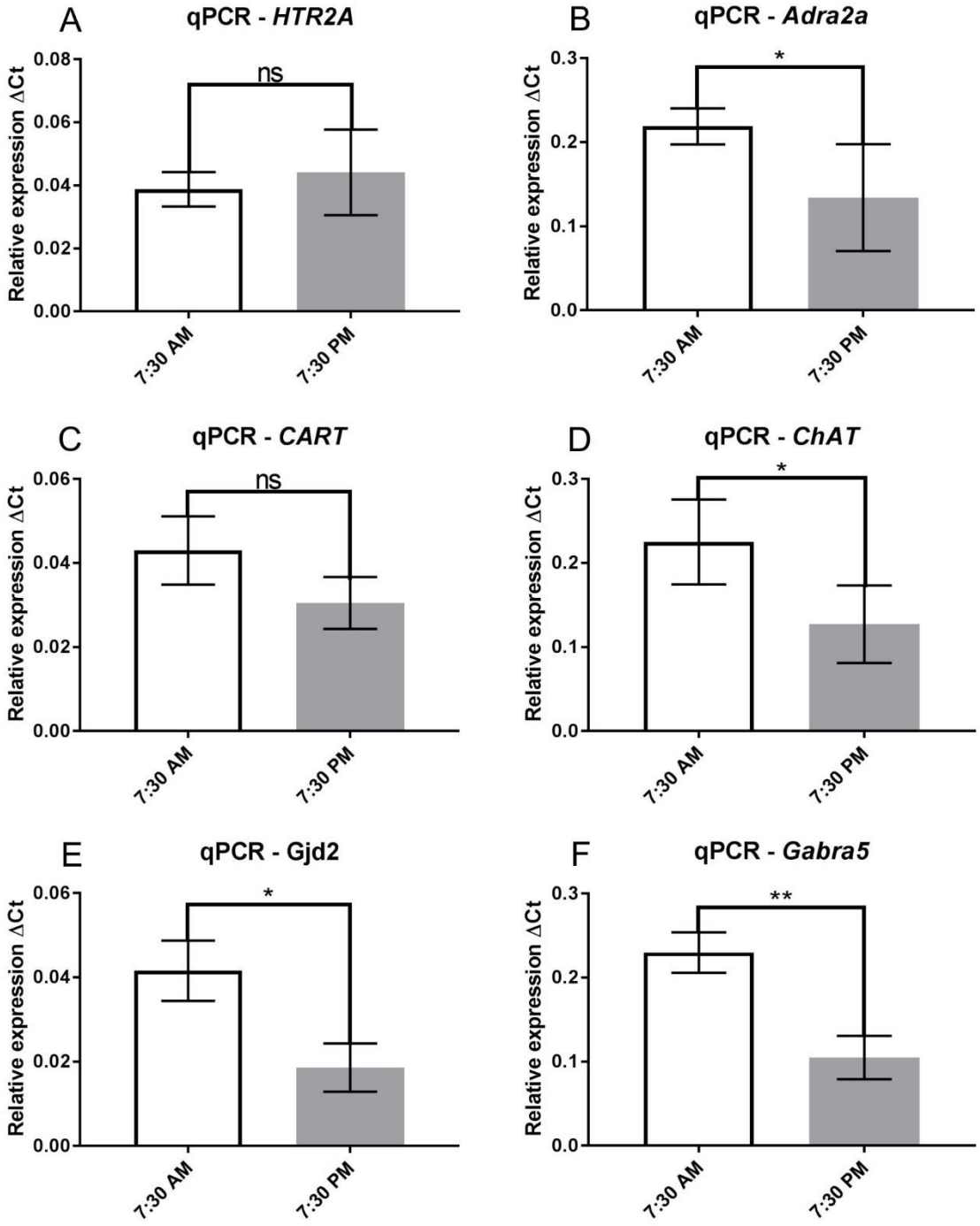

Figure 5.6: The effect of light-dark cycle on candidate genes in IML micropunches. mRNA coding for adrenergic α2 receptor subtype 2a (Adra2a), choline acetyltransferase (ChAT), connexion 36 (Gjd2) and GABAA receptor α5 subunit (Gabra5) displayed diurnal rhythms all being more highly expressed during the morning time point (7:30 AM).
qPCR analysis of candidate gene expression in IML micropunches, results are average of triplicate readings for each animal ±SEM (n=5 animals in each group). Significance measured with Mann-Whitney test: n.s (not significant), * ($p<0.05$), ** ($p<0.01$), *** ($p<0.001$), **** ($p<0.0001$).

Table 5.12: Comparison of differential mean FPKM expression between ChAT- and GAD-positive single cell samples.

Gene	Mean FPKM value (GAD cells)	Mean FPKM value (ChAT cells)	SPN	Ependymal cells	Ventral Horn Motoneurones	Function
Abtb2 - ankyrin repeat and BTB domain containing 2	0	4.7	Yes	No	Yes	The function of this protein is unknown.
Dnaja3 - DnaJ (Hsp40) homolog, subfamily A, member 3	0	1.8	Yes	No	Yes	This protein is involved in protein folding, degradation and multiprotein complex assembly. Within neuromuscular junctions this protein is responsible for clustering acetylcholine receptors for efficient synaptic transmission.
Fosl2 - fos-like antigen 2	0	4.0	Yes	No	Yes	The Fosl2 protein is thought to regulate cell proliferation,

						differentiation, and transformation.
Glra4 - Glycine receptor, alpha 4 subunit	0	4.8	Yes	No	Yes	The protein encoded is a subunit of the glycine receptor. Glycine receptors downregulate neuronal excitability, contributing to inhibitory postsynaptic currents.
Irg1 - Immunoresponsive gene 1	0	5.8	Yes	No	No	This protein is involved in immune response to pathogens.
Isl1 – Isl1 transcription factor, LIM/homeodomain	0	5.7	Yes	No	Yes	This gene encodes for a transcription factor involved in retinal ganglion cell

						differentiation, motor neuron specification and cardiac development.
Plscr4 - Phospholipid scramblase 4	0	6.9	Yes	No	No	This protein is thought to be involved in phospholipid migration and fibrin clot formation.
Pms1 - Postmeiotic segregation increased 1	0	6.9	Yes	No	Yes	This protein is thought to be involved in DNA mismatch repair and DNA damage signalling pathway.
Sdc2 - syndecan 2	2.9	63.6	Yes	Yes	No	A transmembrane protein involved in mediating mediate cell binding, cell signaling, and

						cytoskeletal organization and syndecan receptors.
Tnip2 - TNFAIP3 interacting protein 2	0	19.9	Yes	No	No	This protein is involved in cellular immune response by activating the MEK/ERK signalling pathway.

5.4 Discussion

Very few studies have focussed on using RNA-seq to study to gene expression profiles in the spinal cord. Rosenberg *et al*. is one of the few studies which characterized the gene expression profiles of cell types in RNA samples obtained from spinal cord samples. Cells were clustered into 4 distinct groups of neurons based on the gene expression profile: cerebrospinal fluid contacting cells, cholinergic motor neurons, GABAergic/glycinergic interneurons and glutamatergic interneurons. By identifying the 10 most enriched genes in each cluster the spatial origin within the spinal cord of each neuronal cluster was inferred with some GABAergic cell clusters being found in the IML region however the specific genes expressed within this area were not focussed on (Rosenberg *et al*., 2018).

This study is the first to attempt to produce a gene expression profile for SPNs using IML micropunch/multi-cell and single cell samples. A new rapid, efficient method of spinal cord extraction and single cell aspiration has been developed that does not affect RNA-seq library quality. This new method involved ejecting the spinal cord out of the spinal column using hydraulic pressure, this process removes the meninges around the spinal cord thus eliminating the need to clean the spinal cord prior to processing. It is important to note that this protocol can be performed in adult animals with little damage to the spinal cord. The spinal cord is rapidly frozen in optimal cutting temperature (OCT) compound thus RNA damaging enzymes are unlikely to affect the mRNA of the spinal cord. Images taken of the spinal cord slices following thawing indicate the morphology of the spinal cord slice is not affected by the freezing or thawing process ensuring accurate selection of samples from areas of interest such as the IML. Furthermore, aspirating IML multi-cell or single cell samples from

thawed frozen spinal cord slices had no effect on the quality of the libraries when compared to libraries of IML micropunches and single cell samples obtained from fresh spinal cord slices.

Using frozen sections for both tissue samples and single cell RNA analyses introduces new possibilities for RNA-seq experiments in other tissues and other CNS regions. For example, the nucleus ambiguus (NA) is one example of a CNS region involved in autonomic control in which neurones with different functions are often intermingled – those in the external formation that predominantly control the heart are surrounded by other cells (Izzo *et al*., 1993). The ability to pick single cells from frozen sections means that these cardiac vagal preganglionic neurones could be labelled retrogradely with a fluorescent tracer and picked individually from the frozen sections.

For SPNs, those projecting to different ganglia or to the adrenal gland could be fluorescently labelled retrogradely prior to harvesting cells. Although viruses have been used to transganglionically label SPNs projecting to specific organs (Strack and Loewy, 1990), such viruses influence mRNA processing and so would not likely be beneficial in such studies.

Another use for this approach to investigating SPNs could be to examine gene expression in SPNs in the IML compared to those in the intermediate zone and lamina X. Due to time and financial constraints, this current study focussed only on the IML and SPNs located there. However, all SPNs could be identified in sections by pre-labelling with, for example Fluorogold (Ambalavanar and Morris, 1989) or in TG animals expressing fluorescent reporters in ChAT cells.

A major benefit from using the frozen section approach is that whole tissue can be frozen, sectioned and stored in a -80^{o}C freezer until cell harvesting. This has

the potential to significantly reduce the number of animals required for RNA-seq studies in any tissue or CNS region. Another benefit could be in studies of circadian rhythms – freezing tissue is expected to halt RNA production at the time of freezing, enabling exact timing of tissue collection. Although the experiments in this chapter did not reach this stage, they lay foundations for future studies to do so.

Adrenergic (alpha 1 and 2) Receptors

α_{1B} adrenergic receptor and α_{2A} adrenergic receptor were the highest expressed adrenergic receptor types in both the IML and single cell data sets. Furthermore consulting the Allen brain atlas (ABA) database, IML SPNs in thoracic spinal cord slices selectively express mRNA coding for α_{2A} adrenergic receptor; this suggests that α_{2A} adrenergic receptor as an attractive candidate to utilize to select for IML SPNs. Future work should examine the effectiveness of using α_{2A} adrenergic receptor antibodies to select SPNS, perhaps using ChAT staining and/or fluorogold as in chapter 3.

These receptors are targets for adrenaline and noradrenaline which have both excitatory actions, mediated by interactions with α_1 receptors, and inhibitory, mediated by interactions with α_2 receptors, effects on SPNs (Guyenet and Cabot, 1981, Deuchars and Lall, 2015). Intracellular recording of SPNs using whole-cell patch-clamp technique in neonatal rats found that noradrenaline induced inhibitory hyperpolarization on some SPNs suggesting that α_2 receptors modulate these effects on SPNs (Minoura *et al*., 2018). The ratio of α_1 and α_2 adrenergic receptor types present on SPNs may lead to different responses according to the catecholamine that targets them. Synaptic transmission involving adrenaline or noradrenaline to the SPNs may play a crucial role in

cardiovascular control, previous research has demonstrated excitatory and inhibitory effects of noradrenaline on cardiovascular-projecting SPNs which could potentially effect BP however the downstream effects of this action on SPNs has not been described (Coote *et al.*, 1981; Guyenet and Cabot, 1981; Weidmann *et al*., 1983).

Voltage-Gated Calcium Channels

Each type of voltage-gated calcium channel is made of combination of subunits, these channels are involved in neuronal excitability and synaptic transmission (Catterall, 2000). There was a difference in the L-type calcium channel subunits that were expressed in IML and single cell data with calcium channel, voltage-dependent, L type, $\alpha 1_S$ subunit (Cacna1s) being highly expressed in the IML data set while calcium voltage-gated channel subunit $\alpha 1_C$ (Cacna1c) and calcium voltage-gated channel subunit $\alpha 1_D$ mRNA (Cacna1d) were highest in the single cell data set. Similar subunits of the T-type and voltage-dependent calcium channels were expressed in the IML and single cell data sets. P-type channel subunit ($\alpha 1_A$), as identified in both the single cell and IML data sets is surprising as expression of this channel is usually restricted to the cerebellum however a study by Burgos *et al*. found P-type channels were expressed in rat sympathetic superior cervical ganglion using selective calcium channel blockers (Gonzalez Burgos *et al*., 1995). Interestingly, N-type and P-type calcium channels were the main calcium channel types and play a dominant role in the release of acetylcholine from lumbar SPNs in guinea pigs which were identified using antagonists for those channels (Ireland *et al*., 1999, Jobling *et al*., 2004). The functional output of activation of these calcium channels on these lumbar SPNs was not determined but it was speculated they may play a role in manipulating sympathetic pathways such as those controlling vasoconstriction

(McLachlan *et al.*, 1997; Ireland, Davies and McLachlan, 1999). T-type channel subunit $\alpha 1_I$ is a CNS specific isoform and was the highest LVA isoform in single cells. IHC conducted on mouse embryos found expression of $\alpha 1_I$ in the spinal cord. $\alpha 1_I$ mRNA transcripts were found in the dorsal horn of the spinal cord which agrees with the ISH image from the ABA (Talley *et al*., 1999, Perez-Reyes, 2003). When consulting the ABA, Cacna1c and Cacna1d mRNA was expressed in IML SPNs but also other cell types, with expression in both the dorsal and ventral horns. Cacna1s mRNA expression was expressed at low levels across the thoracic spinal cord slice.

Muscarinic Receptors

Acetylcholine elicits an inhibitory response via muscarinic receptors; there are five types of muscarinic receptors. Muscarinic receptors M2, M3 and M4 were prevalent in the IML and single cell data. M4 was higher in single cells suggesting that perhaps this muscarinic receptor type is more prevalent in SPNs.

Muscarinic receptor M2: Whole cell current-clamp recordings from SPNs found that hyperpolarizing responses were due to M2 receptor activation (Gibson and Logan, 1995). M2 receptors were identified as the main receptor type in the SPNs mediating anti-inflammatory effects. Briefly, mice received injections of bee venom in their hind limb which triggered acetylcholine release in the spinal cord, as measured by counting the number of Fos- and ChAT-double labelled neurons in the thoracic spinal cord slice. Acetylcholine acts on the M2 receptors on SPNs which in turn signal the adrenal medulla to release catecholamines to contribute to the anti-inflammatory response as measured by a reduction in

leukocyte count in exudate fluid collected from the site of inflammation (Yoon *et al*., 2005).

Muscarinic receptor M3: M3 receptors were the highest expressed muscarinic receptor type in the IML data which could be due to other cell types in the IML region that have high expression of M3 receptors.

Muscarinic receptor M4: The M4 receptor was the highest expressed receptor in the single cell data which suggests that this muscarinic receptor type may be prevalent in SPNs.

Muscarinic receptor types are often co-expressed with other receptor types (Tsentsevitsky *et al*., 2017). Therefore these receptors may work in unison to modulate their inhibitory effect on SPN activity. ABA images of thoracic spinal cord slices showed higher levels of M4 receptor mRNA expression throughout the section. Indeed there appeared to be higher M4 receptor mRNA expression in the IML SPN region than the ventral horn region. M3 receptor mRNA expression was sparse across the spinal cord slice but also appeared to be expressed by fewer IML SPNs, which could potentially be related to the function of particular SPNs within this area. Marquez *et al* studied the binding of [3H]-N-methyl-escopolamine, the agonist carbachol and the antagonist pirenzepine to muscarinic receptors in rat forebrains at a series of time points and found that muscarinic receptors binding affinity was lowest during the evening time points suggesting the receptor expression was low during this time period (Marquez, 1990). Activation of muscarinic receptors by intrathecal administration of muscarinic receptor agonist pilocarpine in dogs resulted in a reduction in BP suggesting muscarinic receptors are involved in sympathetic control of vasomotor tone (Bhargava *et al*., 1982). These findings suggest that inhibitory

response to acetylcholine mediated by the muscarinic receptors is potentially reduced during the evening, which is the active period of mice. To date, no such studies have been made on SPNs.

Nicotinic Receptors

Nicotinic receptors causes an excitatory response in SPNs in response to acetylcholine (Yoshimura and Nishi, 1982). In Bhargava's *et al*., study found that intrathecal administration of nicotinic receptor agonist dimethylphenylpiperazinium (DMPP) caused a BP increase; this finding suggests nicotinic receptors play an important role in determining IML SPN influence on sympathetic vasomotor tone (Bhargava *et al*., 1982). These receptors are formed of a pentameric combination of either α, β, δ or ε subunits. Neuronal acetylcholine receptor subunit α1 (CHRNA1) and neuronal acetylcholine receptor subunit α4 mRNA (CHRNA4) are the two types of nicotinic receptor subunits that were expressed in the IML and single cell data. The alpha subunit defines the sensitivity of the nicotinic receptor to acetylcholine. The α1 and α4 subunits were determined to be more sensitive to acetylcholine by measuring acetylcholine-evoked currents in voltage clamped *Xenopus* oocytes (Gross *et al*., 1991). mRNA expression of both neuronal acetylcholine receptor subunit α1 and neuronal acetylcholine receptor subunit α4 does appear to be present in IML SPNs. Neuronal acetylcholine receptor subunit α4 mRNA is highly expressed throughout the slice and in more IML SPNs which appears to be mirrored in the scRNA-seq data as the α4 subunit is more highly expressed. A similar experiment by Mexal *et al*. examined the binding affinity of radiolabelled α-bungarotoxin to nicotinic receptors in the cortex, hippocampus, hypothalamus and striatum at a series of time points and found that the only significant difference was observed in the hypothalamus,

maximal binding occurs during the early morning and late evening (Mexal, 2012). If a similar pattern of expression of nicotinic receptors is found in the spinal cord this suggests an increase in excitatory receptors in SPNs during the evening which is the active period of mice.

$GABA_A$ and $GABA_B$ Receptors

Analysis of GABA receptor expression in samples of IML and single SPNs revealed numerous subunits were potentially present. However, of particular interest were subunits that are rare in the CNS but that could be detected in these samples. These include the θ, α5 and ρ subunits.

α5 *subunit*: the presence of the α5 subunit in RNA-seq analysis is consistent with expression of α5 previously seen with qPCR in rat IML, supported by patch clamp recordings from SPNs in spinal cord slices which indicated that α5 containing receptors underpinned a tonic background inhibition (Wang *et al*., 2008a). Since α5 is considered relatively rare except in the hippocampus, as indicated by regional distribution and immunoprecipitation studies (Pirker *et al*., 2000; Sieghart and Sperk, 2002), SPNs may provide a novel avenue to explore the properties of receptors containing this subunit. In addition, qPCR studies in this chapter revealed that α5 expression varied with time of day, suggesting that the tonic GABA current in SPNs could exhibit circadian variation and so contribute to changes in sympathetic activity. Indeed, expression of α5 was higher in the morning, which in mice could coincide with lower blood pressure consistent with decreased SNA which could be due to enhanced GABAergic inhibition however future work is required to confirm this (Mahadi *et al.*, 2019).

Θ subunit: expression of theta in SPNs was supported by reference to the Allen Spinal Cord Atlas, where the θ subunit appeared to be expressed highly (and

potentially exclusively) in SPNs in the thoracic cord. This subunit is one which has been rarely investigated. It was first reported in 1999 as highly expressed in the striatum, where it co-immunoprecipitated with α2, β1, and γ1 subunits to likely form α2β1γ1θ or α2β1γ2θ receptors (Bonnert *et al*., 1999). Addition of the θ subunit increases the EC50 of GABA but with no effect on actions of many known GABA receptor neuromodulators. Further study suggests that the θ subunit appears to be able to contribute to receptors comprising α3β1εθ and α3β1θ in expression systems at least, where it confers a high efficacy for etomidate, which enhances currents evoked by GABA in α3β1θ receptors by 364% (Ranna *et al*., 2006).

It seems likely that at least some $GABA_A$ receptors in SPNs contain the θ subunit: etomidate profoundly reduces preganglionic nerve activity when administered IV in anaesthetised cats (Skovsted and Sapthavichaikul, 1977) or to decerebrate rabbits (Hughes and Mackenzie, 1978). Indeed, the sensitivity of theta subunit to etomidate may explain the arterial hypotension seen in some patients after etomidate anaesthetic induction (Van Berkel *et al*., 2017, Abou Arab *et al*., 2019). The apparent selectivity of θ subunit expression in the thoracic cord to SPNs could provide a novel target for modulating the activity of sympathetic nerve activity. Unfortunately, when an antibody against the θ subunit was tested in thoracic spinal cord slices using IHC, ventral horn motoneurons were labelled eliminating this subunit to be used for SPN isolation.

ρ1 subunit: single cell and IML RNA-seq indicate that SPNs may express the ρ1 subunit. Indeed, ρ subunits are observed across the thoracic spinal cord slice in ABA images (Figure 5.31E, F). The ρ subunits were once considered to form homomeric ρ containing channels called $GABA_C$ receptors, but with increasing evidence that they can form heteromers with $GABA_A$ subunits are now

considered as part of the $GABA_A$ subfamily (Milligan *et al*., 2004, Olsen and Sieghart, 2008). Whilst it appears that ρ subunits can confer particular pharmacological properties on GABA receptors, the so-called $GABA_C$ receptor agonist CACA was without significant effect on SPNs (Whyment *et al*., 2004, Naffaa *et al*., 2017).

$GABA_A$ receptor composition in SPNs: $GABA_A$ receptors are typically considered to consist of 2 α, 2 β and a γ subunit. The most highly expressed γ subunit in our samples was γ2 and it therefore seems likely that this forms part of $GABA_A$ receptors on SPNs. Considering pharmacological evidence alongside the expression data here, there appears to be at least some receptors containing the α5 subunit and/or the θ subunit. SPNs receive GABAergic innervation from diverse sources that include cells in lamina X, local interneurones and even long-range GABAergic projections from the ventrolateral medulla (Guyenet and Stornetta, 2004, Deuchars *et al*., 2005). In other CNS regions the receptor subunit composition at synapses appears to vary according to the synapse type (Semyanov *et al*., 2004). It would therefore be of interest to determine if this is the case for the different sources of GABAergic input to SPNs.

$GABA_B$: $GABA_B$ receptors are G-protein receptors that play an important role in controlling neuronal excitability at both pre-and post-synaptic sites. Both GABABR1 and GABABR2 subunits were detected in the RNA-seq, with GABABR1 more highly expressed. This is also observed in ABA images with GABABR1 being more highly expressed as indicated by the expression mask (Figure 5.32). Since a functional $GABA_B$ receptor requires GABABR1 to form a heteromer with GABABR2 (Fritzius, 2019), it is perhaps unsurprising that both subunits are detected. Functionally, rat SPNs in spinal cord slices have been

shown to respond to activation of postsynaptic $GABA_B$ receptors with a number of different types of responses, with the differences suggested to be due to distinct second messenger systems in different SPNs, which appears possible due to such diversity observed in other systems (Wang, 2010, Fritzius, 2019).

Glutamate Receptors

AMPA receptor subunits: The AMPA receptors are composed of different combinations of the Gria1, Gria2, Gria3 or Gria4 subunits and may vary with neuronal function which could explain why certain subunits were more highly expressed in the IML and single cell data sets. Glutamate acts through AMPA receptors to initiate fast excitatory postsynaptic potentials of SPNs (Deuchars *et al*., 1995, Llewellyn-Smith *et al*., 1997). An IHC study looking at the presence of AMPA receptor subunits in SPNs located in thoracic level 8 of the spinal cord found that cells had receptors composed of Gria1, Gria2 and Gria3 subunits but were not immunoreactive to Gria4; a high number of SPNs at this level possessed Gria2 subunits (McNair *et al*., 1998). High expression of the Gria4 subunit in the IML data set could be explained by the fact that the entire area was sampled therefore other cell types may have higher expression of Gria4 subunits. mRNA coding for the Gria2 subunit was highly expressed in the single cell data set which agrees with the findings of the McNair study and suggests that the single cells are likely to be SPNs. Gria2, 3 and 4 are highly expressed in the thoracic ABA images all three subunits are highly expressed in the IML region according to expression mask images (Figure 5.36). It is interesting to note that the Gria2 subunit undergoes RNA editing at the mRNA sequence which determines the Q/R site of the protein. RNA editing of the Q/R site of the Gria2 subunit determines the calcium permeability of the channel. This process has been implicated in mediating thiamine deficiency-induced neuronal damage

in cultured cortical neurons where edited R subunits of the Gria2 subunit form calcium impermeable channels protecting cortical neurons from thiamine deficiency-induced cytotoxicity (Lee *et al*., 2010).

Kainate receptor subunits: Kainate receptors play a role in the excitation of SPNs in response to glutamate (Spanswick and Logan, 1990). Glutamate receptor ionotropic kainate 4 (Grik4) and glutamate receptor, ionotropic kainate 5 (Grik5) were the highest expressed kainate receptor subunits in the RNA-seq data sets. These subunits require other kainate receptor subunits to form a functional receptor (Collingridge *et al*., 2009). Glutamate receptor, ionotropic kainate 4 mRNA expression seems to be limited to IML SPNs in ISH and expression images whereas glutamate receptor, ionotropic kainate 5 mRNA expression is more widespread throughout the spinal cord slice.

NMDA receptor subunits: Similar to the AMPA receptors, glutamate can act through NMDA receptors to initiate fast excitatory postsynaptic potentials of SPNs (Clendening and Hume, 1990, Llewellyn-Smith *et al*., 1997). Glutamate [NMDA] receptor subunit 3A (Grin3A) and glutamate [NMDA] receptor subunit ε2 (Grin2B) were highly expressed in the IML and single cell data sets. Glutamate [NMDA] receptor subunit 3A (Grin3A) was previously only described in the dorsal and ventral horn motor neurons in the lumbar spinal cord (Wee *et al*., 2008). Glutamate [NMDA] receptor subunit 3A (Grin3A) is thought to be involved in the development of excitatory synapses acting to prevent strengthening or stabilization of the synapse by limiting the development of dendritic spines (Pérez-Otaño *et al*., 2016). IHC experiments have demonstrated glutamate [NMDA] receptor subunit ε2 (Grin2B) are present in neurons located in the dorsal horn of the lumbar spinal cord (Zhang *et al*.,

2013). A study tracing synapse formation in organotypical hippocampal slices found that overexpression of Grin2B subunits caused an increase in spine motility; conversely a similar study conducted in co-cultures of cerebral cortex and cervical spinal cord slices found that Grin2B was involved in synapse elimination (Ohno *et al*., 2010, Gambrill and Barria, 2011). Previous research has demonstrated that NMDA receptors composed of either Grin3A or Grin2B subunits are required in a ratio to control synapse development; this raises the possibility that these presence of these receptor subunits could affect SPN synapse development or have an ongoing role in synaptic plasticity.

mGLuR receptors: Metabotropic glutamate receptor 5 (GRM5) was highly expressed in both the IML and single cell data sets. This particular receptor is a member of group I metabotropic receptors which depolarize SPNs (Deuchars and Lall, 2015). The presence of metabotropic glutamate receptor 5 have been found in IML SPNs in rat spinal cord using IHC. This receptor is not expressed as highly in ventral horn motor neurons which suggests that this receptor could be used to select for SPNs specifically.

The PVN and RVLM influence IML SPN sympathoexcitatory drive through glutamatergic transmission which in turn can influence cardiovascular parameters such as BP (Deuchars *et al*., 1995; Deuchars *et al*., 1997; Pyner, 2009). The glutamate receptor mRNAs expressed within the IML and scRNA-seq data sets suggests that some of these receptors are present in IML SPNs, future work should target these receptors to determine downstream functional effects on cardiovascular parameters.

5-HT Receptors

5-HT causes excitation or inhibition of SPNs depending on the type of receptors involved. 5-HT_2 receptors cause excitatory responses while 5-HT_{1A} receptors cause inhibitory responses.

5-HT_{1A} receptors: These receptors were highly expressed in the IML and single cell data set. 5-HT_{1A} receptors mediate the biphasic response, an initial depolarization followed by a long hyperpolarization, to 5-HT exhibited by SPNs (Pickering *et al*., 1994, Deuchars and Lall, 2015).

5-HT_2 receptors: 5-HT_{2C} were the highest expressed receptor type of this group in the IML and single cell data set. These receptors play an important role mediating SPN excitability as they mediate strong depolarisation of SPNs by 5-HT (Pickering *et al*., 1994).

5-HT_3 receptors: There was a difference between the data sets in terms of which 5-HT_3 receptor subunits were expressed, with 5-HT_{3A} being higher in the IML while 5-HT_{3B} was higher in the single cell data. The 5-HT_{3A} can form a functional subunit on its own unlike the 5-HT_{3B} subunit (Barnes *et al*., 2009). ISH experiments targeting mRNA of both subunits found neuron populations in the rat dorsal and ventral horn expressing mRNA coding for the subunits (Morales and Wang, 2002). This makes the current study the first in describing these receptor subunits in the mouse spinal cord specifically in the IML and SPNs. Low 5-HT_{3B} mRNA expression was observed in some IML SPNs in the ABA images.

5-HT_5 receptors: 5-HT_{5A} receptors were highly expressed in the IML however, 5-HT_{5B} receptors were highly expressed in the single cell data set. 5-HT has been demonstrated to inhibit sympathetic chronotropic outflow; continuous

intravenous perfusions of 5-HT in a pithed rat preparation prevented tachycardia caused by electrode stimulation of preganglionic sympathetic outflow spanning cervical segment 7 to thoracic segment 1. This inhibition was thought to be solely the result of 5-HT_1 receptors located in the spinal cord however this effect was mimicked when using an agonist for 5-HT_{5A}/5-HT_{5B} receptors suggesting these receptors may play a role in this process as well (Villalón *et al*., 1999, Sánchez-López *et al*., 2003).

5-HT can cause excitation or inhibition of SPNs depending on the type of receptors involved however the downstream effect of this excitation/inhibition is unknown. Previous research has found intrathecal administration of 5-HT agonists and 5-HT release within the thoracic spinal cord correlates to an increase in BP therefore it is highly likely serotonergic neurotransmission is involved in sympathetic BP control at the level of SPNs (Pilowsky *et al.*, 1986; Helke *et al*., 1991; Pilowsky and Goodchild, 2002).

Sodium Channels

Neural sodium channels are composed of α1, β1 and β2 subunits and are essential for the generation and propagation of action potentials. The α subunits are responsible for normal electrophysiological function while the β subunits are considered to be auxiliary subunits however, they do function to regulate sodium channel kinetics and voltage dependence. Previous research has found β2 subunits were widely distributed in the spinal cord. (Wang *et al*., 2017). Nav1.1, encoded by the SCN1A gene, channel subunits are expressed in the axon initial segments and nodes of Ranvier from the cervical to sacral segments of the spinal cord (Black *et al*., 1996, Duflocq *et al*., 2008). The sodium channel, voltage-gated, α1 (SCN1A) and sodium channel subunit β1

(SCN1B) were highly expressed in both the IML and single cell data sets; whether these channel subunits play a role in sympathetic control of vasomotor function is currently unknown. The expression of both subunits in both the IML and single cell data sets suggests that the sodium channels in this area are composed primarily of α1 and β1 subunits.

qPCR analysis of target genes in time point IML micropunches

The mRNA targets depicted potential diurnal rhythms but only Adra2a, ChAT, Gjd2 and Gabra5 were significantly higher in the morning (Figure 5.57). Adra2a and Gabra5 are involved in inhibitory responses in SPNs suggesting that SPNS could be inhibited or less active in the morning when mice have an increased tendency to sleep, consistent with experimentally observed lower levels of sympathetic activity (Wang *et al*., 2008a, Deuchars and Lall, 2015).

GABAergic signalling has a profound inhibitory effect on sympathetic outflow by acting on IML SPNs. Previous work identified α5 subunits as being prevalent in the IML and α5 subunit-containing receptors activation mediate the inhibitory response in SPNs which could prevent the development of high blood pressure (Wang *et al*., 2008a). Gabra5 mRNA which codes for the α5 subunit is more prevalent during the day; taking in account the knowledge that α5 subunit-containing receptors mediate SPN inhibition, an increase in these receptors at night could be involved in reducing the sympathetic outflow influencing blood pressure thereby reducing it. No previous research has examined the diurnal rhythm of Gabra5 in the spinal cord however, diurnal changes in GABAergic tone and in other GABA receptor subunits has been observed in the SCN (Novak and Albers, 2004, Albers *et al*., 2017, Brancaccio *et al*., 2017). GABAergic signalling is very important in the SCN and exhibits a diurnal

rhythm. SCN astrocytes suppress SCN neurons through GABAergic signalling during circadian night. GABAergic tone is decreased during circadian day when the SCN neurons are active (Brancaccio *et al*., 2017). This is opposite to the findings stated earlier for the IML, suggesting that the circadian rhythm of Gabra5 mRNA and GABAergic signalling in the IML is different to that in the SCN.

ChAT mRNA codes for the enzyme choline acetyltransferase which is involved in the synthesis of acetylcholine which has both excitatory and inhibitory effect on SPNs depending on which receptor is activated. ChAT mRNA expression was higher during the morning in the IML while previous studies in the hippocampus have found ChAT mRNA and protein is higher during the evening compared to the morning (NORDBERG and WAHLSTRÖM, 1980, Greco *et al*., 1999). Elevated ChAT mRNA and protein at night suggests a potential increase in acetylcholine however whether this potential increase has any effect on SPN targets such as the ganglia they innervate or the adrenal medulla is unknown.

Connexin-36 (Cx36) is also significantly higher in the morning suggesting that gap junction coupling could be more abundant in SPNs during the day (Figure 5.58E). Gap junction communication mediated by Cx36 in SPNs is thought to play an important role in the generation of rhythmic sympathetic activity which influences cardiovascular parameters such as heart rate (HR) and arterial blood pressure (Lall *et al*., 2017). The increase in Cx36 mRNA expression in the morning suggests a higher level of gap junction expression between SPNs.

GABARa5 and Adra2a receptors have inhibitory effects on SPNs, thus inhibiting or decreasing sympathetic nerve activity which could lead to a decrease in blood pressure. The mRNA coding for these receptors are highly expressed in

the morning. This finding agrees with previous literature which found sympathetic nerve activity and blood pressure were higher during the night which is the active phase of mice therefore sympathetic nerve activity and blood pressure would be reduced during the rest phase for mice which is the morning (Takeda, 2016, Lall, 2017, Mahadi, 2019). These findings also agree with human studies which found that blood pressure and sympathetic nerve discharge are lower during rest periods (Millar-Craig, 1978, Krauchi, 1994). These findings suggest that a potential mechanism for the decrease of blood pressure and sympathetic nerve activity during rest phases could be an upregulation of inhibitory receptors mRNA and proteins.

While these mRNA transcripts are significantly higher during the morning, the time these transcripts are translated into their protein forms are unknown. These processes are most likely regulated by molecular modulators therefore the levels of these proteins in the cells at the time points is unknown. Future diurnal immunofluorescence experiments could answer this question and determine if these and other proteins exhibit a diurnal rhythm in these cell types. This experiment is the first to demonstrate there are diurnal rhythms of gene expression in the IML which is consistent with the diurnal rhythms of activity in the sympathetic nervous system.

Comparison of differentially expressed genes between Chat-positive or GAD-positive single cells

When comparing the mean FPKM values of GAD-positive and ChAT-positive cells, a number of potential SPN marker candidates were identified. The presence of Irg1 and Tnip2 as well as presence of Lgals3 described in chapter 3 suggests that SPNs may play a role in cellular immune response and may be

involved in neuroinflammatory responses within the spinal cord. Furthermore, the expression of Plscr4 suggests another form of response to inflammation with phospholipid movement at the bilayer however how this relates to SPN activity or function is currently unknown. Unlike the other candidates, Plscr4 mRNA expression was high specifically in IML SPNs in ABA images, future work could test whether Plscr4 protein is found only in SPNs using IHC.

The IML and single cell data sets have provided the first attempt at a gene expression profile for SPNs. While there were variations in terms of the expression level of the receptor/channel types and subunits between the two data sets; the same receptor/channel types and subunits were observed in both sample groups. The difference of expression levels could be due to the gene expression of SPNs present in the IML samples being diluted by the gene expression of other cell types. qPCR of IML micropunches found that several target genes exhibit a diurnal rhythm of expression however further study is required to describe the functional effect of the upregulation or downregulation of these genes between morning and evening. The single cell data set provided a number of receptor/channel types and subunits that were previously not described in SPNs whose presence can be tested for using immunohistochemistry. Furthermore some of these receptor/channel types and subunits could play a role in sympathetic control of BP however further testing is required potentially screening receptor agonists/antagonists and recording changes in SPN activity and BP.

Chapter 6
General Discussion

6.1 Summary

SPNs are the last point of control that the CNS has on sympathetic outflow to end organs such as the heart, gastrointestinal tract and liver. The activity of IML SPNs influences cardiovascular parameters such as blood pressure and heart rate. Furthermore, diurnal rhythmicity of blood pressure has been linked to sympathetic activity (Guyenet, 2006, Takeda and Maemura, 2011, Deuchars and Lall, 2015, Lall et al., 2017). This suggests that SPNs possess a molecular clock and the activity of this cell type can exhibit diurnal rhythms of activity, which in turn may drive rhythmic physiological processes in end organs.

In an effort to determine the presence of the molecular clock in SPNs there were two main aims. Firstly, to label SPNs selectively with a goal to separating these cells from spinal cord tissue for qPCR and scRNA-seq. The second aim was to construct a gene expression profile of this cell type using scRNA-seq and characterize the molecular clock within SPNs using qPCR.

Novel findings of this study include:

- Demonstration of SPN labelling using Gal-3 for the first time in mouse spinal cord tissue
- Characterisation of SPN labelling efficiency of ChAT, Gal-3 and NOS1 against FG
- mRNA and protein forms of clock genes, *BMAL1* and *PER2* are present in IML SPNs and display diurnal rhythmicity
- Development of a method to preserve single cell RNA quality by rapid extraction and freezing of the spinal cord
- Successfully produced the first transcriptome of IML SPNs

6.2 Identification of a selective marker for SPNs/VHMNs

The IHC experiments carried out in this study found that most candidate markers did not label SPNs or VHMNs selectively. Antibodies against ChAT, NOS1 and Gal-3 labelled IML SPNs. ChAT antibody labelled the largest number of SPNs in thoracic spinal cord sections when compared to NOS1 and Gal-3 antibodies. ChAT antibody was later used to identify IML SPNs for studying clock protein expression.

Initially flow cytometry was going to be used to isolate SPNs from other spinal cord cell types using a selective marker. Successful selection of cells of interests using flow cytometry is dependent on specific labelling by the antibody. However, no selective marker was identified by the IHC study. The scRNA-seq dataset produced by the experiments summarized in chapter 5 is an invaluable resource and can be used to search for potential markers. These marker candidates can be cross-referenced with the Allen spinal cord atlas to determine expression in SPNs. Potential selective markers for SPNs can be tested using IHC.

6.3 Diurnal rhythms of *BMAL1* and *PER2* mRNA/protein expression within the IML

The qPCR experiments revealed diurnal rhythms for mRNA expression of *BMAL1* and *PER2*. This was determined from whole IML micro-punch samples collected at morning or evening time points. *BMAL1* mRNA expression displayed a trend towards peaking during the evening. In contrast, *PER2* mRNA expression was significantly higher in the morning. Diurnal rhythm in the protein form of *BMAL1* was also observed in IML and IPPe SPNs as shown by IHC. *BMAL1* protein levels were significantly higher in the morning. The rhythmic oscillation of *BMAL1* is further evidence of the molecular clock being present in SPNs, and indicates that the translation loop persists in these cells. *PER2*

protein levels however, did not appear to differ between the morning and evening time point. As previous reports indicate that *PER2* and *BMAL1* act in tandem (Mohawk et al., 2012), this finding is surprising. Potential explanations for the lack of diurnal rhythm in *PER2* protein levels are: (1) there are other proteins that interfere with *PER2* protein levels in SPNs or (2) that the molecular clock functions differently in SPNs however, further work is required to confirm this.

As *BMAL1* and *PER2* are key clock genes, these data provide novel and compelling evidence that cells within the IML possess a molecular clock. As the molecular clock consists of a transcriptional-translational feedback loop, cells of the IML may provide a peripheral clock within the spinal cord, thus providing a mechanism to couple time of day with gene expression, SPN activity and ultimately sympathetic output.

Slices or samples containing the suprachiasmatic nucleus of the hypothalamus (SCN) could be included in future qPCR and IHC studies, providing a well described CNS region containing the master clock (Hastings et al., 2018). This would provide a positive control, enabling comparison of clock gene mRNA and protein levels, between SCN and IML/SPNs. Furthermore, future experiments combining qPCR and IHC could explore the link between the SCN master clock and the peripheral clock in SPNs to determine whether exhibit the same rhythmic patterns of clock gene expression or whether they differ.

6.4 Producing the first transcriptome of single IML SPNs

As a final series of experiments, scRNA-seq was used to determine the genes expressed in single SPNs aspirated from the IML region. A new method was developed for rapid extraction and freezing of the spinal cord to prevent RNA degradation.

The single cells were confirmed as SPNs based on their expression of ChAT. In addition, RNA-seq was used to examine RNA obtained from whole IML micropunches and multi-cell aspirations. When comparing the single cell, whole IML and multi-cell aspiration RNA-seq datasets, receptor/channel subtypes and subunits were focused on. These included: voltage-gated calcium and sodium channels, adrenergic alpha 1/2 receptors muscarinic acetylcholine receptors, nicotinic acetylcholine receptors, $GABA_A$ and $GABA_B$ receptors, glutamate receptors and 5-HT receptors. All examined receptor/channel subtypes and subunits were shown to be present in both datasets, albeit with variable predominant subtypes and relative expression levels. These findings provide a unique insight into the subunit composition of receptors and ion channels expressed by SPNs. While the influence of receptor/channel subtype/subunit composition on downstream functions is variable, this data could be used to identify potential roles of different SPN subtypes. From the scRNA-seq data, target mRNA coding for proteins related to SPN activity were identified. qPCR was then performed to determine whether these mRNA exhibited diurnal rhythms in the IML. Adra2a, ChAT, Gjd2 and Gabra5 mRNA expression levels were found to be higher in the morning, and thus shown to have diurnal rhythm in thoracic spinal cord. These preliminary findings suggest along with the BMAL1/PER2 findings that there does appear to be diurnal rhythms in the IML however further experiments are required to determine characterize diurnal rhythms of gene expression in SPNs and how these rhythms affect the activity of this cell type.

6.5 Future Experiments

The experiments in this thesis have determined there is a functioning molecular clock present in IML SPNs and has produced the transcriptome for this cell type. The findings of this thesis can serve as the foundation to a number of queries regarding diurnal rhythmicity of SPN activity and the downstream effects. Potential future experiments based on the findings of this project are listed below:

- Identification of a selective marker for SPNs

The experiments in chapter 3 did not find a new selective marker for SPNs however the scRNA-seq dataset can be used to identify potential candidates. New candidates for IHC testing have already been discovered using this dataset, proteins Irg1, Plscr4 and Tnip2 are involved in immune response and appear to be selectively expressed in IML SPNs according to ABA images. Other candidates could similarly be cross-referenced with ABA images to see whether they are expressed in SPNs. If marker expression is observed in SPNs further IHC tests could be conducted to observe whether the protein expression of the marker is conserved within SPNs. If a selective marker for SPNs is identified it could be used in flow cytometry experiments in combination with FG and anti-PDGFRβ to select for SPNs.

- Exploring the mechanics of the molecular clock in IML SPNs

qPCR and IF/IHC experiments determined the presence of rhythmically expressed clock genes *BMAL1* and *PER2* in IML SPNs. *PER2* mRNA and *BMAL1* protein displayed diurnal rhythm however *BMAL1* mRNA and *PER2* protein did not which could suggest either interference from other clock genes or that the molecular clock functions differently in this cell type. Future qPCR

and IF/IHC experiments could answer this question by investigating more clock genes such as *CRY1/2* and *CLOCK* and including more time points throughout the day. Furthermore, the inclusion of the SCN as a positive control would be useful as this structure is a well described CNS region of circadian control. The rhythms of the SCN master clock and those of the peripheral clock in SPNs could be compared to determine whether their rhythmic expression patterns align.

- Investigation of the IML SPN transcriptome

As summarized in chapter 5, the scRNA-seq experiments yielded the first transcriptome profile of IML SPNs. This dataset identified all the mRNA coding for ion channel/receptor subtypes and components expressed in single IML SPNs at a given time. The θ subunit of the GABA receptor was highly expressed within the single/multi-cell dataset and IHC experiments confirmed the expression of the θ subunit protein in SPNs. Electrophysiology experiments could target this subunit using agonists or antagonists and characterize any resultant change in SPN activity. A new method of extracting and preserving the spinal cord was developed to facilitate scRNA-seq. Future experiments can refine cell targeting and aspiration through the use of transgenic animals or pre-labelling cells of interest. This method could be used to rapidly extract and freeze spinal cord tissue at specific time points, scRNA-seq could produce the transcriptomes of single SPNs to determine whether gene expression changes with time of day providing further evidence of a functioning molecular clock and diurnal rhythms of activity in this cell type.

6.6 Conclusion

These studies have characterized a gene expression profile of SPNs, demonstrated a molecular clock is likely present in SPNs and furthermore has found preliminary evidence that these cells may exhibit diurnal rhythms of gene expression. Firstly, the IHC study demonstrated, for the first time in mouse tissue, Galectin 3 labels a small population of IC and IML SPNs in the thoracic spinal cord. *BMAL1* and *PER2* mRNA and protein exhibit diurnal rhythms in IML micropunches supporting the notion a molecular clock exists in IML SPNs. A new method of extracting the spinal cord and aspirating multiple and single cells has been developed. scRNAseq is possible with aspirated SPNs, RNA obtained from aspirated single SPN was used to produce cDNA which was subsequently used to produce libraries for sequencing. Using scRNA-seq, a ChaT-positive single cell expression profile was constructed. Gene expression profiles were constructed for IML micropunch and multi-cell samples. IML SPNs possess a molecular clock and displays rhythmic gene and protein expression which may affect rhythmic BP downstream however further work is required to characterize this. Future work could build upon the information in this thesis to isolate and/or manipulate SPNs to unravel the role that the molecular clock in these cells plays in regulating cardiovascular function.

References

Abou Arab, O. *et* al. (2019) Etomidate-induced hypotension: a pathophysiological approach using arterial elastance. *Anaesthesia Critical Care & Pain Medicine,* 38**,** 347-352.

Abraham, P. and Maliekal, T.T. (2017) Single cell biology beyond the era of antibodies: relevance, challenges, and promises in biomedical research. *Cellular and Molecular Life Sciences, 74,* 1177-1189*.*

Affleck, V. S., Coote, J. H. and Pyner, S. (2012) The projection and synaptic organisation of NTS afferent connections with presympathetic neurons, GABA and nNOS neurons in the paraventricular nucleus of the hypothalamus. *Neuroscience*, 219, 48–61.

Akhtar, R.A. *et al*. (2002) Circadian Cycling of the Mouse Liver Transcriptome, as Revealed by cDNA Microarray, Is Driven by the Suprachiasmatic Nucleus. *Current Biology,* 12**,** 540-550.

Albers, H. E. *et al*. (2017) The dynamics of GABA signaling: Revelations from the circadian pacemaker in the suprachiasmatic nucleus. *Frontiers in Neuroendocrinology,* 44**,** 35-82.

Albrecht, U. and Ripperger, J. A. (2009) 'Clock Genes', in Binder, M. D., Hirokawa, N., and Windhorst, U. (eds) *Encyclopedia of Neuroscience*. Berlin, Heidelberg: Springer Berlin Heidelberg, 759–762.

Alvarez, F. J. *et al*. (2000) Differential distribution of metabotropic glutamate receptors 1a, 1b, and 5 in the rat spinal cord. *Journal of Comparative Neurology,* 422**,** 464-487.

Ambalavanar, R. and Morris, R. (1989) Fluoro-Gold injected either subcutaneously or intravascularly results in extensive retrograde labelling of CNS neurones having axons terminating outside the blood-brain barrier. *Brain research*, 505, 171–175.

Anderson, C. R. (1992) Nadph diaphorase-positive neurons in the rat spinal cord include a subpopulation of autonomic preganglionic neurons. *Neuroscience Letters*, 139, 280–284.

Anderson, C. R. and Edwards, S. L. (1994) Intraperitoneal injections of Fluorogold reliably labels all sympathetic preganglionic neurons in the rat. *J The Journal of Neuroscience Methods*, 53, 137–141.

Anderson, C. et al. (1995) Characterisation of neurons with nitric oxide synthase immunoreactivity that project to prevertebral ganglia. *Journal of the autonomic nervous system,* 52**,** 107-116.

Andresen, M. C. *et al.* (2006) Cellular Mechanisms of Baroreceptor Integration at the Nucleus Tractus Solitarius, *Annals of the New York Academy of Sciences*, 940, 132–141.

Anea Ciprian, B. *et al.* (2009) Vascular Disease in Mice With a Dysfunctional Circadian Clock, *Circulation*. American Heart Association. 119, 1510–1517.

Arendt J. (2010) Shift work: coping with the biological clock. *Occupational Medicine,* 60**,** 10-20.

Arlotta, P. *et al.* (2005) Neuronal Subtype-Specific Genes that Control Corticospinal Motor Neuron Development In Vivo. *Neuron,* 45**,** 207-221.

Aschoff, J. (1951) Die 24-Stunden-Periodik der Maus unter konstanten Umgebungsbedingungen. *Die Naturwissenschaften*, 38, 506–507.

Bacon, S. J. and Smith, A. D. (1988) Preganglionic sympathetic neurones innervating the rat adrenal medulla: immunocytochemical evidence of synaptic input from nerve terminals containing substance P, GABA or 5-hydroxytryptamine. *Journal of the autonomic nervous system*, 24, 97–122.

Balsalobre, A. (1998) A Serum Shock Induces Circadian Gene Expression in Mammalian Tissue Culture Cells. *Cell*, 93, 929-937.

Barber, R. P. *et al.* (1984) The morphology and distribution of neurons containing choline acetyltransferase in the adult rat spinal cord: an immunocytochemical study. *Journal of Comparative Neurology*, 229, 329–346.

Barca-Mayo, O. *et al*. (2017) Astrocyte deletion of Bmal1 alters daily locomotor activity and cognitive functions via GABA signalling. *Nature Communications*, 8, 14336.

Barman, S. M. and Gebber, G.L. (1980) Sympathetic nerve rhythm of brain stem origin. *American Journal of Physiology-Regulatory, Integrative and Comparative Physiology*, 239, 42-47.

Barnes, N.M. *et al*. (2009) The 5-HT3 receptor – the relationship between structure and function. *Neuropharmacology*, 56, 273-284.

Baron, R., Jänig, W. and McLachlan, E. M. (1985a) The afferent and sympathetic components of the lumbar spinal outflow to the colon and pelvic organs in the cat. I. The hypogastric nerve, *Journal of Comparative Neurology*, 238, 135–146.

Baron, R., Jänig, W. and McLachlan, E. M. (1985b) The afferent and sympathetic components of the lumbar spinal outflow to the colon and pelvic organs in the cat. II. The lumbar splanchnic nerves. *Journal of Comparative Neurology*, 238, 147-157.

Barondes, S. H. *et al*. (1994) Galectins: a family of animal beta-galactoside-binding lectins. *Cell*, 76, 597-8.

Bartlett, J. and Stirling D. (2003) *PCR protocols*, Totowa, N.J., Humana

Bell-Pedersen, D. *et al.* (2005) Circadian rhythms from multiple oscillators: Lessons from diverse organisms. *Nature Reviews Genetics*, 6, 544–556.

Benarroch, E. E. (2005) Paraventricular nucleus, stress response, and cardiovascular disease. *Clinical Autonomic Research*, 15, 254-263.

Bennett, J. A. *et al.* (1986) The location and characteristics of sympathetic preganglionic neurones in the lower thoracic spinal cord of dog and cat. *Experimental Physiology*, 71, 79–92.

Bhadra, U. *et al.* (2017) Evolution of circadian rhythms: from bacteria to human. *Sleep Medicine*, 35, 49–61.

Bhargava, K. P. *et al*. (1982) Cholinergic influences on the spinal cardiovascular neurones. *Journal of Autonomic Pharmacology*, 2, 225–230.

Bishehsari, F. (2016) Circadian Rhythms in Gastrointestinal Health and Diseases. *Gastroenterology*, 151, 1-5.

Black, J.A. *et al*. (1996) Spinal sensory neurons express multiple sodium channel α-subunit mRNAs. *Molecular Brain Research*, 43, 117-131.

Blessing, W.W. and Nalivaiko, E. (2000) Regional blood flow and nociceptive stimuli in rabbits: patterning by medullary raphe, not ventrolateral medulla. *The Journal of Physiology*, 524, 279-292.

Blottner, D. and Baumgarten, H. (1992) Nitric oxide synthetase (NOS)-containing sympathoadrenal cholinergic neurons of the rat IML-cell column: Evidence from histochemistry, immunohistochemistry, and retrograde labeling. *Journal of Comparative Neurology*, 316, 45–55.

De Boer, R. A., Yu, L. and Van Veldhuisen, D. J. (2010) Galectin-3 in cardiac remodeling and heart failure. *Current Heart Failure Reports*, 7, 1–8.

Bonnert, T. P. *et al*. (1999) theta, a novel gamma-aminobutyric acid type A receptor subunit. *Proceedings of the National Academy of Sciences USA*, 96, 9891-9896.

Brancaccio, M. *et al*. (2017) Astrocytes Control Circadian Timekeeping in the Suprachiasmatic Nucleus via Glutamatergic Signaling. *Neuron*, 93, 1420-1435 e5.

Bray, M. S. *et al.* (2008) Disruption of the circadian clock within the cardiomyocyte influences myocardial contractile function, metabolism, and gene expression. *American Journal of Physiology-Heart and Circulatory Physiology*. American Physiological Society, 294, 1036–1047.

Briaud, S. A., Zhang, B. L. and Sannajust, F. (2004) Continuous Light Exposure and Sympathectomy Suppress Circadian Rhythm of Blood Pressure in Rats. *Journal of Cardiovascular Pharmacology and Therapeutics*, 9, 97–105.

Buhr, E. D. and Takahashi, J. S. (2013) Molecular Components of the Mammalian Circadian Clock. *Circadian Clocks*, 217, 3–27.

Buijs, R. M. *et al*. (2003) The suprachiasmatic nucleus balances sympathetic and parasympathetic output to peripheral organs through separate preautonomic neurons. *Journal of Comparative Neurology*, 464, 36-48.

Buijs, R. M. and Kalsbeek, A. (2001) Hypothalamic integration of central and peripheral clocks. *Nature Reviews Neuroscience*, 2, 521.

Bunger, M. K. *et al*. (2005) Progressive arthropathy in mice with a targeted disruption of the Mop3/Bmal-1 locus. *Genesis*, 41, 122-132.

Cadwell, C. R. *et al*. (2016) Electrophysiological, transcriptomic and morphologic profiling of single neurons using Patch-seq. *Nature Biotechnology*, 34, 199-203.

Cailotto, C. *et al.* (2005) The suprachiasmatic nucleus controls the daily variation of plasma glucose via the autonomic output to the liver: are the clock genes involved? *European Journal of Neuroscience*, 22, 2531–2540.

Cailotto, C. *et al.* (2009) Effects of Nocturnal Light on (Clock) Gene Expression in Peripheral Organs: A Role for the Autonomic Innervation of the Liver. *PloS one*. 4, 5650.

Cano, G. et al. (2004) Dual viral transneuronal tracing of central autonomic circuits involved in the innervation of the two kidneys in rat. *Journal of Comparative Neurology*, 471, 462-481.

Cano, G. et al. (2003) Anatomical substrates for the central control of sympathetic outflow to interscapular adipose tissue during cold exposure. *Journal of Comparative Neurology*, 460, 303-326.

Catterall, W. A. (2000) Structure and Regulation of Voltage-Gated Ca2+ Channels. *Annual Review of Cell and Developmental Biology*, 16, 521-555.

Chen, R. *et al.* (2017) Single-Cell RNA-Seq Reveals Hypothalamic Cell Diversity. *Cell Reports*, 18, 3227-3241.

Chouchou, F. *et al*. (2013) Sympathetic overactivity due to sleep fragmentation is associated with elevated diurnal systolic blood pressure in healthy elderly subjects: the PROOF-SYNAPSE study. *European Heart Journal*, 34, 2122-2131.

Cechetto, D. F. and Saper, C. B. (1988) Neurochemical organization of the hypothalamic projection to the spinal cord in the rat. *Journal of Comparative Neurology*, 272, 579–604.

Challet, E. (2019) The circadian regulation of food intake. *Nature Reviews Endocrinology*, 15, 393–405.

Chalmers, J. A. *et al.* (2008) Vascular circadian rhythms in a mouse vascular smooth muscle cell line (Movas-1). *American Journal of Physiology-Regulatory, Integrative and Comparative Physiology*, 295, 1529–1538.

Chung, K. *et al.* (1979) Sympathetic neurons in the cat spinal cord projecting to the stellate ganglion. *Journal of Comparative Neurology*, 185, 23–29.

Chung, K., La Velle, F. W. and Wurster, R. D. (1980) Ultrastructure of HRP-identified sympathetic preganglionic neurons in cats. *Journal of Comparative Neurology*, 190, 147–155.

Clarke, J. L. (1850) Researches into the Structure of the Spinal Cord. [Abstract]. *Abstracts of the Papers Communicated to the Royal Society of London*. The Royal Society, 6, 1–3.

Clendening, B. and Hume, R. I. (1990) Expression of multiple neurotransmitter receptors by sympathetic preganglionic neurons in vitro. *The Journal of Neuroscience*, 10, 3977.

Collingridge, G. L. et al. (2009). A nomenclature for ligand-gated ion channels. *Neuropharmacology*, 56, 2-5.

Comte, I. *et al* (2011) Galectin-3 maintains cell motility from the subventricular zone to the olfactory bulb. *The Journal of Cell Science*, 124, 2438-2447.

Coote, J. H. *et al.* (1981) The response of individual sympathetic preganglionic neurones to microelectrophoretically applied endogenous monoamines. *Brain Research*, 215, 135–145.

Coote, J. H. *et al.* (1998) Control of sympathetic outflows by the hypothalamic paraventricular nucleus. *Clinical and Experimental Pharmacology and Physiology*, 25, 461–463.

Crnko, S. *et al.* (2019) Circadian rhythms and the molecular clock in cardiovascular biology and disease. *Nature Reviews Cardiology*, 16, 437–447.

Cui, L. N., Coderre, E. and Renaud, L. P. (2001) Glutamate and GABA mediate suprachiasmatic nucleus inputs to spinal-projecting paraventricular neurons. *American Journal of Physiology-Regulatory, Integrative and Comparative Physiology*, 281, 1283-1289.

Cummings, J. F. (1969) Thoracolumbar preganglionic neurons and adrenal innervation in the dog. *Cells Tissues Organs*, 73, 27-37.

Curtis, A. M. *et al.* (2007) Circadian variation of blood pressure and the vascular response to asynchronous stress. *Proceedings of the National Academy of Sciences USA*, 104, 3450–3455.

Dampney, R. *et al.* (2005) Functional Organization of Brain Pathways Subserving the Baroreceptor Reflex: Studies in Conscious Animals Using Immediate Early Gene Expression. *Cellular and Molecular Neurobiology*, 23, 597-616.

Dampney, R. *et al.* (2005) Long-term regulation of arterial blood pressure by hypothalamic nuclei: some critical questions. *Clinical and Experimental Pharmacology and Physiology*, 32, 419–425.

Davidson, A. J. *et al.* (2005) Cardiovascular tissues contain independent circadian clocks. *Clinical and Experimental Hypertension*, 27, 307–311.

Dean, C. *et al*. (1992) Differential control of sympathetic activity to kidney and skeletal muscle by ventral medullary neurons. *Journal of the Autonomic Nervous System*, 37, 1-10.

Dempsey, J. A. *et al*. (2002) Respiratory influences on sympathetic vasomotor outflow in humans. *Respiratory Physiology & Neurobiology*, 130, 3-20.

Deuchars, S. A. (2015) How sympathetic are your spinal cord circuits? *Experimental Physiology*, 100, 365–371.

Deuchars, S. A. and Lall, V. K. (2015) Sympathetic preganglionic neurons: properties and inputs. *Comprehensive Physiology*, 5, 829-869.

Deuchars, S. A. *et al*. (2001) Properties of interneurones in the intermediolateral cell column of the rat spinal cord: role of the potassium channel subunit Kv3.1. *Neuroscience*, 106, 433-446.

Deuchars, S. A. *et al*. (2005) GABAergic Neurons in the Central Region of the Spinal Cord: A Novel Substrate for Sympathetic Inhibition. *Journal of Neuroscience*, 25, 1063-1070.

Deuchars, S. A., Morrison, S. F. and Gilbey, M. P. (1995) Medullary-evoked EPSPs in neonatal rat sympathetic preganglionic neurones in vitro. *Journal of Physiology*, 487, 453–463.

Deuchars, S. A., Spyer, K. M. and Gilbey, M. P. (1997) Stimulation Within the Rostral Ventrolateral Medulla Can Evoke Monosynaptic GABAergic IPSPs in Sympathetic Preganglionic Neurons In Vitro. *Journal of Neurophysiology*, 77, 229–235.

Do, M. T. H. and Yau, K.-W. (2010) Intrinsically Photosensitive Retinal Ganglion Cells. *Physiological Reviews*, 90, 1547–1581.

Dobin, A. *et al*. (2012) STAR: ultrafast universal RNA-seq aligner. *Bioinformatics*, 29, 15-21.

Douma, L. G. and Gumz, M. L. (2018) Circadian clock-mediated regulation of blood pressure. *Free Radical Biology and Medicine*, 119, 108–114.

Duffield, G. E. *et al*. (2002) Circadian Programs of Transcriptional Activation, Signaling, and Protein Turnover Revealed by Microarray Analysis of Mammalian Cells. *Current Biology*, 12, 551-557.

Duflocq, A. *et al*. (2008) Nav1.1 is predominantly expressed in nodes of Ranvier and axon initial segments. *Molecular and Cellular Neuroscience*, 39, 180-192.

Dumic, J., Dabelic, S. & Flögel, M. (2006) Galectin-3: An open-ended story. *Biochimica et Biophysica Acta*, 1760, 616-635.

Dun, N. J. et al. (1992) Nitric oxide synthase immunoreactivity in rat spinal cord. *Neuroscience Letters*, 147, 217-220.

Dun, N. J. et al. (2000). Differential expression of cocaine- and amphetamine-regulated transcript-immunoreactivity in the rat spinal preganglionic nuclei. *Neuroscience Letters*, 294, 143-146.

Durgan, D. J. *et al.* (2005) The intrinsic circadian clock within the cardiomyocyte. *American Journal of Physiology-Heart and Circulatory Physiology*, 289, 1530–1541.

Durgan, D. J. *et al.* (2010) Short communication: Ischemia/reperfusion tolerance is time-of-day- dependent: Mediation by the cardiomyocyte circadian clock. *Circulation Research*, 106, 546–550.

Durgan, D. J. *et al.* (2011) Evidence Suggesting that the Cardiomyocyte Circadian Clock Modulates Responsiveness of the Heart to Hypertrophic Stimuli in Mice. *Chronobiology International*, 28, 187–203.

Eberwine, J. *et al*. (2013) The promise of single-cell sequencing. *Nature Methods*, 11, 25-27.

Edwards, I. J. *et al.* (2013) A simple method to fluorescently label pericytes in the CNS and skeletal muscle. *Microvascular research*, 89, 164–168.

Espinosa-Medina, I. *et al.* (2016) The sacral autonomic outflow is sympathetic. *Science*, 354, 893–897.

Evans, J. A. *et al.* (2015) Shell neurons of the master circadian clock coordinate the phase of tissue clocks throughout the brain and body. *BMC Biology*, 13, 43.

Faden, A. I. and Petras, J. M. (1978) An intraspinal sympathetic preganglionic pathway: anatomic evidence in the dog. *Brain Research*, 144, 358-362.

Fagard, R. H. *et al.* (2009) Night-day blood pressure ratio and dipping pattern as predictors of death and cardiovascular events in hypertension. *Journal of Human Hypertension*, 23, 645–653.

Fenwick, N. M., Martin, C. L. and Llewellyn-Smith, I. J. (2006a) Immunoreactivity for cocaine- and amphetamine-regulated transcript in rat sympathetic preganglionic neurons projecting to sympathetic ganglia and the adrenal medulla. *Journal of Comparative Neurology*, 495, 422-433.

Fenwick, N. M., Martin, C. L. and Llewellyn-Smith, I. J. (2006b) Immunoreactivity for cocaine-and amphetamine-regulated transcript in rat sympathetic preganglionic neurons projecting to sympathetic ganglia and the adrenal medulla. *Journal of Comparative Neurology*, 495, 422-433.

Firsov, D. and Bonny, O. (2018) Circadian rhythms and the kidney. *Nature Reviews Nephrology*, 14, 626–635.

Frankish, A. et al. (2017) Ensembl 2018. *Nucleic Acids Research*, 46, 754-761.

Fu, L. and Lee, C. C. (2003) The circadian clock: pacemaker and tumour suppressor. *Nature Reviews Cancer*, 3, 350-361.

Fu, L. *et al*. (2002) The Circadian Gene Period2 Plays an Important Role in Tumor Suppression and DNA Damage Response In Vivo. *Cell*, 111, 41-50.

Fuzik, J. *et al*. (2016) Integration of electrophysiological recordings with single-cell RNA-seq data identifies neuronal subtypes. *Nature Biotechnology*, 34, 175-183.

Gambrill, A. C. and Barria, A. (2011) NMDA receptor subunit composition controls synaptogenesis and synapse stabilization. *Proceedings of the National Academy of Sciences USA*, 108, 5855-5860.

Gaudet, A. D. *et al*. (2018) Spinal Cord Injury in Rats Disrupts the Circadian System. *eNeuro*, 5, 1-18.

Gekakis, N. *et al.* (1998) Role of the CLOCK protein in the mammalian circadian mechanism. *Science*, 280, 1564–1569.

Gery, S. *et al*. (2006) The Circadian Gene Per1 Plays an Important Role in Cell Growth and DNA Damage Control in Human Cancer Cells. *Molecular Cell*, 22, 375-382.

Giachetti, S. (2002) Chronotherapy of colorectal cancer. *Chronobiology International*, 19, 207-219.

Gibson, I. C. and Logan, S. D. (1995) Effects of muscarinic receptor stimulation of sympathetic preganglionic neurones of neonatal rat spinal cord in vitro. *Neuropharmacology*, 34, 309-318.

Gokce, O. *et al*. (2016) Cellular Taxonomy of the Mouse Striatum as Revealed by Single-Cell RNA-Seq. *Cell Reports*, 16, 1126-1137.

Golubeva, Y. *et al*. (2013) Laser capture microdissection for protein and NanoString RNA analysis. *Methods in Molecular Biology*, 931, 213-257.

Gonsalvez, D. G. *et al*. (2010) Chemical Coding for Cardiovascular Sympathetic Preganglionic Neurons in Rats. *The Journal of Neuroscience*, 30, 11781-11791.

Gonzalez Burgos, G. R. *et al*. (1995) Different calcium channels mediate transmitter release evoked by transient or sustained depolarization at mammalian symphatetic ganglia. *Neuroscience*, 64, 117-123.

González, G. E. *et al*. (2016) Cardiac-deleterious role of galectin-3 in chronic angiotensin II-induced hypertension. *American Journal of Physiology-Heart and Circulatory Physiology*, 311, 1287-1296.

Gordan, R., Gwathmey, J. K. and Xie, L.-H. (2015) Autonomic and endocrine control of cardiovascular function. *World Journal of Cardiology,* 7, 204–214.

Gotts, J. *et al*. (2016) Co-expression of GAD67 and choline acetyltransferase in neurons in the mouse spinal cord: A focus on lamina X. *Brain Research*, 1646, 570-579.

Grassi, G. *et al.* (2003) Effects of Hypertension and Obesity on the Sympathetic Activation of Heart Failure Patients. *Hypertension*, 42, 873-877.

Grassi, G. *et al.* (2008) Adrenergic, metabolic, and reflex abnormalities in reverse and extreme dipper hypertensives. *Hypertension*, 52, 925–931.

Greco, M., Mccarley, R. & Shiromani, P. (1999) Choline acetyltransferase expression during periods of behavioral activity and across natural sleep–wake states in the basal forebrain. *Neuroscience*, 93, 1369-1374.

Greenwood, J. P., Stoker, J. B. and Mary David, A. S. G. (1999) Single-Unit Sympathetic Discharge. *Circulation*, 100, 1305-1310.

Grkovic, I. and Anderson, C. R. (1995) Calretinin-containing preganglionic nerve terminals in the rat superior cervical ganglion surround neurons projecting to the submandibular salivary gland. *Brain Research*, 684, 127-135.

Grkovic, I. and Anderson, C. R. (1997) Calbindin D28K-immunoreactivity identifies distinct subpopulations of sympathetic pre- and postganglionic neurons in the rat. *Journal of Comparative Neurology*, 386, 245-259.

Grkovic, I. *et al*. (1999) Chemically distinct preganglionic inputs to iris-projecting postganglionic neurons in the rat: A light and electron microscopic study. *Journal of Comparative Neurology*, 412, 606-616.

Gross, A. *et al*. (1991) Neuronal nicotinic acetylcholine receptors expressed in Xenopus oocytes: role of the α subunit in agonist sensitivity and desensitization. *Pflügers Archiv: European Journal of Physiology*, 419, 545-551.

Guerler, A. *et al*. (2018) The Galaxy platform for accessible, reproducible and collaborative biomedical analyses: 2018 update. *Nucleic Acids Research*, 46, 537-544.

Guez-Barger, D. *et al*. (2012) FACS purification of immunolabeled cell types from adult rat brain. *Journal of Neuroscience Methods*, 203, 10-18.

Guyenet, P. G. (2006) The sympathetic control of blood pressure. *Nature Reviews Neuroscience*, 7, 335-346.

Guyenet, P. G. and Cabot, J. B. (1981) Inhibition of sympathetic preganglionic neurons by catecholamines and clonidine: mediation by an alpha-adrenergic receptor. *The Journal of Neuroscience*, 1, 908-917.

Guyenet, P. G. and Stornetta, R. L. (2004) The Presympathetic Cells of the Rostral Ventrolateral Medulla (RVLM): Anatomy, Physiology and Role in the Control of Circulation. *Neural Mechanisms of Cardiovascular Regulation*, 187–218.

Hastings, M. H., Maywood, E. S. and Brancaccio, M. (2018) Generation of circadian rhythms in the suprachiasmatic nucleus. *Nature Reviews Neuroscience*, 19, 453–469.

Helke, C. J., Thor, K. B. and Phillips, E. T. (1991) 5-hydroxytryptamine(1C/2) agonists in the thoracic spinal cord: Cardiovascular effects and binding sites in the intermediolateral cell column. *Journal of Pharmacology and Experimental Therapeutics*, 259, 1335–1343.

Henry, J. L. and Calaresu, F. R. (1972) Distribution of cardioacceleratory sites in intermediolateral nucleus of the cat. *American Journal of Physiology-Legacy Content*, 222, 700-704.

Herichova, I. *et al*. (2007) Rhythmic clock gene expression in heart, kidney and some brain nuclei involved in blood pressure control in hypertensive TGR(mREN-2)27 rats. *Molecular and Cellular Biochemistry*, 296, 25-34.

Hermida, R. C. *et al*. (2017) Bedtime Blood Pressure Chronotherapy Significantly Improves Hypertension Management. *Heart Failure Clinics*, 13, 759-773.

Hermida, R. C. *et al*. (2018) Risk of incident chronic kidney disease is better reduced by bedtime than upon-awakening ingestion of hypertension medications. *Hypertension Research*, 41, 342-353.

Herzog, E. D. (2007) Neurons and networks in daily rhythms. *Nature Reviews Neuroscience,* 8, 790-802.

Hinrichs, J. M. and Llewellyn-Smith, I. J. (2009) Variability in the occurrence of nitric oxide synthase immunoreactivity in different populations of rat sympathetic preganglionic neurons. *Journal of Comparative Neurology*, 514, 492–506.

Hosoya, Y. *et al*. (1991) Descending input from the hypothalamic paraventricular nucleus to sympathetic preganglionic neurons in the rat. *Experimental Brain Research*, 85, 10-20.

Huang, J., Chowdhury, S. I. and Weiss, M. L. (2002) Distribution of sympathetic preganglionic neurons innervating the kidney in the rat: PRV transneuronal tracing and serial reconstruction. *Autonomic Neuroscience*, 95, 57-70.

Huangfu, D. H., Koshiya, N. and Guyenet, P. G. (1991) A5 noradrenergic unit activity and sympathetic nerve discharge in rats. *American Journal of Physiology-Regulatory, Integrative and Comparative Physiology*, 261, 393-402.

Hubli, M. and Krassioukov, A. V. (2013) Ambulatory Blood Pressure Monitoring in Spinal Cord Injury: Clinical Practicability. *Journal of Neurotrauma*, 31, 789-797.

Hughes, M. E. *et al*. (2009) Harmonics of circadian gene transcription in mammals. *PloS one*, 5, 1-12.

Hughes, R. L. & Mackenzie, J. E. (1978) An investigation of the centrally and peripherally mediated cardiovascular effects of etomidate in the rabbit. *British Journal of Anaesthesia*, 50, 101-108.

IITAKA, C. *et al*. (2005) A role for glycogen synthase kinase-3beta in the mammalian circadian clock. *Journal of Biological Chemistry*, 280, 397-402.

Ireland, D. R., Davies, P. J. and McLachlan, E. M. (1999) Calcium channel subtypes differ at two types of cholinergic synapse in lumbar sympathetic neurones of guinea-pigs. *Journal of Physiology*, 514, 59–69.

Ishibashi, S. *et al*. (2007) Galectin-1 regulates neurogenesis in the subventricular zone and promotes functional recovery after stroke. *Experimental Neurology*, 207, 302-313.

Izzo, P. N., Deuchars, J. and Spyer, K. M. (1993) Localization of cardiac vagal preganglionic motoneurones in the rat: Immunocytochemical evidence of synaptic inputs containing 5-hydroxytryptamine. *Journal of Comparative Neurology*, 327, 572-583.

Jänig, W. and Häbler, H. J. (2003) Neurophysiological analysis of target-related sympathetic pathways – from animal to human: similarities and differences. *Acta Physiologica Scandinavica*, 177, 255-274.

Jänig, W. and Mclachlan, E. M. (1992) Specialized functional pathways are the building blocks of the autonomic nervous system. *Journal of the Autonomic Nervous System*, 41, 3-13.

Jänig, W. and McLachlan, E. M. (1986) Identification of distinct topographical distributions of lumbar sympathetic and sensory neurons projecting to end organs with different functions in the cat. *Journal of Comparative Neurology*, 246, 104–112.

Jardine, D. L. *et al*. (2007) Cardiac sympathetic nerve activity and ventricular fibrillation during acute myocardial infarction in a conscious sheep model. *American Journal of Physiology-Heart and Circulatory Physiology*, 293, 433-439.

Jin Mo, C., Chung, K. and Wurster, R. D. (1975) Sympathetic preganglionic neurons of the cat spinal cord: horseradish peroxidase study. *Brain Research*, 91, 126-131.

Jobling, P. *et al*. (2004) Differential expression of calcium channels in sympathetic and parasympathetic preganglionic inputs to neurons in paracervical ganglia of guinea-pigs. *Neuroscience*, 127, 455-466.

Julius, S. (1993) Corcoran Lecture. Sympathetic hyperactivity and coronary risk in hypertension. *Hypertension*, 21, 886-893.

Kalsbeek, A. *et al*. (2010) Hypothalamic control of energy metabolism via the autonomic nervous system. *Annals of the New York Academy of Sciences*, 1212, 114-129.

Kalsbeek, A., La Fleur, S. & Fliers, E. (2014) Circadian control of glucose metabolism. *Molecular Metabolism*, 3, 372-383.

Kalsbeek, A. *et al*. (2004) Suprachiasmatic GABAergic Inputs to the Paraventricular Nucleus Control Plasma Glucose Concentrations in the Rat via Sympathetic Innervation of the Liver. *The Journal of Neuroscience*, 24, 7604.

Kalsbeek, A., Perreau-Lenz, S. and Buijs, R. M. (2006) A Network of (Autonomic) Clock Outputs. *Chronobiology International*, 23, 521-535.

Kamosińska, B., Nowicki, D. and Szulczyk, P. L. (1989) Control of the heart rate by sympathetic nerves in cats. *Journal of the Autonomic Nervous System*, 26, 241-249.

Kanbar, R. *et al*. (2011) Regulation of visceral sympathetic tone by A5 noradrenergic neurons in rodents. *The Journal of Physiology*, 589, 903-917.

Karemaker, J. M. (2017) An introduction into autonomic nervous function. *Physiological Measurement*, 38, 89–118.

Kario, K. (2010) Morning surge in blood pressure and cardiovascular risk: Evidence and perspectives. *Hypertension*, 56, 765–773.

Karlsson, B. *et al.* (2005) Total mortality and cause-specific mortality of Swedish shift- and dayworkers in the pulp and paper industry in 1952-2001. *Scandinavian Journal of Work, Environment and Health*, 31, 30–35.

Karlsson, B. *et al.* (2001) Is there an association between shift work and having a metabolic syndrome? Results from a population based study of 27 485 people. *Occupational and Environmental Medicine*, 58, 747-752.

Keesler, G. A. *et al.* (2000) Phosphorylation and destabilization of human period I clock protein by human casein kinase Iε. *NeuroReport*, 11, 951–955.

Kerkhof, G. A., Dongen, H. P. A. V. and Bobbert, A. C. (1998). Absence of Endogenous Circadian Rhythmicity in Blood Pressure? *American Journal of Hypertension*, 11, 373-377.

King, D. P. *et al.* (1997) Positional cloning of the mouse circadian Clock gene. *Cell*, 89, 641–653.

Kishi, T. *et al*. (2002) Cardiovascular Effects of Overexpression of Endothelial Nitric Oxide Synthase in the Rostral Ventrolateral Medulla in Stroke-Prone Spontaneously Hypertensive Rats. *Hypertension*, 39, 264-268.

Knutsson, A. *et al.* (1986) Increased risk of ischaemic heart disease in shirt workers. *The Lancet*, 328, 89–92.

Ko, C. H. and Takahashi, J. S. (2006) Molecular components of the mammalian circadian clock. *Human molecular genetics*, 15, 271–277.

Kume, K. *et al.* (1999) mCRY1 and mCRY2 are essential components of the negative limb of the circadian clock feedback loop. *Cell*, 98, 193–205.

Kuo, D. C., *et al.* (1980) Segmental organization of sympathetic preganglionic neurons of the splanchnic nerve as revealed by retrograde transport of horseradish peroxidase. *Neuroscience Letters*, 17, 11-16.

Lake, B. B. *et al*. (2016) Neuronal subtypes and diversity revealed by single-nucleus RNA sequencing of the human brain. *Science*, 352, 1586-1590.

Lall, V. K. *et al.* (2017) Physiologic regulation of heart rate and blood pressure involves connexin 36-containing gap junctions. *FASEB Journal,* 31, 3966-3977.

Lambert, E. A. *et al.* (2014) Morning surge in blood pressure is associated with reactivity of the sympathetic nervous system. *American journal of hypertension*, 27, 783–792.

Lamia, K. A., Storch, K.-F. and Weitz, C. J. (2008) Physiological significance of a peripheral tissue circadian clock. *Proceedings of the National Academy of Sciences USA*, 105, 15172-15177.

Laposky, A. *et al*. (2005) Deletion of the mammalian circadian clock gene BMAL1/Mop3 alters baseline sleep architecture and the response to sleep deprivation. *Sleep*, 4, 395-409.

Leach, G. *et al*. (2013) Responses of brain and behavior to changing day-length in the diurnal grass rat (Arvicanthis niloticus). *Neuroscience*, 234, 31-39.

Lee, S. *et al*. (2010) ADAR2-dependent RNA editing of GluR2 is involved in thiamine deficiency-induced alteration of calcium dynamics. *Molecular Neurodegeneration*, 5, 1-13.

Lefta, M. *et al.* (2012) Development of dilated cardiomyopathy in Bmal1-deficient mice. *American Journal of Physiology-Heart and Circulatory Physiology*, 303, 475–485.

Leibetseder, V. *et al.* (2009) Clock Genes Display Rhythmic Expression in Human Hearts. *Chronobiology International,* 26, 621–636.

Lesauter, J. *et al.* (2012). Antibodies for assessing circadian clock proteins in the rodent suprachiasmatic nucleus. *PLoS One*, 7, 1-9.

Li, P. *et al*. (2016) Hematopoietic-Derived Galectin-3 Causes Cellular and Systemic Insulin Resistance. *Cell*, 167, 973-984.

Li, Y. W. and Dampney, R. A. L. (1994) Expression of fos-like protein in brain following sustained hypertension and hypotension in conscious rabbits. *Neuroscience*, 61, 613-634.

Liao, Y., Smyth, G. K. and Shi, W. (2013) The Subread aligner: fast, accurate and scalable read mapping by seed-and-vote. *Nucleic acids research*, 41, 1-17.

Llewellyn-Smith, I. J., *et* al. (1997) Glutamate- and GABA-immunoreactive synapses on sympathetic preganglionic neurons caudal to a spinal cord transection in rats. *Neuroscience*, 80, 1225-1235.

Loewy, A. D., Mckellar, S. and Saper, C. B. (1979) Direct projections from the A5 catecholamine cell group to the intermediolateral cell column. *Brain Research*, 174, 309-314.

Lovatt, D., Bell, T. & Eberwine, J. (2015) Single-neuron isolation for RNA analysis using pipette capture and laser capture microdissection. *Cold Spring Harbor Protocols*, 2015, 60-68.

Love, M. I., Huber, W. and Anders, S. (2014) Moderated estimation of fold change and dispersion for RNA-seq data with DESeq2. *Genome biology*, 15, 1-21.

Lowrey, P. L. and Takahashi, J. S. (2011) Chapter 6 - Genetics of Circadian Rhythms in Mammalian Model Organisms. In: BRODY, S. (ed.) *Advances in Genetics. Academic Press*.

Mahadi, K. M. *et al.* (2019) Cardiovascular autonomic effects of transcutaneous auricular nerve stimulation via the tragus in the rat involve spinal cervical sensory afferent pathways. *Brain Stimulation,* 12, 1151-1158.

Malliani, A., Schwartz, P. J. and Zanchetti, A. (1969) A sympathetic reflex elicited by experimental coronary occlusion. *American Journal of Physiology-Legacy Content*, 217, 703-709.

Malpas, S. C. (1998). The rhythmicity of sympathetic nerve activity. *Progress in Neurobiology*, 56, 65-96.

Mancia, G. and Grassi, G. (2014) The Autonomic Nervous System and Hypertension. *Circulation Research*, 114, 1804-1814.

Mancia, G. *et al*. (1999) Sympathetic Activation in the Pathogenesis of Hypertension and Progression of Organ Damage. *Hypertension*, 34, 724-728.

Marcheva, B. *et al*. (2010) Disruption of the clock components CLOCK and BMAL1 leads to hypoinsulinaemia and diabetes. *Nature*, 466, 627-631.

Marina, N., Taheri, M. and Gilbey, M. P. (2006) Generation of a physiological sympathetic motor rhythm in the rat following spinal application of 5-HT. *Journal of Physiology*, 571, 441–450.

Marks, S. A. *et al.* (1990) [3H]Prazosin binding in the intermediolateral cell column and the effects of iontophoresed methoxamine on sympathetic preganglionic neuronal activity in the anaesthetized cat and rat. *Brain Research*, 530, 321–324.

Mayer, M. L. (2005) Glutamate receptor ion channels. *Current Opinion in Neurobiology*, 15, 282-288.

Mclachlan, E. M., Oldfield, B. J. and Sittiracha, T. (1985) Localization of hindlimb vasomotor neurones in the lumbar spinal cord of the guinea pig. *Neuroscience Letters*, 54, 269-275.

McLachlan, E. M. *et al.* (1997) On-going and reflex synaptic events in rat superior cervical ganglion cells. *Journal of Physiology*, 501, 165–181.

Mcnair, C. J. *et al*. (1998) Glutamate receptor subunits associated with rat sympathetic preganglionic neurons. *Neuroscience Letters*, 256, 29-32.

McNamara, P. *et al.* (2001) Regulation of CLOCK and MOP4 by nuclear hormone receptors in the vasculature: A humoral mechanism to reset a peripheral clock. *Cell*, 105, 877–889.

Mehta, N. *et al*. (2015) GRK2 Fine-Tunes Circadian Clock Speed and Entrainment via Transcriptional and Post-translational Control of PERIOD Proteins. *Cell Reports*, 12, 1272-1288.

Mendoza-Viveros, L. *et al*. (2017) Molecular modulators of the circadian clock: lessons from flies and mice. *Cellular and Molecular Life Sciences*, 74, 1035-1059.

Millar-Craig, M., Bishop, C. and Raftery, E. B. (1978) Circadian variation of blood pressure. *The Lancet*, 311, 795–797.

Miller, B. H. *et al.* (2007) Circadian and CLOCK-controlled regulation of the mouse transcriptome and cell proliferation. *Proceedings of the National Academy of Sciences USA*, 104, 3342-3347.

Milligan, C. J. *et al*. (2004) Evidence for Inhibition Mediated by Coassembly of GABAA and GABAC Receptor Subunits in Native Central Neurons. *The Journal of Neuroscience*, 24, 7241-7250.

Minoura, Y. *et al*. (2018) Modulation of sympathetic preganglionic neuron activity via adrenergic receptors. *Hypertension Research*, 41, 499-505.

Mohawk, J. A., Green, C. B. and Takahashi, J. S. (2012) Central and Peripheral Circadian Clocks in Mammals. *Annual Review of Neuroscience*. Annual Reviews, 35, 445–462.

Morales, M. and Wang, S.-D. (2002) Differential Composition of 5-Hydroxytryptamine Receptors Synthesized in the Rat CNS and Peripheral Nervous System. *The Journal of Neuroscience*, 22, 6732-6741.

Mostacada, K. *et al*. (2015) Lack of galectin-3 improves the functional outcome and tissue sparing by modulating inflammatory response after a compressive spinal cord injury. *Experimental Neurology*, 271, 390-400.

Motawei, K. *et al.* (1999) Terminals of paraventricular spinal neurones are closely associated with adrenal medullary sympathetic preganglionic neurones: immunocytochemical evidence for vasopressin as a possible neurotransmitter in this pathway. *Experimental Brain Research*, 126, 68–76.

Murugaian, J. *et al*. (1990) Relative effects of different spinal autonomic nuclei on cardiac sympathoexcitatory function. *Brain Research Bulletin*, 24, 537-542.

Naffaa, M. M. *et al*. (2017) GABA-ρ receptors: distinctive functions and molecular pharmacology. *British Journal of Pharmacology*, 174, 1881-1894.

Nagai, K. *et al*. (1996) Chapter 18 SCN output drives the autonomic nervous system: with special reference to the autonomic function related to the regulation of glucose metabolism. In: BUIJS, R. M., KALSBEEK, A., ROMIJN, H. J., PENNARTZ, C. M. A. & MIRMIRAN, M. (eds.) *Progress in Brain Research*. Elsevier.

Nakamura, T. J. *et al*. (2015) Age-Related Changes in the Circadian System Unmasked by Constant Conditions. *eNeuro*, 2, 1-10.

Nakano, S. *et al.* (1999) Reversed circadian blood pressure rhythm independently predicts endstage renal failure in non-insulin-dependent diabetes mellitus subjects. *Journal of Diabetes and its Complications*, 13, 224–231.

Nakano, Y. *et al.* (2001) Non-dipper phenomenon in essential hypertension is related to blunted nocturnal rise and fall of sympatho-vagal nervous activity and progress in retinopathy. *Autonomic Neuroscience: Basic and Clinical*, 88,181–186.

Narciso, M. S. *et al*. (2009) Sciatic nerve regeneration is accelerated in galectin-3 knockout mice. *Experimental Neurology*, 217, 7-15.

Narkiewicz, K. *et al.* (2002) Relationship between muscle sympathetic nerve activity and diurnal blood pressure profile. *Hypertension*, 39, 168–172.

Navaratnam, V. and Raymond Lewis, P. (1970) Cholinesterase-containing neurones in the spinal cord of the rat. *Brain Research*, 18, 411–425.

Naylor, E. *et al*. (2000) The Circadian Clock Mutation Alters Sleep Homeostasis in the Mouse. *The Journal of Neuroscience*, 20, 8138-8143.

Nichterwitz, S. *et al*. (2016) Laser capture microscopy coupled with Smart-seq2 for precise spatial transcriptomic profiling. *Nature Communications*, 7, 1-11.

Nikodemova, M. *et al.* (2014) Spinal but not cortical microglia acquire an atypical phenotype with high VEGF, galectin-3 and osteopontin, and blunted inflammatory responses in ALS rats. *Neurobiology of Disease*, 69, 43–53.

Nonaka, H. *et al.* (2001) Angiotensin II induces circadian gene expression of clock genes in cultured vascular smooth muscle cells. *Circulation*, 104,1746–1748.

Nordberg, A. and Wahlström, G. (1980) Diurnal fluctuation in striatal choline acetyltransferase activity and strain difference in brain protein content of the rat. *Acta Physiologica*, 108, 385-388.

Novak, C. M. and Albers, H. E. (2004) Novel phase-shifting effects of GABA A receptor activation in the suprachiasmatic nucleus of a diurnal rodent. *American Journal of Physiology-Regulatory, Integrative and Comparative Physiology*, 286, 820-825.

Ohno, T. *et al*. (2010) Specific involvement of postsynaptic GluN2B-containing NMDA receptors in the developmental elimination of corticospinal synapses. *Proceedings of the National Academy of Sciences USA*, 107, 15252-15257.

Oldfield, B. J. and McLachlan, E. M. (1981) An analysis of the sympathetic preganglionic neurons projecting from the upper thoracic spinal roots of the cat. *Journal of Comparative Neurology*, 196, 329–345.

Oldfield, B. J. and McLachlan, E. M. (1977) Uptake and retrograde transport of HRP by axons of intact and damaged peripheral nerve trunks. *Neuroscience Letters*, 6, 135-141.

Olsen, R. W. & Sieghart, W. (2008) International Union of Pharmacology. LXX. Subtypes of γ-Aminobutyric Acid A Receptors: Classification on the Basis of Subunit Composition, Pharmacology, and Function. Update. *Pharmacological Reviews*, 60, 243-260.

Ono, D., Honma, K.-I. and Honma, S. (2015) Circadian and ultradian rhythms of clock gene expression in the suprachiasmatic nucleus of freely moving mice. *Scientific Reports*, 5, 1-10.

Owczarzy, R. et al. (2008) IDT SciTools: a suite for analysis and design of nucleic acid oligomers. *Nucleic acids research*, 36, 163-169.

Pajoohesh-Ganji, A. *et al.* (2012) Characterization of inflammatory gene expression and galectin-3 function after spinal cord injury in mice. *Brain Research*, 1475, 96–105.

Panda, S. *et al.* (2002) Coordinated Transcription of Key Pathways in the Mouse by the Circadian Clock. *Cell*, 109, 307–320.

Panda, S., Hogenesch, J. B. and Kay, S. A. (2002) Circadian rhythms from flies to human. *Nature*, 417, 329–335.

Pando, M. P. *et al.* (2002) Phenotypic rescue of a peripheral clock genetic defect via SCN hierarchical dominance. *Cell*, 110, 107–117.

Pantridge, J. F., Webb, S. W. and Adgey, A. A. J. (1981) Arrhythmias in the first hours of acute myocardial infarction. *Progress in Cardiovascular Diseases*, 23, 265-278.

Park, M. J. and Chung, K. (1999) Endogenous lectin (RL-29) expression of the autonomic preganglionic neurons in the rat spinal cord. *The Anatomical Record*, 254, 53–60.

Pérez-Otaño, I., Larsen, R. S. and Wesseling, J. F. (2016) Emerging roles of GluN3-containing NMDA receptors in the CNS. *Nature Reviews Neuroscience*, 17, 623-635.

Perez-Reyes, E. (2003) Molecular Physiology of Low-Voltage-Activated T-type Calcium Channels. *Physiological Reviews*, 83, 117-161.

Petras, J. M. and Cummings, J. F. (1972) Autonomic neurons in the spinal cord of the rhesus monkey: a correlation of the findings of cytoarchitectonics and sympathectomy with fiber degeneration following dorsal rhizotomy. *Journal of Comparative Neurology*, 146, 189–218.

Pickering, A. E., Spanswick, D. and Logan, S. D. (1994) 5-Hydoxytryptamine evokes depolarizations and membrane potential oscillations in rat sympathetic preganglionic neurones. *Journal of Physiology*, 480, 109–121.

Pierce, M. L., Deuchars, J. and Deuchars, S. A. (2010) Spontaneous rhythmogenic capabilities of sympathetic neuronal assemblies in the rat spinal cord slice. *Neuroscience*, 170, 827-838.

Pilowsky, P. M. *et al.* (1986) Spinal cord serotonin release and raised blood pressure after braintem kainic acid injection. *Brain Research*, 366, 354–357.

Pilowsky, P. M. and Goodchild, A. K. (2002) Baroreceptor reflex pathways and neurotransmitters: 10 Years on. *Journal of Hypertension*, 1675–1688.

Podobed, P. *et al.* (2014) The day/night proteome in the murine heart. *American Journal of Physiology - Regulatory Integrative and Comparative Physiology*, 307, 121-137.

Polson, J. W. *et al.* (2002) 2002. Fos expression in spinally projecting neurons after hypotension in the conscious rabbit. *Autonomic Neuroscience*, 100, 10-20.

Poon, Y.-Y. *et al.* (2016) Endogenous nitric oxide derived from NOS I or II in thoracic spinal cord exerts opposing tonic modulation on sympathetic vasomotor tone via disparate mechanisms in anesthetized rats. *American Journal of Physiology-Heart and Circulatory Physiology*, 311, 555–562.

Portaluppi, F. *et al*. (2012) Circadian rhythms and cardiovascular health. *Sleep Medicine Reviews*, 16, 151-166.

Poulin, J. F. *et al*. (2016) Disentangling neural cell diversity using single-cell transcriptomics. *Nature Neuroscience*, 19, 1131-1141.

Du Pré, B. C. *et al.* (2017) SCA1+ Cells from the Heart Possess a Molecular Circadian Clock and Display Circadian Oscillations in Cellular Functions. *Stem Cell Reports*, 9, 762–769.

Prins, C. A., Almeida, F. M. and Martinez, A. M. B. (2016) Absence of galectin-3 attenuates neuroinflammation improving functional recovery after spinal cord injury. *Neural Regeneration Research*, 11, 92-93.

Pyner, S. (2009) Neurochemistry of the paraventricular nucleus of the hypothalamus: Implications for cardiovascular regulation. *Journal of Chemical Neuroanatomy*, 38, 197–208.

Pyner, S. and Coote, J. H. (1994) Evidence that sympathetic preganglionic neurones are arranged in target-specific columns in the thoracic spinal cord of the rat. *Journal of Comparative Neurology*. Wiley Online Library, 342, 15–22.

Pyner, S. and Coote, J. H. (1995) Arrangement of dendrites and morphological characteristics of sympathetic preganglionic neurones projecting to the superior cervical ganglion and adrenal medulla in adult cat. *Journal of the Autonomic Nervous System*, 52, 35–41.

Pyner, S. and Coote, J. H. (1999) Identification of an efferent projection from the paraventricular nucleus of the hypothalamus terminating close to spinally projecting rostral ventrolateral medullary neurons. *Neuroscience*, 88, 949–957.

Pyner, S. and Coote, J. H. (2000) Identification of branching paraventricular neurons of the hypothalamus that project to the rostroventrolateral medulla and spinal cord. *Neuroscience*, 100, 549–556.

Qiu, S. et al. (2012) Single-neuron RNA-Seq: technical feasibility and reproducibility. *Frontiers in Genetics*, 3, 1-8.

Ramanathan, C. *et al*. (2006) Temporal and spatial distribution of immunoreactive PER1 and PER2 proteins in the suprachiasmatic nucleus and peri-suprachiasmatic region of the diurnal grass rat (Arvicanthis niloticus). *Brain Research*, 1073, 348-358.

Ramos-Vara, J. A. (2017) Principles and Methods of Immunohistochemistry. In: GAUTIER, J.-C. (ed.) *Drug Safety Evaluation: Methods and Protocols*. New York, NY: Springer New York.

Rando, T. A., Bowers, C. W. and Zigmond, R. E. (1981) Localization of neurons in the rat spinal cord which project to the superior cervical ganglion. *Journal of Comparative Neurology*, 196, 73–83.

Ranna, M. *et al*. (2006) Impact of ε and θ subunits on pharmacological properties of α3β1 GABAA receptors expressed in Xenopus oocytes. *BMC Pharmacology*, 6, 1-12.

Ranson, R. N. *et a*l. (1998) The paraventricular nucleus of the hypothalamus sends efferents to the spinal cord of the rat that closely appose sympathetic preganglionic neurones projecting to the stellate ganglion. *Experimental Brain Research*, 120, 164-172.

Reilly, D. F. *et al*. (2008) Peripheral Circadian Clock Rhythmicity Is Retained in the Absence of Adrenergic Signaling. *Arteriosclerosis, Thrombosis, and Vascular Biology*, 28, 121-126.

Romagnano, M. A. and Hamill, R. W. (1984) Spinal sympathetic pathway: An enkephalin ladder. *Science*, 225, 737–739.

Romanov, R. A. *et al*. (2017) Molecular interrogation of hypothalamic organization reveals distinct dopamine neuronal subtypes. *Nature Neuroscience*, 20, 176-188.

Rosenberg, A. B. *et al*. (2018) Single-cell profiling of the developing mouse brain and spinal cord with split-pool barcoding. *Science*, 360, 176-182.

Rotshenker, S. *et al.* (2008) Galectin-3/MAC-2, ras and PI3K activate complement receptor-3 and scavenger receptor-AI/II mediated myelin phagocytosis in microglia. *GLIA*, 56, 1607–1613.

Rubin, E. and Purves, D. (1980) Segmental organization of sympathetic preganglionic neurons in the mammalian spinal cord. *Journal of Comparative Neurology*, 192, 163–174.

Rudic, R. D. *et al*. (2004) BMAL1 and CLOCK, two essential components of the circadian clock, are involved in glucose homeostasis. *PLoS Biology*, 2, 1893-1899.

Sakaguchi, M. *et al*. (2006) A carbohydrate-binding protein, Galectin-1, promotes proliferation of adult neural stem cells. *Proceedings of the National Academy of Sciences USA*, 103, 7112-7117.

Sánchez-López, A. *et al*. (2003) Pharmacological profile of the 5-HT-induced inhibition of cardioaccelerator sympathetic outflow in pithed rats: correlation with 5-HT1 and putative 5-ht5A/5B receptors. *British Journal of Pharmacology*, 140, 725-735.

Saper, C. B., Swanson, L. W. and Cowan, W. M. (1976) The efferent connections of the ventromedial nucleus of the hypothalamus of the rat. *Journal of Comparative Neurology*, 169, 409-442.

Sawchenko, P. E. and Swanson, L. W. (1982) Immunohistochemical identification of neurons in the paraventricular nucleus of the hypothalamus that project to the medulla or to the spinal cord in the rat. *Journal of Comparative Neurology*, 205, 260–272.

von Schantz, M. and Archer, S. N. (2003) Clocks, genes and sleep. *Journal of the Royal Society of Medicine*, 96, 486–489.

Scheer, F. A. J. L. *et al.* (2010) Impact of the human circadian system, exercise, and their interaction on cardiovascular function. *Proceedings of the National Academy of Sciences USA*, 107, 20541–20546.

Scheer, F. A. J. L. *et al.* (2011) The human endogenous circadian system causes greatest platelet activation during the biological morning independent of behaviors. *PLoS ONE*, 6, 1-8.

Scheer, F. A. J. L. *et al.* (2019) Impact of mental stress, the circadian system and their interaction on human cardiovascular function. *Psychoneuroendocrinology*, 103, 125–129.

Scheer, F. A. J. L. and Shea, S. A. (2014) Human circadian system causes a morning peak in prothrombotic plasminogen activator inhibitor-1 (PAI-1) independent of the sleep/wake cycle. *Blood*, 123, 590–593.

Schramm, L. P. *et al.* (1993) Peripheral and central pathways regulating the kidney: a study using pseudorabies virus. *Brain Research*, 616, 251-262.

Schramm, L. P. *et al.* (1975) Preganglionic innervation of the adrenal gland of the rat: a study using horseradish peroxidase. *Experimental Neurology*, 49, 540–553.

Schreihofer, A. M. and Guyenet, P. G. (2002) The baroreflex and beyond: Control of sympathetic vasomotor tone by gabaergic neurons in the ventrolateral medulla. *Clinical and Experimental Pharmacology and Physiology*, 29, 514–521.

Schroder, E. A. *et al.* (2013) The cardiomyocyte molecular clock, regulation of Scn5a, and arrhythmia susceptibility. *American Journal of Physiology - Cell Physiology*, 304, 954-965.

Seifalian, A. and Hart, A. (2019) Circadian Rhythms: Will It Revolutionise the Management of Diseases? *Journal of Lifestyle Medicine*, 9, 1–11.

Semyanov, A. *et al*. (2004) Tonically active GABAA receptors: modulating gain and maintaining the tone. *Trends in Neurosciences*, 27, 262-269.

Sharma, V. K. and Chandrashekaran, M. K. (2005) Zeitgebers (time cues) for biological clocks. *Current Science*, 89, 1136–1146.

Shearman, L. P. *et al.* (2000) Interacting molecular loops in the mammalian circadian clock. *Science*, 288, 1013–1019.

Shimba, S. *et al*. (2005) Brain and muscle Arnt-like protein-1 (BMAL1), a component of the molecular clock, regulates adipogenesis. *Proceedings of the National Academy of Sciences USA*, 102, 12071-12076.

Siaud, P. *et al.* (1994) Superior cervical ganglionectomy suppresses circadian corticotropic rhythms in male rats in the short term (5 days) and long term (10 days). *Brain Research*, 652, 273–278.

Simpson, P. (1983) Norepinephrine-stimulated hypertrophy of cultured rat myocardial cells is an alpha 1 adrenergic response. *The Journal of Clinical Investigation*, 72, 732-738.

Sinturel, F. *et al*. (2017) Diurnal Oscillations in Liver Mass and Cell Size Accompany Ribosome Assembly Cycles. *Cell*, 169, 651-663.

Skovsted, P. and Sapthavichaikul, S. (1977) The effects of etomidate on arterial pressure, pulse rate and preganglionic sympathetic activity in cats. *Canadian Anaesthetists' Society Journal*, 24, 565-570.

Smyth, G. K., Shi, W. and Liao, Y. (2013) featureCounts: an efficient general purpose program for assigning sequence reads to genomic features. *Bioinformatics*, 30, 923-930.

Spanagel, R. *et al*. (2004) The clock gene Per2 influences the glutamatergic system and modulates alcohol consumption. *Nature Medicine*, 11, 35-42.

Spanswick, D. and Logan, S. D. (1990) Sympathetic preganglionic neurones in neonatal rat spinal cord in vitro: electrophysiological characteristics and the effects of selective excitatory amino acid receptor agonists. *Brain Research*, 525, 181-188.

Springell, D. A. *et al.* (2005) Phosphorylated extracellular signal-regulated kinase 1/2 immunoreactivity identifies a novel subpopulation of sympathetic preganglionic neurons. *Neuroscience*, 133,583–590.

St. John, P. A., *et al*. (1986). Analysis and isolation of embryonic mammalian neurons by fluorescence- activated cell sorting. *The Journal of Neuroscience*, 6, 1492-1512.

Stocker, S. D. *et al*. (2006) Water deprivation activates a glutamatergic projection from the hypothalamic paraventricular nucleus to the rostral ventrolateral medulla. *Journal of Comparative Neurology*, 494, 673-685.

Storch, K.-F. *et al.* (2002) Extensive and divergent circadian gene expression in liver and heart. *Nature*, 417, 78-83.

Strack, A. and Loewy, A. (1990) Pseudorabies virus: a highly specific transneuronal cell body marker in the sympathetic nervous system. *The Journal of Neuroscience*, 10, 2139-2147.

Strack, A. M. *et al.* (1988) Spinal origin of sympathetic preganglionic neurons in the rat. *Brain Research*, 455, 187–191.

Stratmann, M. and Schibler, U. (2006) Properties, entrainment, and physiological functions of mammalian peripheral oscillators. *Journal of Biological Rhythms*, 6, 494–506.

Su, C.-K., Chen, Y.-Y. and Ho, C.-M. (2018) Nitric Oxide Orchestrates a Power-law Modulation of Sympathetic Firing Behaviors in Neonatal Rat Spinal Cords. *Frontiers in Physiology*, 9, 1-14.

Sundaram, K., Murugaian, J. and Sapru, H. (1989). Cardiac responses to the microinjections of excitatory amino acids into the intermediolateral cell column of the rat spinal cord. *Brain Research*, 482, 12-22.

Takahashi, J. S. (2016) Transcriptional architecture of the mammalian circadian clock. *Nature Reviews Genetics*, 18, 164-179.

Takano, A. *et al.* (2000) Cloning and characterization of rat casein kinase 1ε. *FEBS Letters*, 477, 106–112.

Takeda, N. and Maemura, K. (2016) Circadian clock and the onset of cardiovascular events. *Hypertension Research*, 39, 383-390.

Takeda, N. and Maemura, K. (2015) The role of clock genes and circadian rhythm in the development of cardiovascular diseases. *Cellular and Molecular Life Sciences*, 72, 3225–3234.

Takeda, N. and Maemura, K. (2011) Circadian clock and cardiovascular disease. *Journal of Cardiology*, 57, 249–256.

Takeda, N. *et al.* (2007) Thrombomodulin is a clock-controlled gene in vascular endothelial cells. *Journal of Biological Chemistry*, 282, 32561–32567.

Talley, E. M. *et al*. (1999) Differential Distribution of Three Members of a Gene Family Encoding Low Voltage-Activated (T-Type) Calcium Channels. *The Journal of Neuroscience*, 19, 1895-1911.

Tang, F. R., Tan, C. K. and Ling, E. A. (1995a) A comparative study by retrograde neuronal tracing and substance P immunohistochemistry of sympathetic preganglionic neurons in spontaneously hypertensive rats and Wistar-Kyoto rats. *Journal of Anatomy*, 186, 197-205.

Tang, F. R., Tan, C. K. and Ling, E. A. (1995b) A light-microscopic study of the intermediolateral nucleus following injection of CB-HRP and fluorogold into the superior cervical ganglion of the rat. *Journal of the Autonomic Nervous System*, 50, 333–338.

Taylor, D. G. and Gebber, T. (1975) Baroreceptor mechanisms controlling sympathetic nervous rhythms of central origin. *American Journal of Physiology-Legacy Content*, 228, 1002-1003.

Taylor, P. (2012) Chapter 16 - Nicotinic Receptors. In: Robertson, D., Biaggioni, I., Burnstock, G., Low, P. A. and Paton, J. F. R. (eds.) Primer on the Autonomic Nervous System (Third Edition). San Diego: Academic Press.

Teclemariam-Mesbah, R. *et al*. (1997) Direct vasoactive intestinal polypeptide-containing projection from the suprachiasmatic nucleus to spinal projecting hypothalamic paraventricular neurons. *Brain Research*, 748, 71-76.

Ter Horst, G. J. *et al*. (1996) Neuroanatomy of Cardiac Activity-regulating Circuitry: A Transneuronal Retrograde Viral Labelling Study in the Rat. *European Journal of Neuroscience*, 8, 2029-2041.

Terazono, H. *et al*. (2003) Adrenergic regulation of clock gene expression in mouse liver. *Proceedings of the National Academy of Sciences USA*, 100, 6795.

Tominaga, K. *et al.* (1992) Effects of 5-HT1A receptor agonists on the circadian rhythm of wheel-running activity in hamsters. *European Journal of Pharmacology*, 214, 79–84.

Trapnell, C. *et al*. (2013) Differential analysis of gene regulation at transcript resolution with RNA-seq. *Nature Biotechnology*, 31, 46-53.

Trapnell, C. *et al*. (2009) TopHat: discovering splice junctions with RNA-Seq. *Bioinformatics* (Oxford, England), 25, 1105-1111.

Trapnell, C. *et al*. (2012) Differential gene and transcript expression analysis of RNA-seq experiments with TopHat and Cufflinks. *Nature Protocols*, 7, 562-578.

Tsentsevitsky, A. N. *et al*. (2017) Muscarinic cholinoreceptors (M1-, M2-, M3- and M4-type) modulate the acetylcholine secretion in the frog neuromuscular junction. *Neuroscience Letters*, 649, 62-69.

Tuck, M. L. (1986) The sympathetic nervous system in essential hypertension. *American Heart Journal*, 112, 877–886.

Tuck, M. L., Stern, N. and Sowers, J. R. (1985) Enhanced 24-hour norepinephrine and renin secretion in young patients with essential hypertension: Relation with the circadian pattern of arterial blood pressure. *The American Journal of Cardiology*, 55, 112–115.

Turek, F. W. *et al*. (2005) Obesity and Metabolic Syndrome in Circadian Clock Mutant Mice. *Science*, 308, 1043-1045.

Ueda, H. R. *et al.* (2005) System-level identification of transcriptional circuits underlying mammalian circadian clocks. *Nature Genetics*, 37, 187–192.

Ueyama, T. *et al.* (1999) Suprachiasmatic nucleus: a central autonomic clock. *Nature Neuroscience*, 2, 1051-1053.

Untergasser, A. *et al.* (2012) Primer3--new capabilities and interfaces. *Nucleic Acids Research*, 40, 1-12.

Vallbo, Å. B., Hagbarth, K.-E. and Wallin, B. G. (2004) Microneurography: how the technique developed and its role in the investigation of the sympathetic nervous system. *Journal of Applied Physiology*, 96, 1262-1269.

Van Berkel, M. A. *et al.* (2017) Increased incidence of clinical hypotension with etomidate compared to ketamine for intubation in septic patients: A propensity matched analysis. *Journal of Critical Care*, 38, 209-214.

Van der veen, D. R. *et al.* (2012) Cardiac atrial circadian rhythms in PERIOD2::LUCIFERASE and per1:luc mice: amplitude and phase responses to glucocorticoid signaling and medium treatment. *PloS One*, 7, 1-13.

Vielhaber, E. *et al.* (2000) Nuclear Entry of the Circadian Regulator mPER1 Is Controlled by Mammalian Casein Kinase I varepsilon. *Molecular and Cellular Biology*, 20, 4888–4899.

Villalón, C. M. *et al.* (1999) 5-Hydroxytryptamine inhibits the tachycardia induced by selective preganglionic sympathetic stimulation in pithed rats. *Life Sciences*, 64, 1839-1847.

Viswambharan, H. *et al.* (2007) Mutation of the Circadian Clock Gene Per2 Alters Vascular Endothelial Function. *Circulation*. American Heart Association, 115, 2188–2195.

Von Schantz, M. and Archer, S. N. (2003) Clocks, genes and sleep. *Journal of the Royal Society of Medicine*, 96, 486-489.

Vrang, N., Mikkelsen, J. D. and Larsen, P. J. (1997) Direct Link From the Suprachiasmatic Nucleus to Hypothalamic Neurons Projecting to the Spinal Cord: A Combined Tracing Study Using Cholera Toxin Subunit B and Phaseolus vulgaris-Leucoagglutinin. *Brain Research Bulletin*, 44, 671-680.

Vujović, N., Davidson, A. J. and Menaker, M. (2008) Sympathetic input modulates, but does not determine, phase of peripheral circadian oscillators. *American Journal of Physiology-Regulatory, Integrative and Comparative Physiology*, 295, 355-360.

Wang, J., Ou, S.-W. and Wang, Y.-J. (2017). Distribution and function of voltage-gated sodium channels in the nervous system. *Channels*, 11, 534-554.

Wang, L. *et al.* (2008a) Tonic GABAergic inhibition of sympathetic preganglionic neurons: a novel substrate for sympathetic control. *Journal of Neuroscience*, 28, 12445–12452.

Wang, L. *et al.* (2008b). Vascular PPARγ Controls Circadian Variation in Blood Pressure and Heart Rate through Bmal1. *Cell Metabolism*, 8, 482-491.

Wang, D., Cui, L. N. and Renaud, L. P. (2003) Pre- and postsynaptic gabab receptors modulate rapid neurotransmission from suprachiasmatic nucleus to parvocellular hypothalamic paraventricular nucleus neurons. *Neuroscience*, 118, 49-58.

Warren, W. S., Champney, T. H. and Cassone, V. M. (1994) The suprachiasmatic nucleus controls the circadian rhythm of heart rate via the sympathetic nervous system. *Physiology & Behavior*, 55, 1091–1099.

Wee, K. S. L., Zhang, Y., Khanna, S. and Low, C.-M. (2008). Immunolocalization of NMDA receptor subunit NR3B in selected structures in the rat forebrain, cerebellum, and lumbar spinal cord. *Journal of Comparative Neurology*, 509, 118-135.

Wehrwein, E. A., Orer, H. S. and Barman, S. M. (2016) Overview of the Anatomy, Physiology, and Pharmacology of the Autonomic Nervous System. *Comprehensive Physiology*, 6, 1239–1278.

Welsh, D. K. *et al.* (2004) Bioluminescence imaging of individual fibroblasts reveals persistent, independently phased circadian rhythms of clock gene expression. *Current Biology*, 14, 2289–2295.

Whyment, A. D. *et al.* (2004) Activation and integration of bilateral GABA-mediated synaptic inputs in neonatal rat sympathetic preganglionic neurones in vitro. *The Journal of Physiology*, 555, 189-203.

Wisor, J. P. *et al.* (2002) A role for cryptochromes in sleep regulation. *BMC Neuroscience*, 3, 1-14.

Xie, Z. *et al.* (2015) Smooth-muscle BMAL1 participates in blood pressure circadian rhythm regulation. *Journal of Clinical Investigation*, 125, 324–336.

Yan, B. *et al.* (2015) Novel association between the reverse-dipper pattern of ambulatory blood pressure monitoring and metabolic syndrome in men but not in women. *Medicine (United States)*, 94, 1-4.

Xu, Y. *et al*. (2005) Functional consequences of a CKIδ mutation causing familial advanced sleep phase syndrome. *Nature*, 434, 640-644.

Yamashita, T. *et al*. (2003) Circadian Variation of Cardiac K+ Channel Gene Expression. *Circulation*, 107, 1917-1922.

Yamazaki, S. *et al*. (2000) Resetting Central and Peripheral Circadian Oscillators in Transgenic Rats. *Science*, 288, 682-685.

Ye, J., *et al*. (2012) Primer-BLAST: a tool to design target-specific primers for polymerase chain reaction. *BMC Bioinformatics*, 13, 134-134.

Yoo, H.I. *et al*. (2017) Neuroanatomical distribution of galectin-3 in the adult rat brain. *Journal Molecular Histology*, 48, 133-146.

Yoo, S.-H. *et al.* (2004) PERIOD2:: LUCIFERASE real-time reporting of circadian dynamics reveals persistent circadian oscillations in mouse peripheral tissues. *Proceedings of the National Academy of Sciences USA*, 101, 5339–5346.

Yoon, S.-Y. *et al.* (2005) The anti-inflammatory effect of peripheral bee venom stimulation is mediated by central muscarinic type 2 receptors and activation of sympathetic preganglionic neurons. *Brain Research*, 1049, 210-216.

Yoshimura, M., Polosa, C. and Nishi, S. (1987) Slow EPSP and the depolarizing action of noradrenaline on sympathetic preganglionic neurons. *Brain Research*, 414, 138–142.

Young, M. E. *et al.* (2014) Cardiomyocyte-specific BMAL1 plays critical roles in metabolism, signaling, and maintenance of contractile function of the heart. *Journal of Biological Rhythms*, 29, 257–276.

Zhang, R. *et al*. (2014) A circadian gene expression atlas in mammals: implications for biology and medicine. *Proceedings of the National Academy of Sciences USA*, 111, 16219-16224.

Zhang, R.-X. *et al.* (2013) Gene silencing of NR2B-containing NMDA receptor by intrathecal injection of short hairpin RNA reduces formalin-induced nociception in C57BL/6 mouse. *International Journal of Neuroscience*, 123, 650-656.

Ziegenhain, C., *et al.* (2017) Comparative Analysis of Single-Cell RNA Sequencing Methods. *Molecular Cell*, 65, 631-643.